DEVELOPMENT OF PROCEDURES FOR CALCULATING STIFFNESS AND DAMPING PROPERTIES OF ELASTOMERS IN ENGINEERING APPLICATIONS, PART III: THE EFFECTS OF TEMPERATURE, DISSIPATION LEVEL AND GEOMETRY

A. J. SMALLEY, ET AL

MECHANICAL TECHNOLOGY INCORPORATED
LATHAM, NEW YORK

NOVEMBER 1975

BEST SELLERS

FROM NATIONAL TECHNICAL INFORMATION SERVICE

NTIS

Solar Heating and Cooling in Buildings: Methods of Economic Evaluation
COM–75–11070/PAT 48 p PC$4.00/MF$2.25

Design and Construction of a Residential Solar Heating and Cooling System
PB–237 042/PAT 233 p PC$8.00/MF$2.25

Performance of a Residential Solar Heating and Cooling System
PB–244 644/PAT 62 p PC$4.50/MF$2.25

Solar Energy
AD–778 846/PAT 478 p PC$12.50/MF$2.25

Stimulation of Geothermal Energy Resources
ERDA–37/PAT 52 p PC$4.50/MF$2.25

An Assessment of Industrial Energy Options Based on Coal and Nuclear Systems
ORNL–4995/PAT 329 p PC$10.00/MF$2.25

Environmental Impact Statements: A Handbook for Writers and Reviewers
PB–226 276/PAT 207 p PC$7.75/MF$2.25

Environmental Protection Guidelines for Construction Contract Specification Writers
ADA–014146/PAT 124 p PC$5.50/MF$2.25

A Review and Analysis of Environmental Impact Assessment Methodologies
ADA–013 359/PAT 21 p PC$3.50/MF$2.25

Procedures for Reviewing Environmental Impact Assessments and Statements for Construction Projects
ADA–015 020/PAT 25 p PC$3.50/MF$2.25

Computers in the 1980's: Trends in Hardware Technology
AD–783 323/PAT 20 p PC$3.50/MF$2.25

Minicomputers: A Review of Current Technology, Systems, and Applications
AD–783 316/PAT 104 p PC$5.50/MF$2.25

Microprocessor/Microcomputer Software Systems: Present and Future
ADA–013 322/PAT 25 p PC$3.50/MF$2.25

An Air Force Guide to Contracting for Software Acquisition
ADA–020 444/PAT 45 p PC$4.00/MF$2.25

A Dictionary for Unit Conversion
PB–249 659/PAT 456 p PC$17.50/MF Not Available

HOW TO ORDER

When you indicate the method of payment, please note if a purchase order is not accompanied by payment, you will be billed an addition $5.00 *ship and bill* charge. And please include the card expiration date when using American Express.

Normal delivery time takes three to five weeks. It is vital that you order by number or your order will be manually filled, insuring a delay. You can opt for *airmail delivery* for a $2.00 charge per item. Just check the *Airmail Service* box. If you're really pressed for time, call the NTIS Rush Order Service. (703) 557-4700. For a $10.00 charge per item, your order will be airmailed within 48 hours. Or, you can pick up your order in the Washington Information Center & Bookstore or at our Springfield Operations Center within 24 hours for a $6.00 per item charge.

You may also place your order by telephone or TELEX. The order desk number is (703) 557-4650 and the TELEX number is 89-9405.

Whenever a foreign sales price is NOT specified in the listings, all foreign buyers must add the following charges to each order: $2.50 for each paper copy; $1.50 for each microfiche; and $10.00 for each Published Search.

Thank you for your interest in NTIS. We appreciate your order.

METHOD OF PAYMENT

☐ Charge my NTIS deposit account no._____

☐ Purchase order no._____

☐ Check enclosed for $_____

☐ Charge to my American Express Card account number

Card expiration date_____

Signature_____

☐ Airmail Services requested

NAME_____

ADDRESS_____

CITY, STATE, ZIP_____

Item Number	Quantity		Unit Price*	Total Price*
	Paper Copy (PC)	Microfiche (MF)		

All Prices Subject to Change
10/76

Sub Total	
Additional Charge	
Enter Grand Total	

Clip and mail to:

NTIS

National Technical Information Service
U.S. DEPARTMENT OF COMMERCE
Springfield, Va. 22161
(703) 557-4650 TELEX 89-9405

DISCLAIMER NOTICE

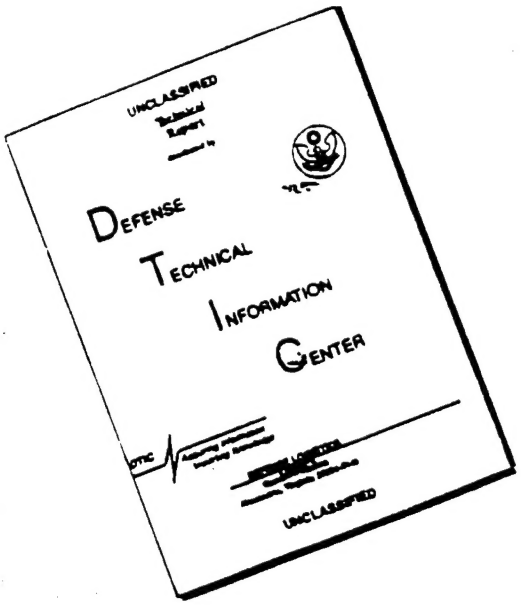

THIS DOCUMENT IS BEST QUALITY AVAILABLE. THE COPY FURNISHED TO DTIC CONTAINED A SIGNIFICANT NUMBER OF PAGES WHICH DO NOT REPRODUCE LEGIBLY.

NASA CR-134939
MTI 76TR5

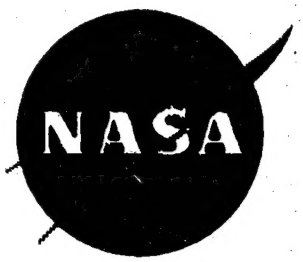

DEVELOPMENT OF PROCEDURES FOR CALCULATING STIFFNESS AND DAMPING PROPERTIES OF ELASTOMERS IN ENGINEERING APPLICATIONS

PART III. THE EFFECTS OF TEMPERATURE, DISSIPATION LEVEL AND GEOMETRY

by

A. J. Smalley
J. M. Tessarzik

MECHANICAL TECHNOLOGY INCORPORATED

Prepared for

NATIONAL AERONAUTICS AND SPACE ADMINISTRATION

NASA – Lewis Research Center

Contracts NAS 3-15334
and NAS 3-18546

Robert E. Cunningham, Project Manager

NOTICE

This report was prepared as an account of Government-sponsored work. Neither the United States, nor the National Aeronautics and Space Administration (NASA), nor any person acting on behalf of NASA:

A.) Makes any warranty or representation, expressed or implied, with respect to the accuracy, completeness, or usefulness of the information contained in this report, or that the use of any information, apparatus, method, or process disclosed in this report may not infringe privately-owned rights; or

B.) Assumes any liabilities with respect to the use of, or for damages resulting from the use of, any information, apparatus, method or process disclosed in this report.

As used above, "person acting on behalf of NASA" includes any employee or contractor of NASA, or employee of such contractor, to the extent that such employee or contractor of NASA or employee of such contractor prepares, disseminates, or provides access to any information pursuant to his employment or contract with NASA, or his employment with such contractor.

Requests for copies of this report should be referred to

National Aeronautics and Space Administration
Scientific and Technical Information Facility
P.O. Box 33
College Park, Md. 20740

Report No.

NASA CR-

4. Title and Subtitle

DEVELOPMENT OF PROCEDURES FOR CALCULATING [illegible] AND DAMPING PROPERTIES OF ELASTOMERS

PART III THE EFFECTS OF TEMPERATURE, DISSIPATION LEVEL AND GEOMETRY

5. Report Date

November [illegible]

6. Performing Organization Code

7. Author(s)

Anthony J. Smalley
Juergen M. Tessarzik

8. Performing Organization Report No

MTI 76TR5

9. Performing Organization Name and Address

Mechanical Technology Incorporated
968 Albany-Shaker Road
Latham NY 12110

10. Work Unit No.

11. Contract or Grant No.

NAS 3-15334
NAS 3-18546

12. Sponsoring Agency Name and Address

National Aeronautics and Space Administration
Washington, DC 20546

13. Type of Report and Period Covered

Contractor Report - Final

14. Sponsoring Agency Code

15. Supplementary Notes

Project Manager, Robert E. Cunningham, Bearings and Mechanical Power Transfer Branch, NASA-Lewis Research Center, Cleveland, OH 44135

16. Abstract

Effects of temperature, dissipation level and geometry on the dynamic behavior of elastomer elements were investigated. Force-displacement relationships in elastomer elements and the effects of frequency, geometry and temperature upon these relationships are reviewed. Based on this review, methods of reducing stiffness and damping data for shear and compression test elements to material properties (storage and loss moduli) and empirical geometric factors are developed and tested using previously generated experimental data. A prediction method which accounts for large amplitudes of deformation is developed on the assumption that their effect is to increase temperature through the elastomers, thereby modifying the local material properties. Various simple methods of predicting the radial stiffness of ring cartridge elements are developed and compared.

Material properties were determined from the shear specimen tests as a function of frequency and temperature. Using these material properties, numerical predictions of stiffness and damping for cartridge and compression specimens were made and compared with corresponding measurements at different temperatures, with encouraging results.

Successful comparisons of high dissipation predictions and measurements were made for the compression specimens but it is shown that, for the shear specimen, strain is an important influential paramenter, even when the temperature rise is small.

The method of reduced variables (which allows frequency dependent data at different temperatures to be collapsed to a single curve in reduced variables) is tested out on the material property results. It is shown that the storage modulus follows the reduced variable law satisfactorily, whereas the loss modulus does not.

PRICES SUBJECT TO CHANGE

17. Key Words (Suggested by Author(s))

Dynamic Properties
Vibration Test Rig
Viscoelastic Models
Analytical Prediction Methods
Elastomers

18. Distribution Statement

Unlimited

19. Security Classif. (of this report)

UNCLASSIFIED

20. Security Classif. (of this page)

UNCLASSIFIED

FOREWORD

This report presents the work performed under NASA contracts NAS3-15334 and NAS3-18546 in the period January, 1974 to July, 1975, with Mr. Robert E. Cunningham, NASA Lewis Research Center as Project Manager. It is the third in a series of reports on the development of procedures for calculating stiffness and damping properties of elastomers in engineering application. The Program Manager for MTI was Dr. A. J. Smalley. Principal Investigator for the analytical portions was Dr. A. J. Smalley and for the experimental portions was Mr. J. M. Tessarzik. The analysis for reduction of test data was developed by Dr. P. K. Gupta. Mr. M. S. Darlow conducted a number of the tests. Principal Technician for all the elastomer tests was Mr. W. G. Spodnewski.

TABLE OF CONTENTS

TABLE OF CONTENTS (concluded)

LIST OF ILLUSTRATIONS

LIST OF TABLES

SUMMARY

This report presents the results of a program of analysis and test to investigate the effects of temperature, dissipation level and geometry on the dynamic behavior of elastomer elements. The report presents, first, a review of force displacement relationships in elastomer elements and the effects of frequency, geometry and temperature upon these relationships. Based on this review, methods of reducing stiffness and damping data for shear and compression test elements to material properties (storage and loss moduli) and empirical geometry factors are developed and tested using previously generated experimental data. A prediction method which accounts for large amplitudes of deformation is developed on the assumption that their effect is to increase temperature through the elastomers, thereby modifying the local material properties. Various simple methods of predicting the radial stiffness of ring cartridge elements are developed and compared.

The test method for all dynamic stiffness and damping measurements involves resonating a mass, supported on the test element, by exciting the base to which the test element is mounted. The specimens tested were: Two rectangular shear specimens; one cylindrical compression specimen; and two cartridge elements of different length. Tests were performed at temperatures between 5 and 93 C and at dissipation levels between 0.022 watts/cm^3 and 4.4 watts/cm^3 material.

Material properties were determined from the shear specimen tests as a function of frequency and temperature. Using these material properties, numerical predictions of stiffness and damping for cartridge and compression specimens were made and compared with corresponding measurements at different temperatures, with encouraging results.

Successful comparisons of high dissipation predictions and measurements were made for the compression specimens but it is shown that, for the shear specimen, strain is an important influential parameter, even when the temperature rise is small.

The method of reduced variables (which allows frequency dependent data at different temperatures to be collapsed to a single curve in reduced variables) is tested out on the material property results. It is shown that the storage modulus follows the reduced variable law satisfactorily whereas the loss modulus does not.

INTRODUCTION

The use of support damping as a means to control rotating machinery vibrations is seeing increasingly wide application in advanced turbomachinery. It will also have an important role to play in advanced, flexible, power transmission shafting. Presently the most common type of damper in these applications is the squeeze-film damper in parallel with some type of mechanical flexure.

Elastomer dampers are an attractive alternative to the squeeze film for rotating machinery and other applications because of their simplicity; their inherent combination of stiffness and damping; their compactness; and their lack of need for seals or oil supply. In the form of O-rings or cartridges they are being considered for low-cost engine applications and for helicopter transmission shafting.

Two of the factors which resist the growth in application of elastomer dampers are the limited availability of design-oriented data on their dynamic behavior and limited quantification of the problems to be encountered in their application. Dynamic testing under controlled conditions, coupled with practical interpretation of the test results is the means to fill this need. Thereby, the influence of important geometrical, environmental and chemical design parameters can be determined.

A program for testing and analysis of elastomer materials has been in progress at MTI since 1971. The objectives of the program are to develop elastomer dynamics technology and to reduce the technology to a form in which it can be readily applied in design.

Experimental and analytical methods are employed in meeting these objectives. Firstly, from a limited number of tests, general properties are sought which characterize an elastomer material. Secondly, prediction methods are sought which employ these material properties, in combination with appropriate geometry effects, to yield values for stiffness and damping of particular elastomer configurations.

This report is the third in a series. Preceding reports (refs. 1 and 2) have described the development and refinement of a powerful test technique, the Base Excitation Resonant Mass (BERM) method, and its initial application to the development of elastomer element properties in a controlled temperature environment under conditions of low dissipation. The BERM method most conveniently supplies data in the 100 Hz to 1000 Hz frequency range - into which the majority of rotating machinery vibration problems fall. Important features of the method are its controlled temperature environment; its ability to apply controlled high or low levels of dissipation at frequencies up to 1000 Hz or higher; its exploitation of mechanical resonance to achieve phase angles clustered around 90 degrees; and its determination

of stiffness and damping from accelerometer signals only, each processed by identical electronics, to minimize spurious phase errors in the data.

The work presented herein provides a much expanded body of test data under a range of frequencies, temperatures and dissipation levels; development of interpretive and predictive methods; application of these methods; and verification of their ability to predict dynamic behavior. As a framework against which this work can be viewed, Figure 1 is presented.

Figure 1 is a statement of the possible interactions between tests, data reduction, analysis, performance prediction and verification. As shown, the starting point for practical information is testing, and the BERM test method provides the main source of test data within this program. The output of the tests is raw data (amplitudes, phase angles, etc) which is converted by automated data analysis methods to specimen properties - that is, stiffness and damping of the elements being tested, as a function of frequency. To replace the discrete data points resulting from tests with a continuous relationship which can be handled mathematically, an appropriate frequency correlation, preferably of minimum complexity, is performed. The output of this correlation provides a compact definition of the dynamic behavior of the elements being tested which, together with similar compact definitions for other elements, yields a specimen catalog; that is, a list of stiffness and damping properties of a series of different elements under different conditions of temperature and power level.

To provide more universally applicable information, the specimen information is processed to yield material properties (which relate stress to strain) as a function of frequency. Where available, other sources of test data may also be employed. The output of this step is a material properties catalog, describing one material or several materials as a function of frequency and temperature.

To apply elastomer material properties (moduli) in the design prediction of elastomer element properties, it is necessary to translate stress-strain relationships back into force - displacement relationships. For each elastomer configuration, there exists a ratio between the stiffness and damping at a particular frequency and temperature and the moduli of the material at the same frequency and temperature. These ratios, or geometry factors, will, in general, be a function of frequency, temperature, amplitude and geometry.

As shown in Figure 1, sources of these ratios are solutions to the continuum equations for the elastomer element, in some cases combined with empirical coefficients obtained by tests. The spectrum

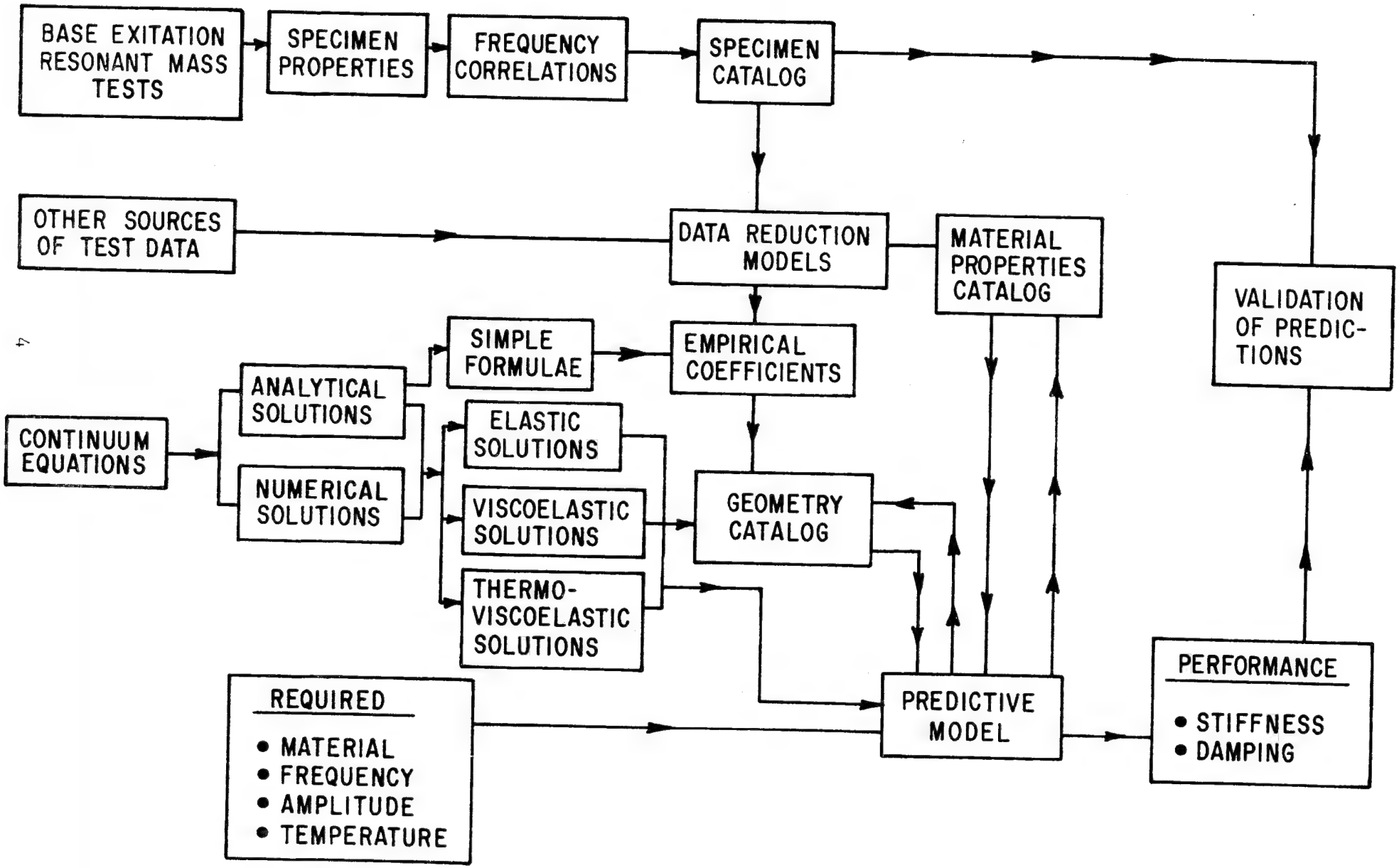

Fig. 1 Block Diagram Illustrating The Interaction of Test, Data Reduction, Analyses and Prediction

of solution complexity can run from a simple algebraic formula to the solution of complex continuum energy and viscoelasticity equations in two or three dimensions. The body of ratios, or geometry factors, determined in one or several ways, is the geometry catalog.

The material properties catalog and the geometry catalog are the two sources of information which embody the predictive model. They make it possible to predict stiffness and damping as a general function of material, geometry, frequency, amplitude and temperature.

Progress along most of the paths of Figure 1 has been made under this program, as will be described in this report.

Important questions to be addressed by this technology program are:

"What level of complexity and sophistication is needed to generate an adequate geometry catalog for design purposes?"

"What are the benefits, in improved accuracy, to be expected from advanced solutions relative to simple solution methods?"

The simplest methods of all provide geometry factors which are independent of frequency, and in two cases such predictive methods have been tested and their accuracy assessed against test data or more complete representations. These methods clearly lack rigor and there are discrepancies between their predictions and measured data. At the same time, for certain application of elastomers, their precision may be adequate. In other applications, the development of, as yet, unavailable sophisticated prediction methods will be required. Given the level of component prediction accuracy to be expected, as indicated in this report, sensitivity studies for particular applications will reveal the likely uncertainties in predicted system performance which will result.

The following sections of the report present, first, a summary of results, conclusions, and recommendations, including the material properties and geometry catalog resulting from the tests and analysis presented in the report. Then follows a review of force-displacement relationships for elastomers; the development of interpretive and predictive models; a description of test methods, including parameter ranges; a presentation of the test results; and a discussion of these results.

SUMMARY OF RESULTS

1. Methods of identifying generalized material properties and their relationship to dynamic behavior of elastomer elements have been developed, applied and tested.

2. Dynamic test data for several geometries has been generated, for dissipation levels from 0.022 to 4.4 watts/cm^3, for temperatures from 5 to 93 C, and for frequencies from 70 to 1500 Hz.

3. The geometries considered are:
   - shear loaded rectangular elastomer strips,
   - compression loaded right solid cylinders, and
   - radially loaded cylindrical cartridges.

4. The material is a broad temperature range (BTR) elastomer-polybutadiene.

5. Material property values (storage and loss moduli) have been generated, as a function of frequency and temperature, from the shear elements.

6. Geometry factor values (analogous to the traditional shape factor coefficient) have been generated for compression loaded right circular cylinders as a function of frequency.

7. These geometry factors have been shown to provide a self-consistent representation of data generated under previously reported work.

8. These geometry factors have provided reasonably effective predictions of stiffness and damping for a range of temperatures other than those for which they were developed.

9. These empirical geometry factors, which depend on frequency, have been compared, in terms of their ability to predict measured stiffness and damping, with use of a frequency independent static shape factor coefficient.

10. Cartridge test specimens and an appropriate test fixture have been designed and fabricated.

11. Predictions of cartridge stiffness and damping have been made as a function of frequency, using two different algebraic expressions. The simplest of these is based on representation of the cartridges as a series of noninteracting beams and column elements.

12. These two simple methods predict results which differ by a factor of two but provide a band within which the great majority of measured values lie.

13. A thermoviscoelastic prediction method indicates some similar trends for stiffness as observed under conditions of high dissipation; that is, decreasing stiffness with increasing dissipation levels. This statement applies particulary to compression test specimens.

14. Although the conductivity is unknown for this material, an effective thermal conductivity value has been generated which gives a good, quantitative match between measured and predicted values of high dissipation stiffness and damping for compression loaded cylinders.

15. Use of the same effective conductivity value for shear elements gives predicted stiffness and damping values which are higher than observed, under high dissipation conditions.

16. Measured stiffness and damping values were correlated against strain and against dissipation. More consistent dependence on strain than on dissipation was observed.

17. A "strain softening" effect is apparent in the shear specimen results.

18. The method of reduced variables was effective in reducing storage modulus data for different temperatures to a single curve of reduced modulus vs reduced frequency, but was not as effective for loss modulus. Strain dependence of the results is shown to be a likely cause of this apparent inconsistency for loss modulus.

19. The material property catalog for the tested elastomer, based on the results presented in this report is as follows:

Temperature	Storage Modulus	Loss Modulus
32 C	$G'(\omega) = 3.686 \times 10^6\ \omega^{0.2037}$	$G''(\omega) = 8.333 \times 10^6\ \omega^{-0.1277}$
43 C	$G'(\omega) = 1.904 \times 10^6\ \omega^{0.2627}$	$G''(\omega) = 3.971 \times 10^6\ \omega^{-0.0637}$
66 C	$G'(\omega) = 1.097 \times 10^6\ \omega^{0.3037}$	$G''(\omega) = 2.423 \times 10^6\ \omega^{-0.0301}$
93 C	$G'(\omega) = 1.197 \times 10^6\ \omega^{0.2450}$	$G''(\omega) = 1.064 \times 10^6\ \omega^{+0.2246}$

20. The geometry catalog for the three tested goemetries is as follows:

Geometry	Basis For Expression	Stiffness	Damping
Shear	Shear, No Bending	$K_1(\omega) = G' Nbx/h$	$K_2(\omega) = G'' Nbx/h$
Compression Cylinder	Empirical Correlation	$K_1(\omega) = G' \frac{N\pi D^2}{4h}\left[1+\beta'\left(\frac{D}{4h}\right)^2\right]$ $\beta' = 12.33\ \omega^{-0.290}$	$K_2(\omega) = G'' \frac{N\pi D^2}{4h}\left[1+\beta''\left(\frac{D}{4h}\right)^2\right]$ $\beta'' = 1.726\ \omega^{0.0299}$
	Static Shape Factor	$K_1(\omega) = G' \frac{N\pi D^2}{4h}\left[1+2\left(\frac{D}{4h}\right)^2\right]$	$K_2(\omega) = G'' \frac{N\pi D^2}{4h}\left[1+2\left(\frac{D}{4h}\right)^2\right]$
Ring Cartridge	Beam-Column	$K_1(\omega) = 2\pi G' NL(r_2+r_1)/(r_2-r_1)$	$K_2(\omega) = 2\pi G'' NL(r_2+r_1)/(r_2-r_1)$
	Beam-Column With Radius Effects	$K_1(\omega) = 4\pi G' NL/\ell n(r_2/r_1)$	$K_2(\omega) = 4\pi G'' NL/\ell n(r_2/r_1)$
	Göbel	$K_1(\omega) = 7.5\ \pi G' NL/\ell n(r_2/r_1) f_1$ $f_1 = 1+0.0097\ L^3/(r_2-r_1)^3$	$K_2(\omega) = 4\pi G'' NL/\ell n(r_2/r_1)$

CONCLUSIONS AND RECOMMENDATIONS

On the basis of the results presented in this report, the following conclusions are drawn.

1. Storage and loss modulus values, obtained as a function of frequency from shear specimen tests, are an effective representation of the dynamic properties of a material.

2. Empirical, frequency dependent coefficients provide a self-consistent representation of the variation of stiffness with shape factor for cylindrical compression elements.

3. For new conditions, the frequency dependent empirical coefficients provide similar predictive ability to the use of a constant, static, coefficient.

4. Either method of prediction for the compression elements incurs errors of 10 to 30 percent (high) relative to test data generated under the present program.

5. Predictive ability, based on simple static analyses, for radially loaded ring cartridges provides upper and lower limits for stiffness and damping within which the great majority of measured data lies.

6. The effect of high dissipation is to reduce stiffness.

7. According to the frequency and geometry damping can be reduced or increased by high dissipation.

8. Self-heating and strain-softening effects are the combined causes of stiffness and damping changes under high dissipation.

9. For all results presented, stiffness and damping depend more consistently on strain than on dissipation rate.

10. Increasing strain up to 0.02 (double amplitude) generally increases the loss coefficient for elements of polybutadiene.

For future investigations, the following recommendations are made.

1. The understanding of the dynamic behavior of elastomer elements will be improved by obtaining further data at very low strain levels, and by relating it to the present data at high strains.

2. Simple methods for including strain dependence of dynamic behavior in elastomer design practice should be developed.

3. The thermal properties of the elastomer material under investigation should be determined.

4. Material and geometrical property tests for a number of different elastomer materials should be performed to determine the extent to which the presently reported results can be generalized.

5. Predictive ability for radially loaded cartridges must be further evaluated in a rotating load environment.

6. Because they are compact, readily available, elastomer elements, the dynamic properties of O-rings should be investigated by analysis and by test, with an effort being made to relate the dynamic properties to the basic material properties of storage and loss moduli.

7. Application studies, analytical then experimental, should be performed to determine the benefits and limitations of elastomer elements as vibration control elements.

8. Successful short-term application tests should be followed by tests for life and survivability to determine the extent to which these problems will limit application.

9. Application studies should be interpreted to reveal what level of predictive accuracy is required for elastomer elements.

10. More sophisticated prediction methods should be developed as indicated by the application studies.

REVIEW OF MATERIAL PROPERTIES AND THE EFFECTS OF GEOMETRY, FREQUENCY, AMPLITUDE AND TEMPERATURE

In this section the relationships between force, displacement, stress and strain in an elastomer specimen are reviewed, with particular emphasis on frequency domain behavior and the influence of geometry, temperature and amplitude.

Relaxation and Hysteresis

Elastomer deformation properties are dominated by the process of relaxation. By this process, the deflection for a given load (strain for a given stress) increases as a function of time - tending towards an asymptotic limit after a period of sufficient length. For very short periods of time, the displacement under a particular load will be significantly lower than the sympototic limit.

If a load cycle is applied repeatedly to an elastomer element, the process of relaxation causes hysteresis - that is, a load deformation curve which depends on the rate of change of load as well as on the load's magnitude - see Figure 2, in which a representative elliptical hysteresis loop is presented. Implicit in such a load deflection curve or hysteresis loop is a loss of energy per cycle equal to the area of the hysteresis loop. Expressed in vibration terminology, elements with such a load-deflection curve provide dissipation, or damping. As shown by Lazan (ref. 3), for an elliptical hysteresis loop, the material behavior is linear, and the damping may be expressed as

$$K_2(\omega) = \frac{D_s}{\pi Y_1^2} \qquad (1)$$

where D_s is the area of the hysteresis loop in energy units and Y_1 is the single amplitude. It is also possible to define stiffness in terms of this loop as the ratio between force at maximum delfection and the value Y_1 of maximum deflection.

$$K_1(\omega) = F_1/Y_1 \qquad (2)$$

where F_1 and Y_1 are defined in Figure 2. In the following paragraphs the relationships between instantaneous force and displacement are developed.

It is noted, at this point, that the linearity of elastomer behavior has been investigated by Warnaka (ref. 4) for materials including neoprene, nitride rubber and BTR elastomer for strains up to 0.1. Using electronics to sense deviations from an elliptical hysteresis loop, Warnaka concluded that linear dynamic

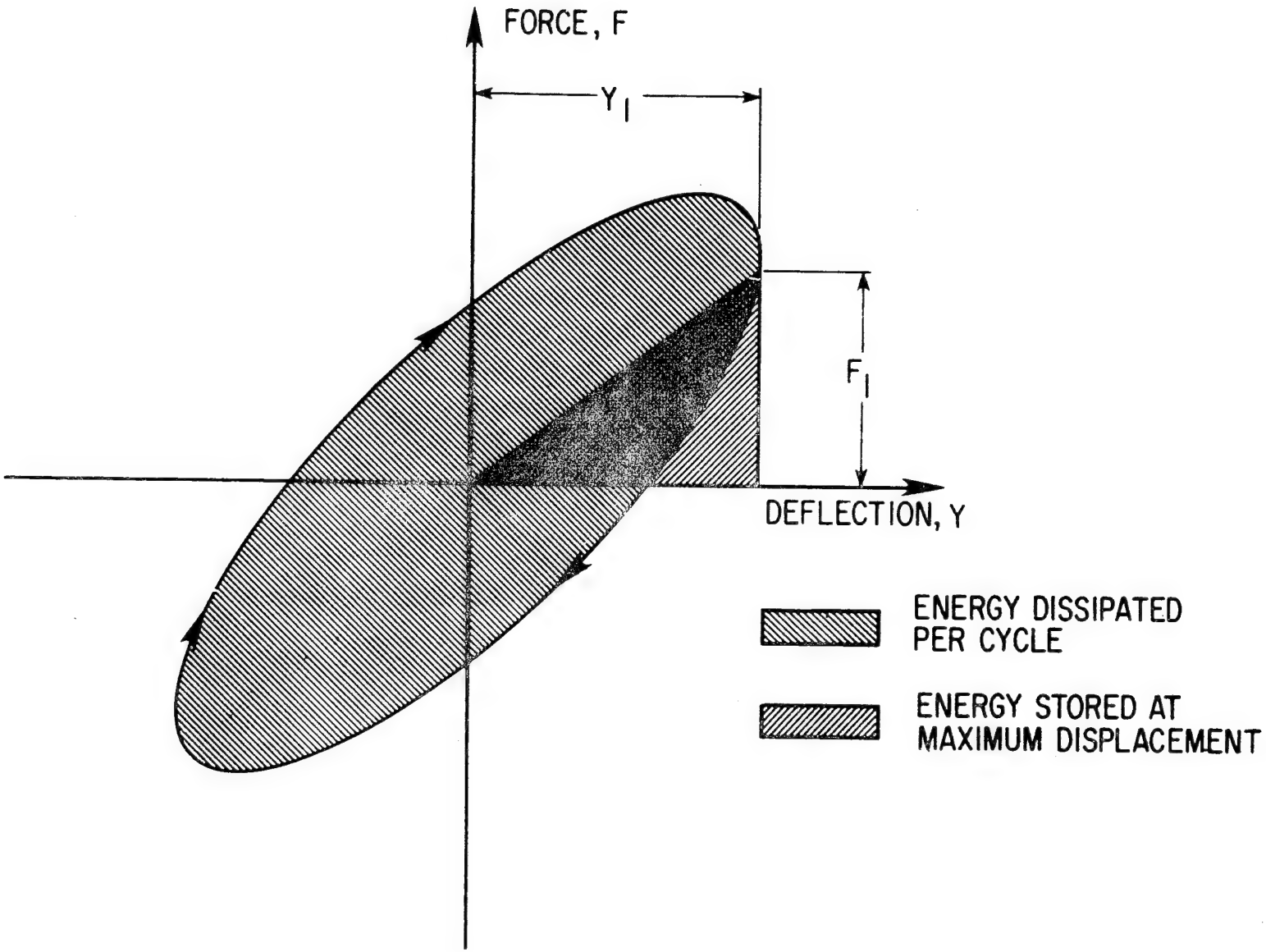

Fig. 2 Load-Deflection Curve For an Elastomer Showing Hysteresis as a Result of The Relaxation Process

behavior within a small discrepancy was exhibited by elastomer elements for even the highest strain at frequencies in the 100-1000 Hz range.

Relationships Between Force And Displacement in The Frequency Domain

A linear elastomer element undergoing a repeated deflection cycle defined by

$$Y = Y^* e^{i\omega t} \tag{3}$$

gives rise to a cyclic force variation described by

$$F = F^* e^{i\omega t} \tag{4}$$

where: ω is the frequency (rad/sec)
Y is the instantaneous displacement (m)
F is the instantaneous force (N)
t is time
Y^*, F^* are complex numbers defining the amplitude and phase of the displacement and force variations, (and it is understood that only the real parts of expressions (3) and (4) are used to establish values for Y and F).

The force and displacement may be related by

$$F = K^* Y \tag{5}$$

where K^* is a complex number

$$K^* = K_1 + iK_2 \tag{6}$$

and is, generally, a function of frequency. The quantities K_1 and K_2 will be referred to as the stiffness and dmaping of the elastomer element. The K_1 and K_2, which depends on frequency, temperature amd amplitude characterize the dynamic behavior of the element. The damping ability of an elastomer element is sometimes expressed in terms of a loss coefficient (nondimensional) which relates damping to stiffness, or the energy dissipated percycle (D_s) to the energy stored at maximum displacement (U_s)

$$\eta = \frac{K_2(\omega)}{K_1(\omega)} = \frac{D_s}{2\pi U_s} \tag{7}$$

Relationships Between Stress And Strain

Considering any elastomer element, its geometry can, normally, be characterized by a certain area of the element (A) which is stressed and a certain dimension of the element, h, which is strained. Figure 3 shows two elastomer element geometries which have been

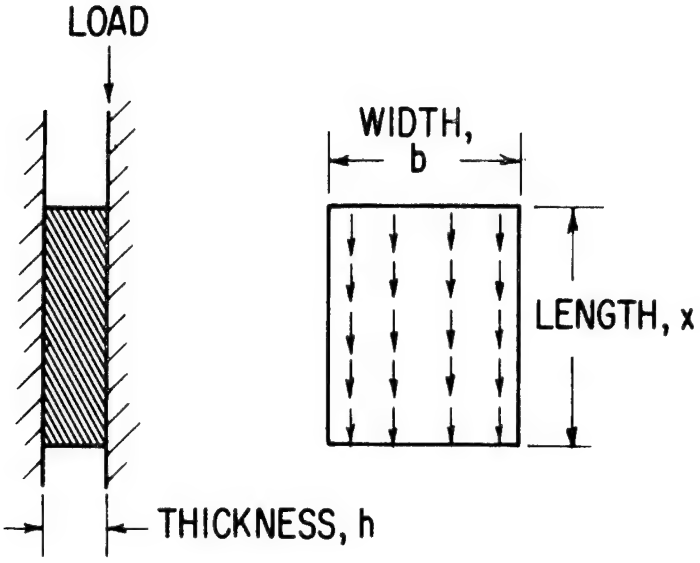

A. SHEAR ELEMENT

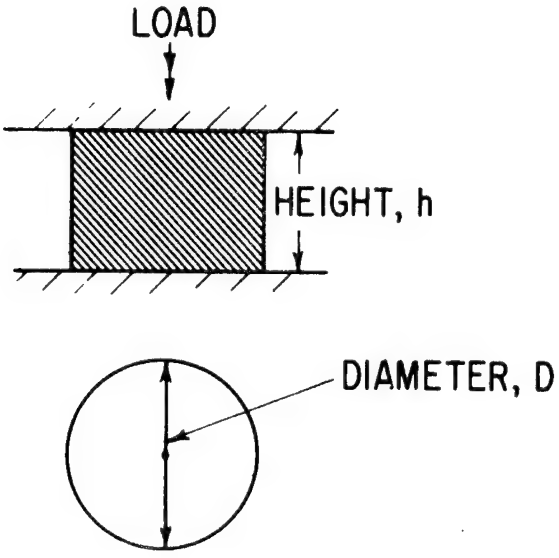

B. COMPRESSION ELEMENT

Fig. 3 Test Elements For Shear and Compression Loading

tested for dynamic stiffness and damping, and which illustrate the effects of geometry. For the shear element (Fig. 3A), the stressed area, A, is its width times its length (b·x) and the strained dimension is its thickness, h. For the compression element (Fig. 3B), the stressed area is the top area of the cylinder ($\pi D^2/4$) and its strained dimension is the height, h.

For the shear element stiffness and damping can be related to effective moduli as follows.

$$\text{Stiffness:} \quad K_1 = G'_{eff} \frac{A}{h} \tag{8}$$

$$\text{Damping:} \quad K_2 = G''_{eff} \frac{A}{h} \tag{9}$$

where G'_{eff}, G''_{eff} are shear moduli, commonly referred to as the effective storage and loss moduli, respectively.

For the compression element stiffness and damping can be related to the effective moduli as follows.

$$\text{Stiffness:} \quad K_1 = 3\, G'_{eff} \frac{A}{h} \tag{10}$$

$$\text{Damping:} \quad K_2 = 3\, G''_{eff} \frac{A}{h} \tag{11}$$

where the factor of 3 arises from the classical elasticity relationship $E = 2(1 + \nu)G$ and the fact that elastomer Poisson's ratios are typically in the range 0.4945 to 0.4999 (Holownia, ref. 5). Any errors in applying this classical elasticity relationship to dynamic behavior of a viscoelastic material will be implicit in the statement that G'_{eff}, G''_{eff} are effective moduli. G'_{eff}, G''_{eff} are, generally functions of the material, the frequency, the amplitude of loading, the temperature, the initial strain and the geometry. They are, therefore, component rather than material properties. Further discussion will explore the relationships between effective and "true" moduli.

The Effects of Geometry

For static loading the effects of bending can be shown (ref. 6) to cause the following relationship between effective and true modulus for the shear element of Figure 3A.

$$(G'_{eff})_o = G'_o \left[\frac{1}{1 + h^2/3X^2}\right] \tag{12}$$

where X is the dimension of the sheared area in the direction parallel to the loading, h is the thickness, and the subscript, o, implies static loading. In Figure 4, the stiffness correction factor

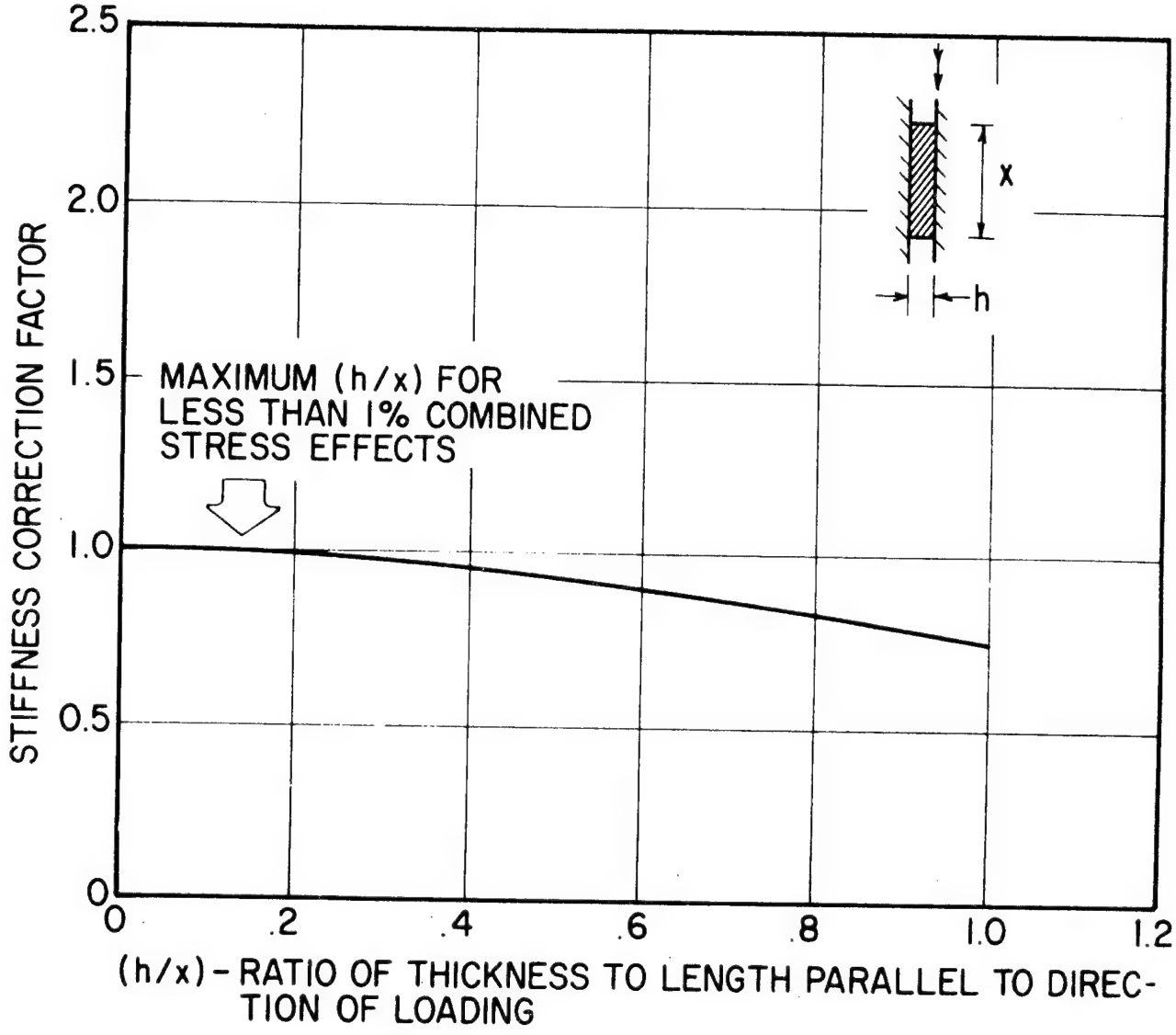

Fig. 4 Static Stiffness Correction Factor. Rectangular Shear Specimen

(G'_{eff}/G'_o) is plotted as a function of X/h for a rectangular shear element. Under static compression loading, the interaction of axial, radial and circumferential stresses was shown by Gent and Lindley (ref. 7), Hattori and Takei (ref. 8), and Payne (ref. 9) to give the following relationship between apparent, or effective static modulus and actual, or true, static modulus:

$$(G'_{eff})_o = G'_o (1 + \beta S^2) \tag{13}$$

where S is a shape factor defined as the ratio of the loaded area to the unloaded area (D/4h for a cylinder) and β is a coefficient, shown by Gent and Lindley (ref. 7) to be equal to 2.

A more complete expression based on the work of Gent and Lindley (ref. 7), which attempts to account for bulk compressibility effects is:

$$\frac{G'_o}{(G'_{eff})_o} = (1 + \beta S^2)^{-1} + \frac{3\,G'_o}{B} \tag{14}$$

where B is the bulk modulus for the material. However, this expression has been tested by Moghe and Neff (ref. 10) using classical elasticity solutions and shown also to be incomplete for large values of S in that an additional dependence on Poisson's ratio occurs. For values of S less than 10, however, neither the second term in Eq. (14) nor the inadequacies due to Poisson's ratio effects should be significant.

In Figure 5, the static stiffness correction factor $((G'_{eff})_o/G'_o)$, as given by Eq. (13) with $\beta = 2$, is plotted against the ratio of diameter to height, for a compression loaded cylinder

The existence of such a square law dependence on shape factor has been verified experimentally by Payne (ref. 9). He showed that, for natural rubbers, the shape coefficient, β, was close to 2 but, for harder materials the coefficient β could fall by as much as 50 percent.

Under low frequency dynamic loading (10 Hz) Payne also demonstrated that the effective storage modulus varied with shape factor according to a square law.

The analytical or experimental quantification of the effects of geometry (shape) at higher frequencies appears to be limited. Nashif, Cannon and Jones (ref. 11) have demonstrated that shape has a pronounced influence on the effective storage modulus of cylindrical specimens, in the frequency range of 250 to 500 Hz, but have not generalized their results.

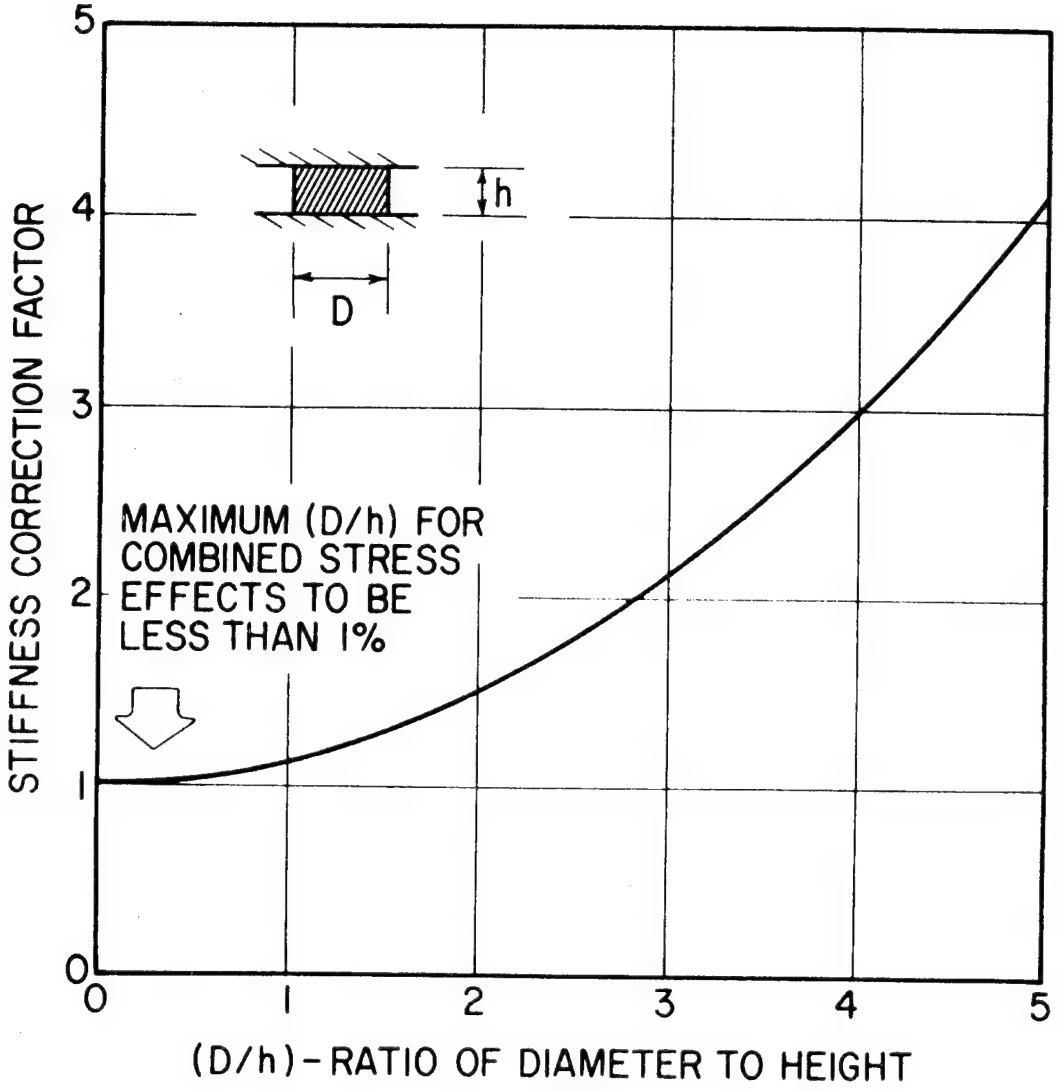

Fig. 5 Static Stiffness Correction Factor. Cylindrical Compression Element

The Effects of Frequency

As might be expected from a material whose behavior is governed by time dependent relaxation processes, the slope and area of the hysteresis loop, together with the stiffness, damping, and loss coefficient are functions of the frequency with which the load cycle is executed. It is generally observed that the dynamic stiffness is higher than the static value, and that stiffness tends to increase with increasing frequency. Shown on a scale which may cover many decades of frequency, the general form of elastomer behavior variation has three regions (ref. 12):

- Rubbery
- Transition (Leathery)
- Glassy

These are illustrated in Figure 6.

In the rubbery region, the behavior is, as implied "rubbery." Elastomer elements are resilient and the damping is usually of the order of 10 to 30 percent of the stiffness. The hysteresis loop is a rather narrow ellipse. As the frequency increases, the transition region is encountered. Both stiffness and damping increase more rapidly in this region but the damping moves ahead of the stiffness and the hysteresis ellipse becomes broader.

For a limited frequency range, damping (K_2) becomes higher than stiffness (K_1) and the loss coefficient becomes greater than 1. For further increases in frequency the stiffness increases more than the damping and in the glassy region both quantities level off at values giving a loss factor which again tends to be 0.3 or less.

The rubbery and transition regions are those normally encountered in elastomers and offer the best opportunity for use in vibration control.

Representation of Frequency Dependence

Observed variation of stiffness and damping with frequency gives rise to discrete data points. For mathematical purposes it is convenient to seek, for an element, a continuous relationship between force and displacement (or stress and strain) which closely matches observed behavior. There are several possible approaches to this problem, with different levels of sophistication and convenience, as discussed below.

1. Generalized Viscoelastic Models. An approach to representing the variation of stiffness and damping of an elastomer element with frequency is to replace the elastomer with a mechanical analog, consisting of a series of springs and viscous dashpots. The simplest

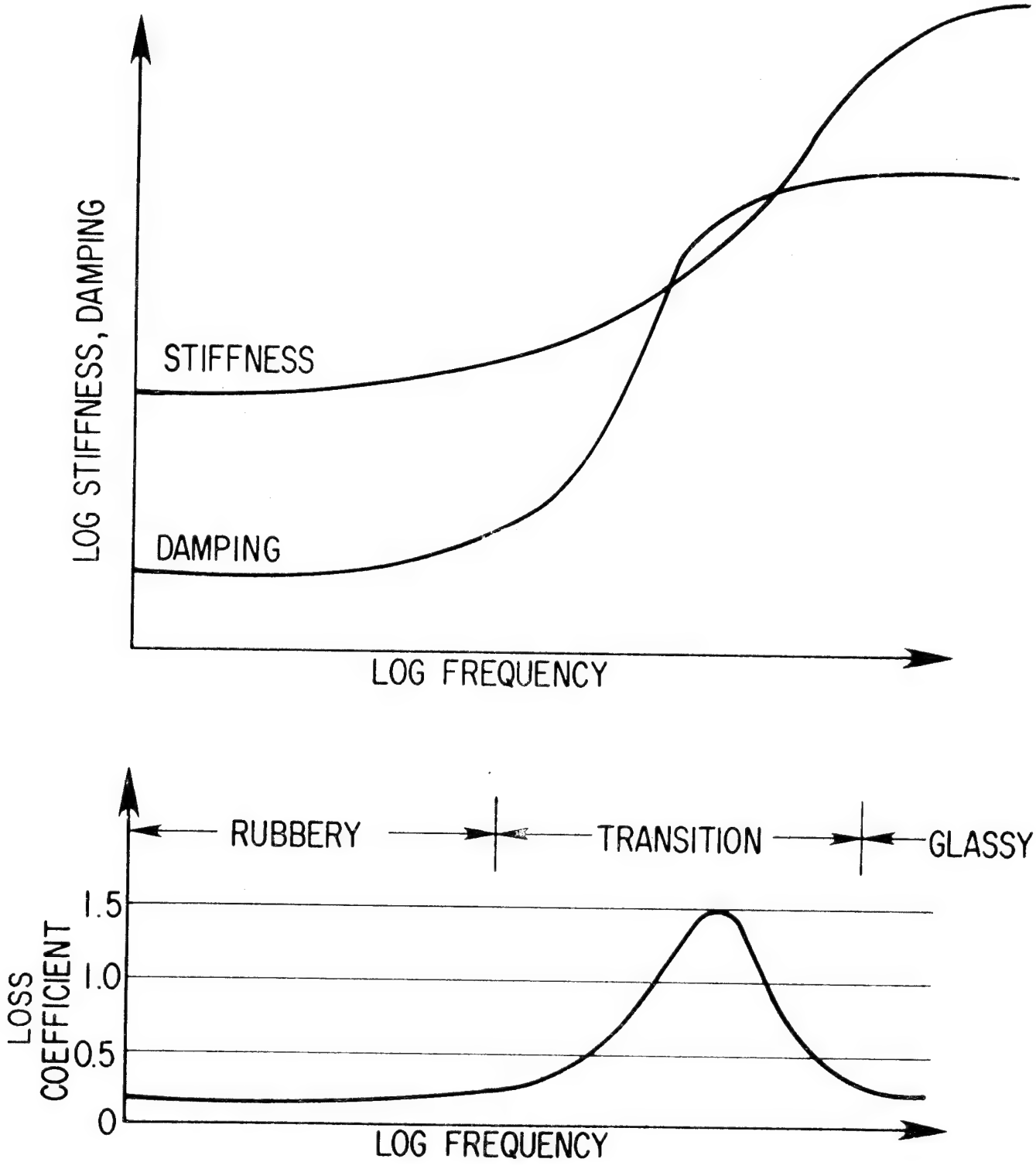

Fig. 6 **Regimes of Elastomer Dynamic Behavior**

of these models are the Maxwell and Voigt elements (Fig. 7). Using these basic elements as building blocks, more complex systems of springs and dashpots may be developed, such as those shown in Figure 8.

The application of a triparameter model, as shown in Figure 9, to elastomer specimen test data generated by the BERM method was demonstrated by Chiang, Tessarzik and Badgley (ref. 1). The methodology to determine, for a selected general viscoelastic model, the element values to best fit a particular variation of stiffness and damping with frequency was developed and demonstrated by Gupta, Tessarzik and Cziglenyi (ref. 2).

2. Generalized Force - Displacement Relationships. An alternative approach for representing the variation with frequency is to assume a general linear differential relationship between force and displacement:

$$a_o F + a_1 \frac{dF}{dt} + a_2 \frac{d^2F}{dt^2} + a_3 \frac{d^3F}{dt^3} + \ldots = c_o Y + c_1 \frac{dY}{dt} + c_2 \frac{d^2Y}{dt^2} + \ldots \qquad (15)$$

For sinusoidal loading and displacement:

$$F = F^* e^{i\omega t} \qquad (16)$$

$$Y = Y^* e^{i\omega t} \qquad (17)$$

So that Eq. (15) becomes:

$$(a_o + i\omega a_1 - \omega^2 a_2 - i\omega^3 a_3 + \ldots)F^* = (c_o + i\omega c_1 - \omega^2 c_2 - \ldots)Y^* \qquad (18)$$

and

$$\frac{F}{Y} = \frac{c_o + i\omega c_1 - \omega^2 c_2 - i\omega^3 c_3 + \ldots}{a_o + i\omega a_1 - \omega^2 a_2 - i\omega^3 a_3 + \ldots} \qquad (19)$$

A close connection between this generalized force displacement relationship and the generalized viscoelastic models exists since, for

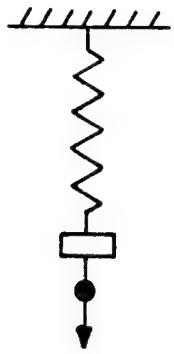

a. MAXWELL ELEMENT

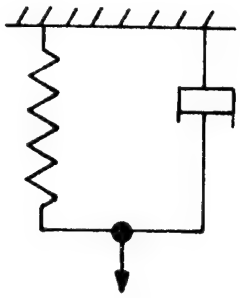

b. VOIGT ELEMENT

Fig. 7 Maxwell and Voigt Elements

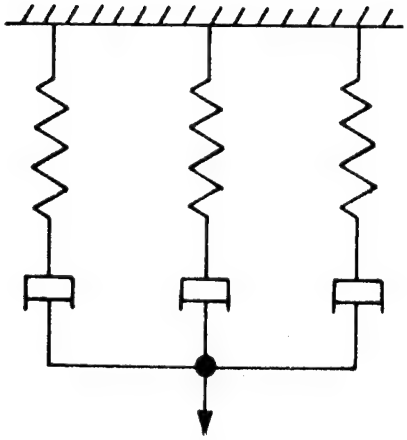

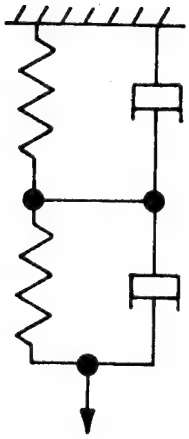

Fig. 8 Combination Systems

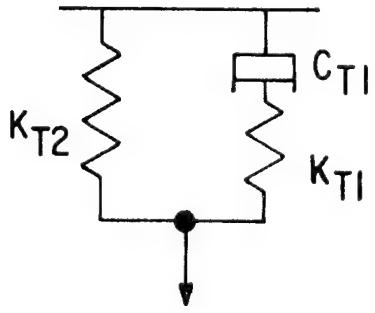

Fig. 9 Triparameter Model

a given order of expansion on left- and right-hand sides of Eq. (15), there exists a corresponding combination of springs and dashpots (ref. 12), which will give the same force-displacement relationship.

For example the differential equation for the triparameter model (Fig. 9) is

$$F + \frac{C_{T1}}{K_{T1}} \frac{dF}{dt} = K_{T2}Y + \frac{C_{T1}}{K_{T1}} (K_{T2} + K_{T1}) \frac{dY}{dt} \qquad (20)$$

so that the nonzero coefficients of Eq. (15) for the triparameter model are

$$\begin{aligned} a_o &= 1 \\ a_1 &= C_{T1}/K_{T1} \\ c_o &= K_{T2} \\ c_1 &= C_{T1} (K_{T2} + K_{T1})/K_{T_1} \end{aligned} \qquad (21)$$

3. Direct Fit of Mathematical Expressions. A direct approach to the problem is to impose upon the data some correlation function and to seek those coefficients which give the best match between the function and the data. Polynomial, trigonometrical, or power law ($K_1 = A_1\omega^{B1}$) relationships are some of the options available for this approach. It was found by Gupta, et al (ref. 2), that the use of a power law relationship was quite adequate to represent the behavior of elements of polybutadiene in the frequency range 100 to 1000 Hz. For engineering purposes, a known relationship between stiffness, damping and frequency for elastomer elements of different geometries is all that is required to use these elements in design for control of machinery vibrations. In essence this approach may be considered as the use of a generalized Voigt element in which the storage and dissipative elements are a continuous function of frequency.

Influence of temperature. Elastomer behavior is, in general, strongly influenced by temperature. Thus complete characterization of elastomer elements must provide their dynamic behavior over the frequency and temperature ranges of interest. In considering the effects of temperature the following observations are often made.

1. Temperature tends to be most influential where frequency is also strongly influential.
2. Increasing temperature tends to produce the same results as decreasing frequency and vice versa.

Starting from these observations, an elegant method of reducing the

dynamic behavior of elastomers (and other polymers), covering a range of frequencies and temperatures, to a single curve relating appropriate reduced properties, was developed by Ferry, Fitzgerald, Grandine and Williams (ref. 13). The method is sometimes referred to as the WLF law, due to a paper by Williams, Landell and Ferry (ref. 14), in which the mechanics of its implementation are described and demonstrated. The mathematical statement of this method is as follows

$$(G_r)_{\omega,\theta} = (G_r)_{a_\theta \omega, \theta_c} \tag{22}$$

$$\text{Log}_{10}\, a_\theta = \frac{-8.86\ (\theta - \theta_c)}{101.6 + (\theta - \theta_c)} \tag{23}$$

$$(G_r)_{\omega,\theta} = (G)_{\omega,\theta}\ \frac{\theta_c}{\theta} \tag{24}$$

where θ_c is a characteristic temperature given by

$$\theta_c = \theta_t + (50^o \pm 5^o)\ K \tag{25}$$

and θ_t is the transition temperature between the rubbery and glassy states of the material.

G is the observed modulus at temperature θ and frequency ω.

G_r is the reduced modulus.

a_θ is the coefficient by which test frequency is multiplied to obtain the corresponding reduced frequency at temperature θ_c.

By these relationships, knowledge of a modulus as a function of frequency at several temperatures may be interpreted as knowledge of reduced modulus over a wide frequency range at the characteristic temperature. This knowledge may be further interpreted to give the variation of modulus over a wide frequency range at any temperature between θ_c and the maximum temperature tested.

The method has been demonstrated to be applicable to material properties of storage and loss moduli or to element properties of stiffness and damping. The additional information needed to implement and use the methods, beyond the elastomer dynamic data is the value of θ_c.

The transition temperature, θ_t, may be measured independently or θ_c may be inferred from a sufficiently large volume of dynamic data.

Influence of large amplitude displacements. Observed properties of an elastomer element tend to be a function of amplitude of loading, as well as frequency and temperature. This is shown, for example, by references 15, 16 and 17. No specific and complete explanation of this mechanism has been produced. It may be hypothesized, however, that a major contribution is the increase in temperature of the element when a significant dissipation rate is imposed. As will be discussed, further, in relation to the test data a second, nonthermal, mechanism has also been shown to cause degradation in stiffness at high strains.

INTERPRETATION OF BASE EXCITATION RESONANT MASS TEST DATA

The preceding review of elastomer material properties was presented as a framework against which the methods of dynamic testing described in this report and the methods of data reduction and interpretation may be viewed.

The BERM method has been applied in the generation of dynamic properties of three categories of elastomer element: shear elements; compression elements; and ring cartridge elements. The shear and compression elements have been illustrated in Figure 3. The ring cartridge element is shown in Figure 10.

Table I summarizes the range of conditions covered by this data and the periods when it was generated. The 1973, Phase II, data was previously reported by Gupta, Tessarzik and Cziglenyi (ref. 2) in terms of stiffness and damping as a function of frequency. To obtain a continuous mathematical representation of the dependence of stiffness and damping on frequency, a power law relationship was fitted to the test data and the results of this data analysis are presented in Table II.

Prior to the generation of the Phase III test data presented in this report, an effort was undertaken to develop methods of exploiting the information generated by the BERM test method, to yield material properties and geometry factors which can be applied in engineering design. The data of Table II was used to implement and test these methods.

Generation of Material Properties

In the previous section, it was shown that stiffness and damping values can be interpreted in terms of relationships between stress and strain. It was also shown that combined stress effects can be instrumental in making the effective moduli for the shear and compression element different from uniaxial moduli. Table III summarizes the static stiffness correction factor $(G'_{eff})_o/G'_o$ which would be expected on the basis of Eqs. (12) and (13) for the shear and compression elements tested under Phase II and III.

In all but two of the elements tested the predicted effects of combined stress are greater than ten percent. While this data is for static behavior of the elements, and no rigorous basis exists for applying it to dynamic behavior, it is assumed that the two shear elements for which the static stiffness correction factor is within two percent of unity are also likely to show small combined stress effects under dynamic loading conditions. All the other elements tested are likely to show significant combined stress effects.

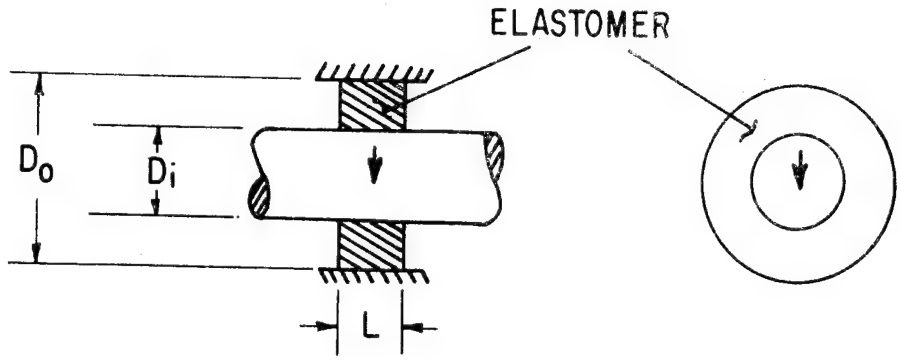

Fig. 10 Ring Cartridge Element

TABLE I

SUMMARY OF DYNAMIC TEST CONDITIONS

Material Tested - Polybutadiene

Phase	Date	Geometry	Dimensions (cm)							N	Temperature	Nominal Dissipation W/cm^3
			h	x	b	d	D_i	D_o	L			
II	1973	Shear	0.3175	0.508	4.877					20	32 C	0.022
			0.3175	1.27	4.877					8	32 C	0.022
			0.3175	2.54	4.877					4	32 C	0.022
		Compression	0.3175			1.27				3	32 C	0.022
			0.635			1.27				10	32 C	0.022
			1.27			1.27				30	32 C	0.022
III	1975	Shear	0.3175	1.27	4.877					8	32 C	0.062
			0.3175	1.27	4.877					8	50 C	0.062
			0.3175	1.27	4.877					8	66 C	0.062
			0.3175	1.27	4.877					3	93 C	0.062
			0.3175	2.54	4.877					4	32 C	0.035
			0.3175	2.54	4.877					4	32 C	0.176
			0.3175	2.54	4.877					4	32 C	0.352
			0.3175	2.54	4.877					4	32 C	0.704
			0.3175	2.54	4.877					4	32 C	1.76
										4	32 C	4.40
	1974	Compression	0.635			1.27				10	5 C	0.062
			0.635			1.27				10	66 C	0.062
			0.635			1.27				10	93 C	0.062
			0.635			1.27				10	32 C	0.44
			0.635			1.27				10	32 C	1.1
			0.635			1.27				10	32 C	2.2
	1975	Cartridge					1.905	2.858	0.476	4	32 C	0.022
							1.905	2.858	0.476	4	43 C	0.022
							1.905	2.858	0.476	4	66 C	0.022
							1.905	2.858	0.476	4	80 C	0.022
							1.905	2.858	0.476	4	32 C	0.11
							1.905	2.858	0.476	4	32 C	0.22
							1.905	2.858	0.476	4	32 C	0.88
							1.905	2.858	0.953	4	32 C	0.044
							1.905	2.858	0.953	4	43 C	0.044
							1.905	2.858	0.953	4	66 C	0.044
							1.905	2.858	0.953	4	80 C	0.044
							1.905	2.858	0.953	4	32 C	0.1[illegible]
							1.905	2.858	0.953	4	32 C	0.[illegible]
							1.905	2.858	0.953	4	32 C	1.0
							1.905	2.858	0.953	4	32 C	1.8

TABLE II

SUMMARY OF ELASTOMER TEST DATA FROM PHASE II TESTS

MATERIAL = Polybutadiene
TEMPERATURE = 32 deg-C

COMPLEX STIFFNESS K = K1 + iK2 lb/in
CORRELATION FORM Y = A*OMEGA**B (ω in rad/sec)

SPECIMEN DETAILS	K1 MEAN lb/in	K1 A	K1 B	K2 MEAN lb/in	K2 A	K2 B	AMPLITUDE MEAN in	AMPLITUDE A	AMPLITUDE B
0.50IN-30/C/2.5	7.541E+04	2.224E+04	1.589E-01	8.347E+03	1.873E+04	-1.051E-01	1.055E-03	3.854E-01	-7.677E-
0.50IN-30/C/5.0	7.809E+04	2.545E+04	1.458E-01	8.657E+03	1.507E+04	-7.212E-02	1.042E-03	3.401E-01	-7.529E-
0.25IN-10/C/2.5	8.042E+04	2.871E+04	1.325E-01	9.266E+03	2.809E+04	-1.427E-01	3.806E-04	2.040E-01	-8.082E-
0.25IN-10/C/5.0	8.026E+04	3.577E+04	1.044E-01	9.447E+03	2.753E+04	-1.382E-01	3.924E-04	1.764E-01	-7.889E-
0.125IN-3/C/2.5	7.662E+04	7.312E+04	6.368E-03	1.190E+04	1.378E+04	-2.004E-02	2.501E-04	2.407E-02	-6.216E-
0.125IN-3/C/5.0	8.892E+04	7.007E+04	3.227E-02	1.295E+04	1.854E+04	-4.859E-02	2.250E-04	3.547E-02	-6.854E-
0.5IN-8 /S/0.	1.798E+05	5.330E+04	1.548E-01	1.720E+04	3.457E+04	-8.886E-02	3.186E-04	2.478E-01	-8.473E-
0.5IN-8 /S/2.5	1.666E+05	5.003E+04	1.530E-01	1.737E+04	3.138E+04	-7.521E-02	3.498E-04	4.985E-01	-9.232E-
0.5IN-8 /S/5.0	1.598E+05	5.361E+04	1.391E-01	1.653E+04	2.678E+04	-6.142E-02	3.462E-04	2.162E-01	-8.198E-
1.0IN-4 /S/0.	1.453E+05	2.569E+04	2.199E-01	1.624E+04	2.800E+04	-6.912E-02	3.497E-04	2.844E-01	-8.503E-
1.0IN-4 /S/2.5	1.351E+05	2.550E+04	2.135E-01	1.631E+04	2.388E+04	-4.882E-02	3.799E-04	1.502E-01	-8.309E-
1.0 IN-4 /S/5.0	1.307E+05	2.263E+04	2.238E-01	1.563E+04	1.923E+04	-2.647E-02	3.820E-04	2.035E-01	-8.339E-
0.2IN-20 /S/0.	1.625E+05	3.708E+04	1.881E-01	1.689E+04	5.700E+04	-1.548E-01	3.395E-04	2.168E-01	-8.220E-
0.2IN-20 /S/2.5	1.549E+05	3.336E+04	1.936E-01	1.681E+04	5.867E+04	-1.576E-01	3.398E-04	2.630E-01	-8.386E-
0.2IN-20 /S/5.0	1.452E+05	3.689E+04	1.743E-01	1.600E+04	4.833E+04	-1.406E-01	3.683E-04	2.240E-01	-8.156E-

CUMPLEX STIFFNESS K = K1 + iK2 New/m
CORRELATION FORM Y = A*OMEGA**B

SPECIMEN DETAILS	K1 MEAN New/m	K1 A	K1 B	K2 MEAN New/m	K2 A	K2 B	AMPLITUDE MEAN m	AMPLITUDE A	AMPLITUDE B
0.50IN-30/C/2.5	1.321E+07	3.894E+06	1.589E-01	1.462E+06	3.280E+06	-1.051E-01	2.679E-05	9.790E-03	-7.677E-0
0.50IN-30/C/5.0	1.368E+07	4.457E+06	1.458E-01	1.516E+06	2.640E+06	-7.212E-02	2.646E-05	8.639E-03	-7.529E-0
0.25IN-10/C/2.5	1.408E+07	5.027E+06	1.325E-01	1.623E+06	4.920E+06	-1.427E-01	9.668E-06	5.180E-03	-8.082E-0
0.25IN-10/C/5.0	1.406E+07	6.264E+06	1.044E-01	1.654E+06	4.822E+06	-1.382E-01	9.968E-06	4.480E-03	-7.889E-0
0.125IN-3/C/2.5	1.342E+07	1.281E+07	6.370E-03	2.084E+06	2.414E+06	-2.004E-02	6.354E-06	6.114E-04	-6.216E-0
0.125IN-3/C/5.0	1.557E+07	1.227E+07	3.227E-02	2.268E+06	3.247E+06	-4.859E-02	5.715E-06	9.010E-04	-6.854E-0
0.5IN-8 /S/0.	3.149E+07	9.335E+06	1.548E-01	3.012E+06	6.054E+06	-8.886E-02	8.092E-06	6.294E-03	-8.473E-0
0.5IN-8 /S/2.5	2.918E+07	8.762E+06	1.530E-01	3.042E+06	5.497E+06	-7.521E-02	8.885E-06	1.266E-02	-9.232E-0
0.5IN-8 /S/5.0	2.799E+07	9.389E+06	1.391E-01	2.895E+06	4.689E+06	-6.141E-02	8.794E-06	5.491E-03	-8.198E-0
1.0IN-4 /S/0.	2.545E+07	4.499E+06	2.199E-01	2.844E+06	4.903E+06	-6.912E-02	8.881E-06	7.223E-03	-8.503E-0
1.0IN-4 /S/2.5	2.366E+07	4.465E+06	2.135E-01	2.857E+06	4.183E+06	-4.883E-02	9.648E-06	6.356E-03	-8.309E-0
1.0 IN-4 /S/5.0	2.289E+07	3.963E+06	2.238E-01	2.737E+06	3.369E+06	-2.647E-02	9.703E-06	6.692E-03	-8.339E-0
0.2IN-20 /S/0.	2.846E+07	6.494E+06	1.881E-01	2.959E+06	9.984E+06	-1.548E-01	8.624E-06	5.506E-03	-8.220E-0
0.2IN-20 /S/2.5	2.713E+07	5.843E+06	1.936E-01	2.944E+06	1.028E+07	-1.576E-01	8.631E-06	6.680E-03	-8.386E-0
0.2IN-20 /S/5.0	2.542E+07	6.461E+06	1.743E-01	2.803E+06	8.464E+06	-1.406E-01	9.355E-06	5.691E-03	-8.156E-0

N.B. Frequency OMEGA in the correlation function is in rad/sec.

A sample consists of several specimens of elastomer arranged in a prescribed configuration.

"Specimen details" code given in the table is derived as follows:

(1) Compression Sample: (Specimen thickness) IN - No. of Specimens/C/ (% Preload).
The diameter of all compression specimens is 1/2

(2) Shear Sample: (Specimen length) IN - No. of Specimens/S/ (% Preload)
The specimen thickness and width normal to direction of deformation for all shear specimens are respectively 1/8 in and 1.92 in.

TABLE III. ELASTOMER TEST ELEMENTS - EFFECTS OF COMBINED STRESSES

Element Type	Length (cm)	No.	Diameter (d,cm)	Strained Dimension (h,cm)	Width (b,cm)	$\frac{(G_{eff})_o}{G_o}$
Shear	2.54	4		0.3175	4.877	0.995
Shear	1.27	8		0.3175	4.877	0.980
Shear	0.508	20		0.3175	4.877	0.884
Compression		30	1.27	1.27		1.125
Compression		10	1.27	0.635		1.5
Compression		3	1.27	0.3175		3.0

This assumption leads to the following approach to interpretation of the test data.

1. From dynamic stiffness and damping data for the shear elements of 1.27 cm and 2.54 cm length (parallel to loading direction) the material properties of storage and loss modulus should be inferred - neglecting whatever small effects of geometry occur.

   From these elements, values of storage and loss modulus at a particular frequency are calculated as follows:

$$G'(\omega) = \frac{K_1(\omega)\, h}{N\, A} \qquad (26)$$

$$G''(\omega) = \frac{K_2(\omega)\, h}{N\, A} \qquad (27)$$

   With values of stiffness and damping available for more than one specimen at a particular frequency, the values of $G'(\omega)$, $G''(\omega)$ are calculated which minimize the rms deviation between stiffness and damping predicted using the $G'(\omega)$, $G''(\omega)$ and the measured stiffness value for the element.

2. From test data for the compression elements of different shape should be extracted empirical coefficients which account for the effects of geometry.

With material property data available from shear specimen tests, values of shape factor coefficient are determined which minimize the deviation between predictions and measurements of compression specimen stiffness and damping. Separate coefficient values, β' and β'', are determined for stiffness and damping so that

$$K_1(\omega) = G'(\omega) \frac{\pi D^2 N}{4h} \left[1 + \beta' S^2\right] \quad (28)$$

$$K_2(\omega) = G''(\omega) \frac{\pi D^2 N}{4h} \left[1 + \beta'' S^2\right] \quad (29)$$

Implementation of Methods of Data Interpretation

Using the Phase II shear element data for three preloads and two length values (six sets in all) rms best fit values of G' and G'' were determined over the frequency range 100 to 1000 Hz and the resultant set of discrete G', G'' frequency points were then refitted to power law expressions. As a result:

$$G'(\omega) = 4.136 \times 10^6 \, \omega^{0.184} \quad (30)$$

$$G''(\omega) = 3.369 \times 10^6 \, \omega^{-0.0793} \quad (31)$$

Using the Phase II compression element data for two preloads and three different heights, independent, best fit values of β', β'' were determined at discrete frequency values between 100 and 1000 Hz and their frequency dependence was then expressed as a power law relationship so that

$$G'_{eff}(\omega) = G'(\omega) \left[1 + 12.33 \, \omega^{-0.2896} \left(\frac{D}{4h}\right)^2\right] \quad (32)$$

$$G''_{eff}(\omega) = G''(\omega) \left[1 + 1.726 \, \omega^{0.02992} \left(\frac{D}{4h}\right)^2\right] \quad (33)$$

Verification of Methods For Determining Material Properties And Geometry Factors

Based upon the preceding results, individual shear elements of polybutadiene would be expected to exhibit the following values of stiffness and damping (neglecting bending effects):

$$K_1(\omega) = 4.136 \times 10^6 \, \omega^{0.184} \frac{b\,X}{h} \qquad (34)$$

$$K_2(\omega) = 3.369 \times 10^6 \, \omega^{-0.0793} \frac{b\,X}{h} \qquad (35)$$

and compression elements of polybutadiene would be expected to exhibit the following values of stiffness and damping:

$$K_1(\omega) = 4.136 \times 10^6 \, \omega^{0.184} \frac{\pi D^2}{4h} \left[1 + 12.33 \, \omega^{-0.2896} \left(\frac{D}{4h}\right)^2\right] \qquad (36)$$

$$K_2(\omega) = 3.369 \times 10^6 \, \omega^{-0.0793} \frac{\pi D^2}{4h} \left[1 + 1.726 \, \omega^{0.02992} \left(\frac{D}{4h}\right)^2\right] \qquad (37)$$

To determine the "goodness of fit" given by the above expressions with the measured data from which they were derived, predicted stiffness and damping of shear and compression specimens are presented in Figures 11 through 22. Three different frequencies, 100, 300 and 1000 Hz have been selected and at each of these, stiffness and damping has been plotted against a geometrical parameter representative of the difference among the specimens of a particular class. For the shear specimens, this parameter is the ratio of sheared length to thickness (X/xh), for which data over a range from 0.2 to 1.0 is available. For the compression specimens, the independent variable is the ratio of diameter to height (D/h), for which data over a range from 1 to 4 is available.

The consistency between the predictions and the test data is generally reasonable, although scatter in the test data leads to individual discrepancies of up to 20 percent of the predicted value. The mean discrepancy is about ten percent of the predicted value.

The results presented in Figures 11 through 22 are taken as providing a satisfactory check of the methods presented for modeling and data interpretation. The same approach to development of material property data from shear specimen tests will be applied to the Phase III data to be presented subsequently. This data covers a much wider temperature range and also reflects improvements in the test method which evolved during the Phase III tests.

Alternative Correlations For Shape

The work of Nashif, Cannon and Jones (ref. 10) provides data on the stiffness of cylinders in compression. Dynamic stiffness values for a range of diameter to height ratios between 0.25 and 4.85 are given at 250 and 500 Hz. The material tested is paracryl (a Buna Nitrile elastomer manufactured by UniRoyal). Just as for the polybutadiene

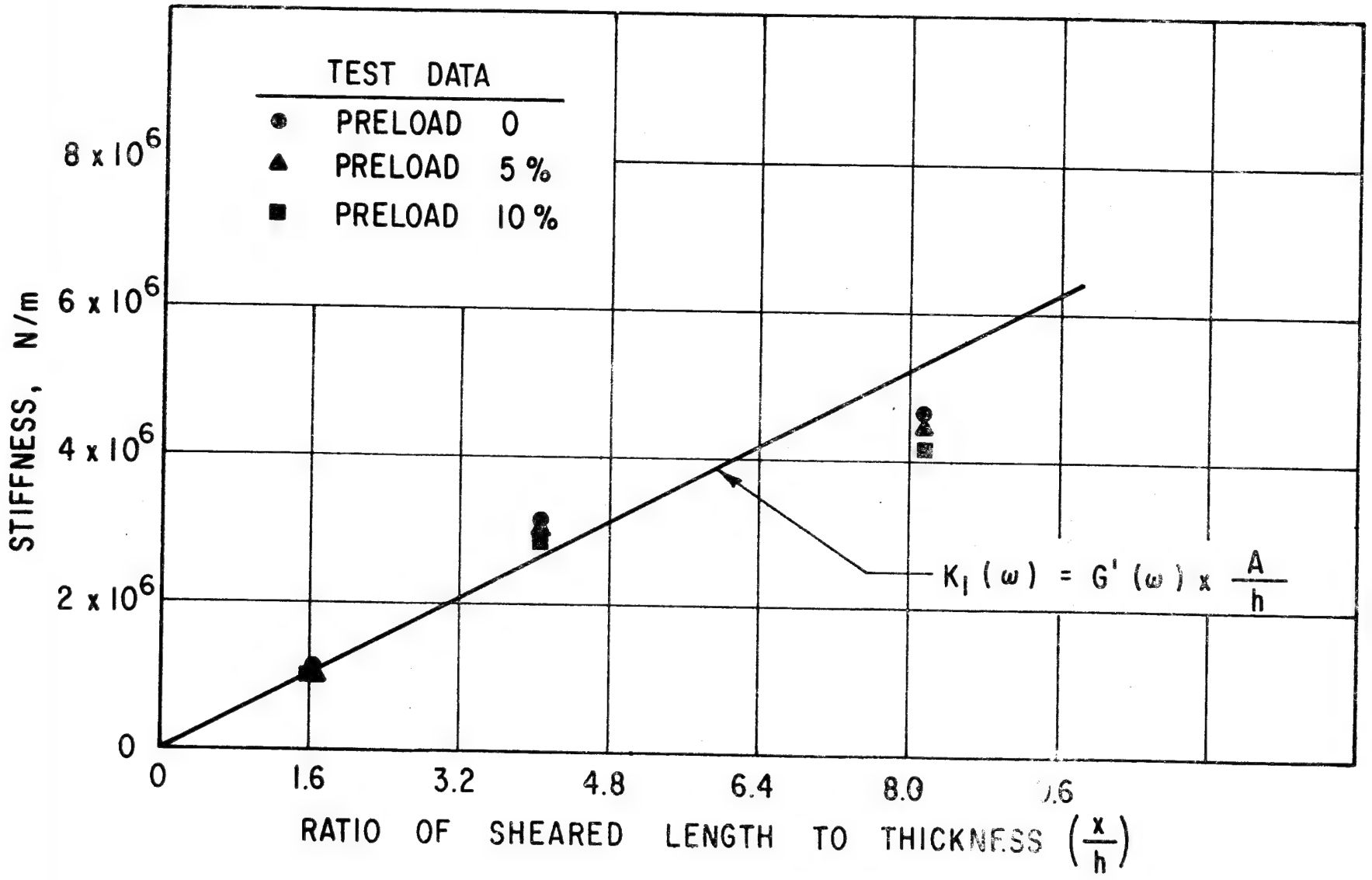

Fig. 11 Phase II Material Property Data. Self-Consistency Test. Sample Shear Element. 100 Hz Stiffness

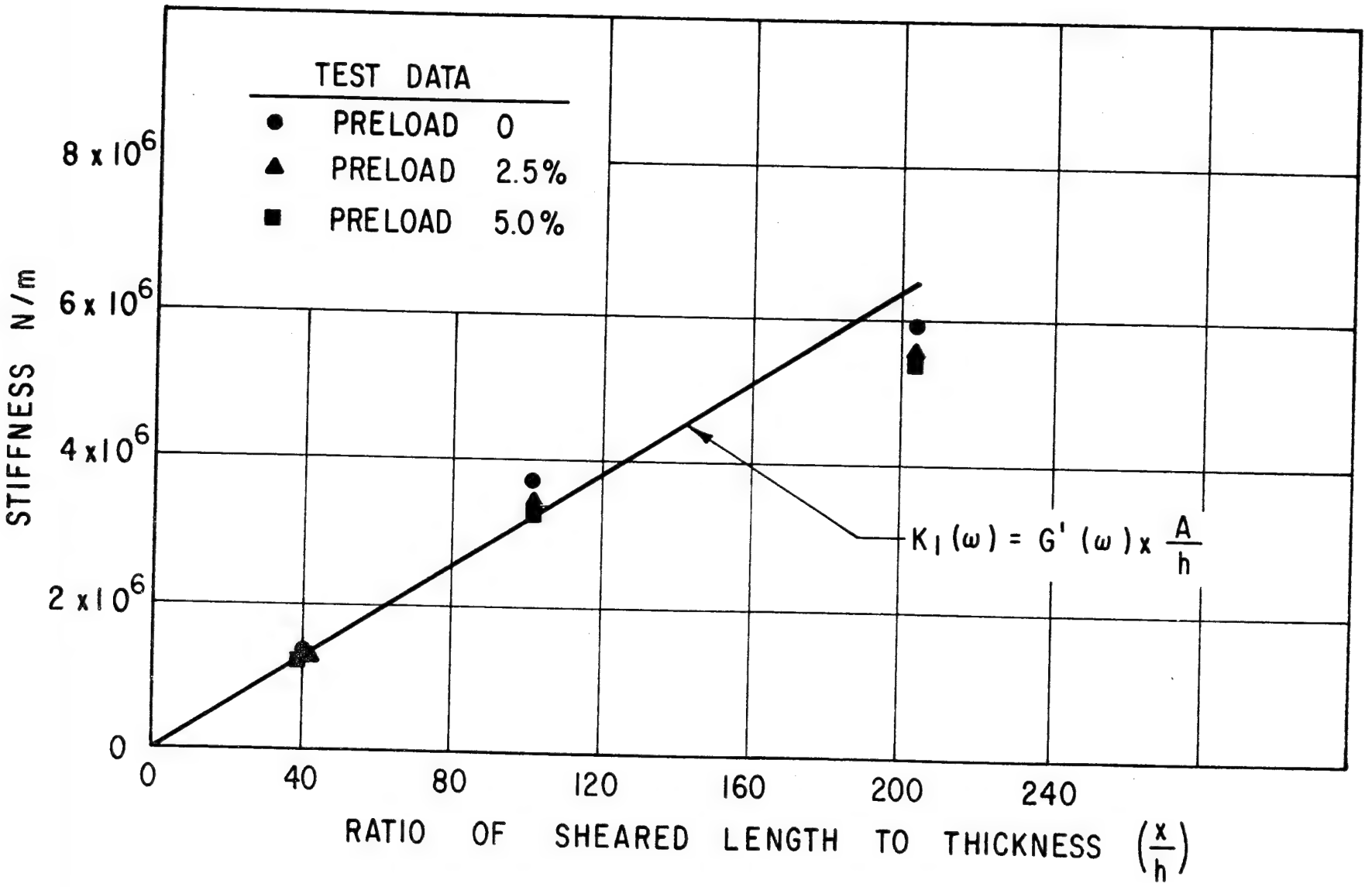

Fig. 12 Phase II Material Property Data. Self-Consistency Test. Sample Shear Element. 300 Hz Stiffness

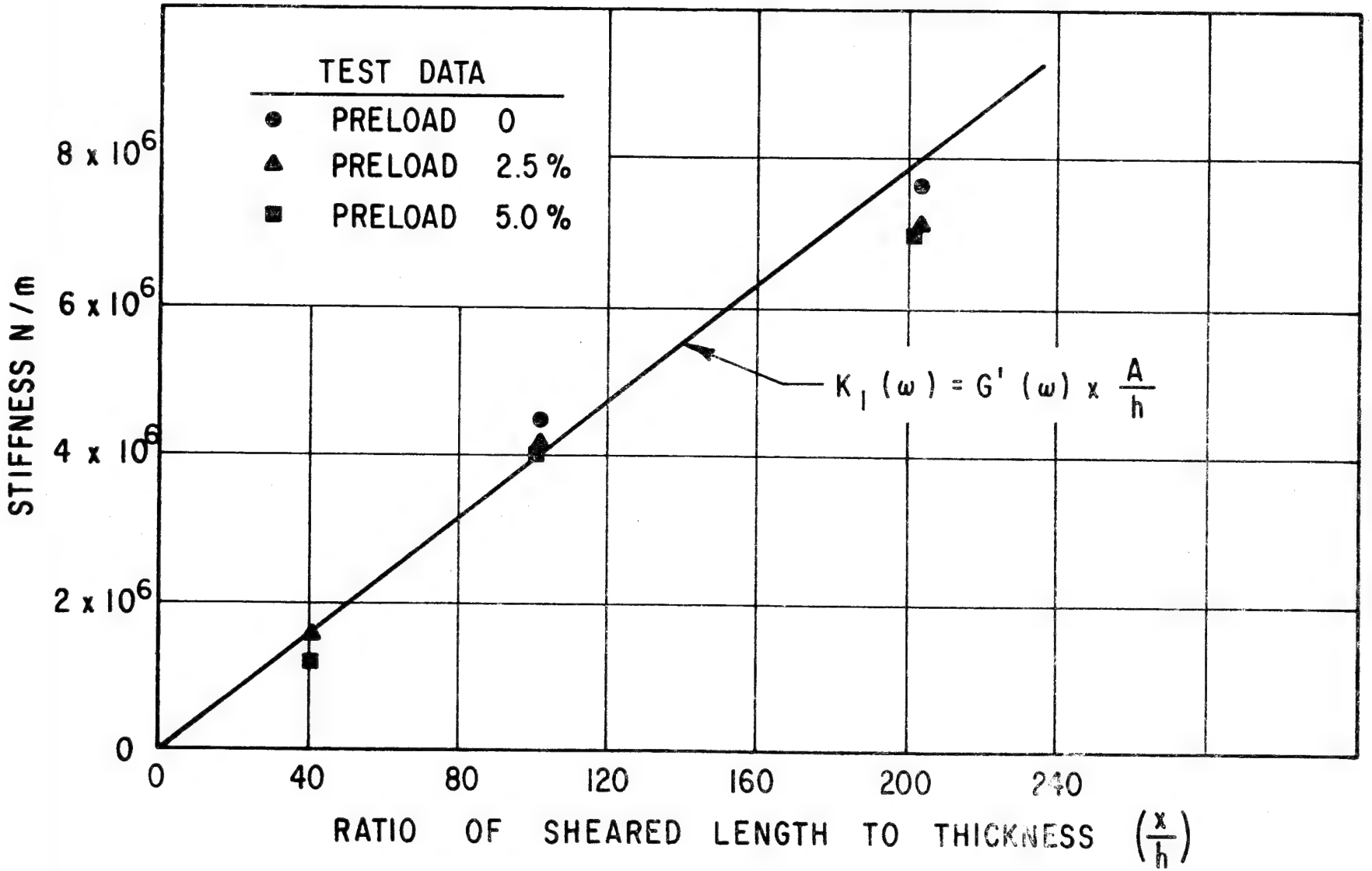

Fig. 13 Phase II Material Property Data. Self-Consistency Test. Sample Shear Element. 1000 Hz Stiffness

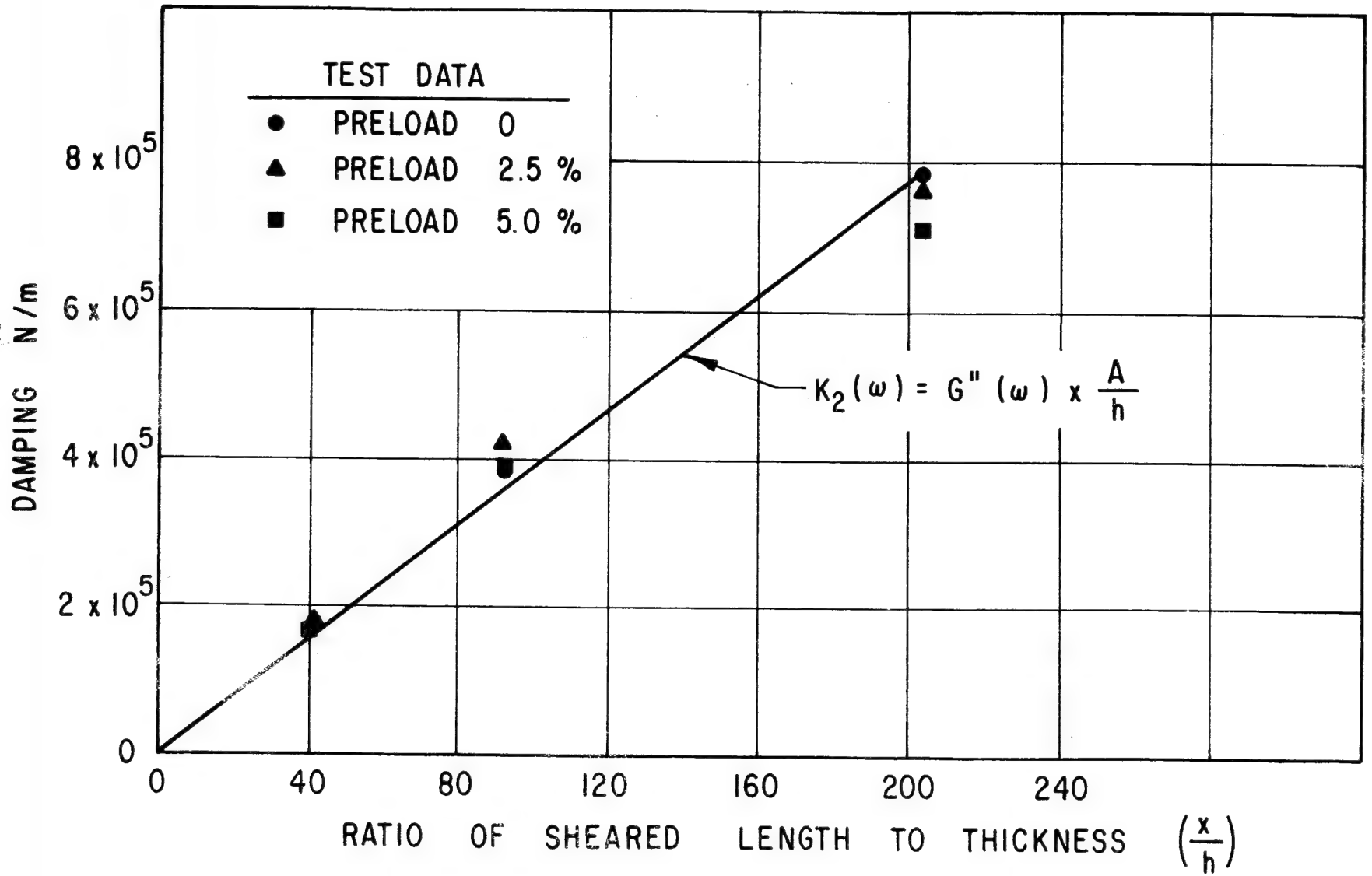

Fig. 14 Phase II Material Property Data. Self-Consistency Test. Sample Shear Element. 100 Hz Damping

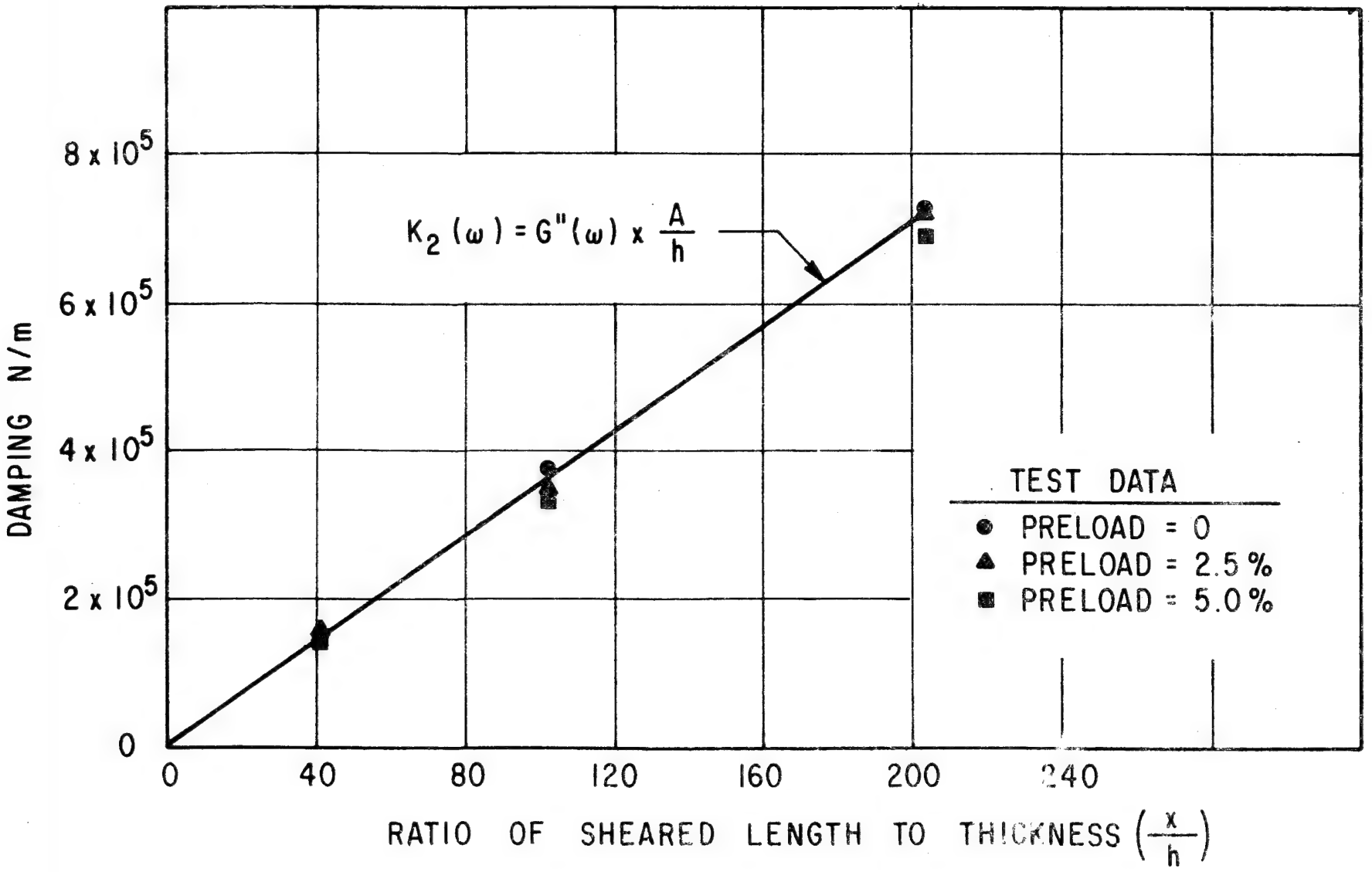

Fig. 15 Phase II Material Property Data. Self-Consistency Test. Sample Shear Element. 300 Hz Damping

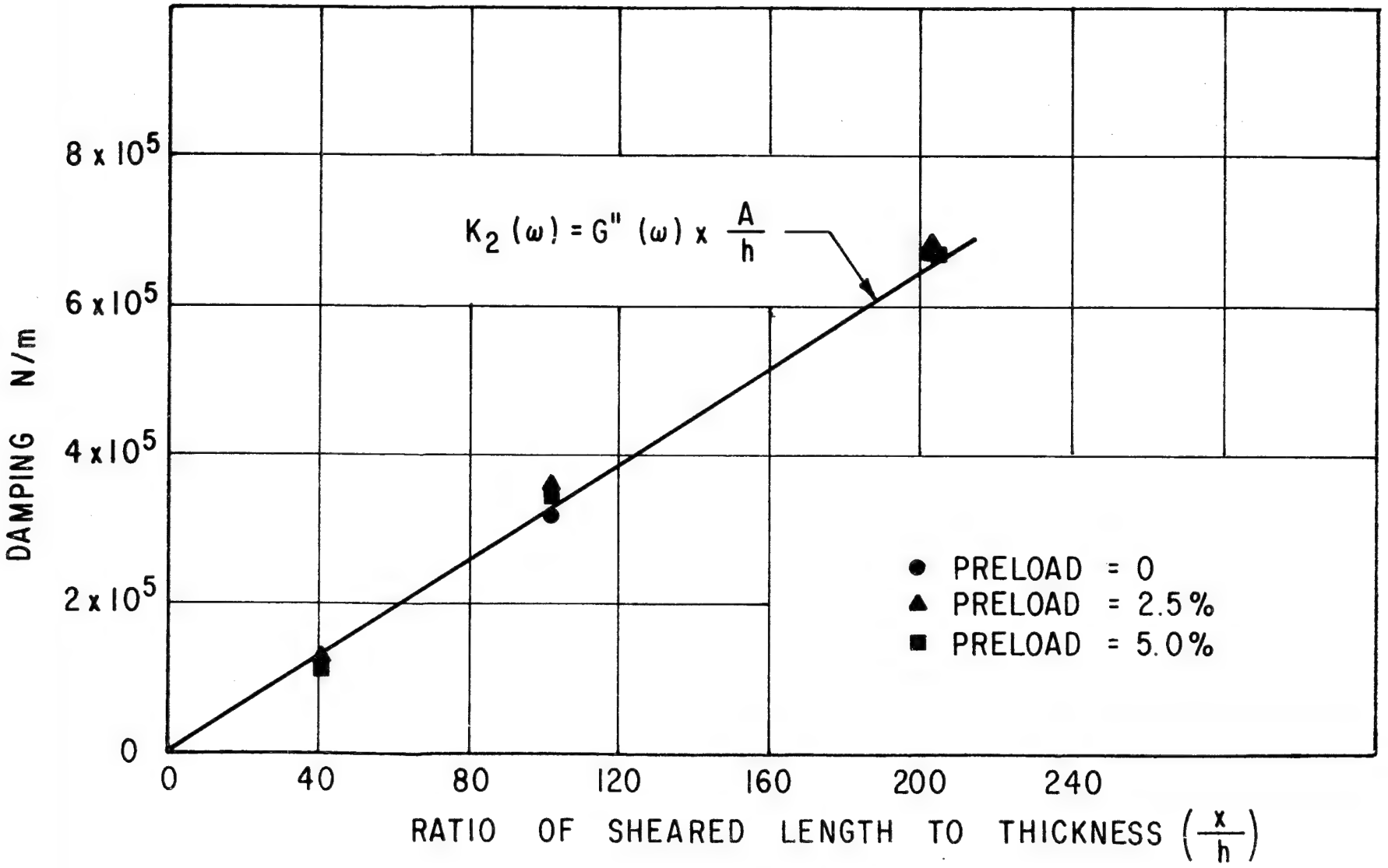

Fig. 16 Phase II Material Property Data. Self-Consistency Test. Sample Shear Element. 1000 Hz Damping

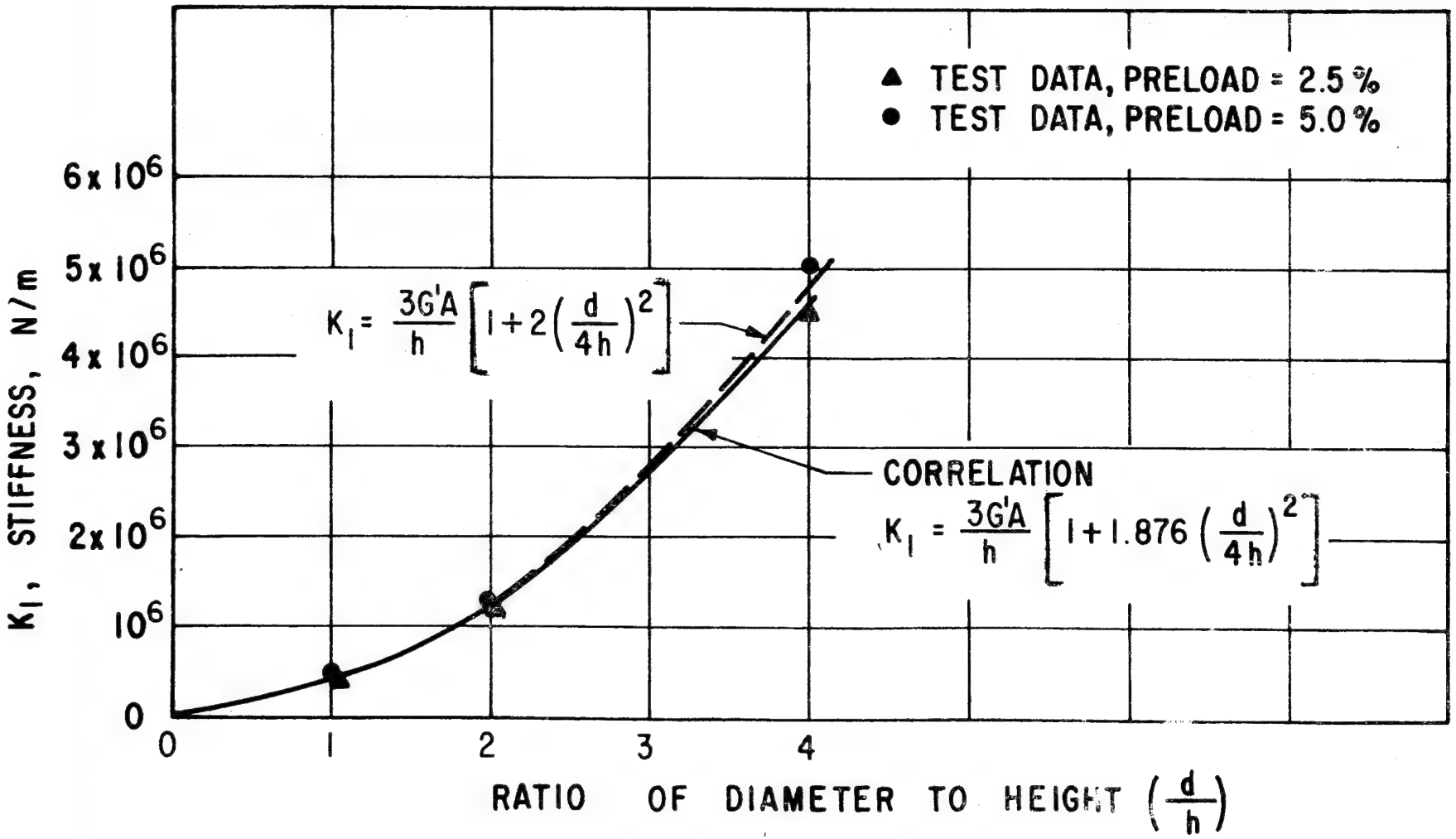

Fig. 17 Phase II Correlation for Shape. Single Compression Element Diameter 0.5 In., 100 Hz Stiffness

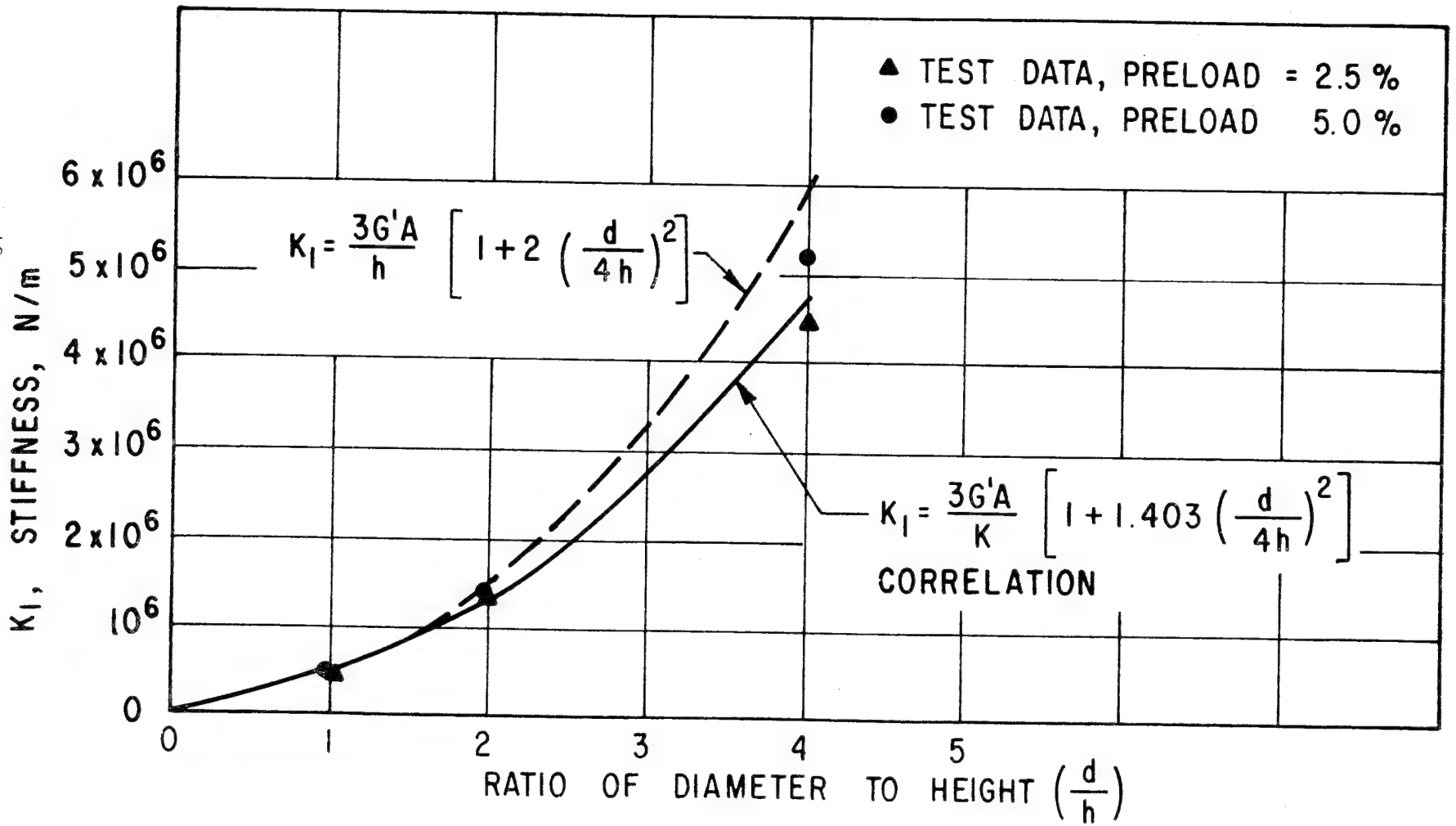

Fig. 18 Phase II Correlation. Single Compression Element. Diameter 0.5 In., 300 Hz Stiffness

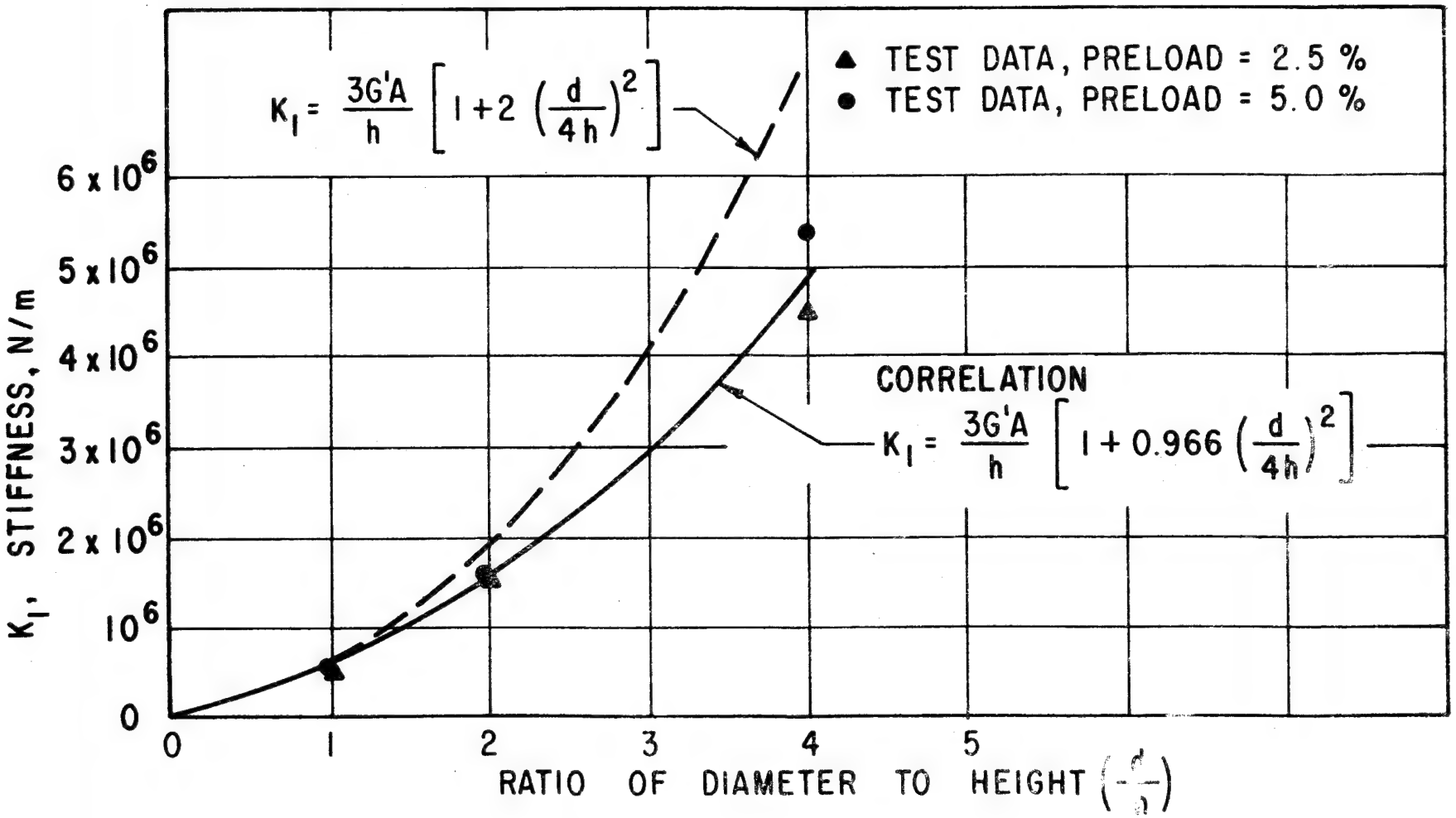

Fig. 19 Phase II Correlation For Shape - Single Compression. Diameter 0.5 In., 1000 Hz

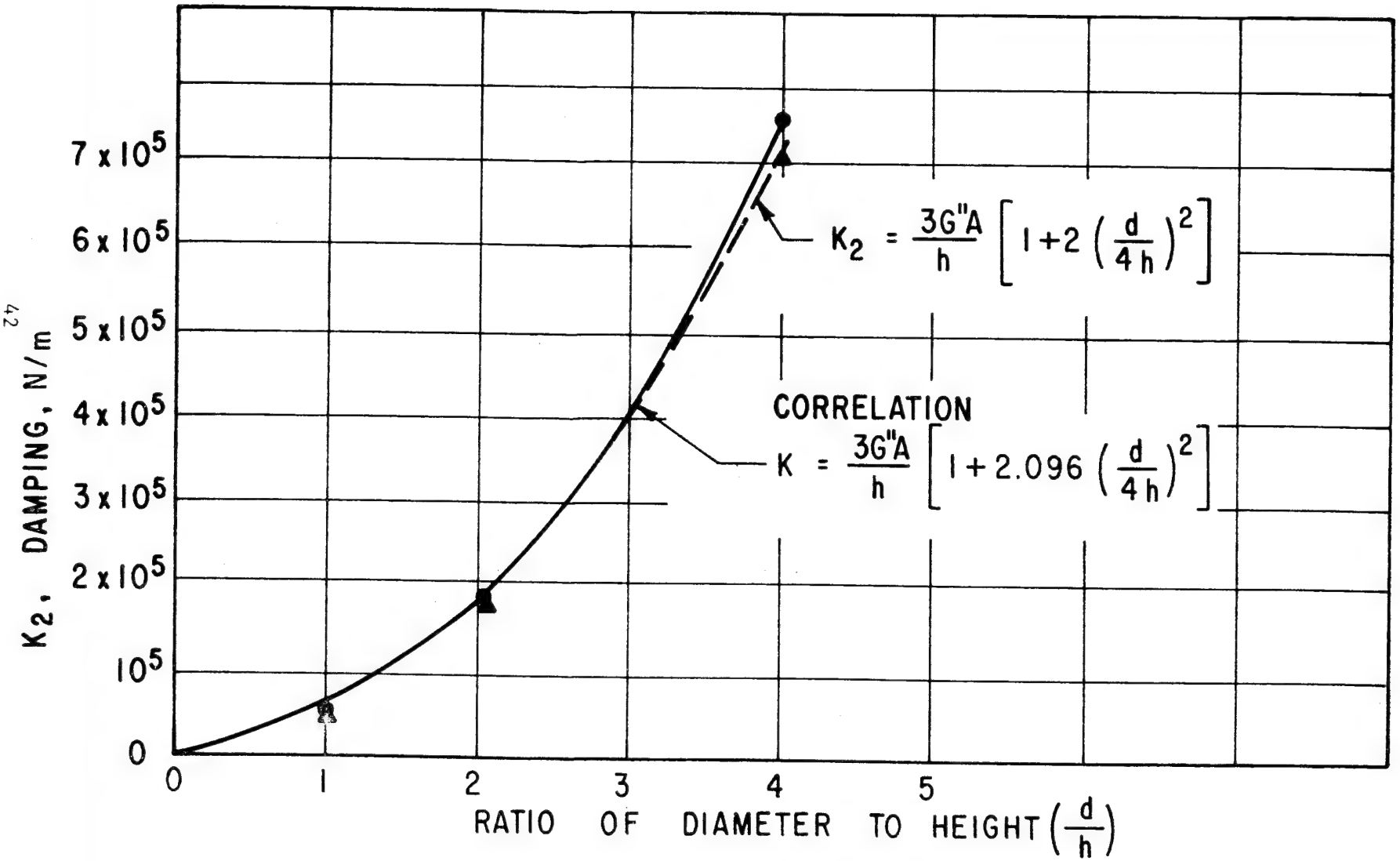

Fig. 20 Phase II Correlation for Shape - Single Compression Element. Diameter 0.5 In., 100 Hz Damping

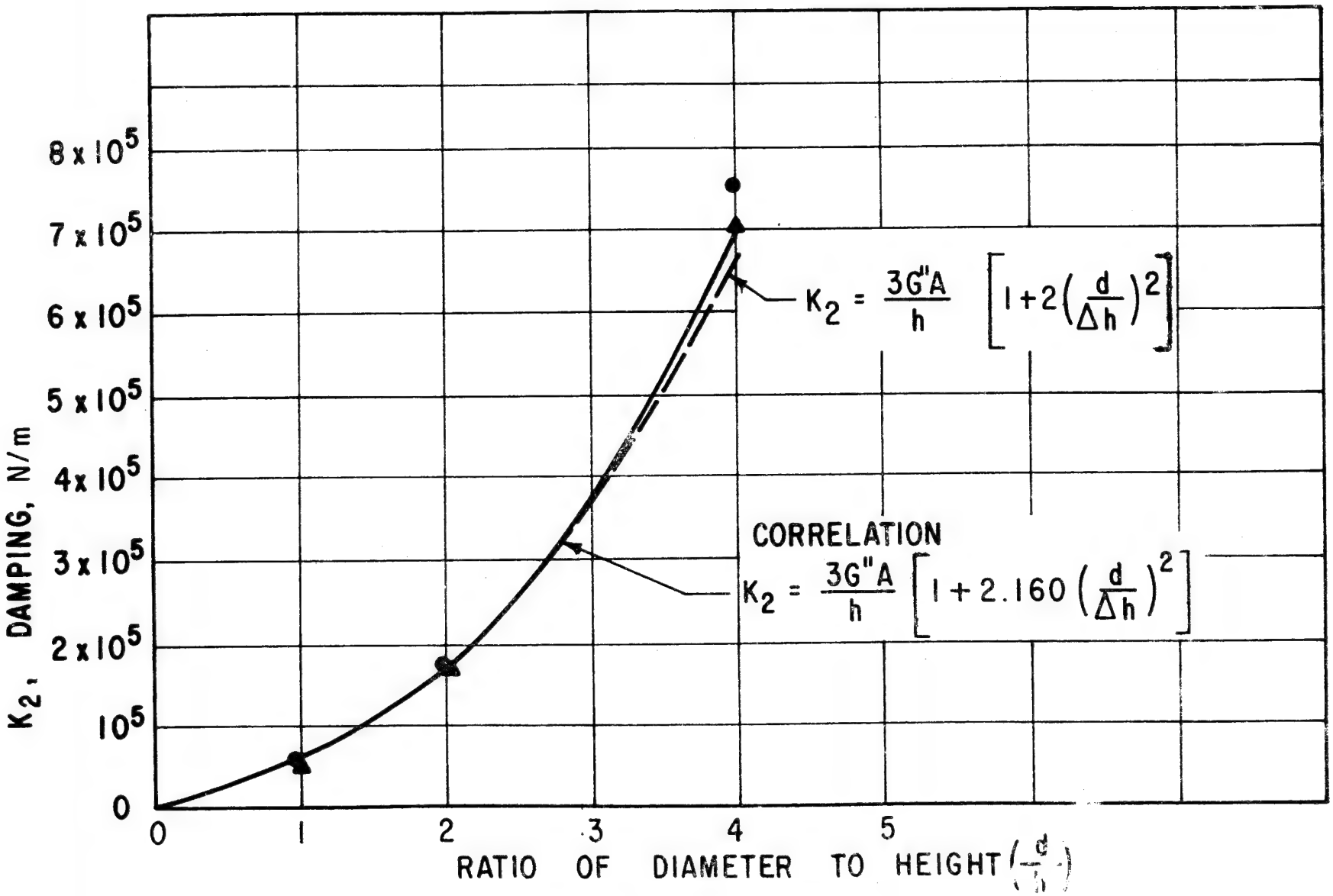

Fig. 21 Phase II Correlation for Shape - Single Compression Element. Diameter 0.5 In., 300 Hz Damping

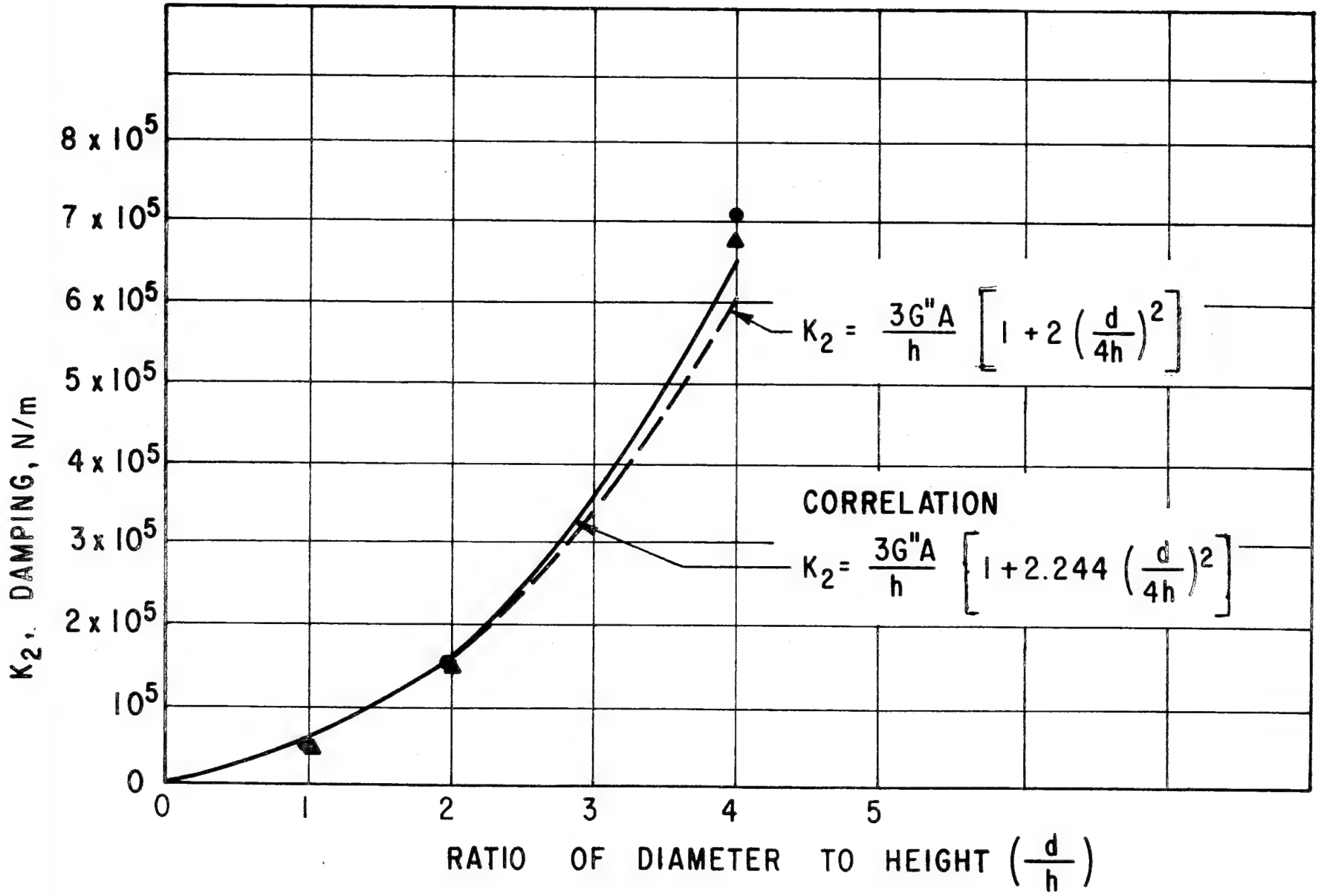

Fig. 22 Phase II Correlation for Shape - Single Compression Element. Diamter 0.5 In., 1000 Hz Damping

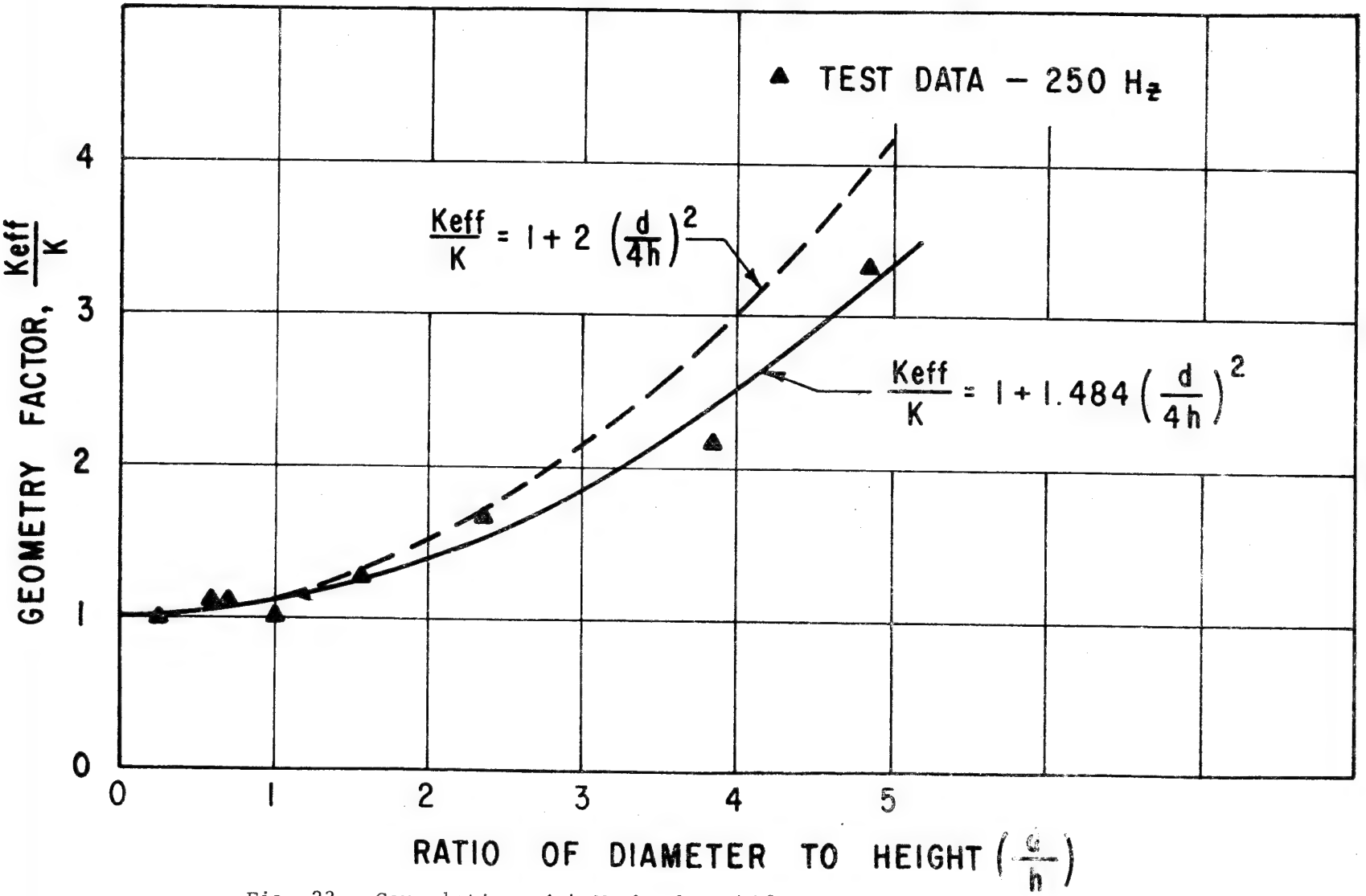

Fig. 23 Correlation with Work of Nashif, Cannon and Jones (Ref. 11). Dynamic Stiffness of Cylindrical Elastomer Test Specimen.

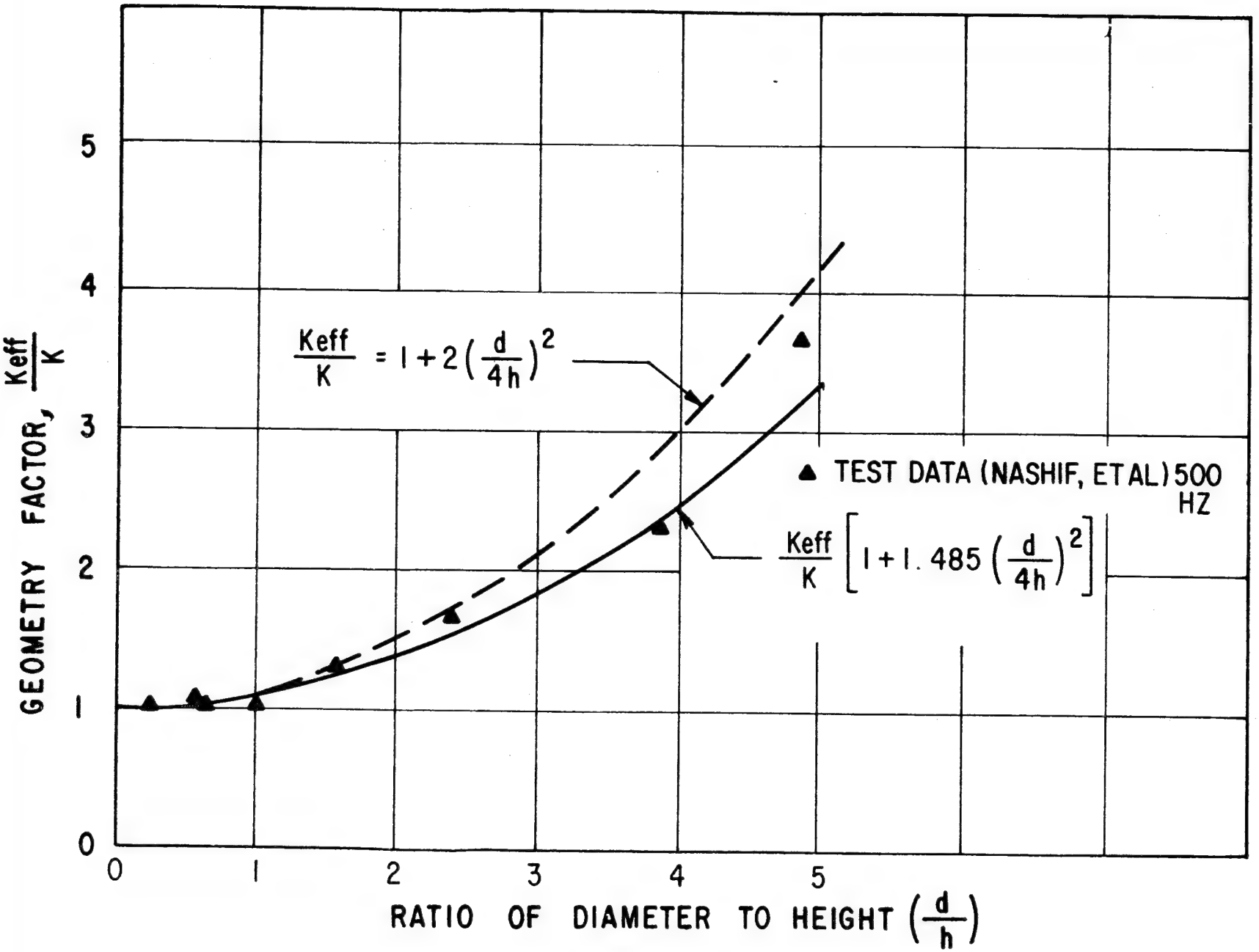

Fig. 24 Correlation with Work of Nashif, Cannon and Jones (Ref. 11). Dynamic Stiffness of Cylindrical Elastomer Test Specimen

stiffness data, this set of data has been used to calculate shape factor coefficient values for the correlation:

$$\text{Stiffness: } K_1 = \frac{G'A}{h}\left[1 + \beta'\left(\frac{D}{4h}\right)^2\right] \qquad (38)$$

and the results for 250 and 500 Hz are $\beta' = 1.484$ and 1.485, respectively. The corresponding results for polybutadiene are 1.45 and 1.29. Comparisons between these correlations and the test data of reference 11 are plotted in Figures 23 and 24 in terms of the ratio of actual stiffness to stiffness predicted for uniaxial stress.

This independent confirmation of the ability of a square law correlation between stiffness correction factor and diameter to height ratio to match test data adds support to the use of such an empirical approach for consolidating the present compression data.

Use of a Constant Shape Factor Coefficient

As discussed previously in this report, the most commonly used value of static shape factor coefficient (β), for cylindrical compression elements is two. A very straightforward method of predicting dynamic stiffness and damping could be based on this coefficient value, as follows

$$K_1(\omega) = 3G'(\omega)\frac{\pi D^2}{4h}\left[1 + 2\left(\frac{D}{4h}\right)^2\right] \qquad (39)$$

$$K_2(\omega) = 3G''(\omega)\frac{\pi D^2}{4h}\left[1 + 2\left(\frac{D}{4h}\right)^2\right] \qquad (40)$$

No analytical justification exists for this application of static coefficients but, since it has the appeal of simplicity and generality, the likely errors in the approach have been tested. Superimposed on Figures 17 through 22 are the above expressions. At high frequencies the predictions of these expressions for stiffness are 50 percent high relative to the more representative lines based on frequency-dependent coefficients. At lower frequencies the discrepancy for stiffness is less and the discrepancy for damping is closer to ten percent under all conditions.

Effects of Temperature And High Dissipation

Since the Phase II data did not include temperature as a varied parameter it cannot be used to evaluate any means of representing the effects of temperature. However, in anticipation of the Phase III data for high temperature and high dissipation, a model intended to tie the effects of high dissipation to the change in properties as a

result of temperature increases, generated by energy dissipation in the elastomer, has been developed. This model simply needs to have available values of G' and G'' as a function of frequency and temperature

$$G'(\omega,T) \tag{41}$$

$$G''(\omega,T) \tag{42}$$

The hypothesis of this model is that, when large amplitude vibrations are imposed upon an elastomer element, they give rise to dissipation of energy throughout the element. As a result there is a tendency for the elastomer to heat up. The temperature distributions in the elastomer are governed by the equations of thermal conduction and appropriate boundary conditions. As a result of the distribution of temperature in the elastomer, and the dependence of elastomer moduli on temperature there is a distribution of material properties through the elastomer. Stress equilibrium within the elastomer, accounting for this distribution of properties, governs the forces generated by the elastomer, and its apparent stiffness and damping.

The implementation of such a model in two or three dimensions could be very complicated. However, to typify the results given by such a model, and to identify the major items of information needed, while minimizing the complexity, a one-dimensional development has been undertaken.

An important, valid, assumption is that the time scale associated with the vibrational phenomena (less than 0.01 second) is short compared to the time scale associated with changes in the thermal condition of the material ($h^2 \rho C_p/k$, which is of the order of 40 seconds and higher).

<u>One-Dimensional Model For Large Dissipation Effects</u>

This model is directed at either a shear or a compression element in which uniaxial stress prevails. The temperature distribution is one-dimensional and the flow of heat is normal to the stressed area. The equations to be solved are:

1. The energy equation, in terms of cycle average temperature, T

$$\frac{\partial}{\partial Z}\left[k \frac{\partial T}{\partial Z}\right] - \rho C_p \frac{\partial T}{\partial t} = - \gamma G'' \left(\left|\frac{\partial U}{\partial Z}\right|\right)^2 \frac{\omega}{2} \tag{43}$$

2. The dynamic stress-equilibrium equation for uniaxial stress

$$\frac{\partial}{\partial Z}\left[G^* \frac{\partial U}{\partial Z}\right] = 0 \tag{44}$$

where U is the amplitude of displacement relative to the base of the elastomer element.

3. The dependence of properties on frequency and temperature

$$G^* = G^* (\omega, T) \tag{45}$$

4. Boundary conditions

$$T = T_a \text{ at } Z = 0, h \tag{46}$$

$$U = 0 \text{ at } Z = 0 \tag{47}$$

5. For imposed displacement at the top of the element

$$U = Y^* \text{ at } Z = h \tag{48}$$

6. For base excitation, the equation of motion for the supported mass

$$G^* \frac{\partial U}{\partial Z} A \gamma - M\omega^2 U = M\omega^2 Y_o^* \tag{49}$$

where Y^* is the amplitude of displacement of top relative to base,
Y_o^* is base excitation amplitude (absolute),
γ is a factor equal to one for shear elements, three for compression elements,
M is the supported mass,
ω is the base excitation frequency
A is the stressed area, and
T_a is the temperature at base and top.

The complete development of Equations (43) to (45) is presented in Appendix A.

Solution of the Equations. As a result of the dependence of G^* on temperature the system of equations is nonlinear. While steady-state results are of most interest, solution in the time domain has been selected as more convenient to implement than an iterative solution. The solution method is a modification of the second order Crank-Nicholson Method (ref. 17), in which nonlinear terms are evaluated by extrapolation forward one-half time-step.

The energy equation is written to apply at the time $t + \Delta t/2$.

$$1/2 \left\{\frac{\partial}{\partial Z}\left[k \frac{\partial T}{\partial Z}\right]\right\}_t + 1/2 \left\{\frac{\partial}{\partial Z}\left[k \frac{\partial T}{\partial Z}\right]\right\}_{t+\Delta t}$$

$$- \rho C_p \frac{(T_{t+\Delta t} - T_t)}{\Delta t}$$

$$= \left\{-\gamma G'' \left|\frac{\partial U}{\partial Z}\right|^2 \frac{\omega}{2}\right\}_{t+\Delta t/2} = R_{t+\Delta t/2} \qquad (50)$$

The left-hand side has a linear operator and consists of known quantities at time t and unknown quantities at time t + Δt. The right-hand side is unknown since it is a function of temperature at time t + Δt/2, but can be approximated by the linear extrapolation from known quantities:

$$R_{t+\Delta/2} = (3/2)R_t - (1/2)R_{t-\Delta t} \qquad (51)$$

The equation for U is solved at time t + Δt, once $T_{t+\Delta t}$ and the associated values of G^* are known.

The time integration solution is continued until results for successive time steps indicate that thermal equilibrium has been reached. The equilibrium distribution of temperature, material properties, and deflection will determine the behavior which will be observed once the initial thermal transients have died out.

An interesting feature of the thermal transient behavior occurs when the base excitation boundary conditions apply and the frequency of excitation and supported mass are such that the element causes subresonant vibrations when the element is cold but vibrates above resonance when the element gets hot due to self-heating. In this case there is a wide swing in phase angle during the thermal transient and an inability to hold subresonant conditions for levels of dissipation higher than a certain limit. Figure 25 illustrates the behavior to be expected for a range of different input amplitudes and this phenonmenon is discussed further in the Results and Discussion Sections of this report. Observed stiffness and damping of the element at any time during the time integration, including equilibrium, are calculated as

$$K_1 = \frac{\gamma A}{Y^*} \mathrm{Re}\left\{G^* \frac{\partial U}{\partial Z}\right\}_{Z=h} \qquad (52)$$

$$K_2 = \frac{\gamma A}{Y^*} \mathrm{Im}\left\{G^* \frac{\partial U}{\partial Z}\right\}_{Z=h} \qquad (53)$$

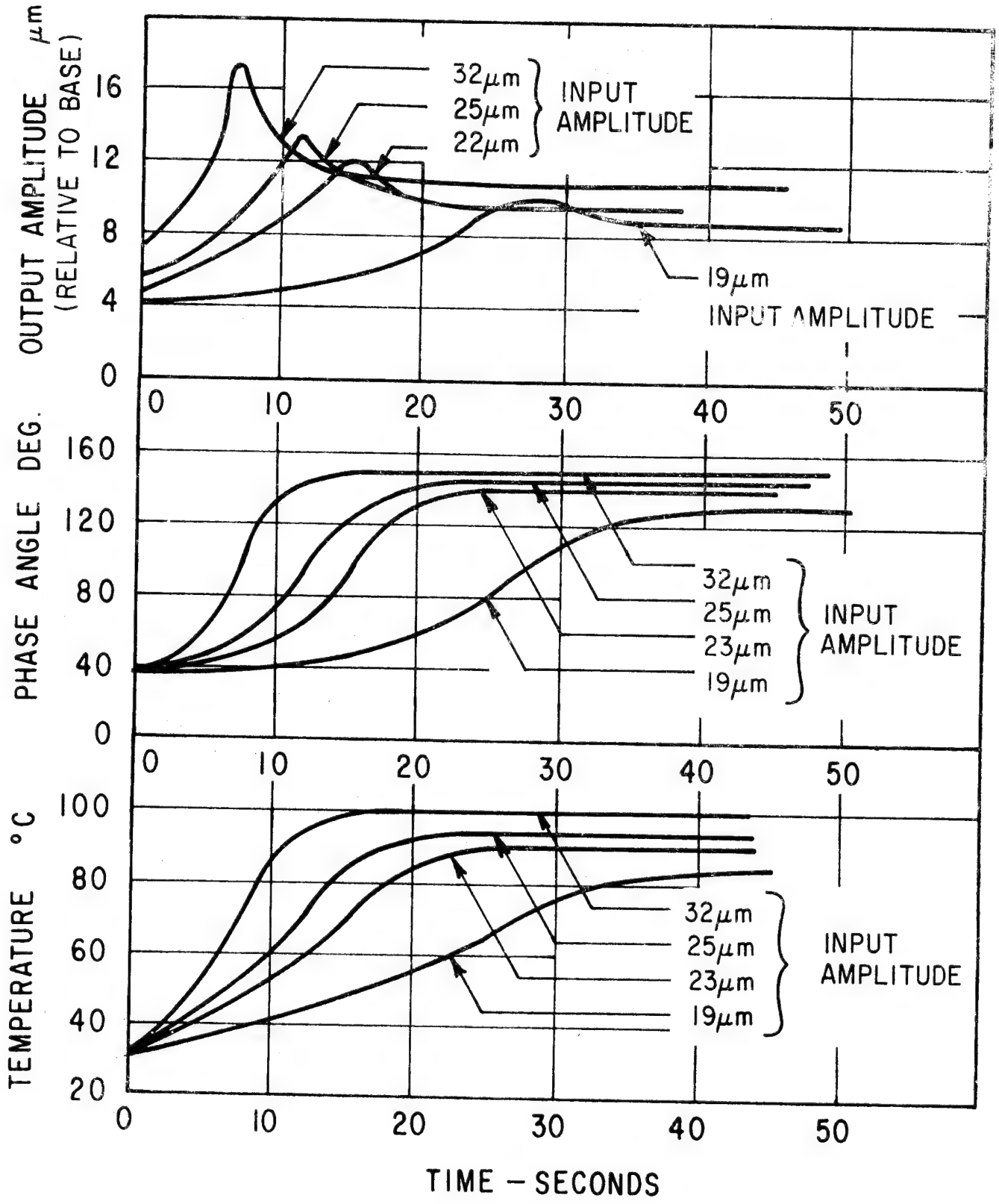

Fig. 25 High Dissipation Predictions Influence of Input Amplitude. 1.816 Kg Mass, 380 Hz, 32 C Ambient, Compression Specimen, 10 Elements, 1.27 cm Diameter, 0.635 cm High

It is important to note that a number of material properties not included in the dynamic tests are needed to implement this analysis; in particular, density, specific heat and conductivity.

In addition, if this analysis is to be applied with meaning to compression elements in which the stiffness correction factor is of order 1.5 and above, some account must be taken of the stiffness correction factor. In the present case, the significant assumption has been made that the stiffness correction factors follow the functional dependence on frequency and geometry determined empirically for cylindrical elements and that the increase in effective modulus should take place on a local basis, and be reflected in the equilibrium equation:

$$\frac{\partial}{\partial Z}\left[G^{*}_{eff}\ \frac{\partial U}{\partial Z}\right] = 0 \qquad (54)$$

PREDICTION OF CARTRIDGE DYNAMIC PROPERTIES

One of the objectives of the work reported is to develop, and evaluate, relatively simple predictive methods for practical elastomer configurations, such as radially loaded ring cartridges. In this Section a number of alternative methods of prediction of radial stiffness are developed and numerical values are obtained for the particular cartridge configurations selected for testing.

Figure 10 illustrated the geometry of the elastomer ring cartridge. The elastomer material separates the inner diameter of one cylinder from the outer diameter of a second, smaller cylinder. The loading of interest is radial; that is, it tends to move one cylinder radially eccentric to the other.

Three predictive methods have been tested:

- Beam-Column Method
- Method of Göbel (ref. 19)
- Predictions Based Upon Plane Stress Analysis

Each of these is a 'static' prediction method; that is, it seeks a ratio of element stiffness to storage modulus which is a function of the geometry only and applies that ratio in the determination of dynamic stiffness and of damping. The approach is not rigorously justifiable, but may be given credibility by empirical verification.

Beam-Column Method

In this development the cartridge is assumed to be made up of a series of noninteracting, elemental column/beams, whose variation of thickness due to radius effects is small. Figure 26 illustrates the cartridge and the Beam-Column element, whose mean loaded area is

$$da = \bar{r}\, \ell d\theta \tag{55}$$

where ℓ is the length of the cartridge
$\bar{r}$ is the mean radius = $(r_1 + r_2)/2$.

Consider the rigid inner member to be displaced radially by a small radial distance Y, relative to the rigid outer member. The compression deflection of the element is Y cos θ, if θ is the angle the radial line to the element makes with the direction of displacement. The shear deflection of the element is Y sin θ. So, considering the element to act independently of adjacent elements, the elemental compression and shear forces, df_c, df_s are

$$df_c = Y \cos\theta\, E \frac{\bar{r}\, \ell d\theta}{(r_2 - r_1)} \tag{56}$$

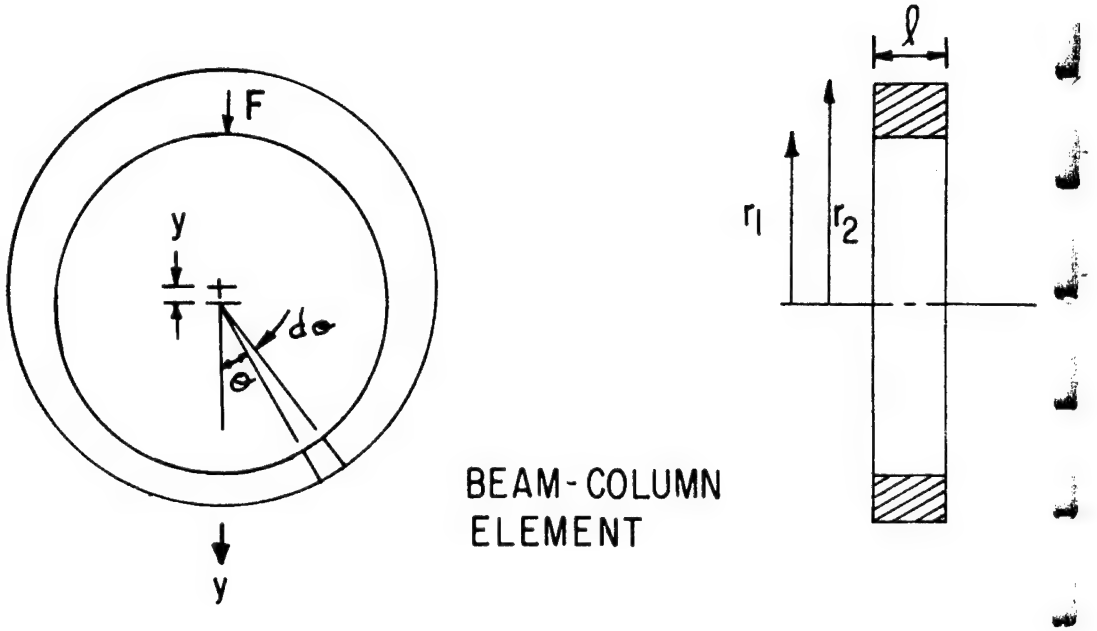

Fig. 26 Cartridge Showing Beam-Column Element

$$df_s = Y \sin\theta \, G \, \frac{\bar{r} \, \ell d\theta}{(r_2 - r_1)} \qquad (57)$$

and the total force exerted at the mean radius is

$$F = \int_o^{2\pi} \frac{Y \bar{r} \, \ell}{(r_2 - r_1)} \left[E \cos^2\theta \, d\theta + G \sin^2\theta \, d\theta \right]$$

$$= \frac{Y \bar{r} \, \ell \, \pi}{(r_2 - r_1)} \left[E + G \right] \qquad (58)$$

so that, if we assume E = 3G (Poisson's ratio $\nu = 0.5$ implied), then

$$K_r = \frac{F}{Y} = 2\pi \frac{(r_2 + r_1)}{(r_2 - r_1)} G\ell \quad \underline{\text{BEAM-COLUMN RESULT}} \qquad (59)$$

A slightly different result is obtained if the tapering of beams and columns due to radius effects is accounted for.

$$K_r = \frac{4\pi \, G\ell}{\ell_n (r_2/r_1)} \quad \underline{\text{ACCOUNTING FOR RADIUS EFFECTS}} \qquad (60)$$

But, as Table IV shows, the reduction in stiffness due to radius effects is less than four percent for radius ratios up to two.

TABLE IV. REDUCTION IN STIFFNESS DUE TO RADIUS EFFECTS
(Relative to Beam-Column Result)

r_2/r_1	Reduction
1.1	0.08%
1.5	1.35%
2.0	3.82%

The radius ratio selected for testing is 1.5, for which radius effects are only 1.35 percent, and have been neglected.

Method of Göbel

The method of Göbel initially follows a very similar development to the Beam-Column method accounting for radius effects, with the intermediate result:

$$K_r = \frac{\pi \, \ell}{\ell_n \, (r_2/r_1)} (G + E) \qquad (61)$$

However, Göbel then claims that, for $\frac{\ell}{(r_2 - r_1)} = 1$, the effective E-modulus is given by

$$E_{eff} = 6.5\ G \tag{62}$$

and, in addition that, for other length to radius ratios, a correction factor, f_1, should be applied, so that

$$K_r = \frac{7.5\ \pi \ell\ G f_1}{\ell_n\ (r_2/r_1)} \tag{63}$$

Göbel presents f_1 as a graphical function of $\ell/(r_2 - r_1)$. Payne and Scott (ref. 6) in their book ENGINEERING DESIGN WITH RUBBER present a cubic fit to Göbel's function:

$$f_1 = 1 + 0.0097\ \ell^3/(r_2 - r_1)^3 \tag{64}$$

which agrees closely with Göbel's graphical presentation. The basis for f_1, or for the statement E = 6.5 G is not made clear in Göbel's book. These are not presented as empirical results, since no test data is given for this geometry. Göbel's method implies that E_{ff} = 6.5 G is an asymptotic condition for very short length cartridges. This implication is surprising.

One set of static test data for the cartridge configuration (Adkins and Gent, ref. 7) has been identified and this data is compared with the prediction of the Beam-Column method and the method of Göbel in Figure 27. It shows good agreement at higher values of $\ell/(r_2 - r_1)$ between Gobel and test data but at lower $\ell/(r_2 - r_1)$, the Beam-Column method appears to come closer, due to a much sharper drop in stiffness of the test element. This comparison suggests that E_{eff} = 6.5 G is not a valid asymptotic condition for short cartridges.

Predictions Based Upon Plane Stress Analysis

The value of using a plane stress elastic analysis was also investigated. In this case, only a quarter of the cartridge was modeled and appropriate symmetry and antisymmetry boundary conditions were imposed. The quarter cartridge was embedded in a rectangular finite difference mesh and a finite displacement of the inner member relative to the outer member was imposed. An existing computer program (MTI Program No. 444) was used to solve for the internal displacement field within the cartridge. Since it is not possible to employ a Poisson's ratio of 0.5 in this computer program, a value of 0.4983 was used, together with a shear modulus value of 1.795×10^7 N/m^2. This combination of Poisson's ratio and shear modulus corresponds to a bulk modulus of 5.28×10^9 N/m^2, which is within the range of bulk moduli determined by Rightmire (ref. 18).

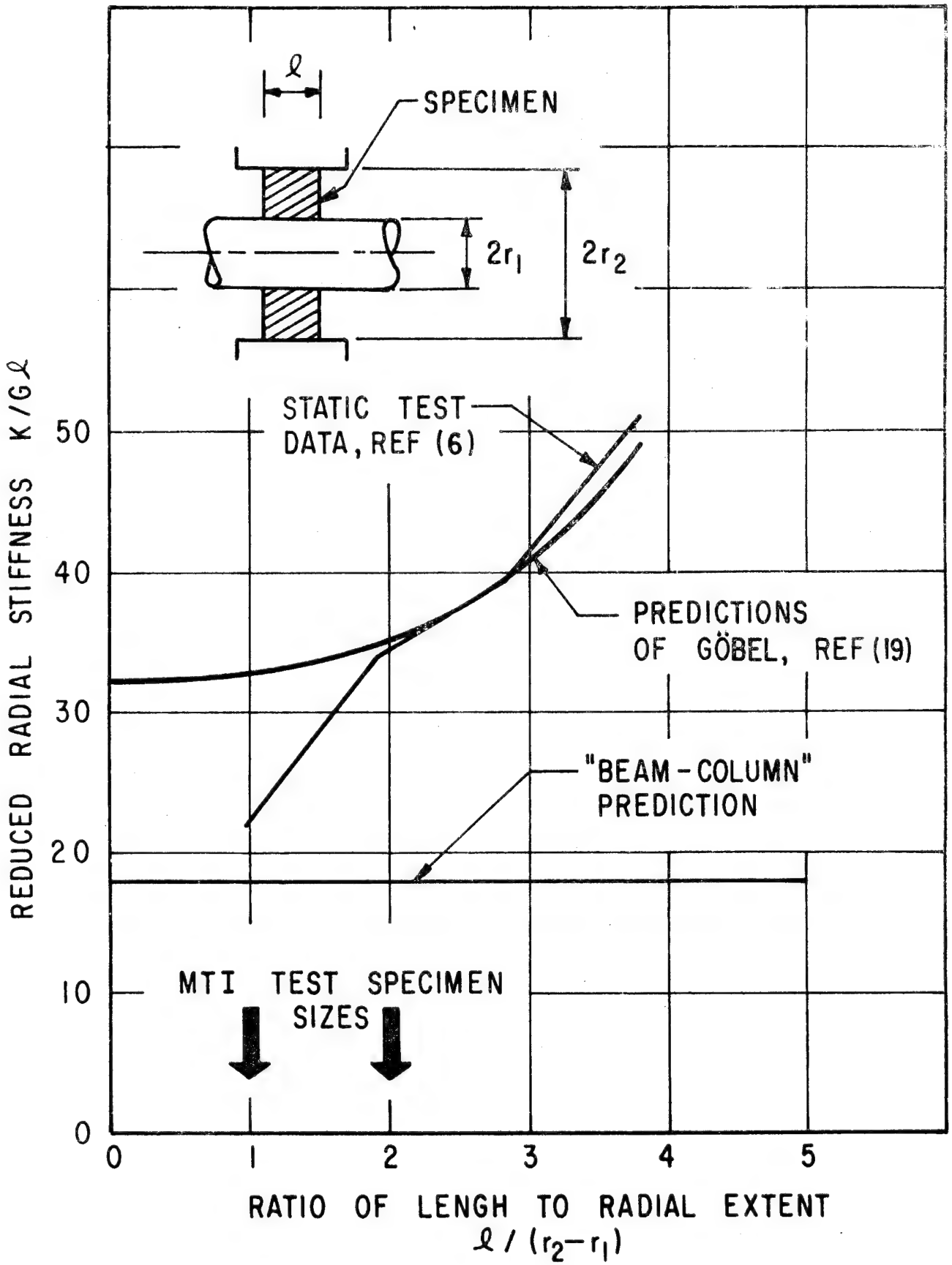

Fig. 27 Comparison of Prediction Methods for Cylindrical Cartridge

The stiffness is calculated by determining the component of shear and direct stress in the direction opposing the displacement x and integrating over the active cartridge surface to obtain the net force. The stiffness is, then, the ratio of net force to displacement.

Numerical Predictions of Cartridge Stiffness and Damping

Each of the predictive methods described for the ring cartridge has been applied to the geometry selected for testing. The results are presented in Table V in nondimensional form; that is, the ratio of stiffness to the product of shear modulus and length is presented.

TABLE V. NONDIMENSIONAL STIFFNESS FOR CARTRIDGES SELECTED FOR TESTING (Inner and Outer Diameters: 1.905 and 2.858 cm)

Method	$K/G\ell$ For ℓ = 0.476 cm	$K/G\ell$ For ℓ = 0.953 cm
Göbel	58.7	62.6
Plane Stress	35.1	35.1
Beam-Column	31.4	31.4

It is seen that only the Göbel method reveals any dependence of this nondimensional stiffness on length of the cartridge, and that the level of the Göbel predictions is substantially higher than that of the Plane Stress and Beam-Column predictions.

The assumption necessary to apply the Göbel and Plane Stress predictions in the determination of dynamic stiffness and damping is that:

$$\frac{K^*}{G^*\ell} = \frac{K}{G\ell} \qquad (65)$$

where $K^* = K_1 + iK_2$ is the complex impedance of the cartridge and $G^* = G' + iG''$ is the complex modulus. That is, the relative distribution of stresses is independent of time under sinusoidal loading and displacement.

The simple Beam-Column method, without accounting for radius effects, since it assumes no interaction between elements, may be developed directly using either G or G^*. In other words, beyond the significant assumptions in its development already presented, no further assumptions are necessary in applying it to dynamic stiffness and damping.

Using these assumptions where appropriate, the predictions of Table V may be applied to the cartridges tested by the BERM method. The non-dimensional stiffness from Table V is simply multiplied by the length of the cartridge and the storage and loss modulus values at the frequency of interest.

The results of this prediction approach are compared with test results later in this report.

EXPERIMENTAL DESIGN AND DESCRIPTION OF TESTS

A forced vibration, resonant mass type of apparatus was used to test the dynamic properties of the elastomer samples. The apparatus was designed as a base excitation, electromagnetic shaker driven mass-spring system which could be brought to resonance for a range of differently sized vibrating masses on top of the elastomer 'spring'. Acquisition of data was, however, not limited to the resonance condition of the system. In fact, data obtained at the resonant frequency of each mass-spring combination was just one of several data points acquired at several vibration frequencies around resonance, where significant amplitude ratios between base and mass vibration existed. The following sections present a description of the test rig, the design of the elastomer test samples, the instrumentation as it was used for the recording of test data, and the range of test parameters investigated.

Description of Elastomer Test Rig

The basic features of this test rig have largely been developed in the course of work conducted under previous phases of NASA Contract NAS3-15334. Reference 2 provides a complete description of test rig capabilities and an analysis of the dynamic characteristics of the test rig components. Figure 28 is a schematic showing all the components.

For the tests reported herein, not all of the available features of the test rig were used. In particular, for test frequencies above 100 Hz, neither the mass support air spring nor the guide spokes (guide bearings) were used. The simplified test rig consisted of a shake table mounted base plate to which the elastomer samples were bonded, and a second plate bonded to the free side of the elastomer samples. A piston with Bellofram seals and various amounts of deadweight were attached to the second plate which vibrated freely on the elastomer spring when the base plate was subjected to sinusoidal vibrations from the shake table.

The piston cavity was externally pressurized with air and served to preload the elastomer sample in a static sense. An overall view of the simplified test rig preload cylinder is given in Figure 29, where a small mass is attached to the free end of the preload piston protruding from the cylinder. Preload was provided on all tests conducted with elastomer compression samples and on a few tests of the cartridge configuration. (The presence or absence of preload is noted on all test results.) All tests with elastomer samples stressed in shear and the majority of the cartridge tests were made without static preload on the sample, and for these tests, the rig was further simplified by removing the piston and seals. Without piston and seal, all test rig components and features with interactive or additive dynamic contributions to the test system had been eliminated. What remained was a dynamically "clean" test rig which, of its own, did not contribute any identifiable dynamic "noise" or distortion of test results.

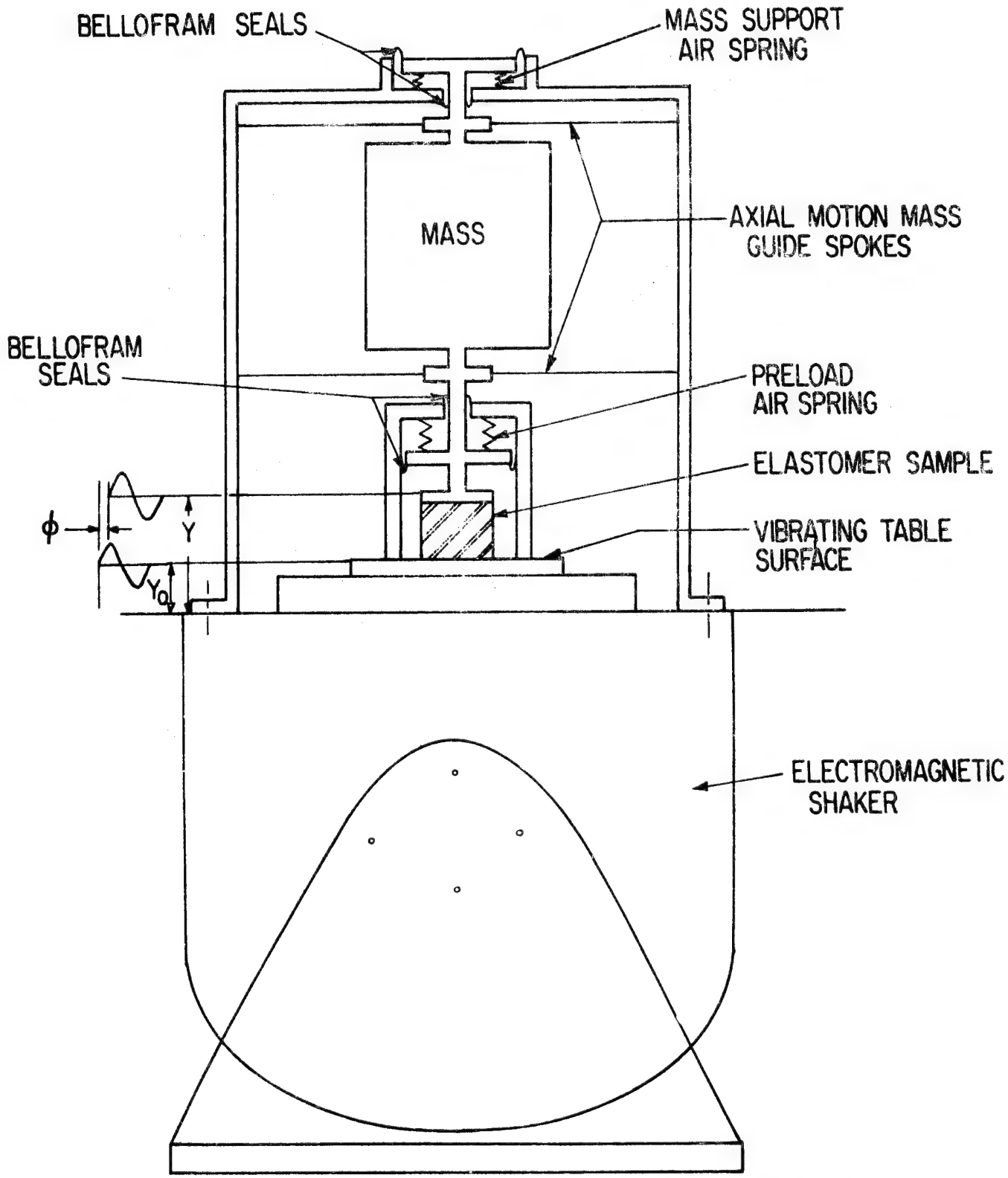

Fig. 28 Schematic of Elastomer Test Rig Showing All Components

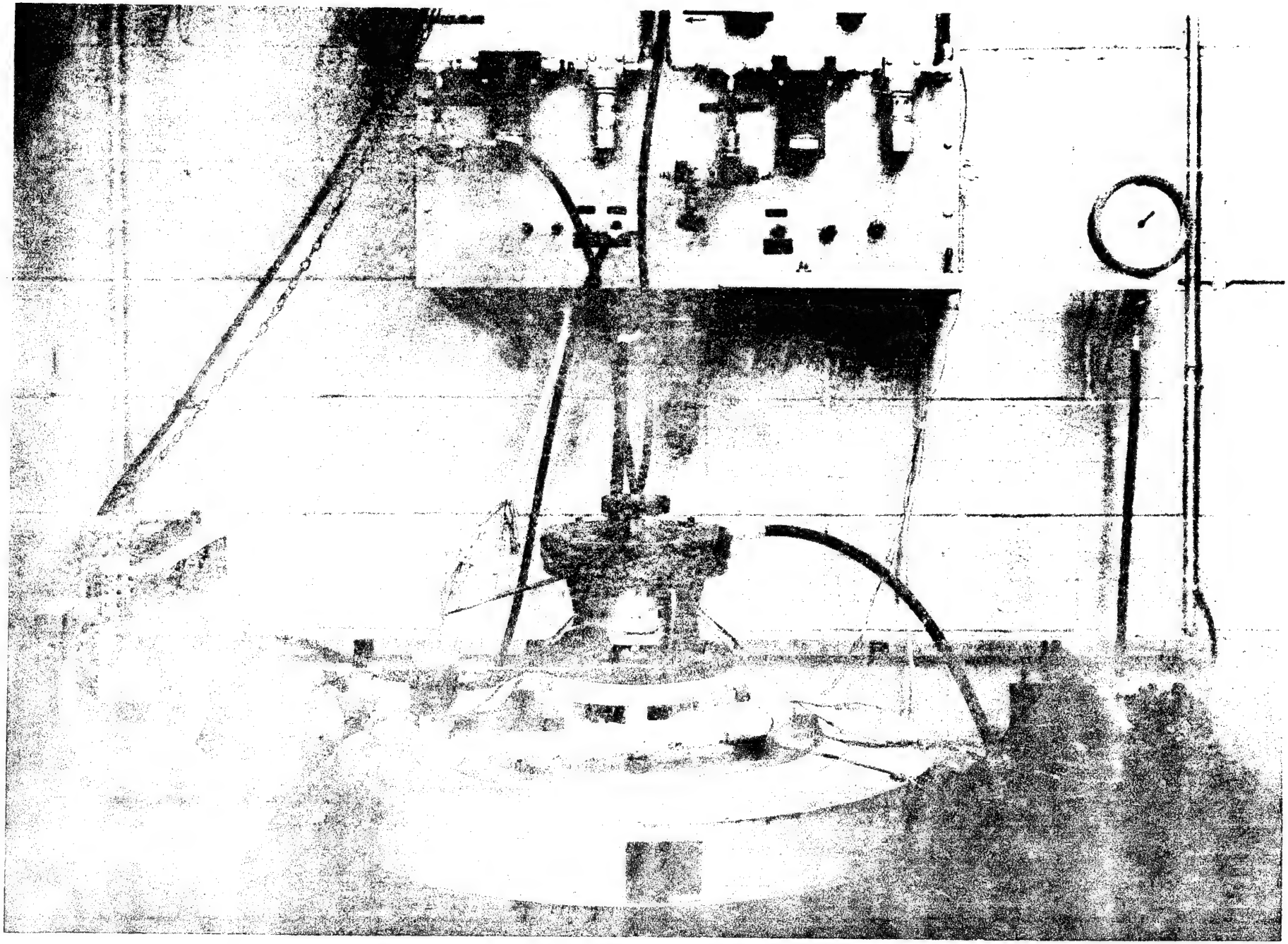

Fig. 29 View of Shake-Table Mounted Elastomer Test Rig With Preload Cylinder and Small Mass

MTI-16654

The vibration input to the test rig in all tests was obtained from a commercially-available electromagnetic shaker system* capable of delivering 66,700 N (15,000 lb) force in the sinusoidal mode of vibration.

The ambient temperature within the elastomer test specimen cavity was controlled through the combined effect of electric heating cables and water-cooled tubes installed in the base plate below the test specimens and heated or cooled air blown directly to the test specimen cavity. For higher than ambient temperatures, the electric heaters were automatically controlled by a temperature controller, which obtained the necessary feedback from the thermocouple embedded in the metal of the base plate. For ambient temperatures down to 2 C, the air supply to the test specimen cavity was passed through cooling coils embedded in dry ice.

Details of the temperature control system and of the temperature recording system are shown in Figure 30.

Elastomer Test Samples - Material Selection

The initial selection of polybutadiene as test material had already taken place during an earlier phase of this program, reported in reference 2. Restated briefly, the choice of polybutadiene, which is classed as Broad Temperature Range (BTR) elastomer, was primarily based upon the desire to test a material that was not overly sensitive to small variations in ambient temperatures nor to the temperature variation induced in the sample through vibration testing.

The choice of polybutadiene among BTR elastomers was based upon the manufacturer's** recommendation founded on manufacturing considerations, such as the achievement of consistent material properties from batch-to-batch. This material, which carries the manufacturer's designation NEX156G, has a nominal hardness of 70 durometers (or Shore A Hardness) and has the highest hardness and damping of those available from the manufacturer.

Elastomer Test Samples - Configurations

Three sample configurations were tested:

- Shear Type Samples
- Compression Type Samples
- Cartridge Type Samples

*Ling Electronics, Model 335A Shaker with PP-35/70 VC Power Amplifier SCO-100 Servo Control Center.

**Nichols Engineering, Incorporated, Shelton, Connecticut.

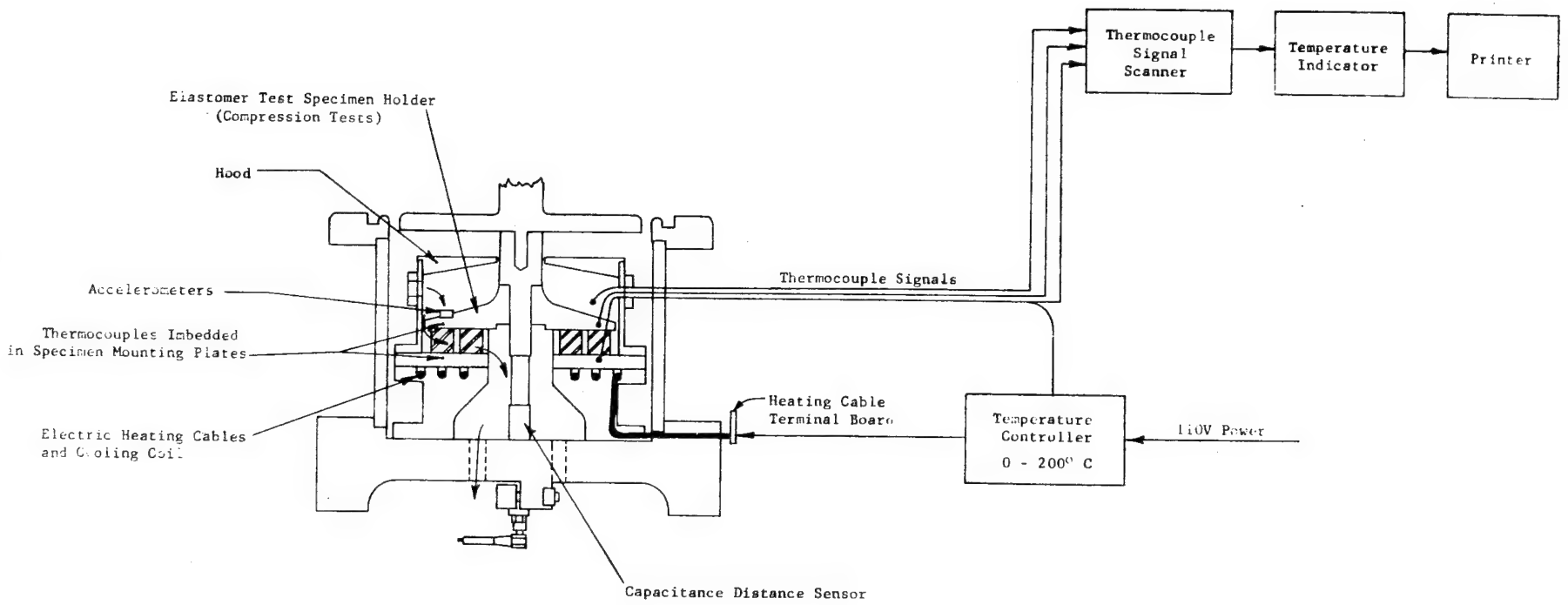

Fig. 30 Temperature Control System For Elastomer Tests

Shear Test Samples. Two shear test samples were used for testing in this phase of the contract. One shear test sample was made up from eight individual elastomer strips, each measuring 12.7 mm in height, 48.8 mm in length and 3.2 mm in thickness (0.5 x 1.42 x 0.125 inch) (Fig. 31). A second shear sample consisted of four individual elastomer strips, each having twice the height (25.4 mm) of the eight-strip sample (Fig. 32).

One individual strip was glued, on its large face to each of the sides of a square aluminum block, with the other large face of each strip glued to an additional aluminum holding block. A cyanoacrylate glue was used (Eastman 910 MHP). In the eight-strip sample, two such assemblies, each consisting of four strips, were placed on top of each other and tested together. In the assembly of the test fixture, the four holding blocks were bolted to the shake table, while the elastomer supported center block was attached to, and therefore became part of, the resonant mass.

Compression Test Sample. The compression test sample consisted of ten individual elastomer cylinders, each measuring 12.7 mm in diameter and 6.4 mm in height (0.5 by 0.25 inch). These cylinders were arranged in a circular pattern and glued with their faces to two aluminum plates (see Fig 33). The bottom plate was anchored to the shake table and the top plate connected to the resonant mass.

Like the shear test sample, the compression test sample had originally been made for the investigations reported in reference 2. Details of manufacture and test results for two other compression test samples made up of three cylinders 3.2 mm in height and of thirty cylinders each 12.7 mm in height may also be found in reference 2.

Cartridge Test Samples. Individual cartridge test specimens were made up of an annular elastomer body with rectangular cross-section held between the cylindrical bore of a rectangular shell structure and a round shaft of smaller diameter.

The elastomer ring was molded to the shaft and bonded to the surrounding shell, which was of split design to facilitate initial assembly and later, static preloading prior to testing.

Figure 34 shows one cartridge specimen before and after assembly of the outer shell around the bonded elastomer ring on the shaft.

Cartridge dimensions were chosen so that four individual cartridges in parallel would have a combined spring stiffness that, in combination with the minimum mass arrangement in the test rig (top plate only), would result in a system resonant frequency of at least 700 Hz. Frequencies to 1000 Hz could then be achieved by testing to about 1.4 times

Fig. 31 Test Assembly of Eight Elastomer Shear Specimens, Each 1.27 cm (0.5 In.) High

MTI-16657

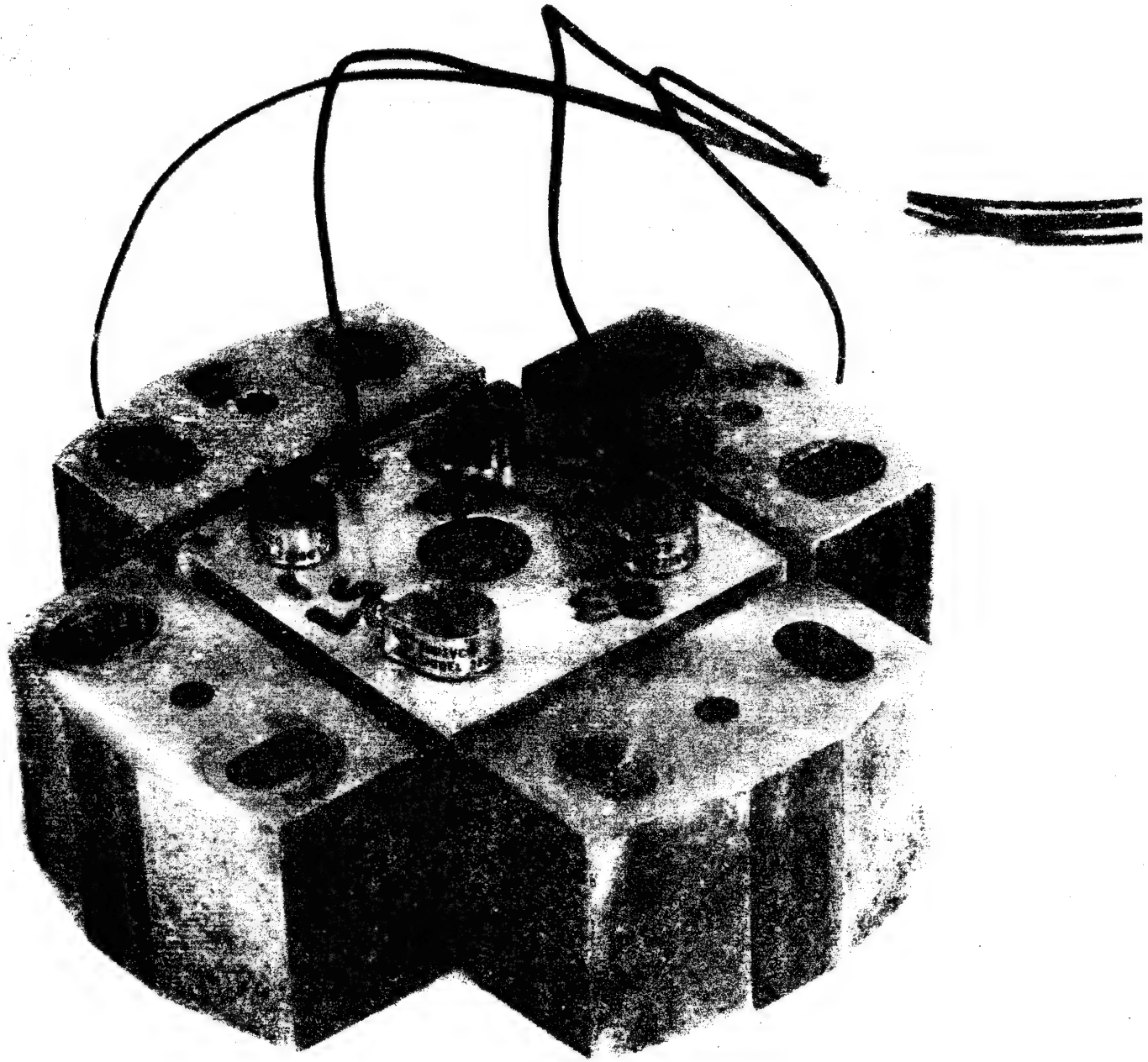

Fig. 32 Test Assembly of Four Elastomer Shear Specimens, Each 2.54 cm (1.0 In.) High

MTI-16656

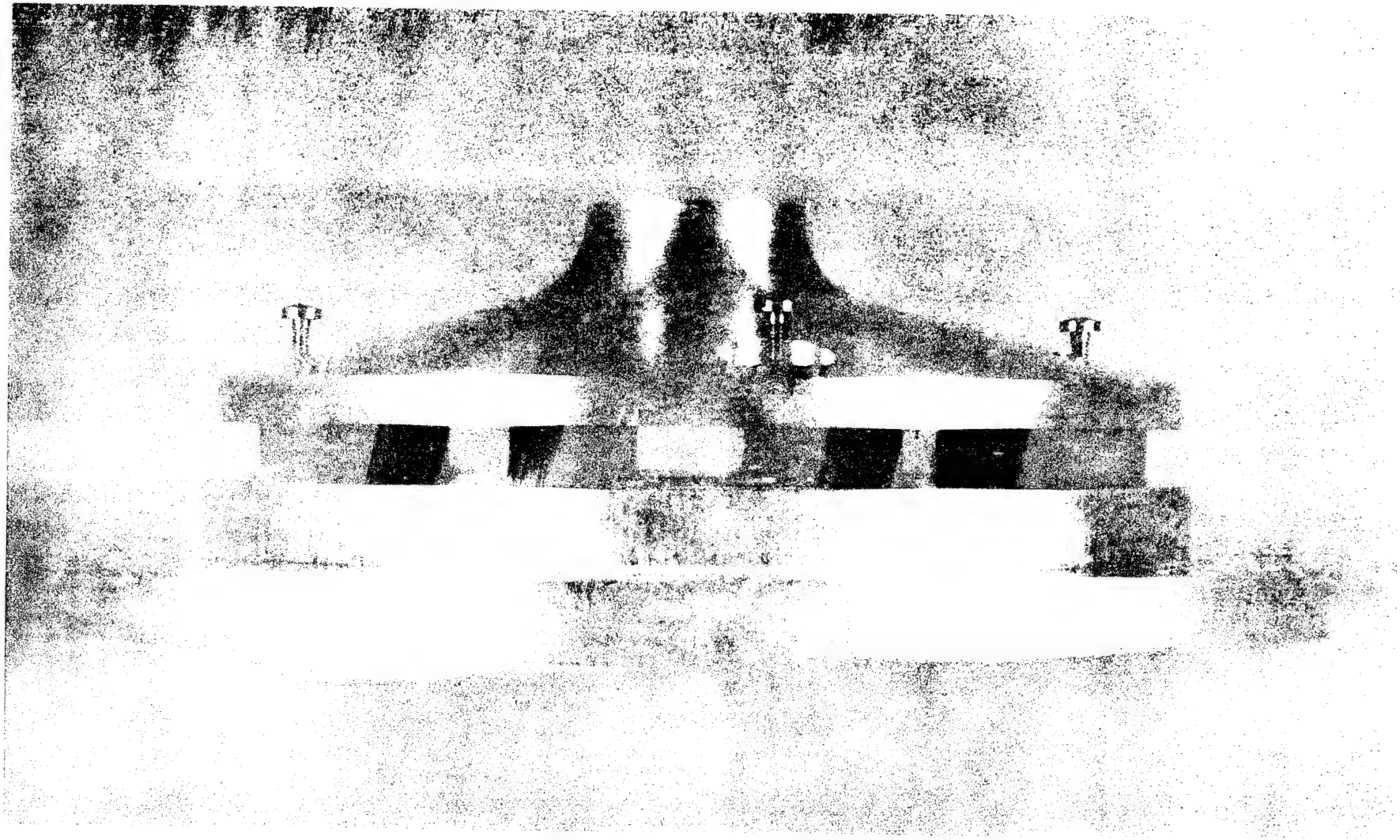

Fig. 33 Compression Test Sample Without Instrumentation

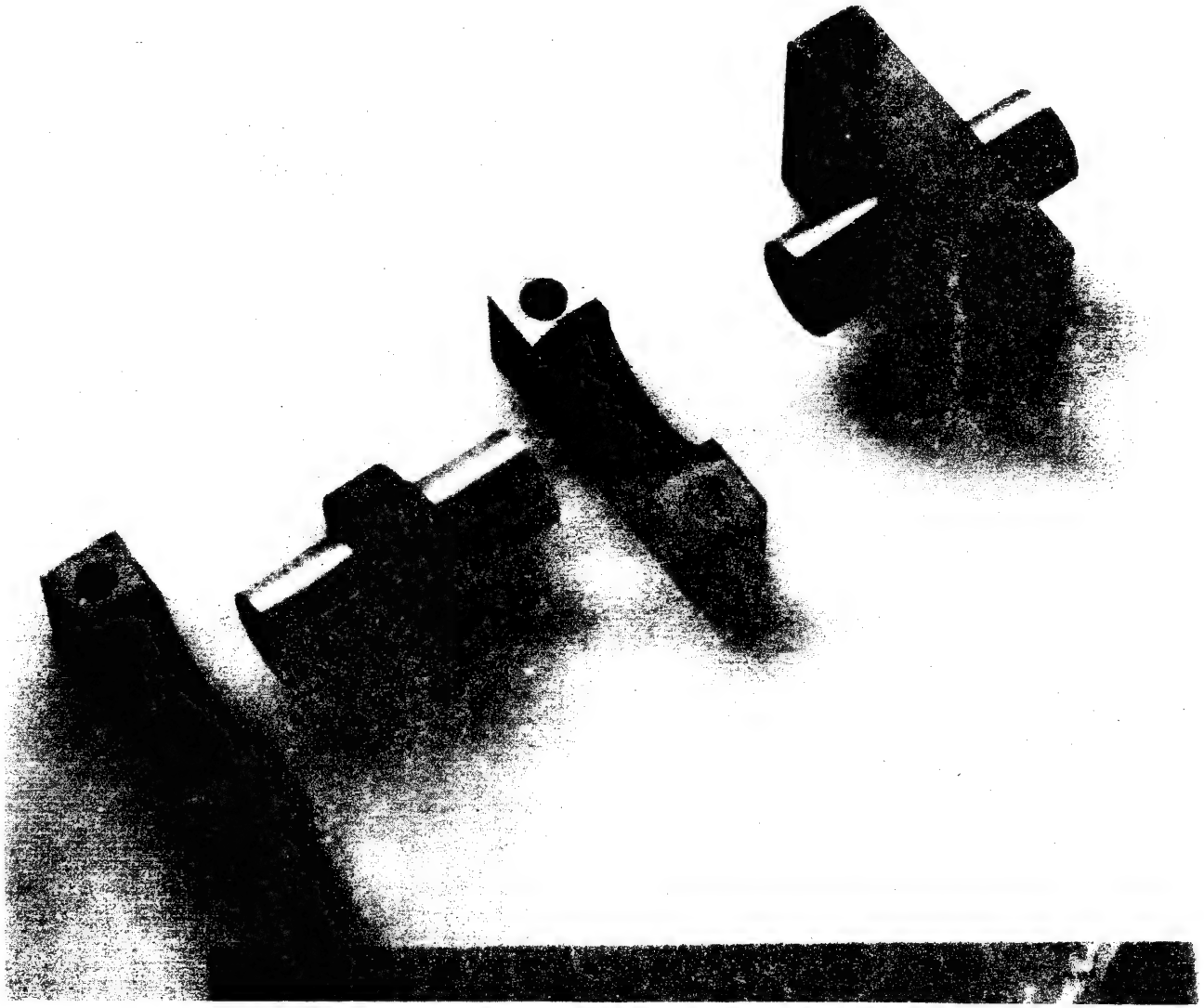

Fig. 34 Elastomer Cartridge Specimen Before Bonding of Outer Shell (Left) and with Outer Shell in Place (Right)

the highest resonant frequency and, through mass addition, resonant frequencies lower than 200 Hz could be achieved.

A second set of cartridge specimens was designed with identical metal dimensions but with only half the elastomer width of the first set. For this set the upper limit of the frequency range was reduced in proportion to the square root of the stiffness change, or by a factor of 1.4.

The elastomer dimensions (in mm) of the individual specimens for the two sets were as follows:

Width	Outer Diameter	Inner Diameter
9.5	28.6	19.1
4.7	28.6	19.1

A manufacturing drawing of the cartridge elastomer specimens is shown in Figure 35. The manufacturing process of the cartridge elements evolved from discussions with the manufacturer. Since a split shell was desired to allow a positive radial preload to be applied for testing, molding of the elastomer to both shaft and outer shell was not considered feasible because tensile stresses setup in the elastomer due to material shrinkage would not be circumferentially symmetrical. In the selected manufacturing process, the elastomer was first molded on the shaft and then ground on the outer diameter to the dimension of the circular hole in the assembled shell. With a small interference tolerance, the outer shell was then clamped around the elastomer and the assembly heat cured. Bonding of the elastomer to the shell was facilitated by a special coating applied to the bore of the shell prior to assembly. (The coating in the shell is clearly visible in Fig. 34.)

Prior to assembly into a complete test sample, all cartridge elements received a uniform preload of 5.3 percent of their uncompressed radial heights. Preloading was accomplished by replacing the shims measuring 1.625 mm between the halves of the outer shell with reduced thickness shims only 1.120 mm thick. The assembly of the individual elastomer cartridges into the complete test sample is depicted in Figures 36 through 38. An assembly of four cartridges was the largest number which could effectively be packaged within the existing size constraints of the test rig. In Figure 36 the four elastomer cartridges are shown next to the top plate to which they will be clamped with two clamps each. In the following picture (Figure 37) the cartridges have been placed into their locations and in Figure 38, the clamps have been placed over the cartridge element shafts and locked to the plate with bolts from beneath. At this stage, the elevations of the individual cartridge element shells were measured,

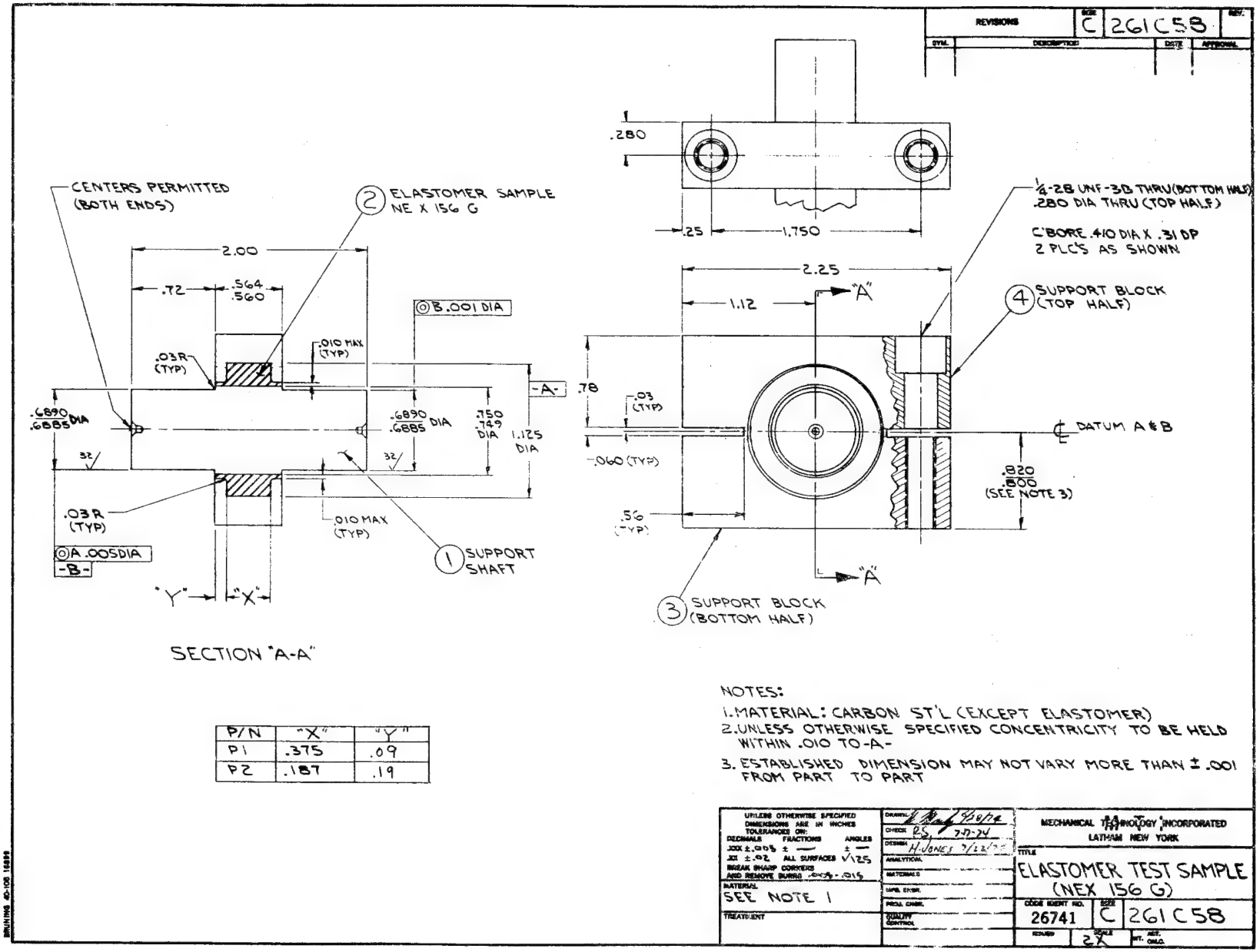

P/N	"X"	"Y"
P1	.375	.09
P2	.187	.19

NOTES:

1. MATERIAL: CARBON ST'L (EXCEPT ELASTOMER)
2. UNLESS OTHERWISE SPECIFIED CONCENTRICITY TO BE HELD WITHIN .010 TO -A-
3. ESTABLISHED DIMENSION MAY NOT VARY MORE THAN ± .001 FROM PART TO PART

UNLESS OTHERWISE SPECIFIED DIMENSIONS ARE IN INCHES
TOLERANCES ON:
DECIMALS FRACTIONS ANGLES
.XX ±.03 ± — ± —
.XXX ±.02 ALL SURFACES √125
BREAK SHARP CORNERS AND REMOVE BURRS .005-.015
MATERIAL SEE NOTE 1
TREATMENT

DRAWN 7/20/74
CHECK RS 7-7-74
DESIGN H. JONES 7/22/74
ANALYTICAL
MATERIALS
SAFE. ENGR.
PROJ. ENGR.
QUALITY CONTROL

MECHANICAL TECHNOLOGY INCORPORATED
LATHAM NEW YORK

TITLE
ELASTOMER TEST SAMPLE (NEX 156 G)

CODE IDENT NO. 26741 SIZE C 261C58
REVISED SCALE 2X WT. ONLY

Fig. 35 Elastomer Test Sample

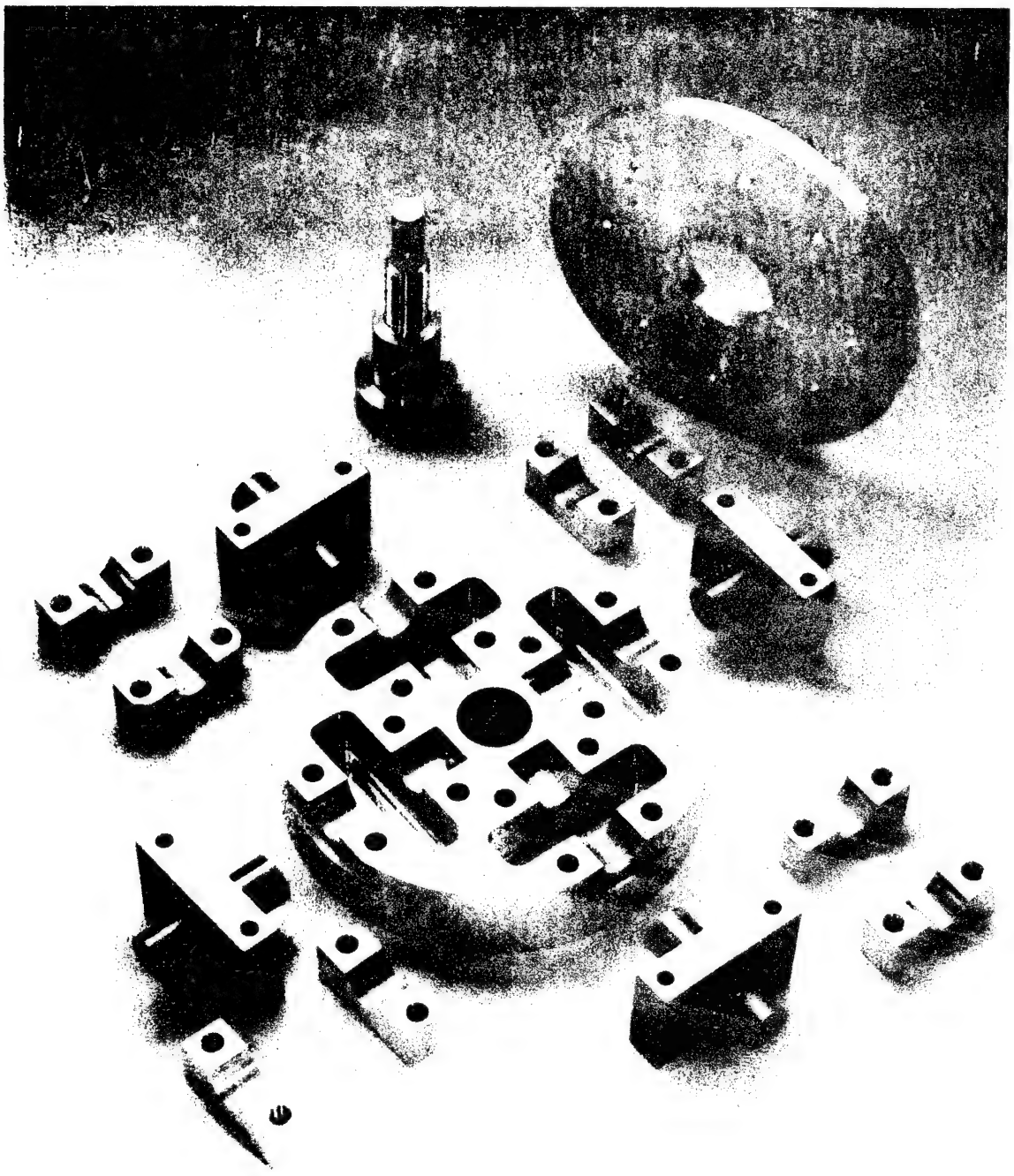

Fig. 36 Elastomer Cartridge Elements and Mounting Hardware for Top and Bottom Plates

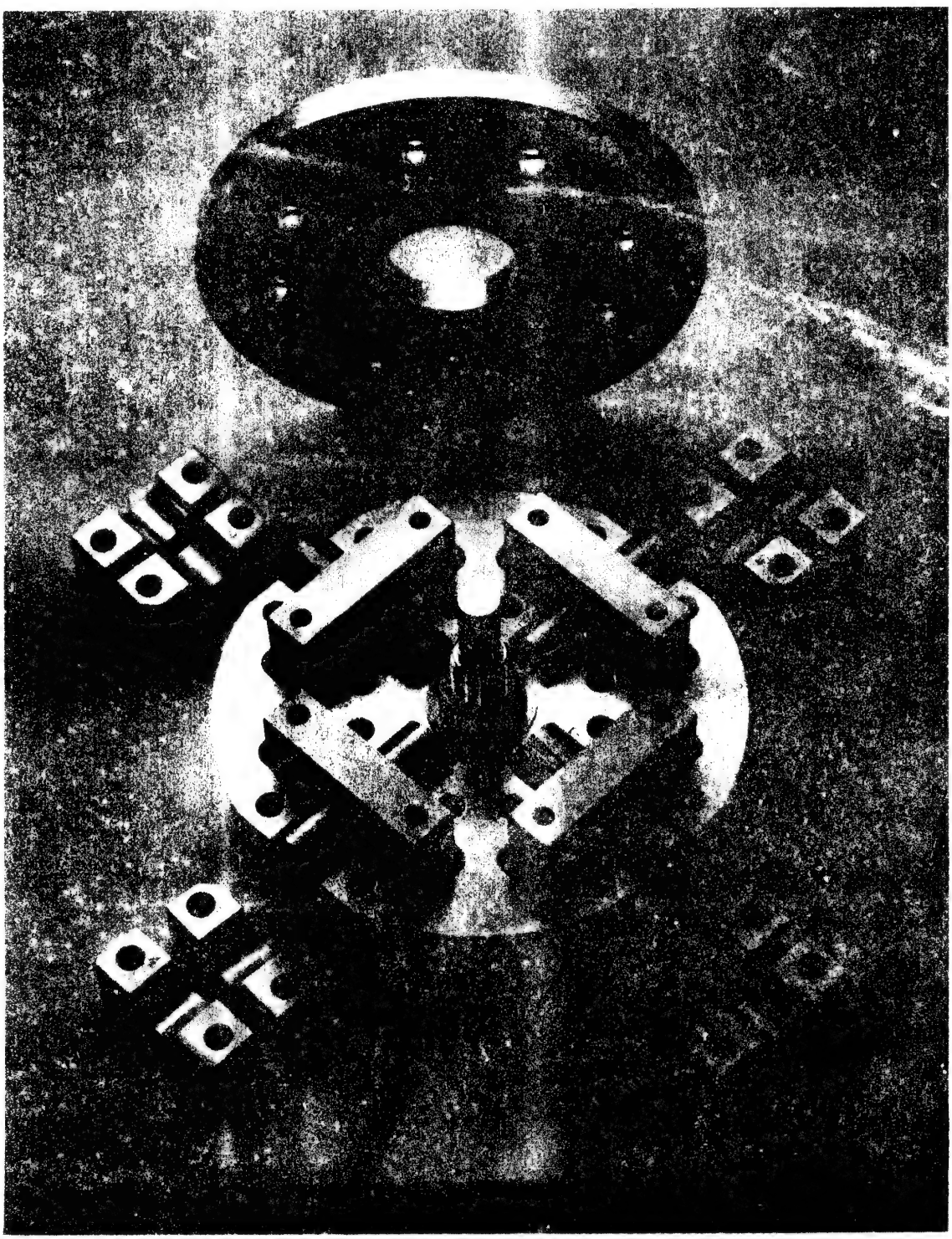

Fig. 37 Elastomer Cartridge Placed in Top Plate (Inverted Position)

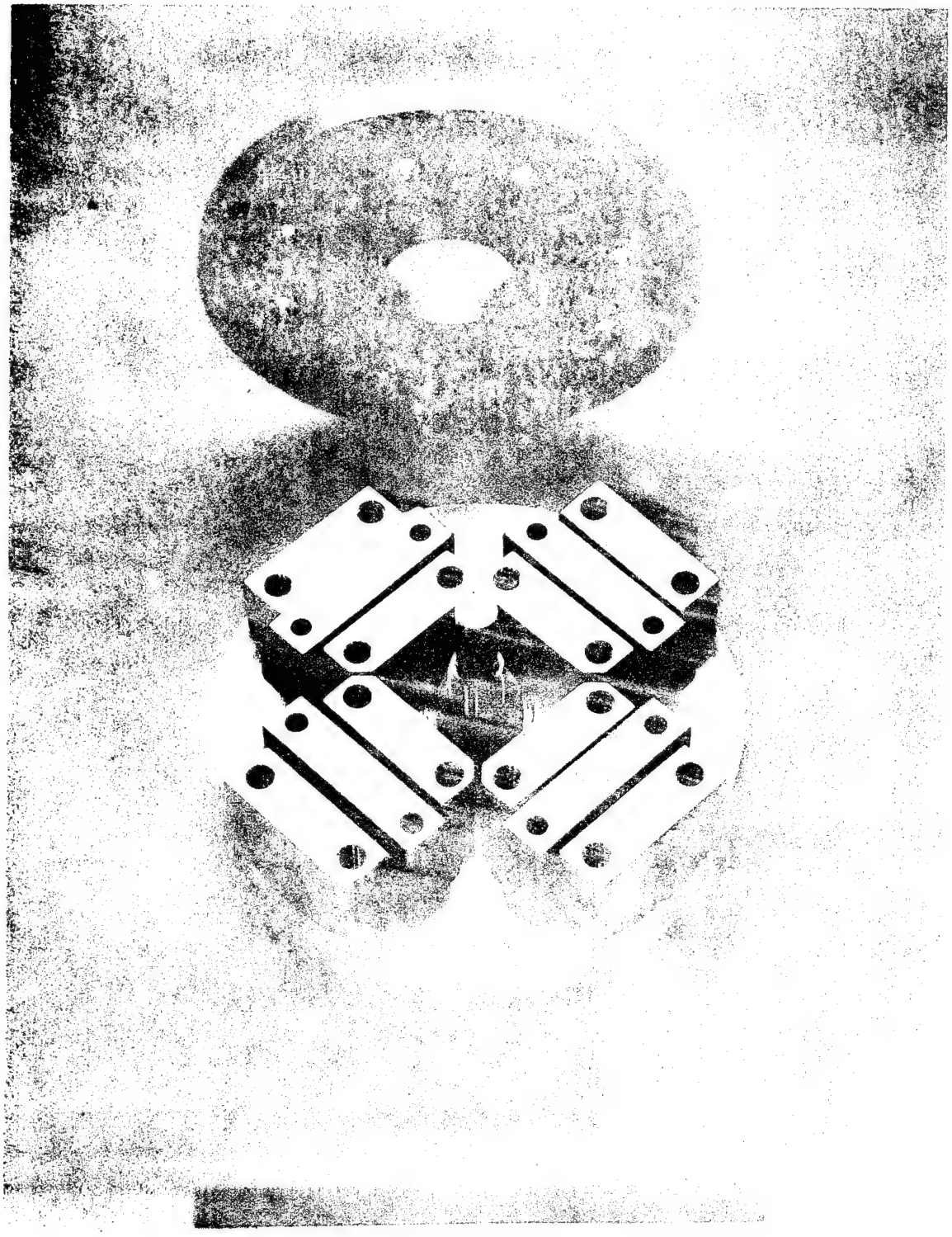

Fig. 38 Elastomer Cartridges Assembled in Top Plate

and shims were prepared for placement between the flat surface of the cartridge shell and the base plate (shown standing behind the assembly in Fig. 38). With shimming in place, differences in elevations between individual cartridge shells were held to less than 0.025 mm. The assembly of the second set of cartridge elements (narrow elastomer elements) received a very light grinding cut to remove some lack of parallelism between the flat shell surfaces and the bottom plate on two of the elements.

Instrumentation

The uncomplicated measurement requirements of the base excitation resonant mass testing method have been expounded before (see reference 1). Restated briefly, the measurement requirements for the experimental investigation of the elastomer dynamic properties are as follows:

1. Displacement measurement of elastomer support plate attached to the vibration table, relative to ground;
2. Displacement measurement of elastomer support plate attached to the resonant mass, relative to ground;
3. Phase angle measurement between displacement measurements (1) and (2) above;
4. Displacement measurement between two elastomer support plates (relative amplitude across the elastomer);
5. Vibration frequency;
6. Temperature of elastomer support plates and ambient air temperature in test specimen cavity;
7. Vibrational power dissipation across the elastomer test sample.

For convenience, acceleration was measured in (1) and (2) instead of displacement, but since the motions were sinusoidal the displacements were directly derivable from the accelerations. The very low level of motion of the shaker body (from which the shaker table is isolated by air springs with a very low resonant frequency) was also measured by accelerometers.

The input acceleration (1) was measured by an accelerometer located on the support base for the elastomer test samples. Output acceleration on the resonant mass (2) was determined from three accelerometers mounted directly to the top plate attached to the elastomer specimens. The use of three accelerometers, spaced 90 degrees apart, with their output signals displayed on one oscilloscope screen, permitted immediate detection of nonaxial motions of the resonant mass. When nonaxial motions of the resonant mass occur, they manifest themselves either as amplitude or phase angle variations among the three signals, or as a combination of both (testing experience revealed that noticeable nonaxial

motions occurred only in a few instances at certain test frequencies. Test data was generally discarded when nonaxial motions were observed.)

The displacement measurement (4) between the two elastomer support plates (relative amplitude across the elastomer) was accomplished with a noncontacting capacitance-type sensor.

Chromel-alumel type thermocouples were used to measure the temperature in the metal directly adjacent to one or two elastomer specimens in each assembly at a distance of approximately 1.6 mm from the elastomer surfaces. In the shear sample the thermocouples were embedded at the midface location. In the compression test samples the thermocouples were directly above and below the center point of the flat surfaces of the cylindrical specimens. In the cartridge specimens one thermocouple was located in the axis of the shaft at the midpoint of the elastomer and two additional thermocouples were placed diametrically opposite in the metal of the outer shell, approximately 1.6 mm from the outer diameter of the elastomer ring and also at the axial midpoint location of the elastomer ring.

Displacement and acceleration data, together with temperatures from individual thermocouples were displayed visually in digital form for monitoring purposes. As a permanent record, this data was also recorded on a 21-column digital printer.

Amplitude signals, from the four accelerometers and one displacement sensor, were sequentially switched by an analog scanner into a two-channel tracking filter, which provided a visual readout of vibration frequency and of two filtered amplitude signals. The base amplitude signal (acceleration) was fed at all times into one of the two channels of the tracking filter and from there into a phase meter where it served as a reference signal for the measurement of the phase angle of the three output acceleration signals and the displacement signal. The d-c values proportional to phase angle and amplitude from the phase meter and the tracking filter were than converted into digital form in digital voltmeters and printed. Each printed line contained phase angle and amplitude from one sensor, together with the vibration test frequency and the temperature indication from one thermocouple. (See Figure 39 for a schematic of the data acquisition system.)

To monitor the power dissipation in the test sample during testing, a previously developed power meter was used. This meter utilizes available acceleration and displacement signal inputs. The three (unfiltered) accelerometer signals from the top plate of the specimen holder (resonant mass signals) are averaged, to give a signal proportional to the net force on the resonant mass. This signal is therefore almost equal to

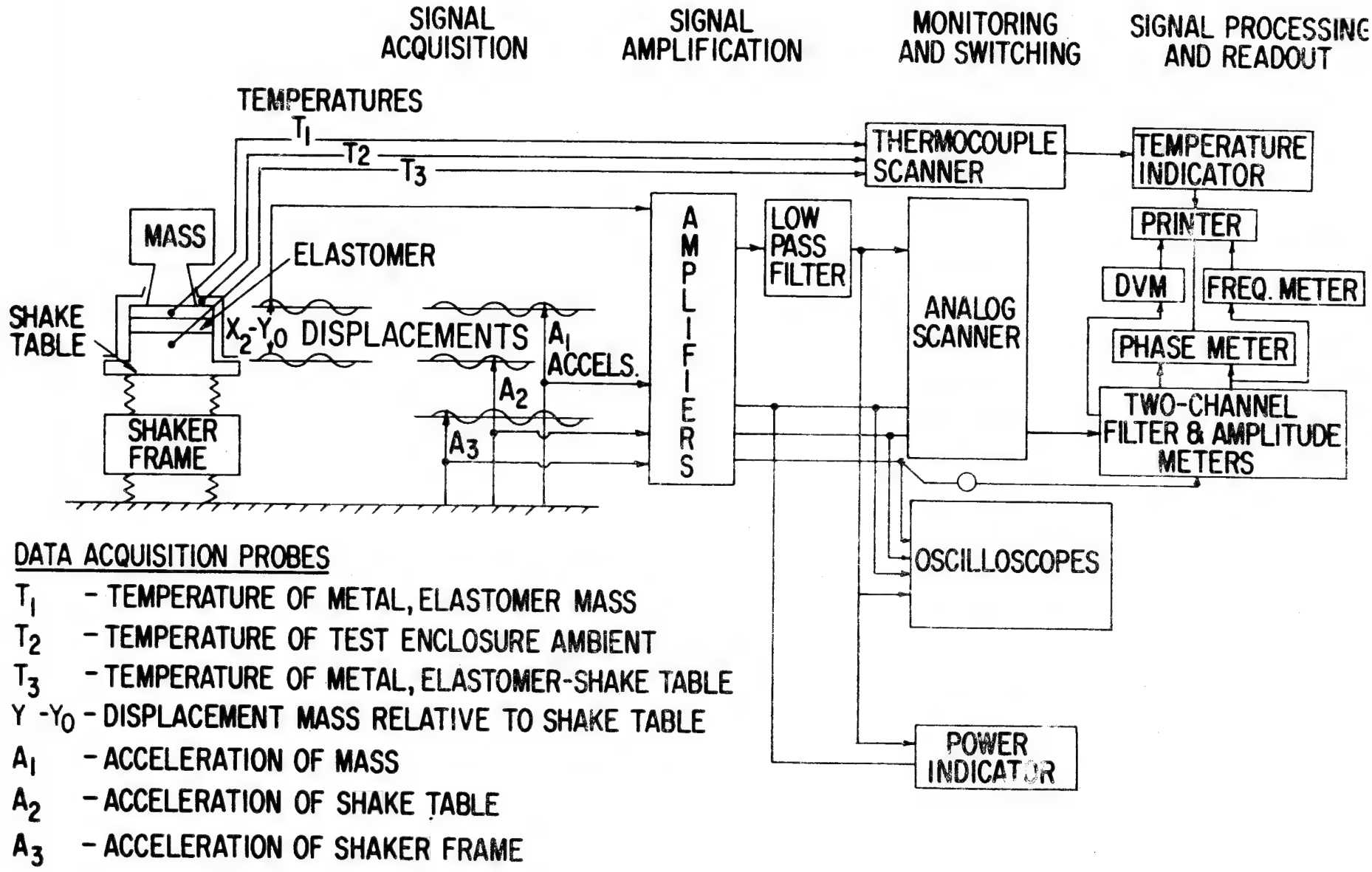

Fig. 39 Schematic of Data Acquisition System For Measurement of Elastomer Dynamic Properties

that portion of the force acting through the elastomer sample which is due to dynamic displacement (differing only by dynamic displacement forces in the air cylinder in those cases where static preload is applied to the test sample). The displacement signal, which indicates relative motion across the sample, is differentiated to give a signal proportional to rate of deformation (relative velocity). The force and velocity signals are multiplied together to give the instantaneous power. The instantaneous power consists of a d-c (average) component and a sinusoidally varying component and, by filtering out the sinusoidally varying component, the average power dissipation is obtained.

Testing Procedures

One of the major features of the current test program was the performance of the scheduled tests at near-resonance conditions. Since phase angle between base excitation and resonant mass response is an accurate indicator of the amount of damping in the region of resonance, measurements should preferably be made in the phase angle range between approximately 15 and 165 degrees (as discussed in reference 2). This requires that the test frequency be approximately 0.7 to 1.5 times the critical frequency of the elastomer-resonant mass system. Coverage of the full test frequency range of 100 to 1000 Hz with sufficient test points, therefore, necessitates changes in the size of the resonant mass. Typically, between five and seven different mass arrangements ranging from 0.5 to 15 kg were found sufficient to cover the desired test range. The smallest mass consisted of the elastomer test sample top plate only, with no additional weight attached. Increasingly larger mass combinations were obtained by attaching weights of up to 15 kg directly to the top plate. In the case of the compression sample, which was tested with preload applied through the air piston cylinder arrangement, weights up to 10 kg were directly attached to the preload piston.

Once any one of the elastomer test samples had been mounted on the shake table and the necessary instrumentation installed and connected, a typical test sequence proceeded as follows:

1. A resonant mass was selected and installed.
2. In the case of the compression tests, the elastomer sample was statically preloaded.

3. The elastomer test sample cavity was enclosed and the temperature control system given time to adjust ambient temperature to the desired value.

4. With low vibration levels applied to the base of the elastomer holding fixture, frequency scans were conducted until the approximate resonant frequency of the system was found. (For selected cases an exact determination of the system resonant frequency was subsequently made by tracing, on an X-Y plotter, the d-c value proportional to the resonant mass acceleration amplitude as a function of the base excitation frequency.) It may be noted here that, for a base-excited single-degree of freedom spring-damper-mass system, resonance occurs at an angle smaller than 90 degrees. The deviation from 90 degrees is essentially determined by the amount of damping in the system.

5. While the predetermined vibrational power dissipation level in the elastomer test sample was maintained by adjustment of the shaker power input level, the vibration frequency was reduced until the phase angle decreased to a value between 15 and 25 degrees. Provided none of the acceleration and displacement signals showed signs of abnormalities (distortions, or indications of nonaxial motion of the resonant mass), a data point was recorded. The recording of one data point consisted of one complete printout of all amplitudes (up to six individual signals), associated phase angles and test frequency, and all temperatures from the thermocouples located in the test specimen holding plates.

6. Stepwise increases in vibration frequency were imposed and between six and eight data points were recorded until the phase angle reached approximately 165 degrees.

7. Tests, comprising steps 1 through 6, were then repeated with each of the remaining masses in turn, each mass giving a dynamic system with a different resonant frequency.

8. Shake table power was turned off and, for the compression tests the preload on the elastomer sample was increased to the next higher value.

9. Steps 4 through 7 were repeated until data at all desired preloads were obtained.

10. Shaker table power was turned off and, for the compression sample, all preload on the elastomer removed. The elastomer test sample was then given time (at least one hour) to recover its original, uncompressed height (as indicated

by displacement probe readings) before tests at either higher ambient temperatures or a higher power dissipation level were commenced.

The result of this test sequence is a printed data set defining the measured amplitudes for each vibration sensor, and the temperature values at each frequency point for a series of mass values. Together with data specifying the test conditions, this data set is entered directly onto punched cards which are processed by a computer. All required editing and averaging functions are performed by the computer, then stiffness K_1, and damping, K_2, are calculated at each frequency as follows:

$$K_1 = \frac{\omega^2 M [\alpha^2 - \alpha \cos \varphi]}{\alpha^2 - 2\alpha \cos \varphi + 1} \tag{66}$$

$$K_2 = \frac{\omega^2 M \alpha \sin \varphi}{\alpha^2 - 2\alpha \cos \varphi + 1} \tag{67}$$

where α is the transmissibility, that is the ratio of absolute values of output to input acceleration; and
φ is the phase angle between input and output acceleration signals.

The development of these expressions for stiffness and damping is presented in Appendix B.

Test Parameter Ranges

It is the purpose of this Section to provide an overall guide to the test cases reported for this investigation and to indicate the range of parameters covered in each case. The method of presentation chosen is predominantly that of data plots showing calculated elastomer stiffness and damping (in N/m) versus test frequency. These plots were originally prepared by computer line-printer, and offered a rapid, economical means to evaluate the combined effect of such constant test parameters as dissipation power level in the specimen and ambient temperatures. The purpose of presenting these plots in this section is to indicate the extent of parameters, particularly in the frequency domain. Lines through individual data points have, therefore, not been extrapolated beyond either the lowest or the highest frequency data point. (The following section of the report presents the test data in expanded format, one frame for each test condition, together with theoretical correlations and comparisons.)

Tests Performed on Shear Samples

Tests were performed on two different shear samples. One sample consisted of eight elastomer strips, each 1.27 cm high and the second

sample was made up of four strips each having twice the height (2.54 cm) of the eight-strip group. The eight-strip sample was tested over a range of ambient temperatures and the four-strip sample was tested over a range of power dissipation levels. Testing of the eight-strip sample was suspended because it was believed that chemical decomposition of the elastomer had been initiated when the ambient temperature had been allowed to go up to 100-110 C during the 93 C tests. Evidence of damage was inconclusive - a retest at 32 C (Fig. 40) did not show significantly different behavior from original tests, but subsequent tests at 5 C ambient temperature showed elastomer damping behavior that appeared anomalous when compared to data obtained at other temperatures.

The range of test parameters (frequency and ambient temperature) covered in tests of the eight-strip sample are shown in Figure 41. The ranges of power level and frequency covered in tests of the four-strip sample are shown in Figure 42. A listing of shear test cases is given in Table VI.

The power dissipation levels are nominal values, representing the average of values calculated, after the fact, from measured frequency, damping and amplitude (power = $0.5\ \omega\ Y^{*2}\ K_2$). The values for shear and compression specimens are generally higher than planned. It was intended that each test would be conducted at a constant power level but it was identified, towards the end of the series of shear specimen tests, that a constant power meter setting actually resulted in a variation with frequency: low frequency dissipation was higher than average and high frequency dissipation was lower than average. The average value was also higher than intended. This characteristic is shown in Figure 43. Following a recalibration of the meter it was possible, during the cartridge tests, to maintain more consistent, targeted, dissipation levels.

The highest test frequency is limited by the lightest resonant mass without the preload piston. This limit is 0.5 Kg and frequencies for the stiffest shear specimen are as high as 1600 Hz. The lowest test frequency is governed by the highest mass which can be resonated without rocking motion and without applying an excessive preload (arbitrarily limited to one percent). The normal upper mass limit was 15 Kg. It may be seen, in Figures 41 and 42 that, with these limitations, the test frequency range covered shifts downwards as the stiffness of the test specimen falls - either with increasing temperature or with increasing dissipation.

Figures 44, 45 and 46 present some interesting comparisons which relate mainly to the test method. In Figure 44 test series 4-01→06 and 4-19→24 are compared. The conditions for each set were identical but the two tests were separated by a two week time delay in which the rig was disassembled and reassembled. The agreement between the two is good and indicates that good repeatability can be achieved with the test method.

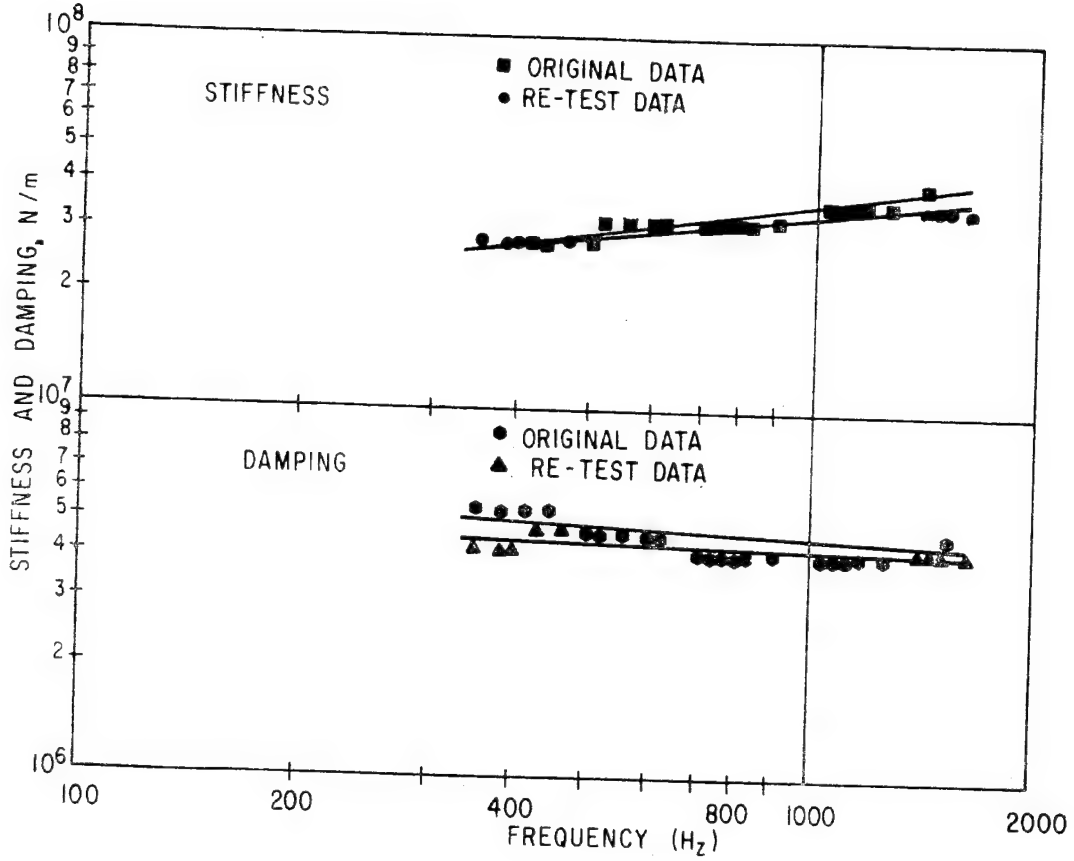

Fig. 40 Stiffness and Damping for Eight-Strip Elastomer Shear Specimen at 32 C Ambient Temperature and 0.062 watt/cm^3 Power Dissipation

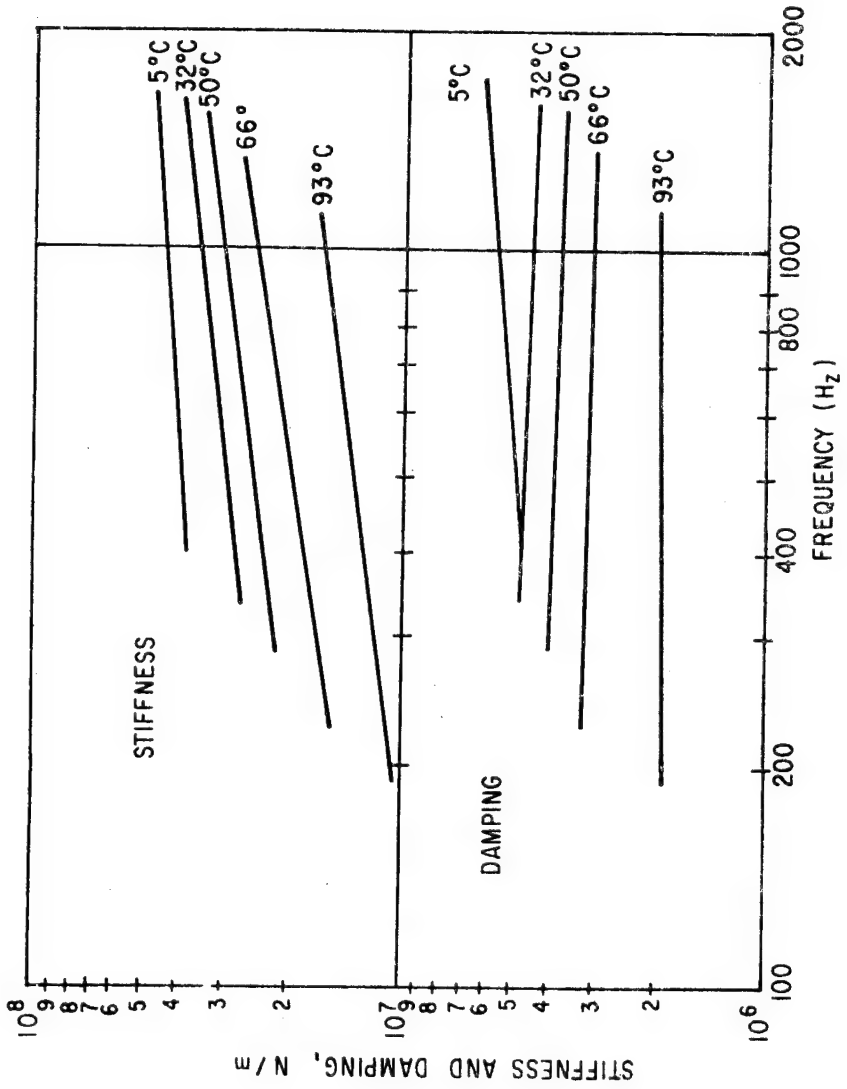

Fig. 41 Stiffness and Damping for Eight-Strip Elastomer Shear Specimen at Ambient Temperatures of 5, 32, 50, 66, and 93 C and 0.062 watt/cm^3 Power Dissipation

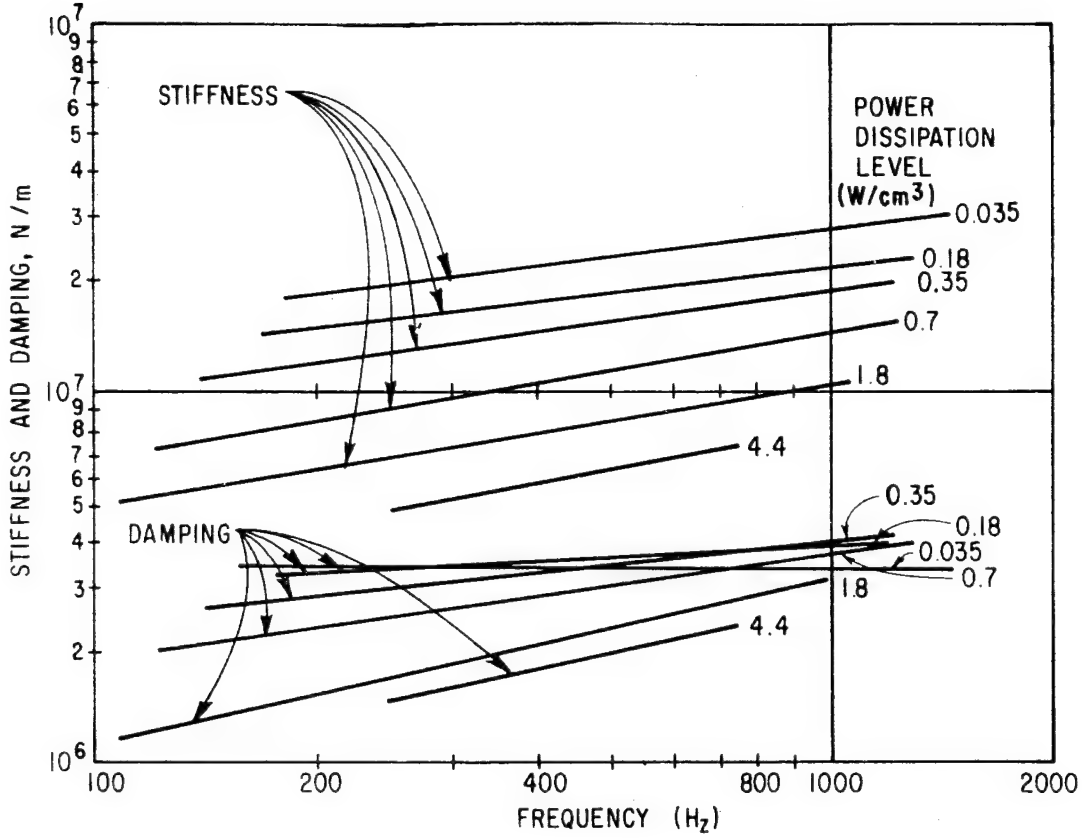

Fig. 42 Stiffness and Damping for Four-Strip Elastomer Specimen at 32 C and Six Power Dissipation Levels

TABLE VI. LISTING OF SHEAR SAMPLE TEST CASES

[Test Conditions Common To All Tests]
Preload On Sample: None

Test Case Number	Ambient Temperature (C)	Mass On Elastomer (Kg)	Power Dissipation Level watt/cm^3	Remarks
Shear Sample With 8 Strips				
8-01→05	32	0.45, 0.75, 1.37, 2.34, 4.85	0.062	
8-07→11	50	↓	↓	
8-12→16	66		0.062	
8-12→21	93		0.031	
8-22→26	5		0.062	
8-27→28	32	↓		
Shear Sample With 4 Strips				
04-01→06	32	0.45, 0.75, 1.37, 2.34, 4.81, 9.6	0.062	
04-07→12	66	↓	↓	
04-13→18	5			
04-19→24	32			
04-25→30	66			
04-31→35	32	1.04, 1.97, 2.94, 5.75, 10.3	0.062	With Air Cylinder, Holes Closed
04-38→43	32	↓	0.035	With Air Cylinder, Holes Closed
04-44→49	32		↓	With Air Cylinder, Holes Open
04-50→55	66			With Air Cylinder, Holes Closed
04-56→61	66			With Air Cylinder, Holes Open
04-62→67	32	0.45, 0.75, 1.37, 2.34, 4.81, 9.6	0.035	Nominal Power Dissipation Level
04-68→73	32	↓	0.176	5X Nominal Power Dissipation Level
04-74→79	32		0.352	10X
04-80→85	32		0.704	20X
04-86→91	32		1.76	50X
04-92→95	32	↓	4.40	125X ↓

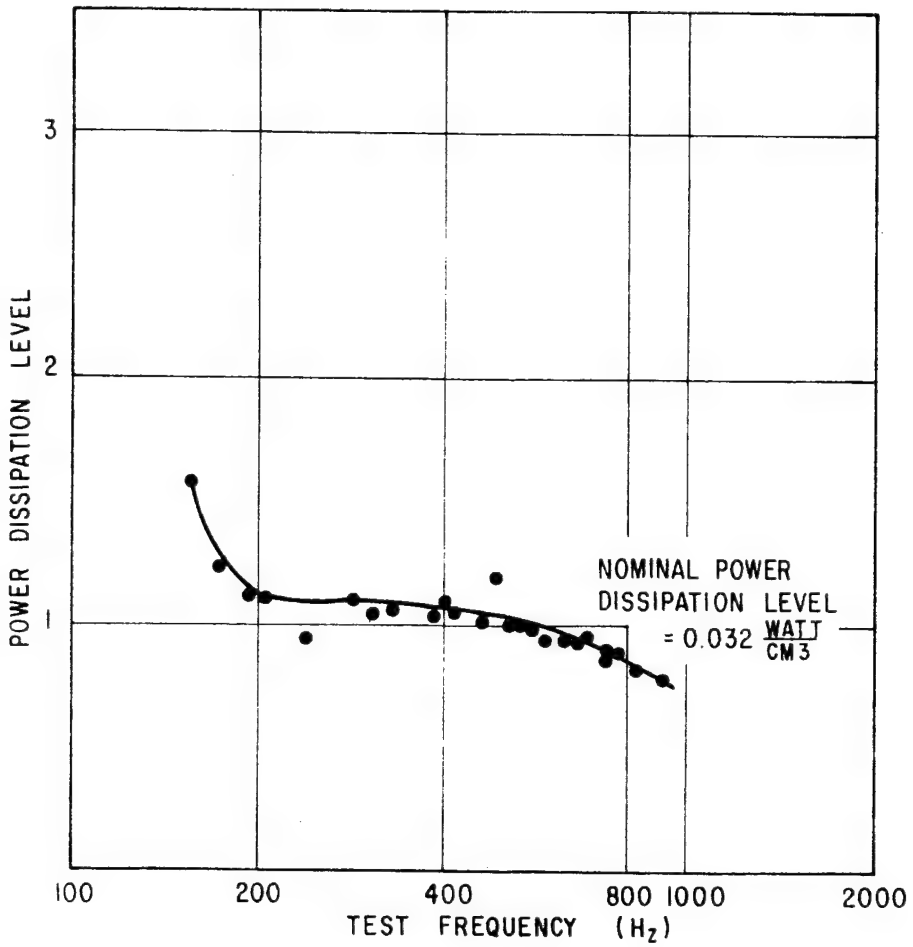

Fig. 43 Actual Power Dissipation Values for Test Case 4-56-61 (Four-Strip Shear Specimen at 66 C)

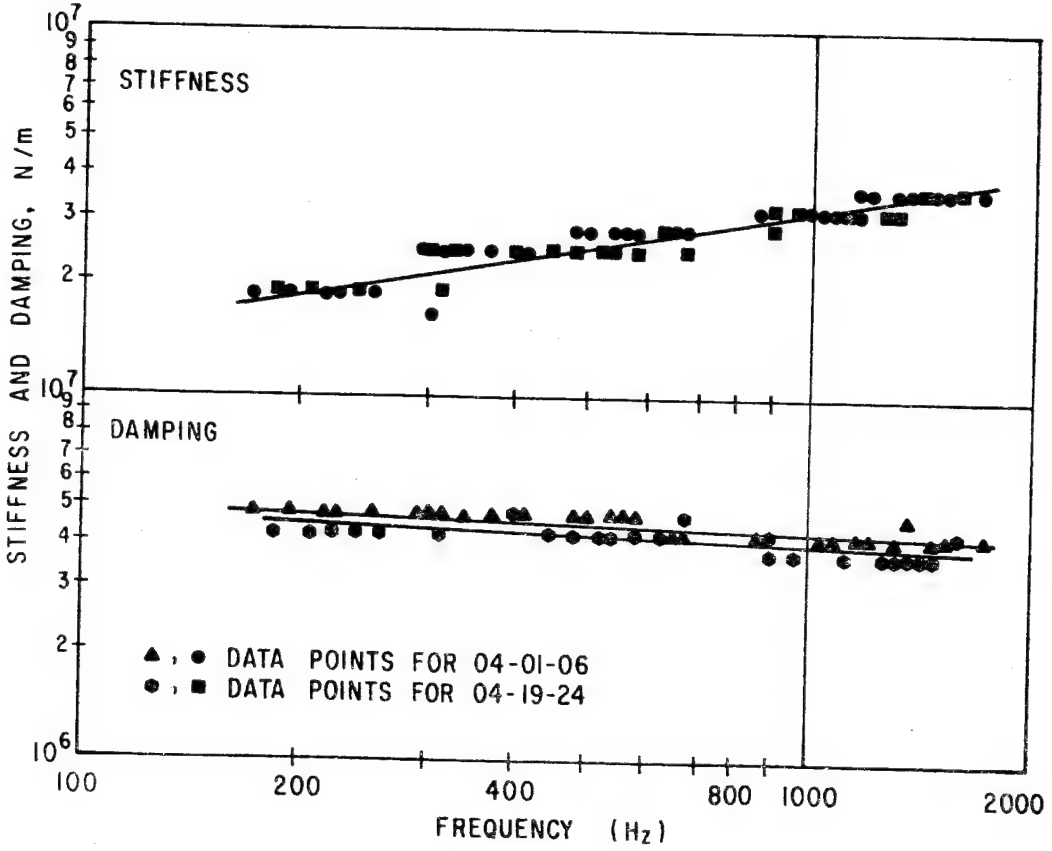

Fig. 44 Stiffness and Damping. Comparison for Two Sets of Shear Specimen Test Taken Under Identical Test Conditions at 32 C Ambient Temperature and 0.062 watt/cm^3 Power Dissipation

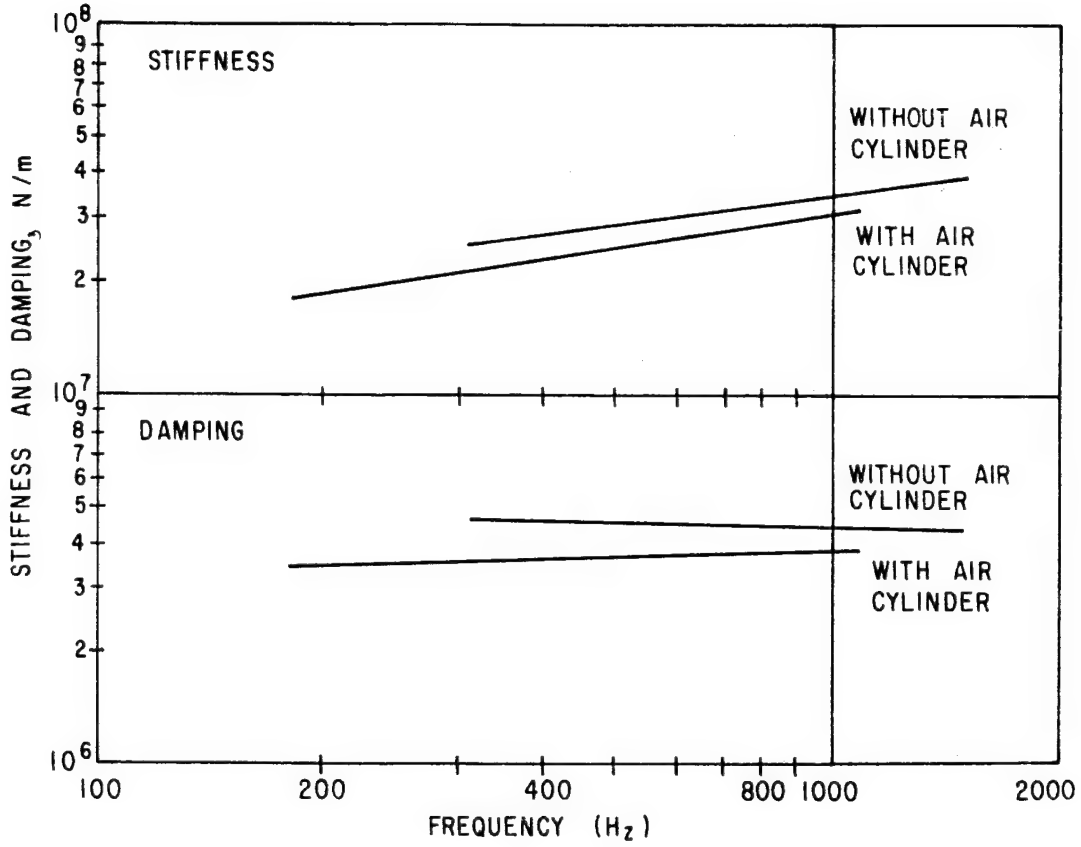

Fig. 45 Stiffness and Damping for Shear Test Specimen at 32 C with and Without Lower Air Cylinder of Test Rig

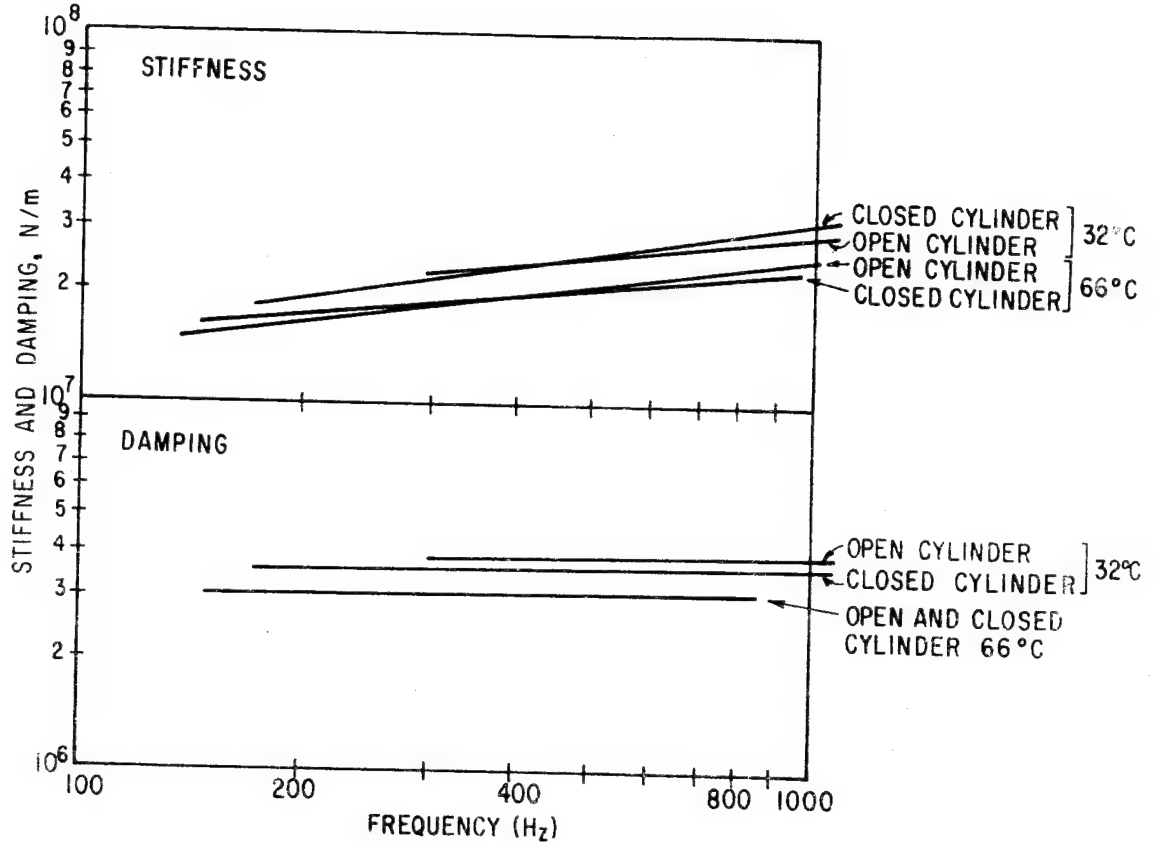

Fig. 46 Stiffness and Damping for Shear Specimen at 32 and 66 C With Lower Air Cylinder Vent Holes Open and Closed

In Figure 45 data sets 4-38→43 and 4-62→67 are compared. The first set was obtained without the air cylinder (preload piston) and the second set was obtained with the air cylinder in place, and sealed, but not pressurized. In other words, apart from the presence of the piston, the conditions are identical. The differences between the two sets of data are small, but they are undeniably in the direction of lower stiffness and damping with the cylinder in place. This result is surprising, since analysis of the test rig mechanics indicates that the air spring stiffness and damping will both tend to act in parallel with the test specimen. However, the result was fully confirmed by data sets 04-01→06 or 04-19→24 and 04-31→35 (not shown in graphical presentation). This anamolous trend is not fully understood at this time, but is assumed to be the result of flexibility in test rig elements (for example, the piston or cylinder head).

In Figure 46 data sets 4-38→43 and 4-44→49 for 32 C are compared and data sets 4-50→55 and 4-56→61 for 66 C are compared. In each comparison the preload piston is present, but between the first and second set, the only difference is that vent holes in the cylinder have been opened. The effect of this change is clearly negligible, leading to the conclusion that anomalous behavior of the air cylinder is not a result of pressure fluctuations.

These anomalies with the preload piston confirm that small uncertainties are introduced in tests with the piston and that the most reliable elastomer specimen data will be obtained without the preload piston.

Tests Performed on Compression Samples

Under Phase III all compression sample tests were performed on an assembly of ten elastomer specimens 12.7 mm in diameter and 6.35 mm in height (see Fig. 35). Tests were generally conducted at 2-1/2 percent preload and then repeated (for each series of masses) at five percent preload. At a nominal power dissipation level of 0.062 watt/cm^3, the compression sample was tested at three ambient temperatures; 2, 66 and 93 C. At 32 C ambient temperature the sample was tested at increased power dissipation levels of approximately 0.50, 1.1 and 2.2 watt/cm^3. (Results from tests at 32 C and low nominal power dissipation level (0.062 watt/cm^3) were available from a previously conducted test series in Phase II.)

The frequency range covered in compression sample tests extended from approximately 150 Hz for high temperature tests to 1000 Hz for low temperature tests. Coverage at the high frequency end was generally not as high as for the shear sample tests, due to the preload piston which increased minimum mass.

Test range parameters for all compression sample tests are shown in Table VII.

Graphical representations of the test ranges covered for the compression

TABLE VII. LISTING OF COMPRESSION TEST SAMPLE CASES

Test Case Number	Mass On Elastomer (Kg)	Ambient Temperature (C)	Preload On Sample (%)	Power Dissipation Level (watt/cm^3)
10-01→05	0.91, 1.81, 2.78, 3.73, 5.35	66	2.5	0.062
10-06→09	0.91, 1.81, 2.78, 3.73, 5.35	60	5	0.062
10-10→13	0.91, 1.81, 2.78, 3.73, 5.35	93	2.5	0.062
10-14→17	0.91, 1.81, 2.78, 3.73, 5.35	93	5	0.062
10-18→21	5.35, 3.72, 1.81, 0.91	32	2.5	0.44
10-32→36	0.41, 1.81, 3.73, 5.35	32	5	0.55
10-25→28	0.41, 1.81, 3.73, 5.35	32	2.5	1.1
10-29→32	0.41, 1.81, 3.73, 5.35	32	5	1.1
10-37→39	0.41, 1.81, 3.73, 5.35	32	2.5	2.2
10-41→44	0.41, 1.81, 3.73, 5.35	2	2.5	0.062
10-45→48	0.41, 1.81, 3.73, 5.35	2	5	0.062

sample are shown in Figures 47 and 48. Both figures are for the 2-1/2 percent preload test case only; very similar results were obtained with five percent preload on the test sample. The consistency of the stiffness and damping values obtained for the compression test sample appears to be good, following very much the trend lines already observed and discussed for the shear test sample.

Test Performed on Cartridge Samples

Two cartridge type samples were tested, one with elastomer elements 9.55 mm wide and a second with elements half as wide (4.75 mm). Both samples were first tested at four ambient temperatures: 32, 43, 66 and 80 C, and then at several power dissipation levels with ambient temperatures controlled at 32 C. The frequency range covered in these tests is indicated, for each ambient temperature and power dissipation level test case, in Figures 49 and 50 for the wide cartridge; and in Figures 52a & 52b for the narrow cartridge. Due to the lower overall stiffness of the narrower element sample the test frequency range did shift somewhat towards lower frequencies.

The effect of static preload produced by the air cylinder (2-1/2 and 5 percent deflection of the height of the elastomer material annulus) was investigated for the wide cartridge specimen only. In Figure 51 results without the preload piston attached are compared with results obtained with the piston attached and pressurized to both 2-1/2 and 5 percent preload. The effect of introducing the piston appears to be much stronger than the effect of doubling the preload. While no direct comparison, showing the effect of the piston alone, is available for the cartridge specimen, the indications are, just as for the shear specimens, that the introduction of the piston reduces the observed stiffness and damping.

A listing of all cartridge sample test cases is given in Table VIII.

Static Tests

Static stiffness tests were conducted with the elastomer samples mounted in the test rig and the displacement probe output used for automatic recording of elastomer specimen deflection. Using the same environmental control as for dynamic tests, static deflection data was obtained at temperatures between 2 and 93 C. Application of load was controlled manually by pressurization of the preload cylinder.

Static deflection tests of elastomer materials differ drastically from those associated with most engineering materials. An elastomer under load will deflect rapidly to a certain extent as the load is applied and then continue deflecting at a much lower rate for an appreciable amount of time. The rate of deflection decreases with time after each step in load application, but for the presently considered material, increases with increased total load on the sample.

One example of a typical load deflection relationship, as obtained for

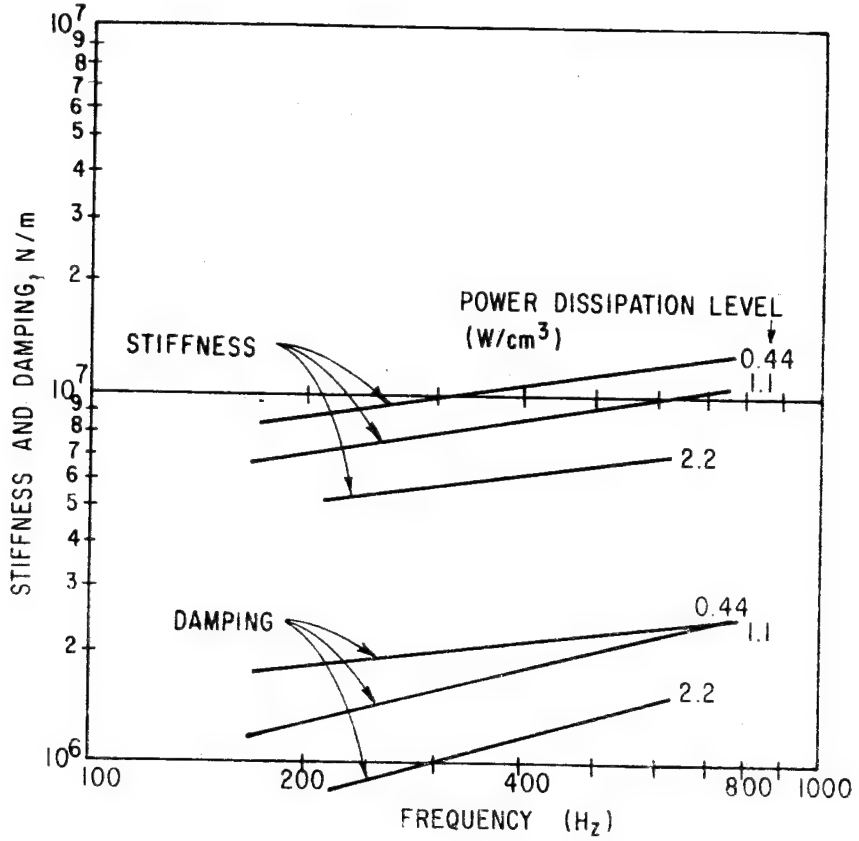

Fig. 47 Stiffness and Damping for Compression Test Specimen with 2-1/2 Percent Preload at 32 C for Various Power Dissipation Levels

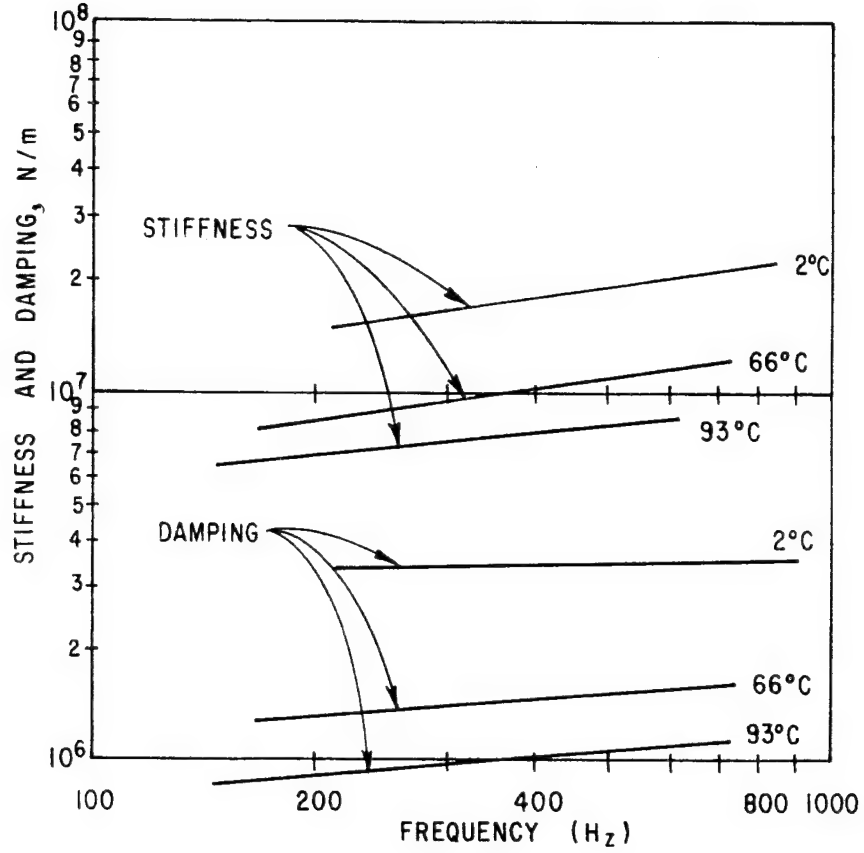

Fig. 48 Stiffness and Damping for Compression Test Specimen with 2-1/2 Percent Preload and 0.062 Watt/cm^3 Power Dissipation at Various Ambient Temperatures

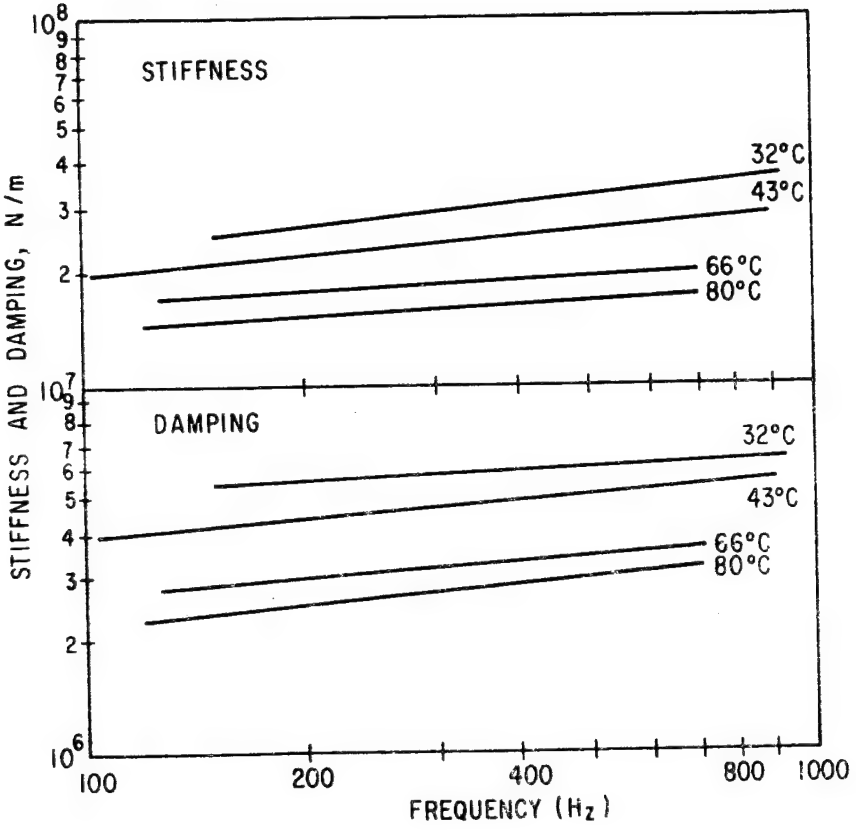

Fig. 49 **Stiffness and Damping for Wide (9.55 mm) Cartridge Element Specimen at Ambient Temperatures of 32, 43, 66 and 80 C and 0.044 watt/cm^3 Power Dissipation**

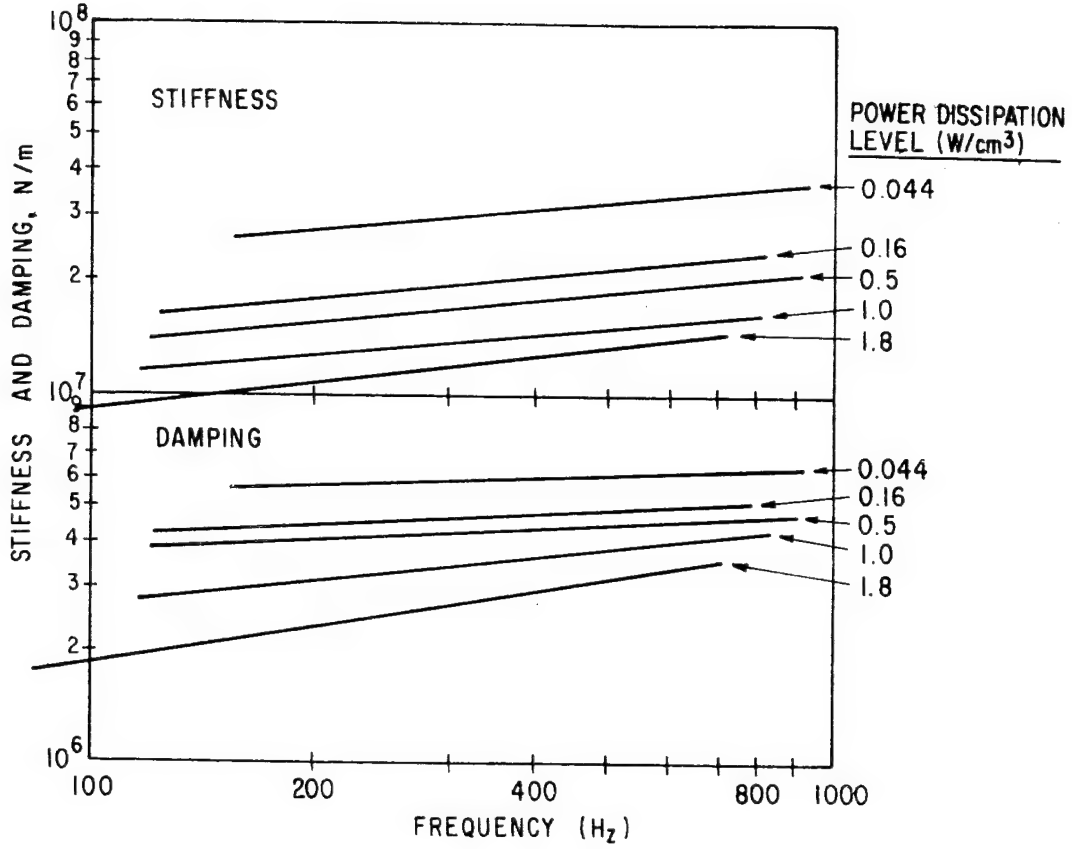

Fig. 50 Stiffness and Damping for Wide (9.55 mm) Cartridge Element Specimen at 32 C Ambient Temperature and Five Power Dissipation Levels

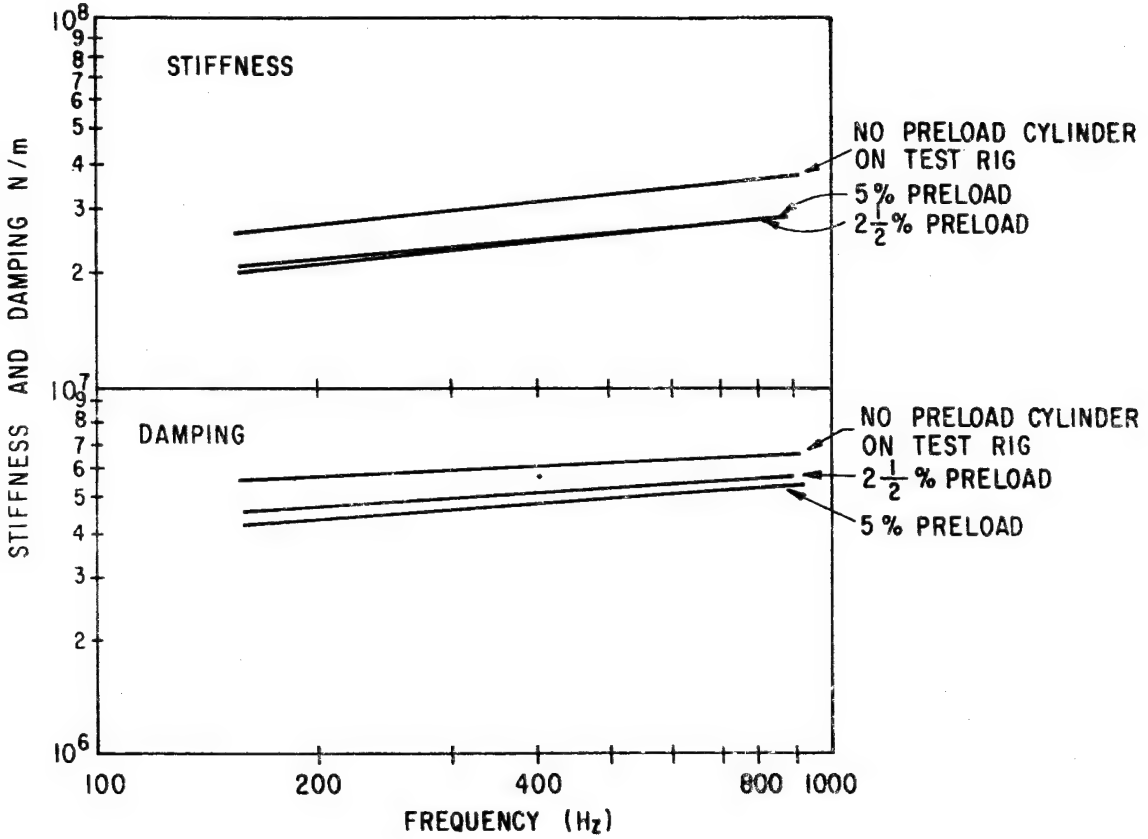

Fig. 51 Stiffness and Damping for Wide (9.55 mm) Cartridge Element Specimen at 32 C Ambient Temperature with 2-1/2 and 5 Percent Preload and Without Preload Cylinder In Place (0.044 watt/cm^3 Power Dissipation)

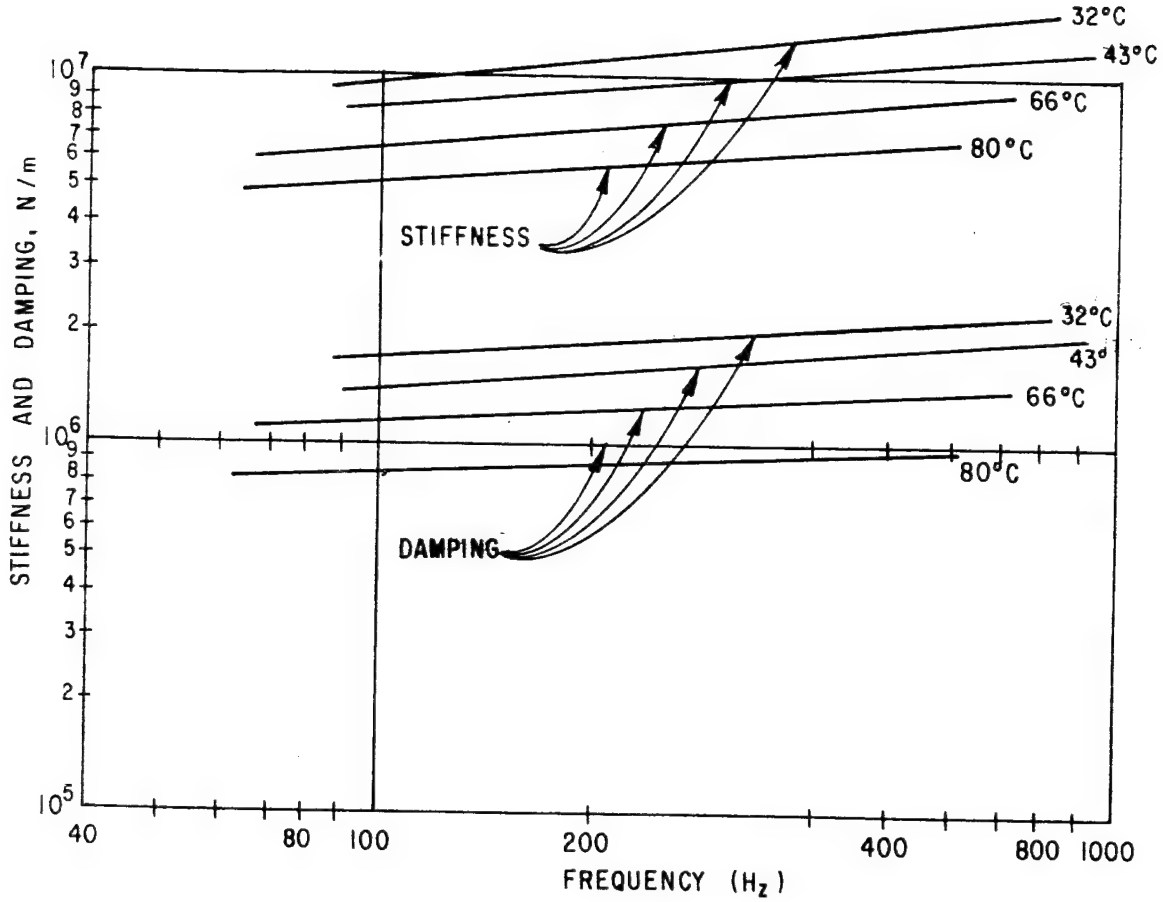

Fig. 52a Stiffness and Damping for Narrow (4.75 mm) Element Cartridge Specimen at 32, 45, 66 and 80 C Ambient Temperature and 0.022 watt/cm^3 Power Dissipation

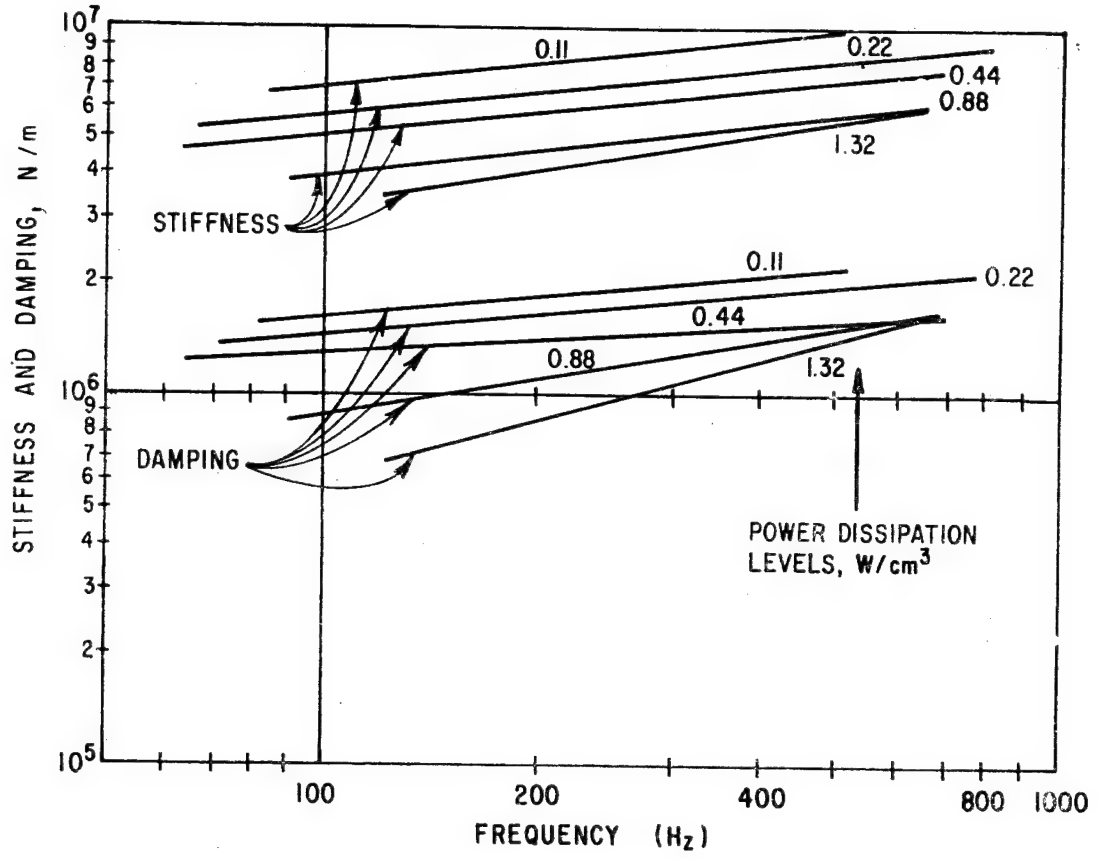

Fig. 52b Stiffness and Damping for Narrow (4.75 mm) Element Cartridge at 32 C Ambient Temperature and 5 Percent Power Dissipation Levels

TABLE VIII. LISTING OF CARTRIDGE TEST SAMPLE CASES

Test Case Number	Ambient Temperature (C)	Mass On Elastomer (Kg)	Power Dissipation Level (watt/cm^3)
Sample Element Width 9.55 mm			
4C-01→06	32	2.06, 2.98, 3.96, 6.51, 11.27, 15.65	0.044
4C-07→13	43	↓	0.044
4C-14→20	66	↓	0.044
4C-21→26	32	↓	0.16
4C-27→32	32	↓	0.5
4C-33→38	32	↓	1.0
4C-39→44	32	↓	1.8
4C-45→50	80	↓	0.044
*4C-51→54	32	2.26, 3.46, 4.46, 11.77	0.044
**4C-55→58	32	2.56, 4.46, 11.77, 16.14	0.044
Sample Element Width 4.75 mm			
4C2-01→04	32	2.06, 3.96, 6.51, 15.67	0.022
4C2-05→08	43	↓	0.022
4C2-09→12	66	↓	0.022
4C2-13→16	80	↓	0.022
4C2-17→20	32	↓	0.11
4C2-21→24	32	↓	0.22
4C2-25→28	32	↓	0.44
4C2-29→32	32	↓	0.88
4C2-33→36	32	↓	1.32

*With Piston (2-1/2% Preload).
**With Piston (5% Preload).

the elastomer cartridge sample at 66 C, is shown in Figure 53. Beginning at time zero with no load on the sample (upper left-hand corner in Figure 53) the output of the displacement sensor (digital voltmeter reading) is high, indicating a large gap between sensor and target. As the air pressure in the loading cylinder on the test rig is increased, first to 4 psi and then successively in 4 psi steps to 16 psi, the voltmeter reading decreases sharply at first and then much more slowly. Approximately twelve minutes after application of each load step the plotter pen was brought back to the left side of the paper and the pressure in the loading cylinder was increased.

From Figure 53 and similar data curves the plots for the shear and cartridge samples - Figures 54 and 55 - have been assembled. The load was plotted against the last deflection value for each load. Similar loading was applied to the compression specimen but, in this case, a mechanical dial indicator was used for deflection measurement. Figure 56 shows compression specimen deflection data.

Examination of the load versus deflection curves for the shear sample (Fig. 54) shows several trends which may also be observed for the compression sample tests (Fig. 56), but are less pronounced for the cartridge sample (Fig. 55).

1. The load versus delfection curve is nonlinear at small deflections only.

2. The degree of nonlinearity decreases with decreasing elastomer stiffness.

3. Elastomer stiffness decreases with increasing ambient temperature.

Details of the nonlinear portion of the stiffness curve for the shear sample (Fig. 54) were confirmed, with greater precision, through substitution of deadweight loading for air cylinder pressurization.

For the cartridge sample (Fig. 55) the deflection curves do not seem to 'straighten out' within the test range as they do for the other samples. The limited range of cartridge sample deflections (about 0.33 mm), may be directly responsible, which was the result of displacement sensor limitations.

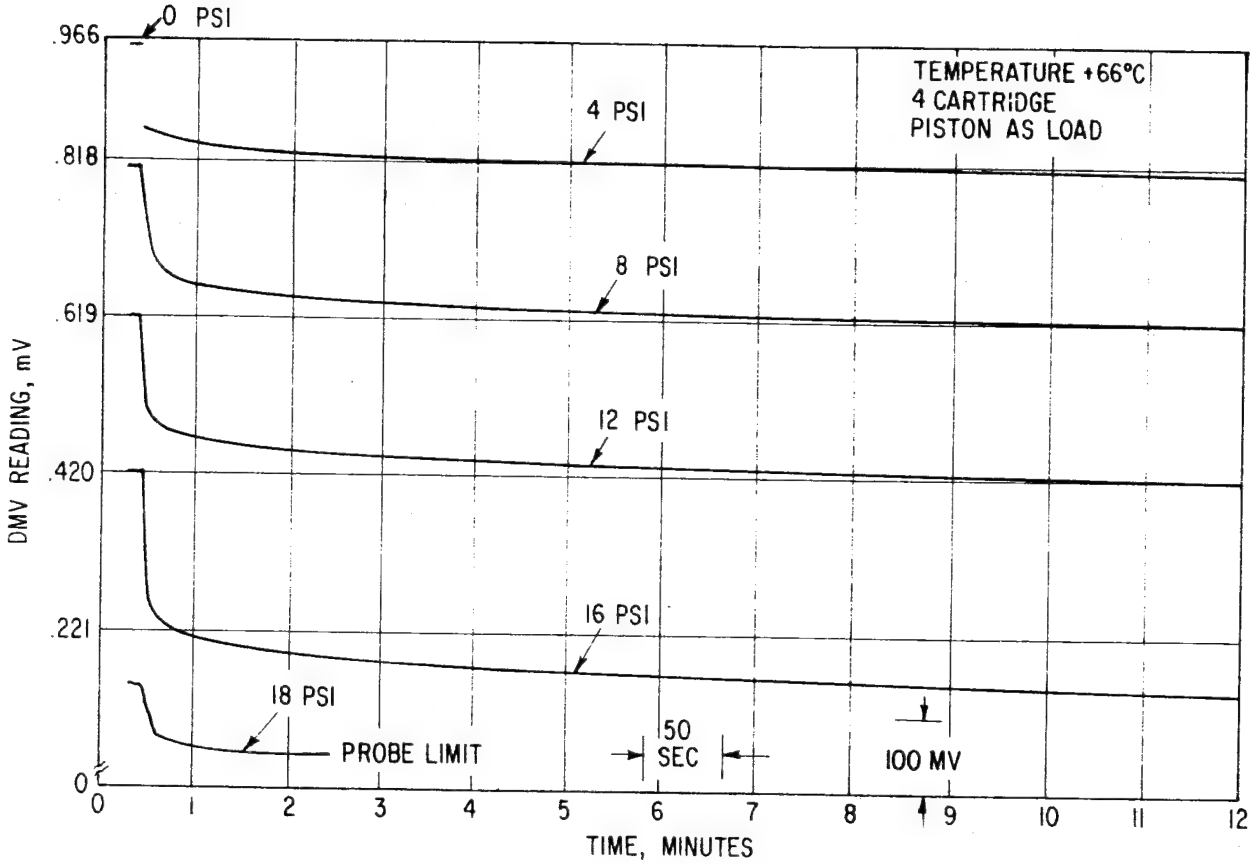

Fig. 53 Load vs Deflection Curves for Elastomer Cartridge at 66 C

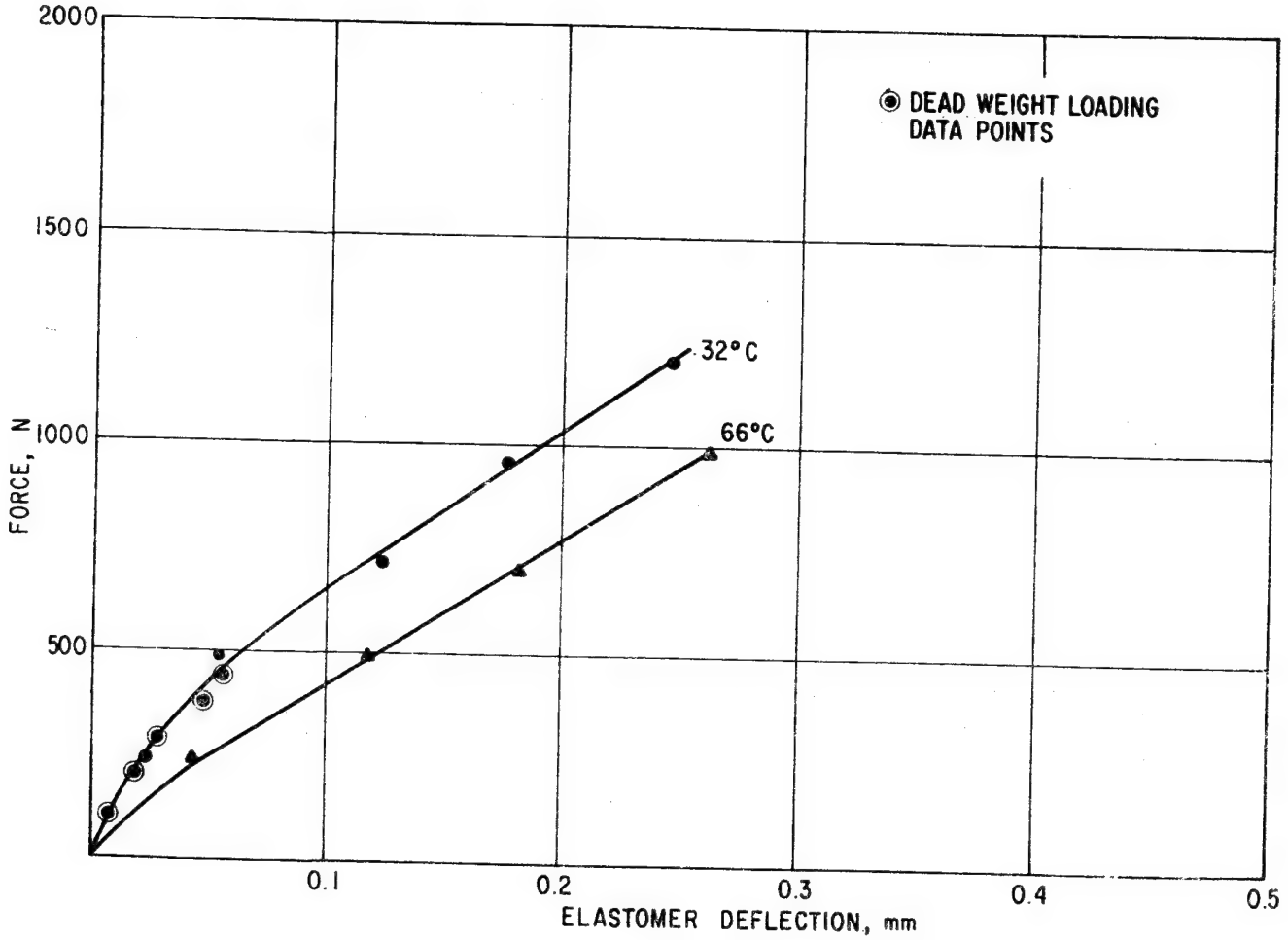

Fig. 54 Static Deflection vs Force for Shear Specimen (Four Elements) at 32 and 66 C

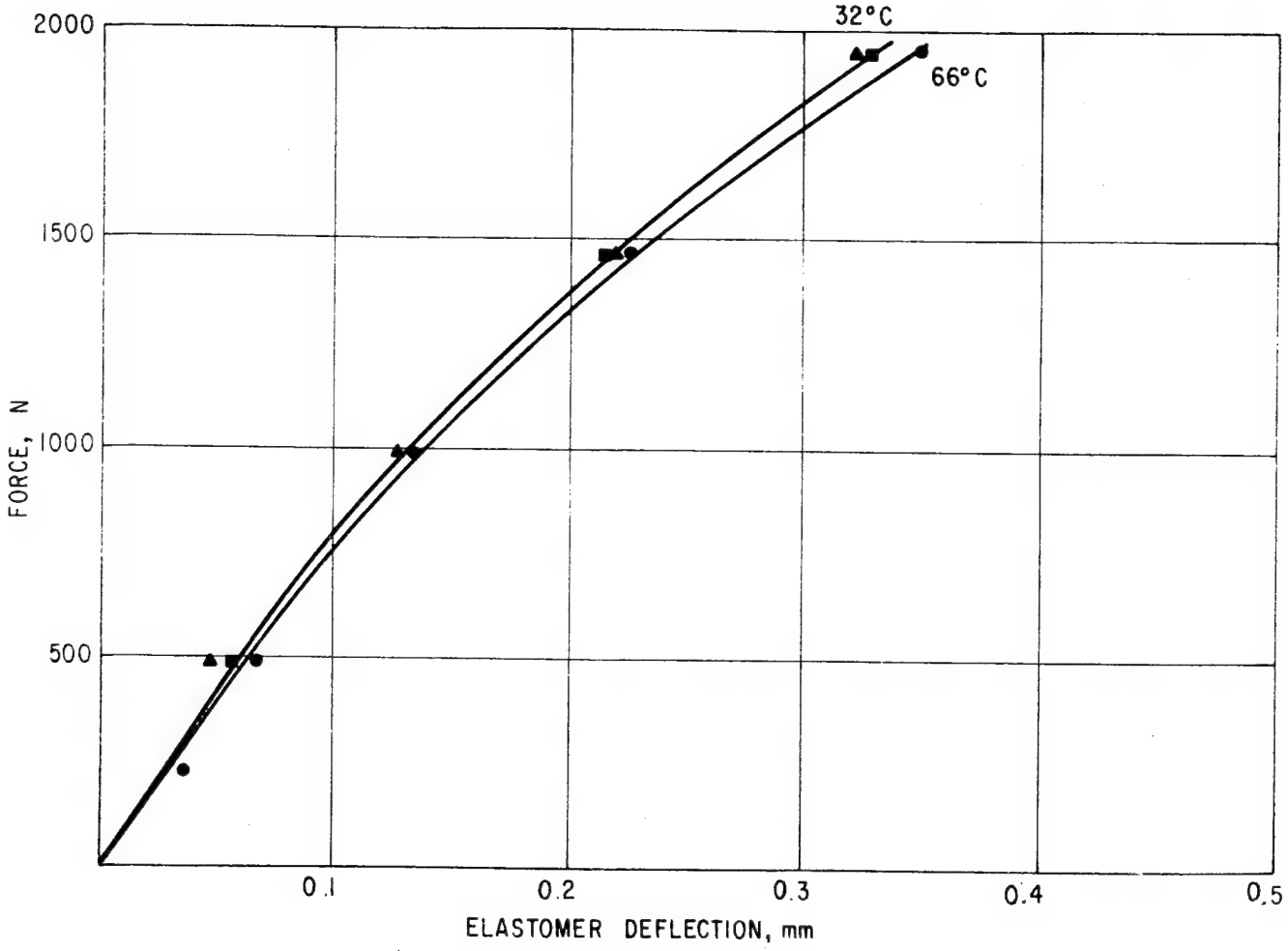

Fig. 55 Static Deflection vs Force for Cartridge Element Specimen at 32 and 66 C

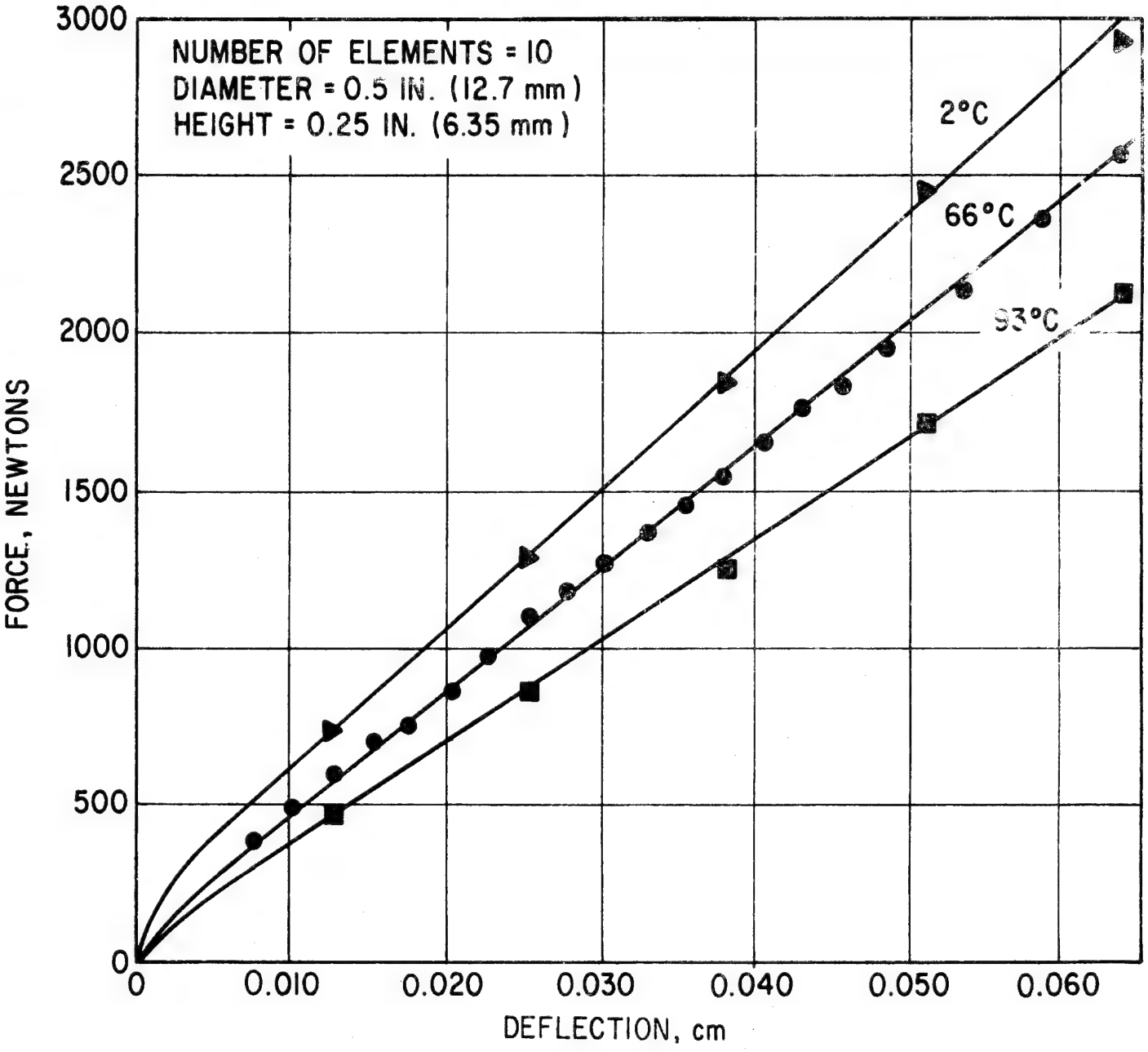

Fig. 56 Static Deflection vs Force for Compression Element Specimen at Various Temperatures

TEST RESULTS

The tests described in the previous sections generated discrete values for stiffness and damping of shear, cylindrical and ring cartridge elastomer elements at different values of frequency, temperature and dissipation level. The purpose of this section is to present this data in its entirety, as well as to provide an appropriate summary of it. The data presented forms the basis for further interpretation. The basic medium of presentation is the plot of stiffness and damping versus frequency. One frame is presented for each set of conditions of:

- Geometry
- Temperature
- Dissipation Level
- Preload (where appropriate)

On each frame discrete stiffness and damping values are plotted, as well as a line representing the least squares best fit power law relationship between stiffness, damping and frequency, in the form:

$$K_1 = A_1 \omega^{B_1} \tag{68}$$

$$K_2 = A_2 \omega^{B_2} \tag{69}$$

The shear specimen power law expressions for different temperatures are used to develop a catalog of material properties for this material. The material properties catalog is subsequently used as part of the basis for predicting stiffness and damping of the cylindrical compression and cartridge specimens.

A brief description of the various sets of test results follows.

Shear Specimen Tests at Different Temperatures

These tests were performed with the eight-element shear specimens, each element having a dimension of 1.27 cm in the direction of loading. The tests were performed with the simplest configuration possible - a mass symmetrically supported by the shear elements which are mounted on the table. The preload piston which has been used in previous tests was not used, eliminating any effects of tare damping.

The data is presented in Figures 57 through 60 for temperatures of 32, 50, 66 and 93 C. The consistent effect of temperature is to reduce stiffness and damping. The data shows reasonable consistency for the three higher temperatures, but at 32 C some scatter is encountered at the highest frequency. The power law relationship provides, in each case, a reasonable fit to the data and, certainly, no more sophisticated representation would be justified.

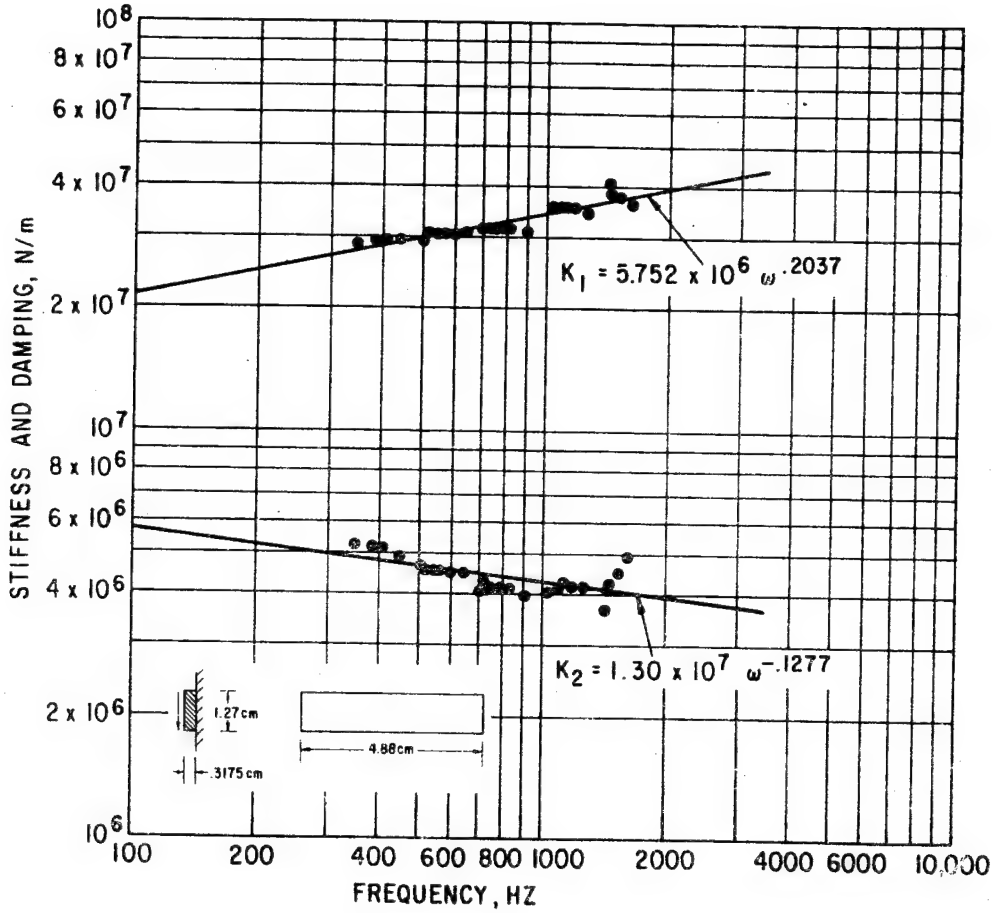

Fig. 57 Stiffness and Damping vs Frequency. Shear Specimen at Zero Preload. 32 C (Eight Elements with Dimensions as Shown). Nominal Dissipation 0.062 watts/cm^3

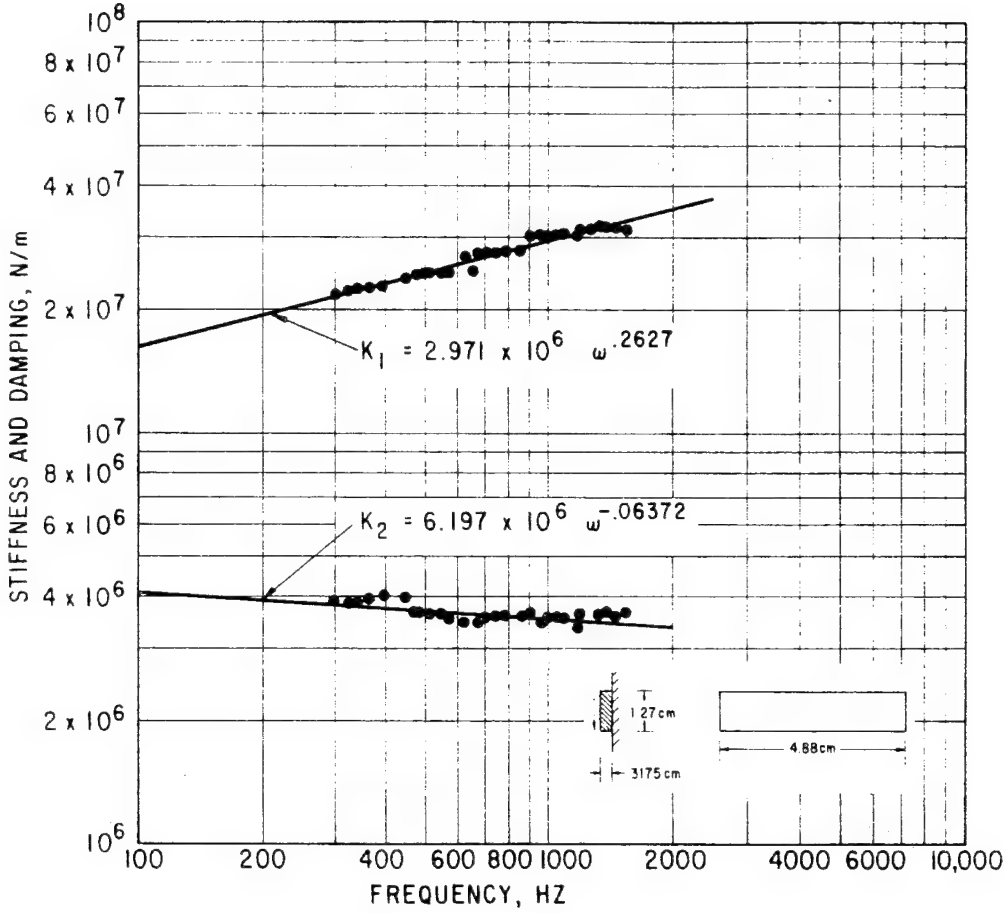

Fig. 58 Shear Specimen at Zero Preload, 50 C (Eight Elements as Shown). Nominal Dissipation 0.062 watts/cm^3

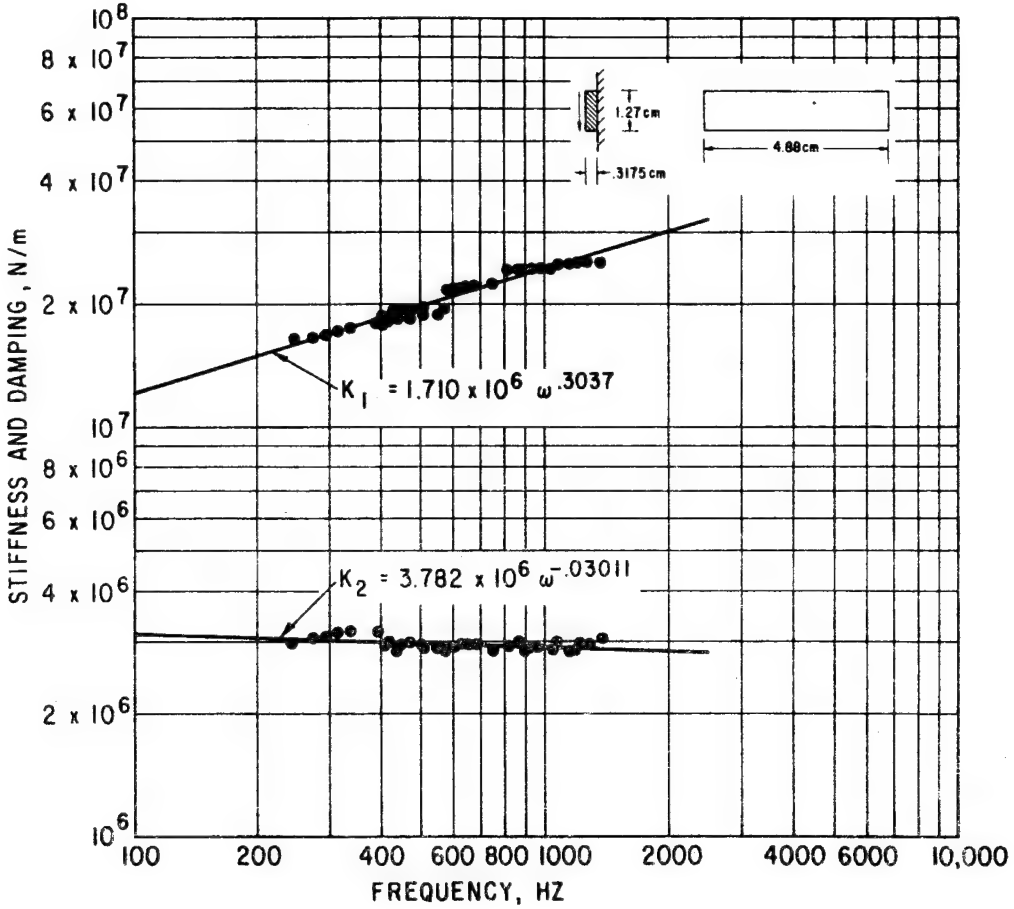

Fig. 59 Shear Specimen at Zero Preload, 66 C (Eight Elements as Shown). Nominal Dissipation 0.062 watts/cm^3

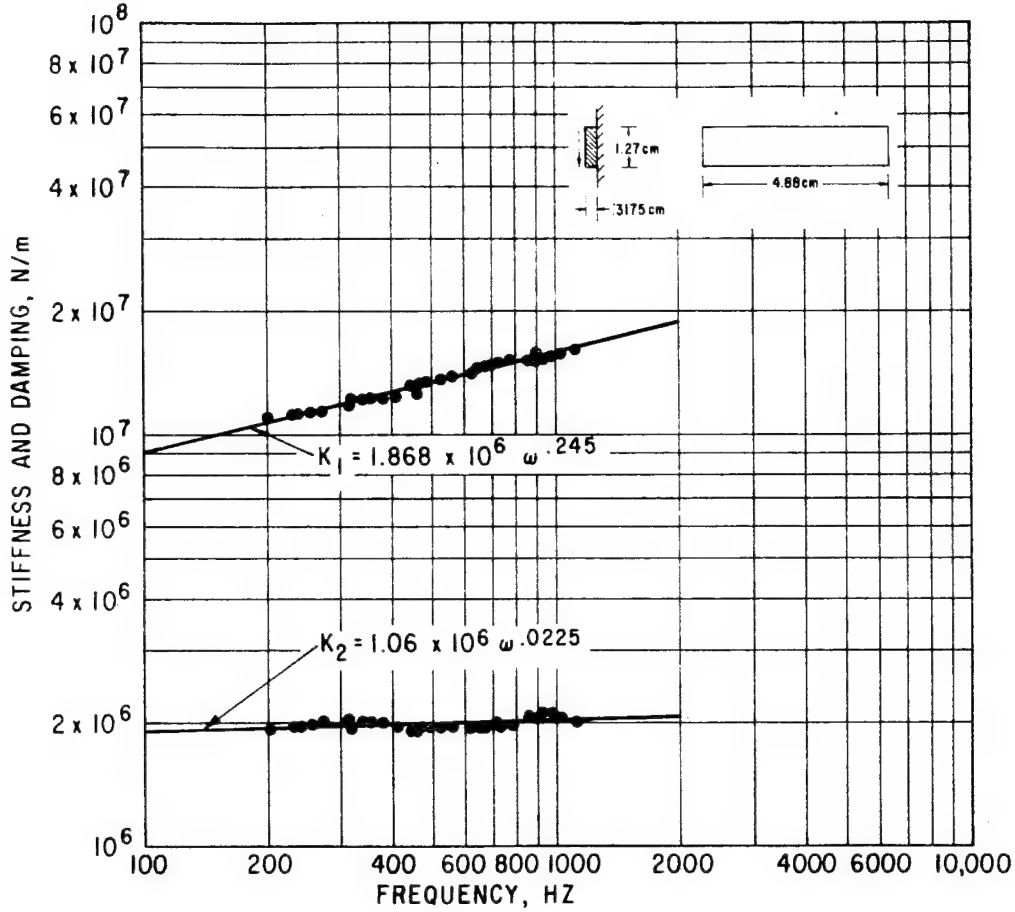

Fig. 60 Shear Specimen at Zero Preload, 93 C (Eight Elements as Shown). Nominal Dissipation 0.062 watts/cm^3

Material Properties Catalog

Applying to the shear specimen test data the interpretive formula:

$$G' = \frac{K_1 \, h}{nA} \tag{70}$$

$$G'' = \frac{K_2 \, h}{nA} \tag{71}$$

where h is the strained dimension (0.3175 cm),
nA is the total stressed area (49.55 cm^2).

A power law relationship between storage and loss moduli (G', G'') and frequency has been obtained, as shown graphically in Figures 61 and 62. The coefficient values are shown in Table IX.

TABLE IX. MATERIAL PROPERTIES CATALOG FOR POLYBUTADIENE, NICHOLS NEX 156G

Temperature	Storage Modulus	Loss Modulus
32 C	$G' = 3.686 \times 10^6 \, \omega^{0.2037}$	$G'' = 8.333 \times 10^6 \, \omega^{-0.1277}$
43 C	$G' = 1.904 \times 10^6 \, \omega^{0.2627}$	$G'' = 3.971 \times 10^6 \, \omega^{-0.06372}$
66 C	$G' = 1.097 \times 10^6 \, \omega^{0.3037}$	$G'' = 2.423 \times 10^6 \, \omega^{-0.03011}$
93 C	$G' = 1.197 \times 10^6 \, \omega^{0.2450}$	$G'' = 1.064 \times 10^6 \, \omega^{+0.2246}$

Together with the geometry factors developed in preceding sections, this material properties data has been applied in the prediction of stiffness and damping of the cylindrical and cartridge specimens. For simplicity of application, it is convenient to have available the values of G', G'' at 100 and 1000 Hz, and these values, based on Table IX are presented in Table X.

TABLE X. VALUES OF STORAGE AND LOSS MODULI FOR POLYBUTADIENE, NICHOLS NEX 156G AT 100 AND 1000 HERTZ

Temperature	G' 100 Hz N/m^2	G' 1000 Hz N/m^2	G'' 100 Hz N/m^2	G'' 1000 Hz N/m^2
32 C	1.369×10^7	2.189×10^7	3.659×10^6	2.728×10^6
43 C	1.035	1.894	2.633	2.274
66 C	0.7755	1.5606	1.996	1.862
93 C	0.5803	1.0201	1.2297	1.2949

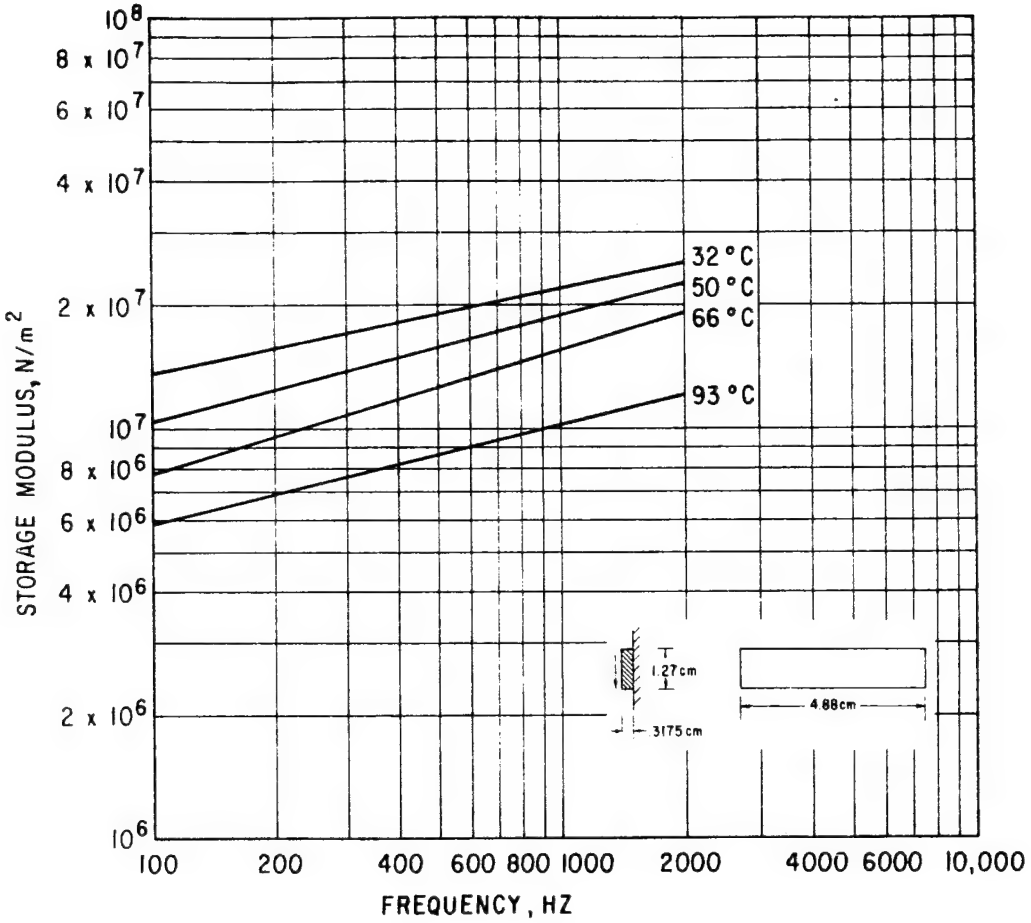

Fig. 61 Influence of Temperature on Storage Modulus (Shear Specimen Data, Eight Elements)

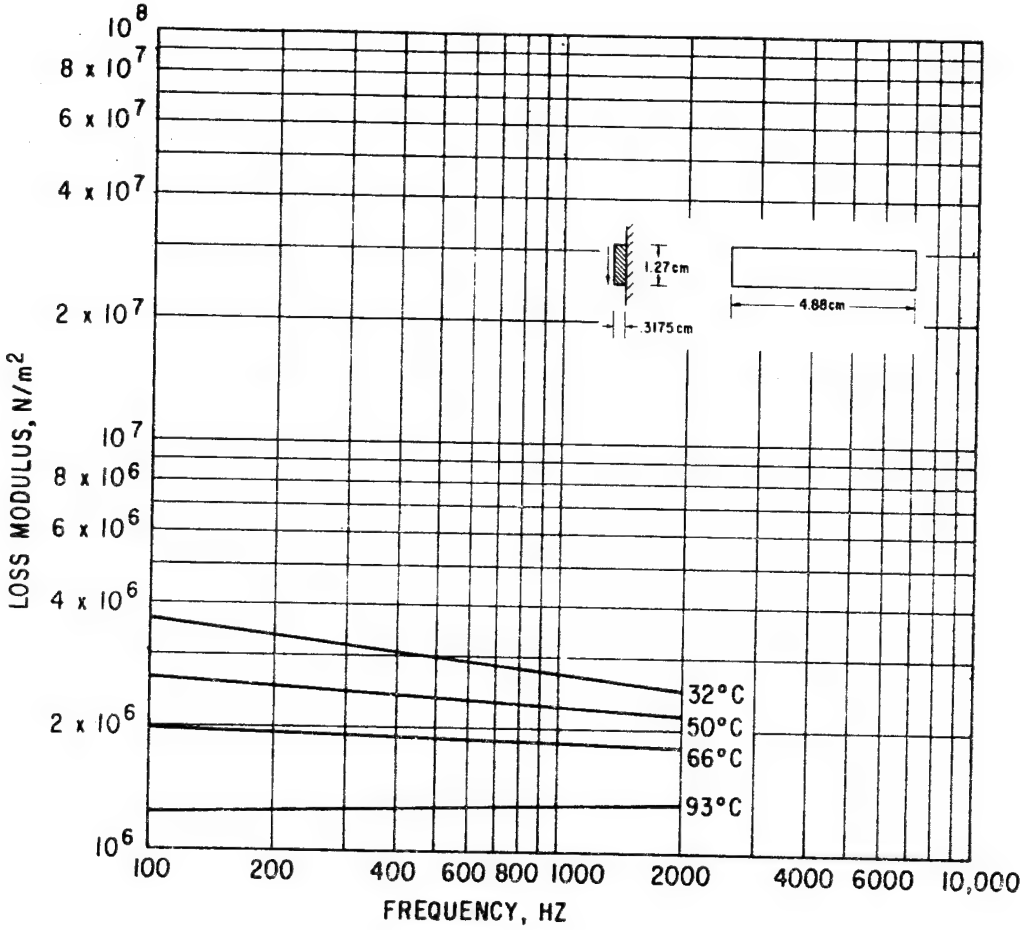

Fig. 62 Influence of Temperature on Loss Modulus (Shear Specimen Data, Eight Elements)

Compression Specimen Tests at Different Temperatures

This series of tests was performed with the ten-element compression specimens, each element 1.27 cm in diameter and 0.635 cm high. In this case, the preload piston was a necessary feature of the tests to satisfy the requirement that the compression elements not be allowed to experience tension. Geometrical preload values of 2.5 and 5 percent were applied. Temperature values tested were 66, 93 and 5 C.

These test results are presented in Figures 63 through 68. Again, reasonable consistency between the test data and the fitted line was obtained. The consistent trend, as for the shear specimens, was that stiffness and damping fall with increasing temperature.

Included in the figures for 66 and 93 C are predictions of stiffness as a function of frequency using the empirical geometry coefficients developed on the basis of previous (Phase II) test data and using the material property values obtained from the present shear specimen tests, as presented in Table IX. In addition, predictions using the static shape coefficient value ($\beta' = \beta'' = 2$) are presented on this figures.

Very similar predictions are obtained with either approach. The predictions of stiffness are within ten percent of measurement at 66 C and within twenty percent at 93 C. Predictions of damping are within 25 percent at 66 C and within twenty percent at 93 C. No predictions are made at 5 C since material property data was not generated at this temperature.

While the stiffness predictions show similar trends to the measurements, in terms of rate of increase with frequency, the damping predictions indicate a slight decrease with frequency and the measurements reveal a more pronounced increase with frequency.

Compression Specimen Tests at Different Dissipation Rates

These tests were performed with the ten-element compression specimens at 32 C. Preloads of both 2.5 and 5 percent were investigated by using the preload piston.

The variation of stiffness and damping with frequency at different nominal dissipation levels is presented in Figures 69 through 73. The corresponding variation of amplitude is shown in Figures 74 and 75 and, using these two sets of data, the details of each test point in terms of amplitude, frequency and temperature may be recreated.

The general effect of increasing dissipation is to decrease both stiffness and damping, at all frequencies, for these compression specimens. As previously discussed, it is hypothesized that a major reason for this degradation is the increase in the material temperature. The comparison between this measured data and predictions of the simple thermoviscoelastic model will be presented in the next Section of the report.

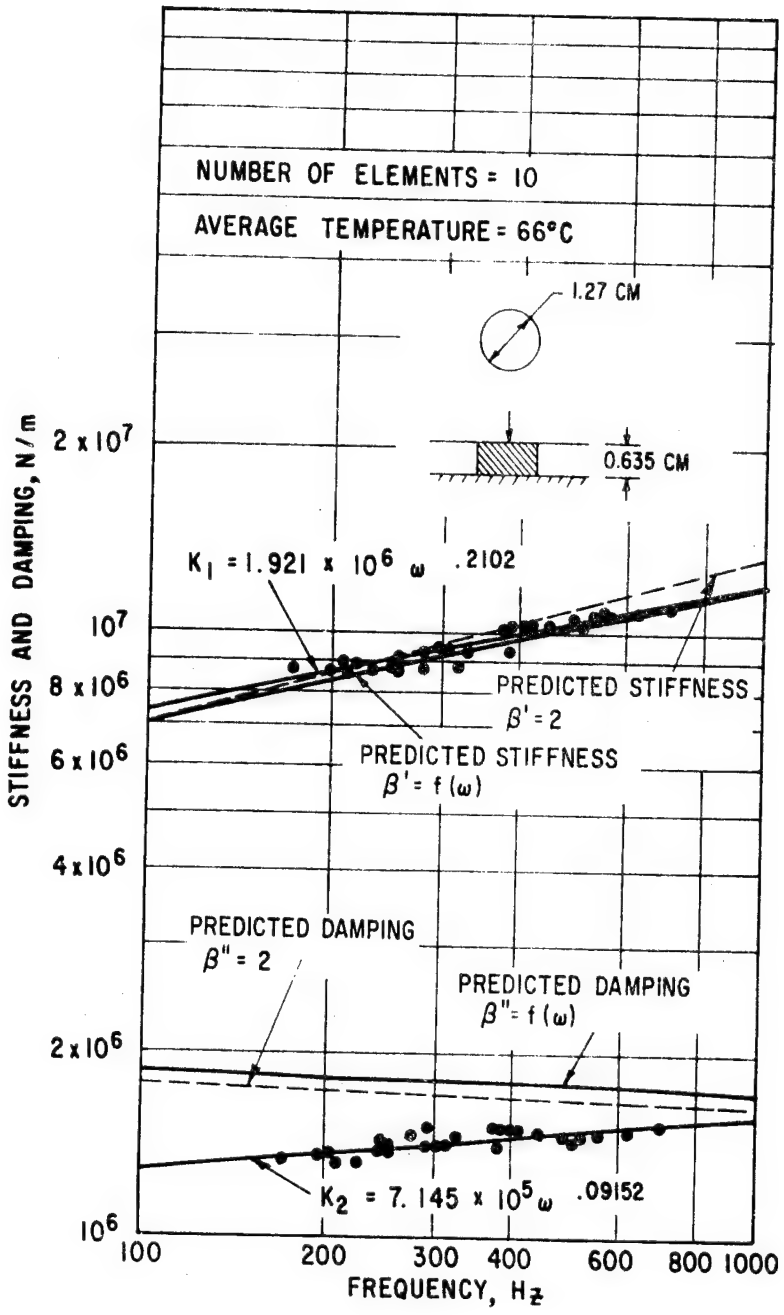

Fig. 63 Stiffness and Damping vs Frequency. Compression Specimen (Ten Elements with Dimensions as Shown). 2-1/2 Percent Preload, 66 C. Nominal Dissipation 0.062 watts/cm^3.

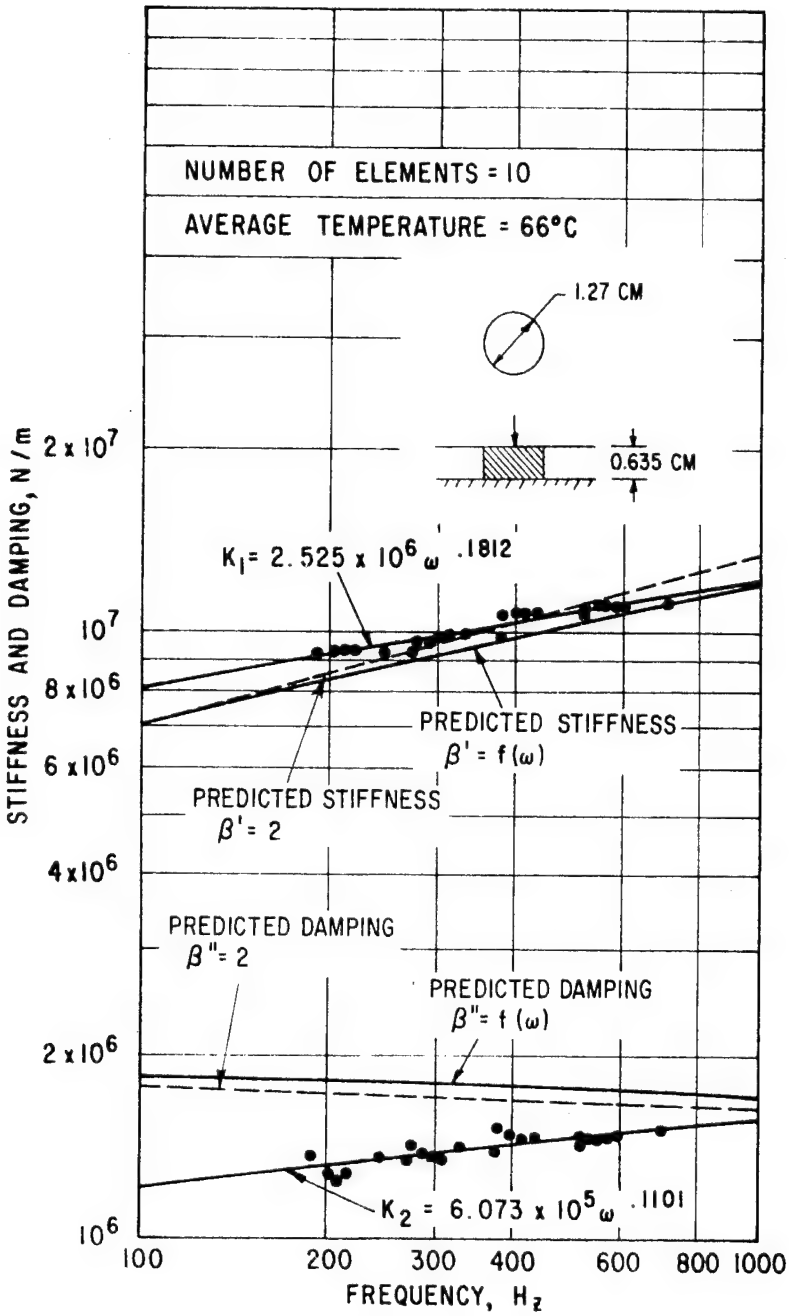

Fig. 64 Stiffness and Damping vs Frequency. Compression Specimen. Five Percent Preload, 66 C. (Ten Elements with Dimensions as Shown). Nominal Dissipation 0.062 watts/cm^3. 2-1/2 Percent Preload.

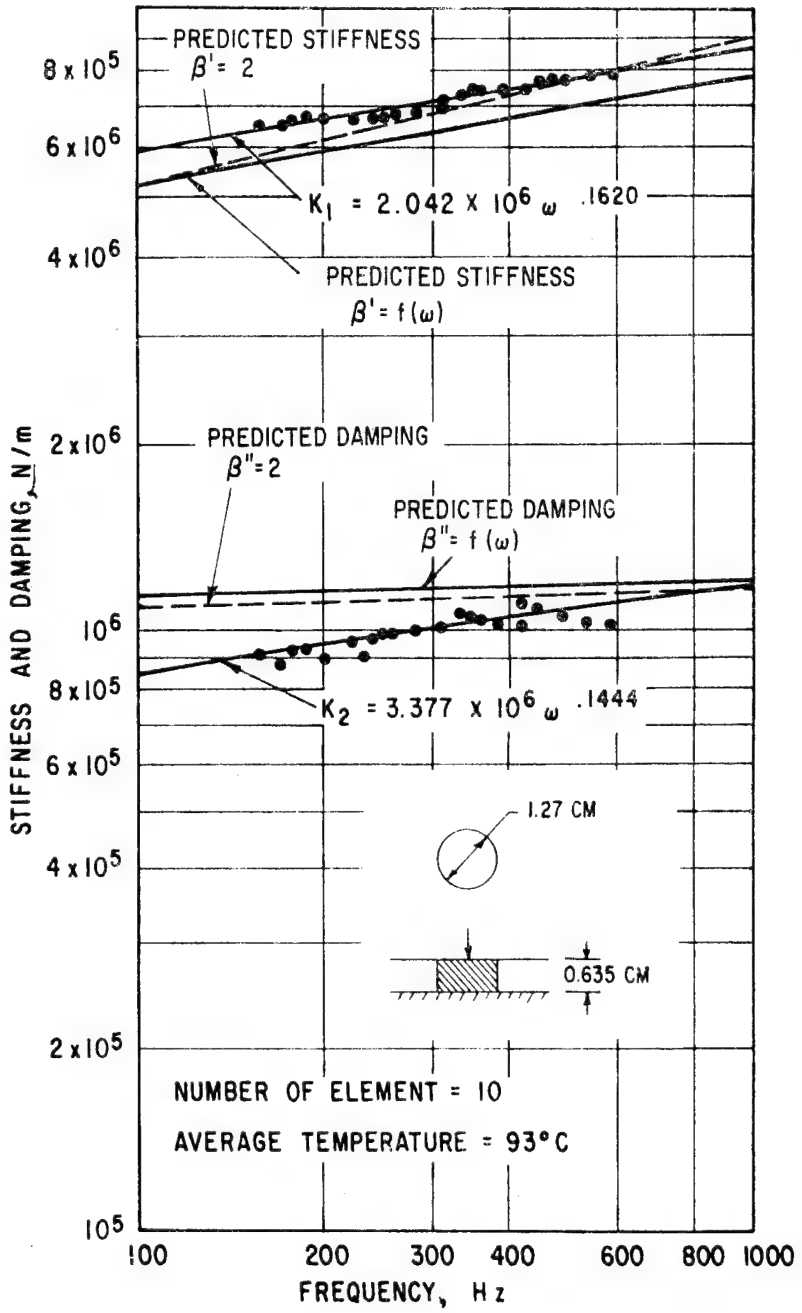

Fig. 65 Stiffness and Damping vs Frequency. Compression Specimen. 2-1/2 Percent Preload, 93 C. Nominal Dissipation 0.062 watts/cm^3

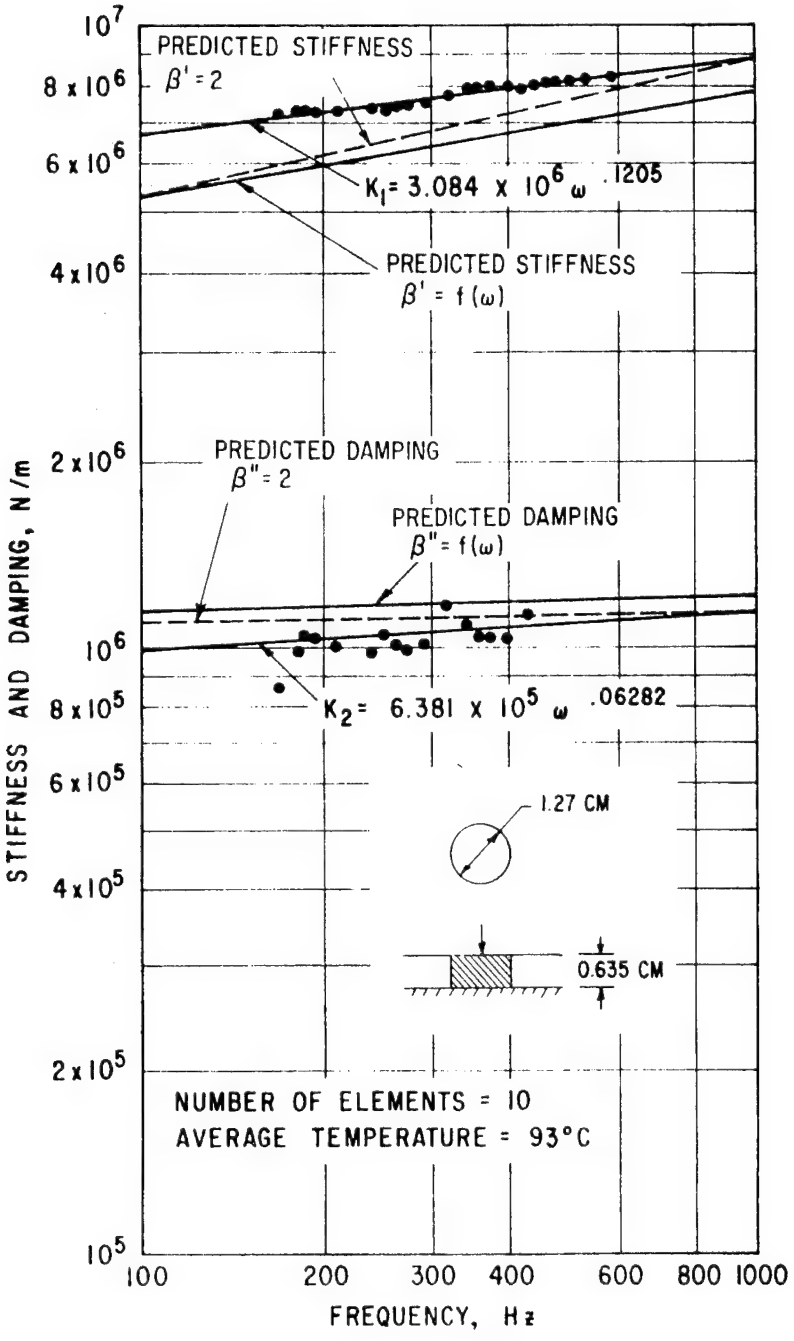

Fig. 66 Stiffness and Damping vs Frequency. Compression Specimen. Five Percent Preload, 93 C. Nominal Dissipation 0.062 watts/cm^3

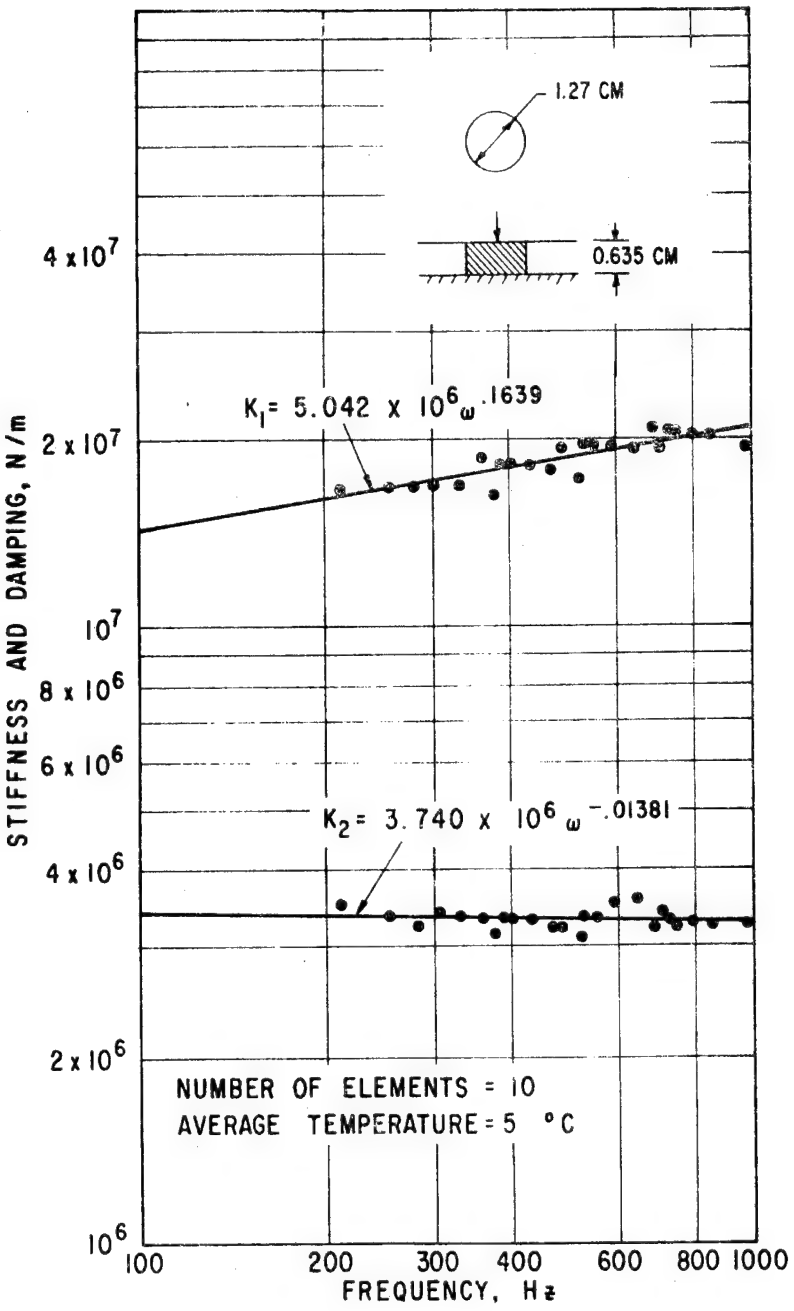

Fig. 67 Stiffness and Damping vs Frequency. Compression Specimen. 5 C. 2-1/2 Percent Preload; Nominal Dissipation 0.062 watt/cm^3.

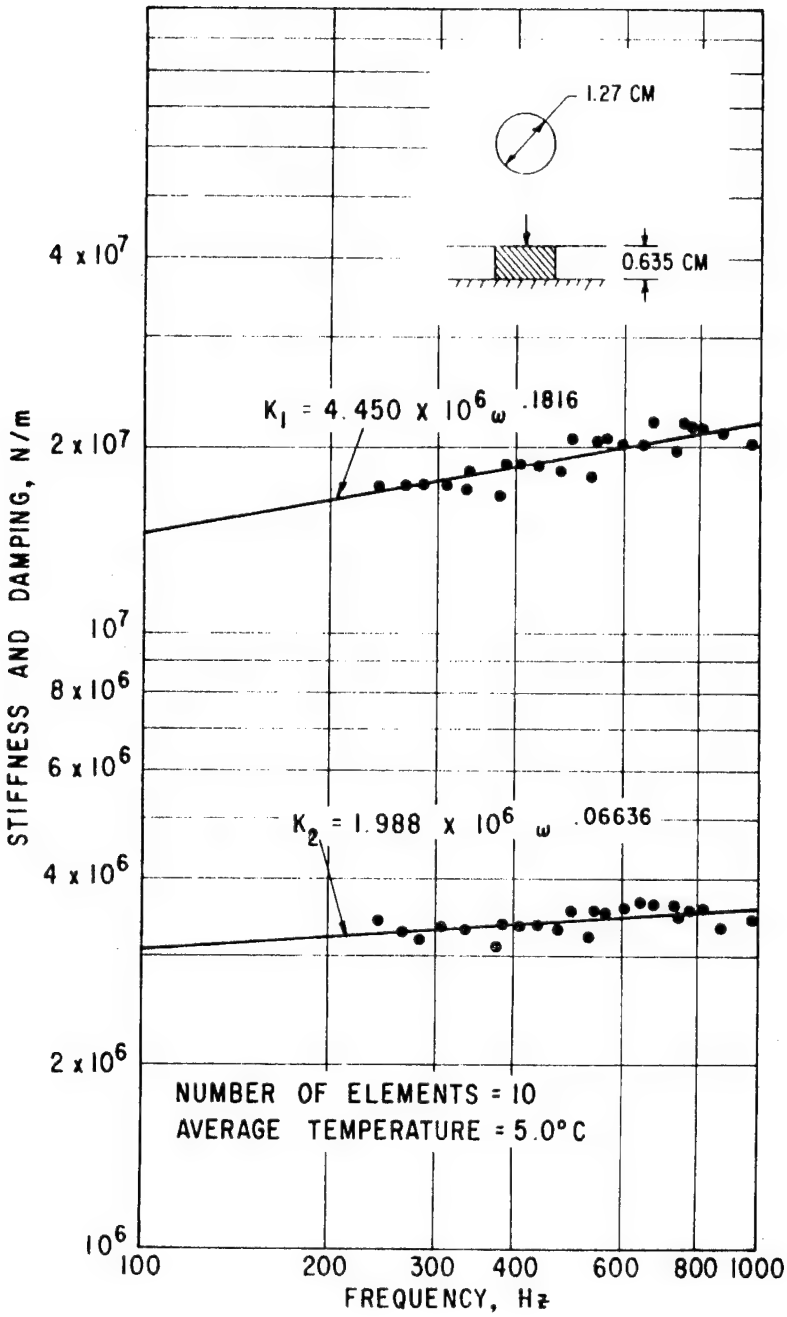

Fig. 68 Stiffness and Damping vs. Frequency. Compression Specimen. 5 C, 5 Percent Preload; Nominal Dissipation 0.062 watt/cm^3.

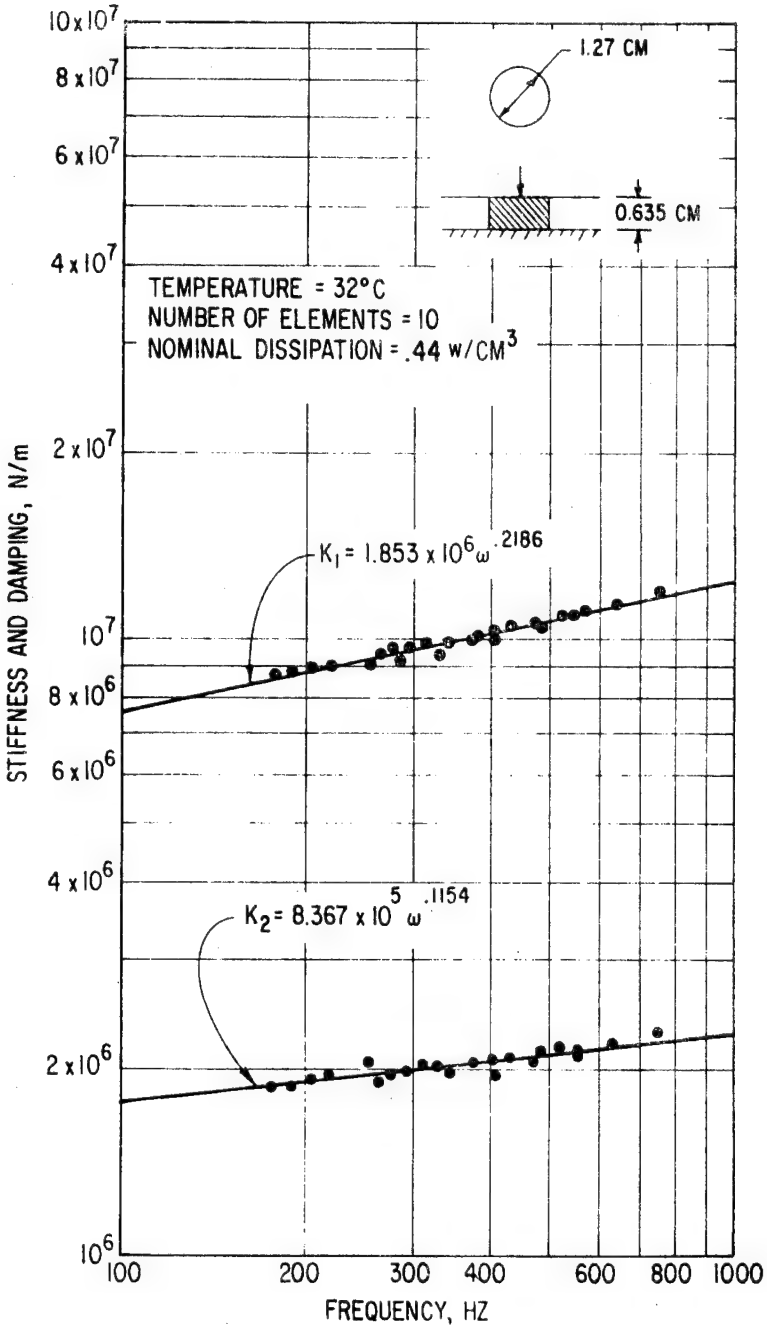

Fig. 69 Stiffness and Damping vs Frequency. Compression Specimen. 32 C. Nominal Dissipation 0.44 watt/cm^3

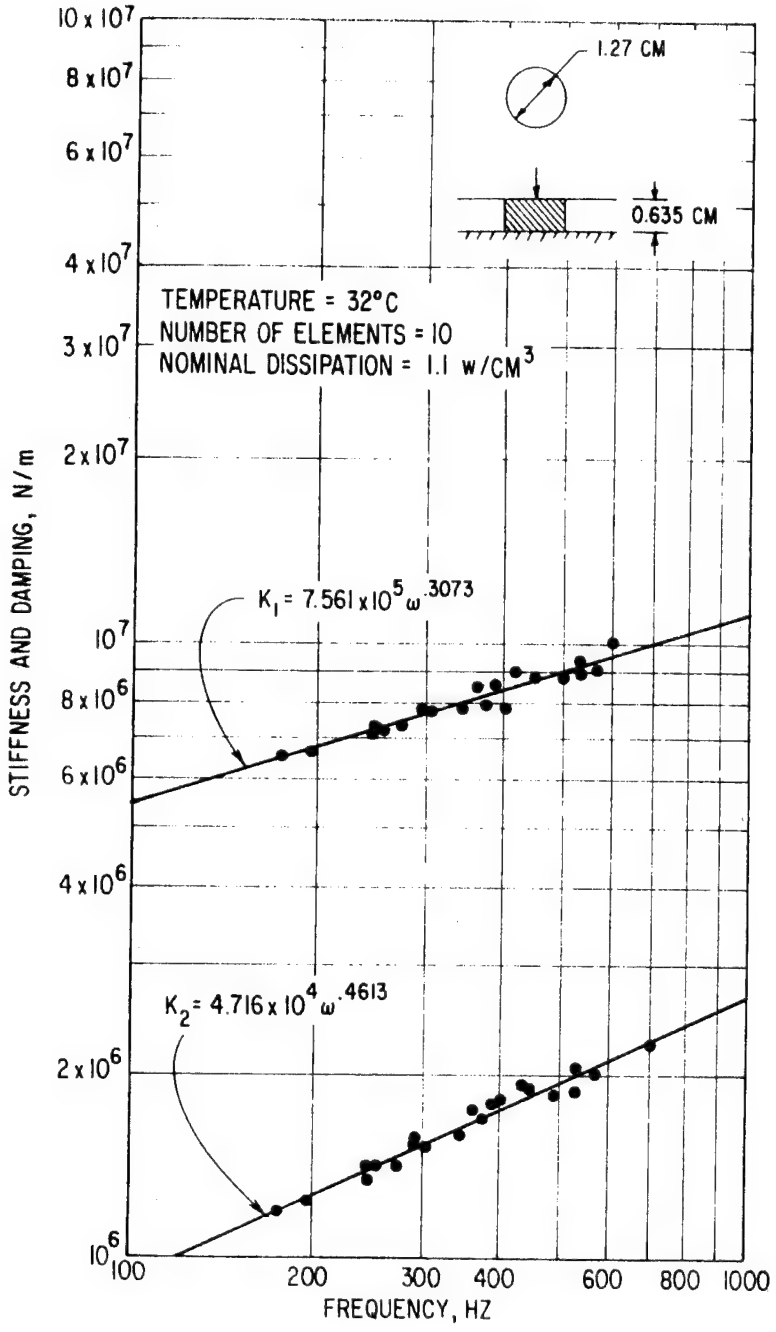

Fig. 70 Stiffness and Damping vs Frequency. Compression Specimen. 2-1/2 Percent Preload, 32 C. Nominal Dissipation 1.1 watts/cm^3

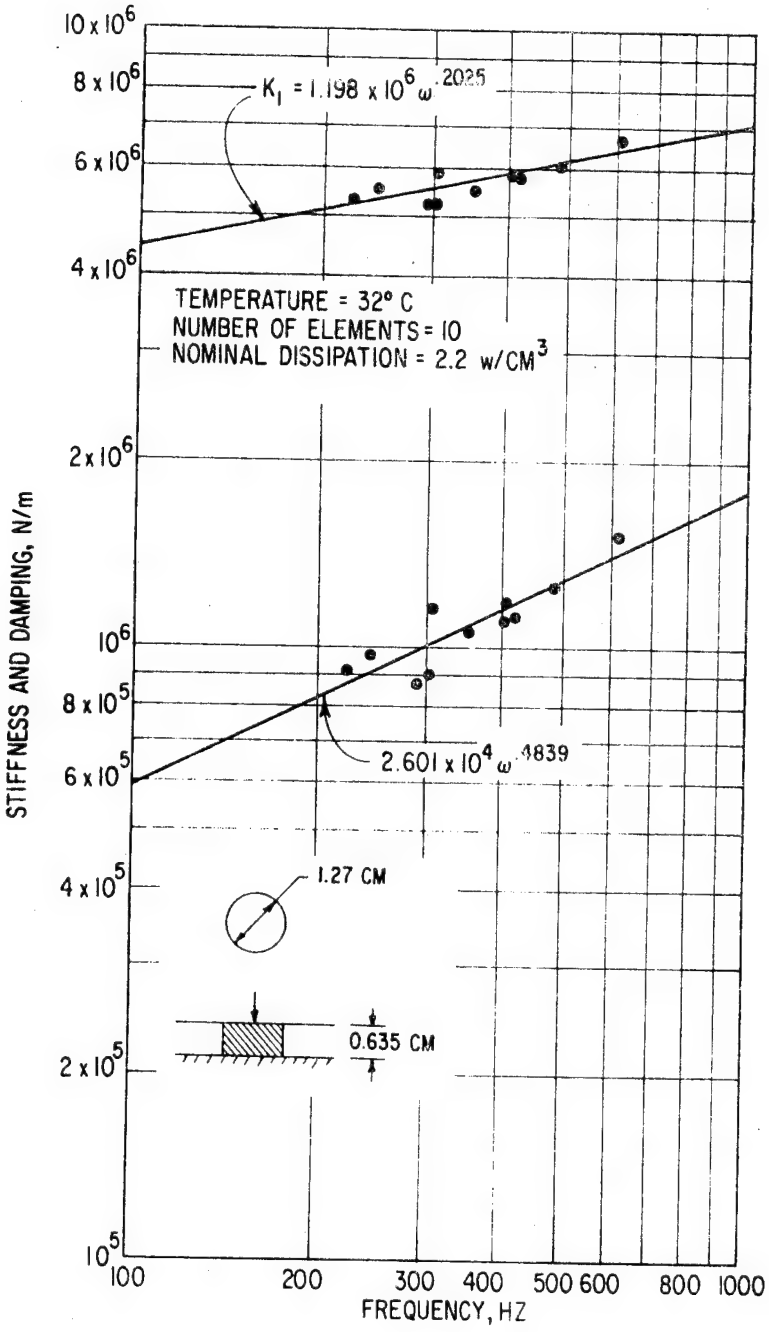

Fig. 71 High Dissipation Stiffness and Damping vs Frequency. Compression Specimen. 2-1/2 Percent Preload, 32 C. Nominal Dissipation 2.2 watts/cm^3

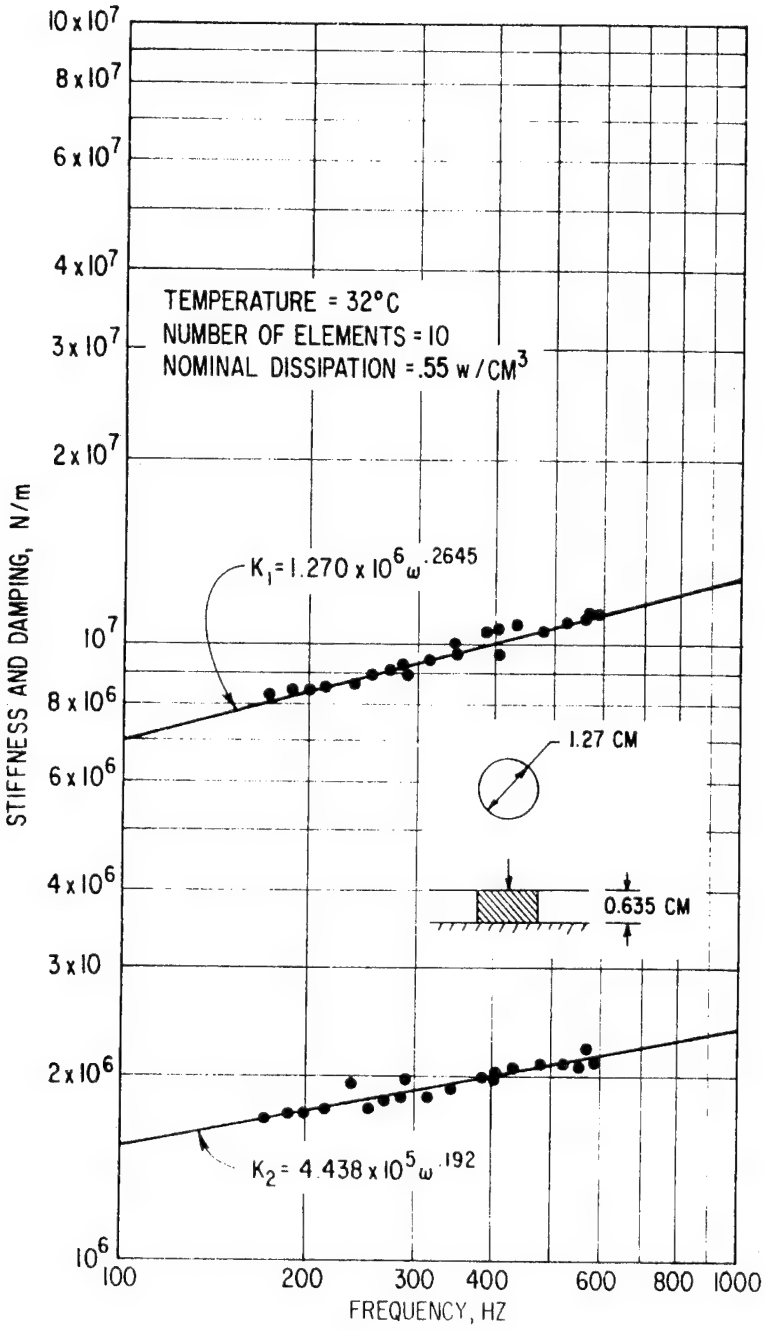

Fig. 72 Stiffness and Damping vs Frequency. Compression Specimen. 5 Percent Preload, 32 C. Nominal Dissipation 0.55 watts/cm^3

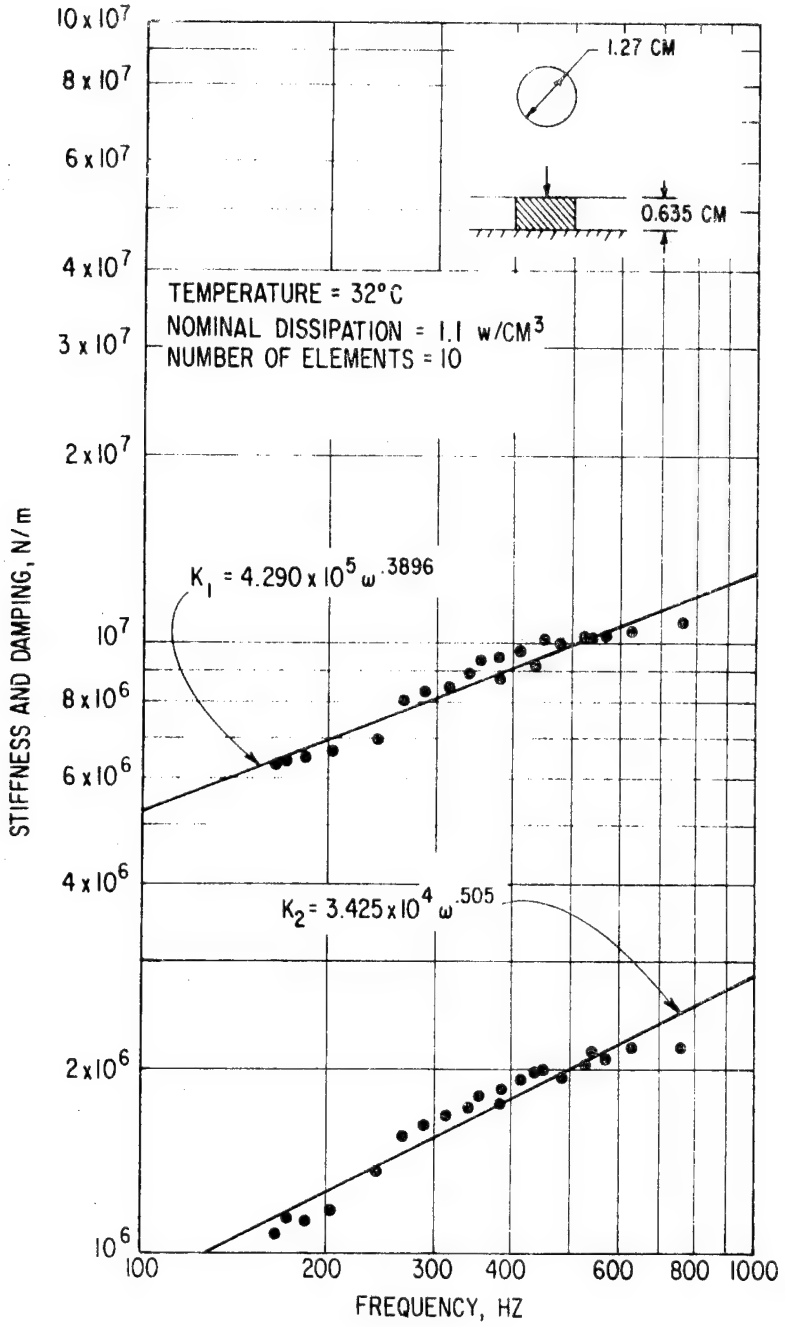

Fig. 73 Stiffness and Damping vs Frequency. Compression Specimen. 5 Percent Preload, 32 C. Nominal Dissipation 1.1 watts/cm^3

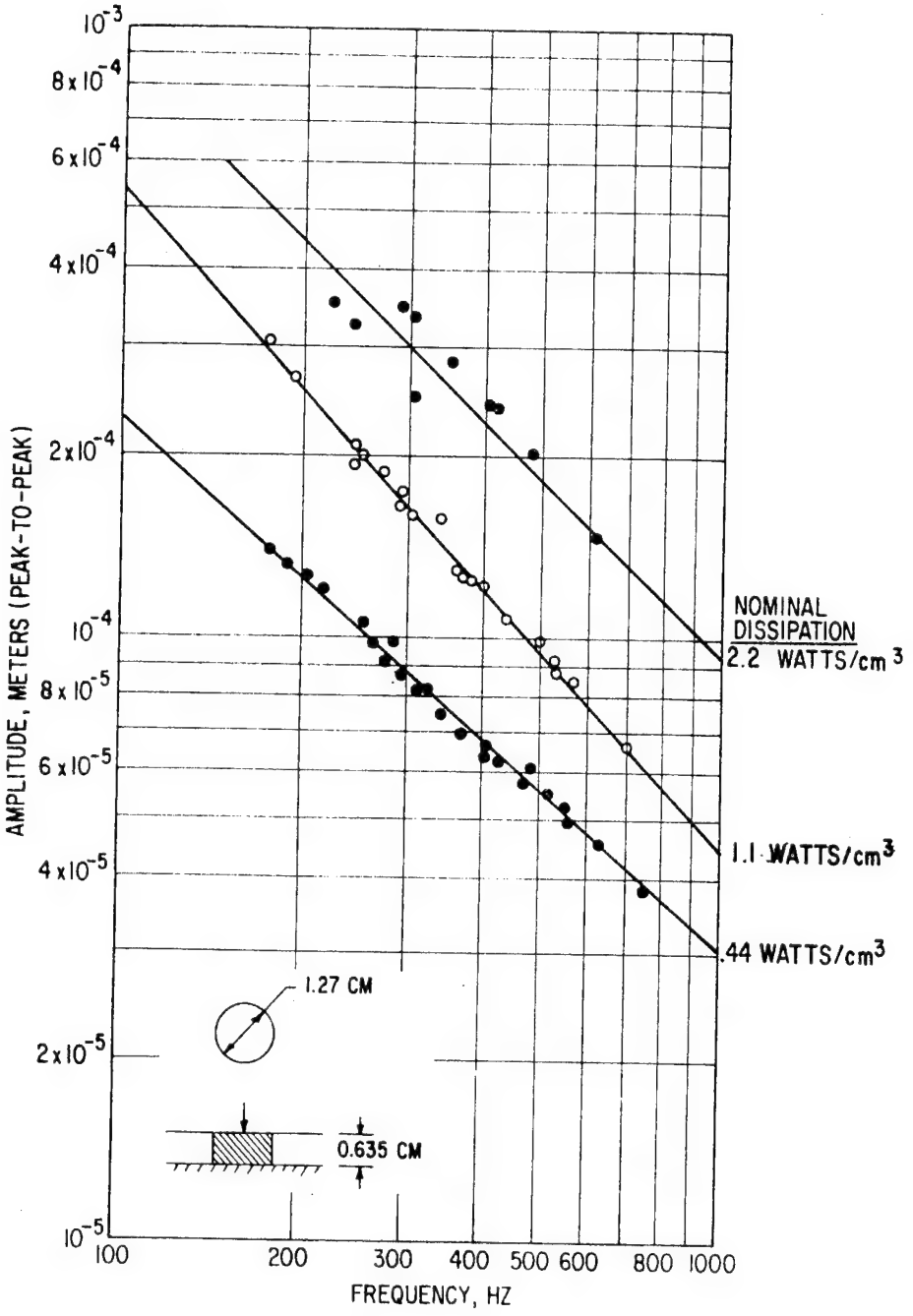

Fig. 74 Amplitude as a Function of Frequency. Compression Specimen. 2-1/2 Percent Preload, 32 C (Ten Elements with Dimensions as Shown)

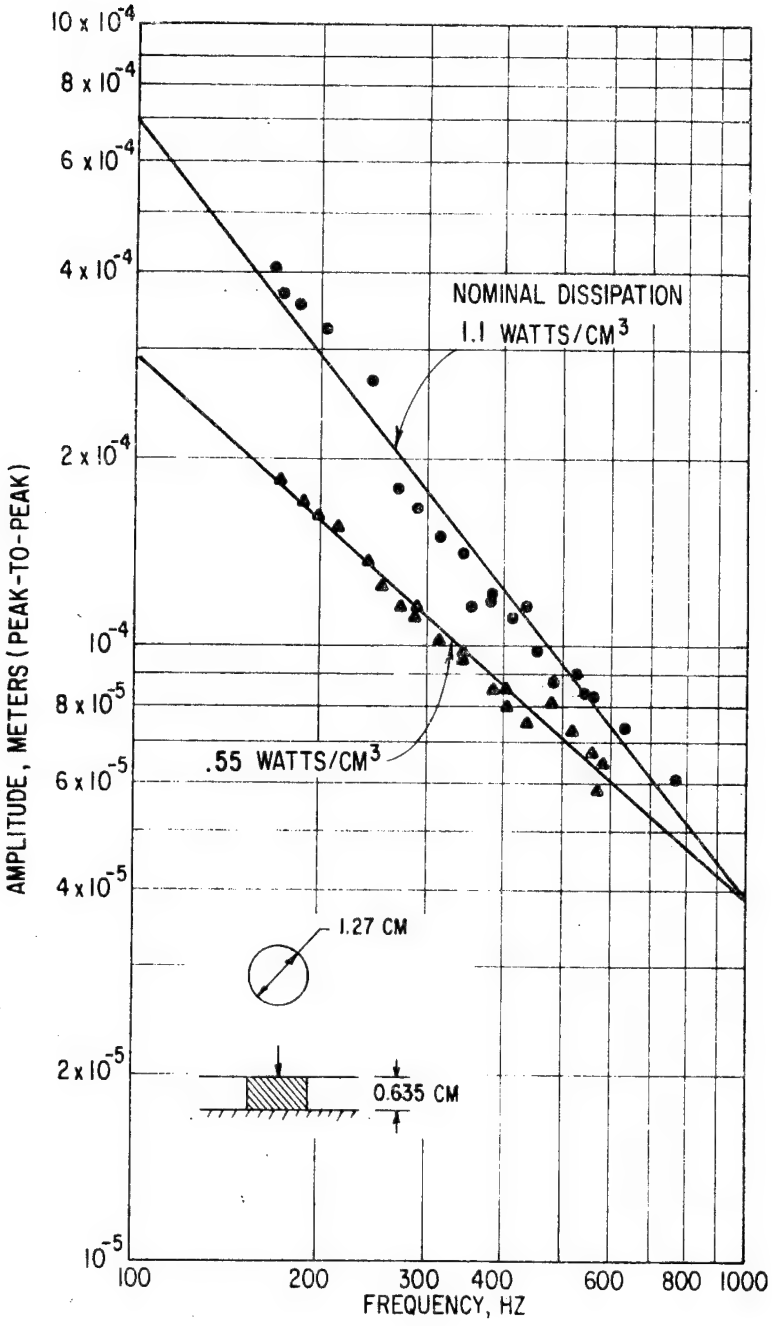

Fig. 75 Amplitude as a Function of Frequency. Compression Specimen. 5 Percent Preload, 32 C (Ten Elements with Dimensions as Shown).

Shear Specimen Tests For Different Dissipation Rates

These tests were performed with four-element shear specimens. Each element is 2.54 cm long in the direction of loading, the strained dimension is 0.3175 cm thick, and the width of the elements is 4.877 cm. As with the eight-element shear specimen, it is possible to perform these tests without the uncertainties introduced by the presence of the preload piston. All the high dissipation tests were performed at a temperature of 32 C.

As a reference, a low dissipation level of 0.035 watt/cm^3 has been tested, followed by nominal dissipation values 5, 10, 20, 50 and 125 times the reference. The data, in terms of stiffness and damping, is presented in Figures 76 through 81 and the amplitudes as a function of frequency in Figure 82.

Reasonable consistency between the test data and the fitted line is obtained, with scatter of the order of ten percent of the stiffness and damping level. Scatter increases at the highest dissipation levels.

It is generally a trend that both stiffness and damping fall with increasing dissipation level.

The slope of the lines also tend to increase with increasing dissipation levels - indicating a more pronounced effect of high dissipation at low frequencies. This could result from the power meter characteristic discussed in the previous Section.

Cartridge Tests at Different Temperatures

These tests were preformed on two different cartridge test specimens. Each consisted of four elements mounted in the same fixtures and holders. The inner and outer diameters of the elements were the same for the two specimens (1.90 cm and 2.86 cm); the difference was the length - 0.47 cm in one case and 0.95 cm in the other. Data for the shorter elements are presented in Figures 83 through 86 and for the larger elements in Figures 87 through 90. The temperature range covered is 32 to 80 C. The energy dissipation rate is 0.022 watts/cm^3.

The data is generally consistent with the fitted power law line, except that at low frequencies, for the shorter length elements, the damping values fall with frequency before starting to increase with frequency above 150 to 200 Hz. The influence of increasing temperature is to decrease the stiffness and damping. In general, the influence of frequency is to increase both stiffness and damping at a similar rate.

Superimposed on these test data plots are predictions using the various methods of prediction for the cartridge geometry previously discussed. In all cases, the Göbel predictions and Beam-Column predictions are included. In most cases the plane stress line is also included.

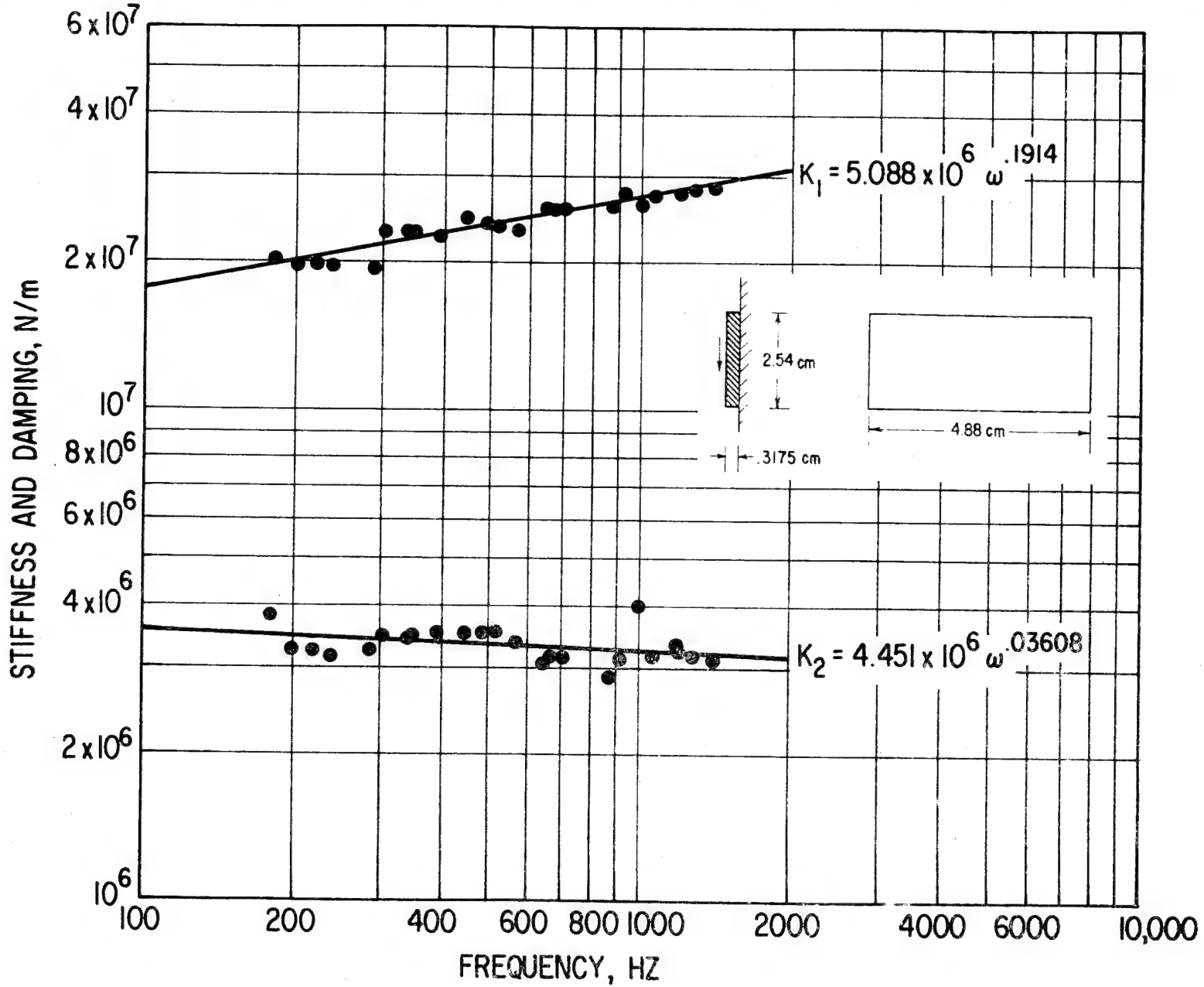

Fig. 76 Stiffness and Damping vs Frequency. Shear Specimens
Zero Preload, 32 C. Nominal Dissipation 0.035 watts/cm^3

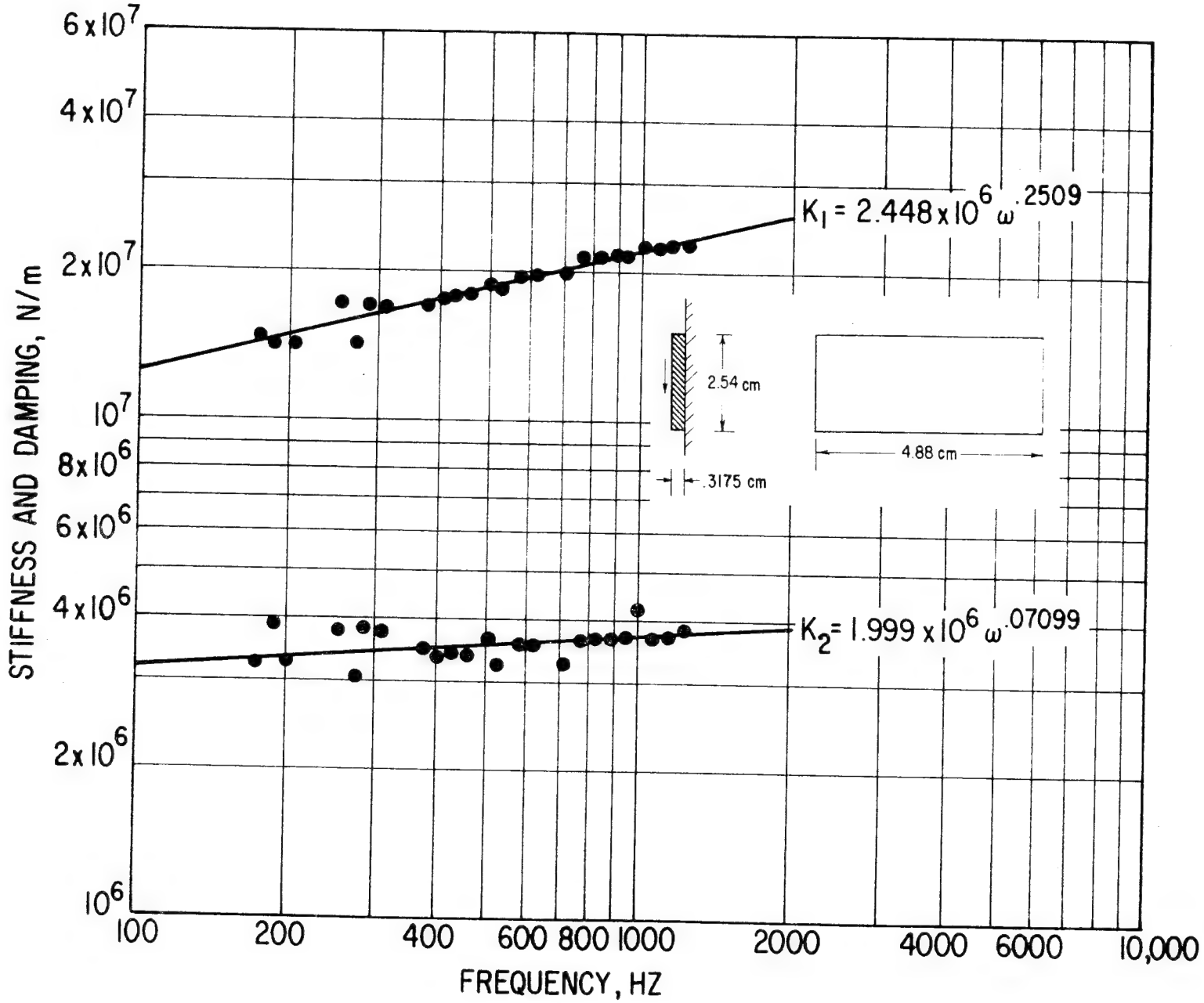

Fig. 77 Stiffness and Damping vs Frequency. Shear Specimen. Zero Preload, 32 C. Nominal Dissipation 0.176 watts/cm^3

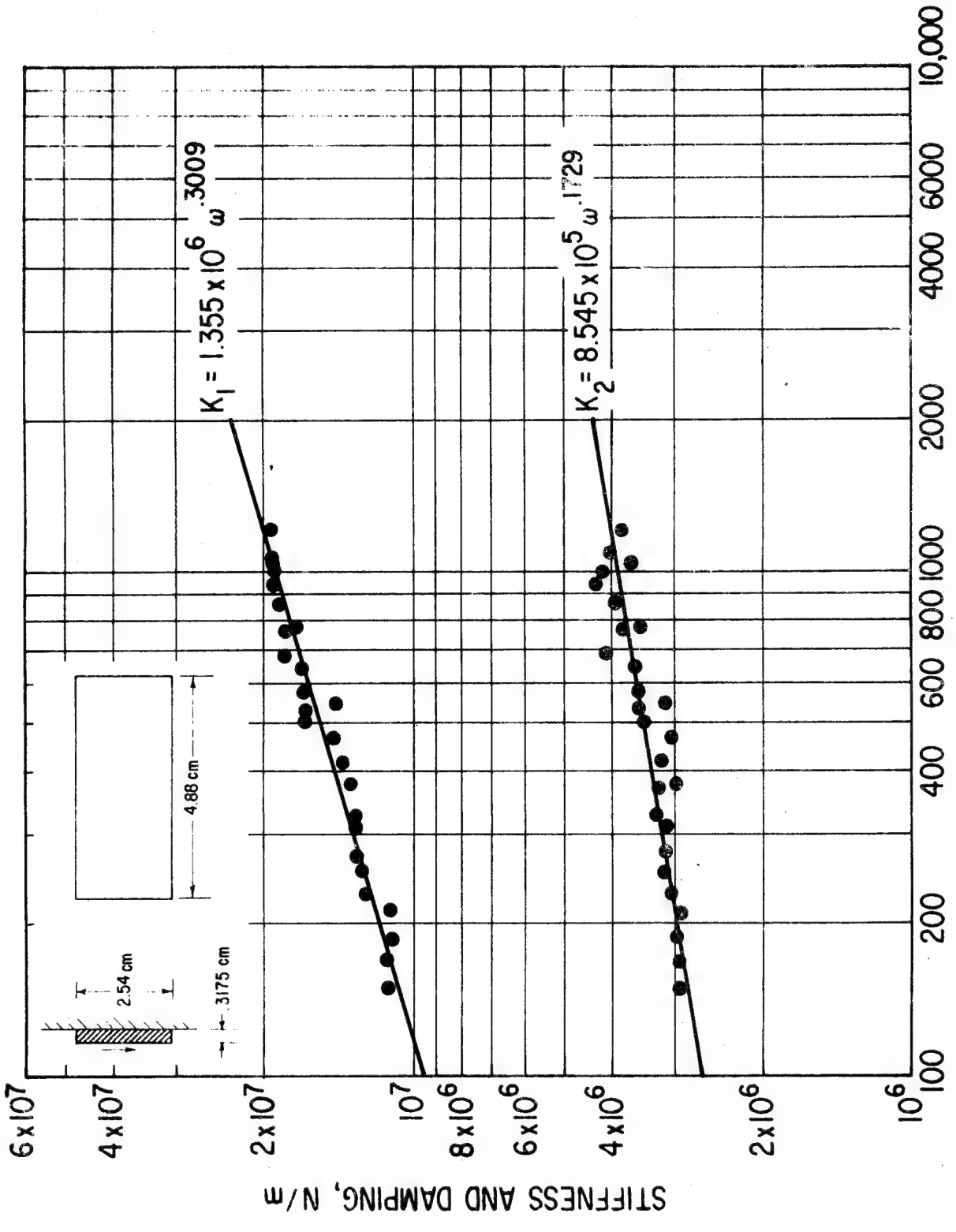

Fig. 78 Stiffness and Damping vs Frequency. Shear Specimens. Zero Preload, 32 C. Nominal Dissipation 0.352 watts/cm^3

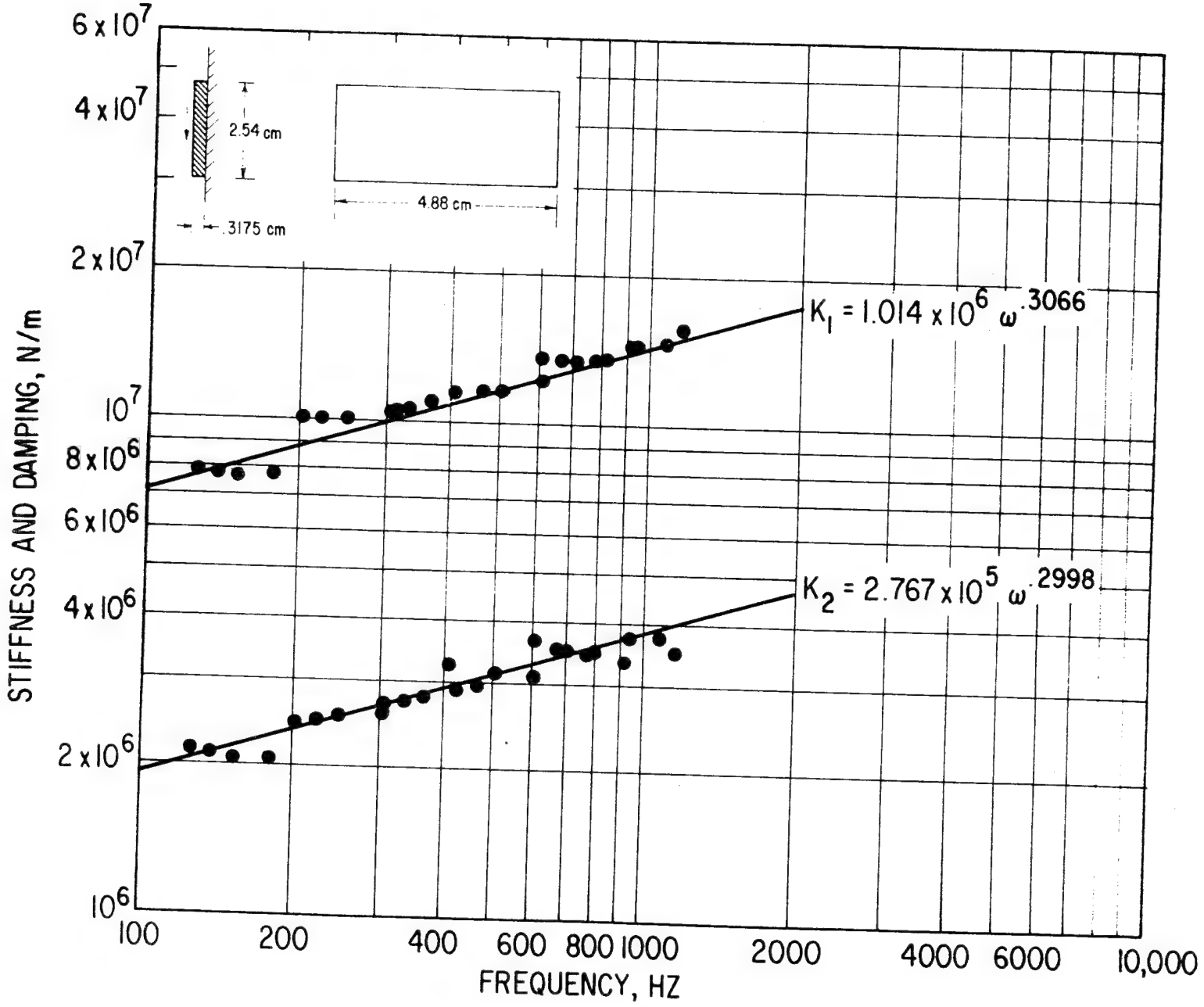

Fig. 79 Stiffness and Damping vs Frequency. Shear Specimens. Zero Preload, 32 C. Nominal Dissipation 0.704 watts/cm^3

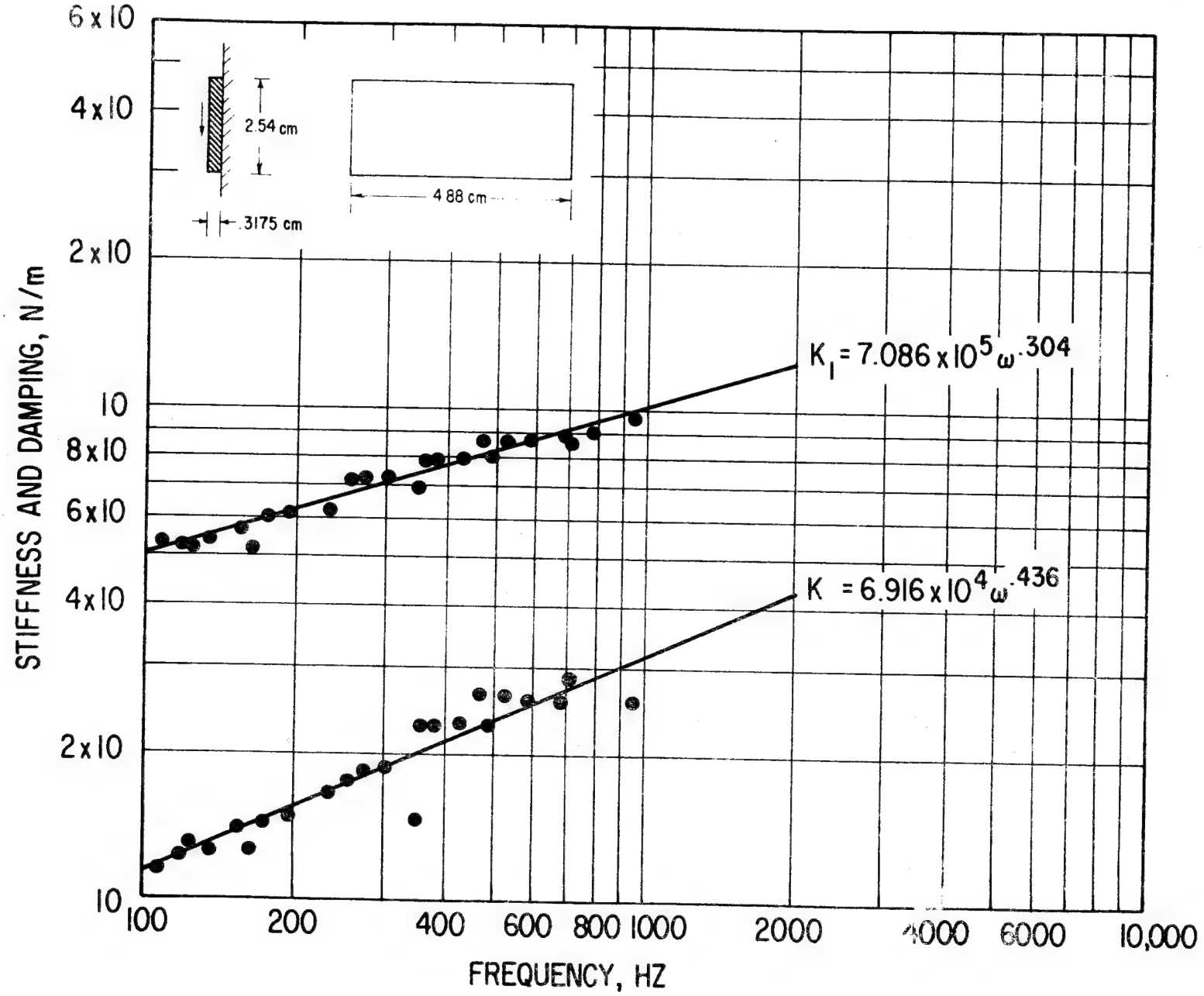

Fig. 80 Stiffness and Damping vs Frequency. Shear Specimens. Zero Preload, 32 C. Nominal Dissipation 1.76 watts/cm^3

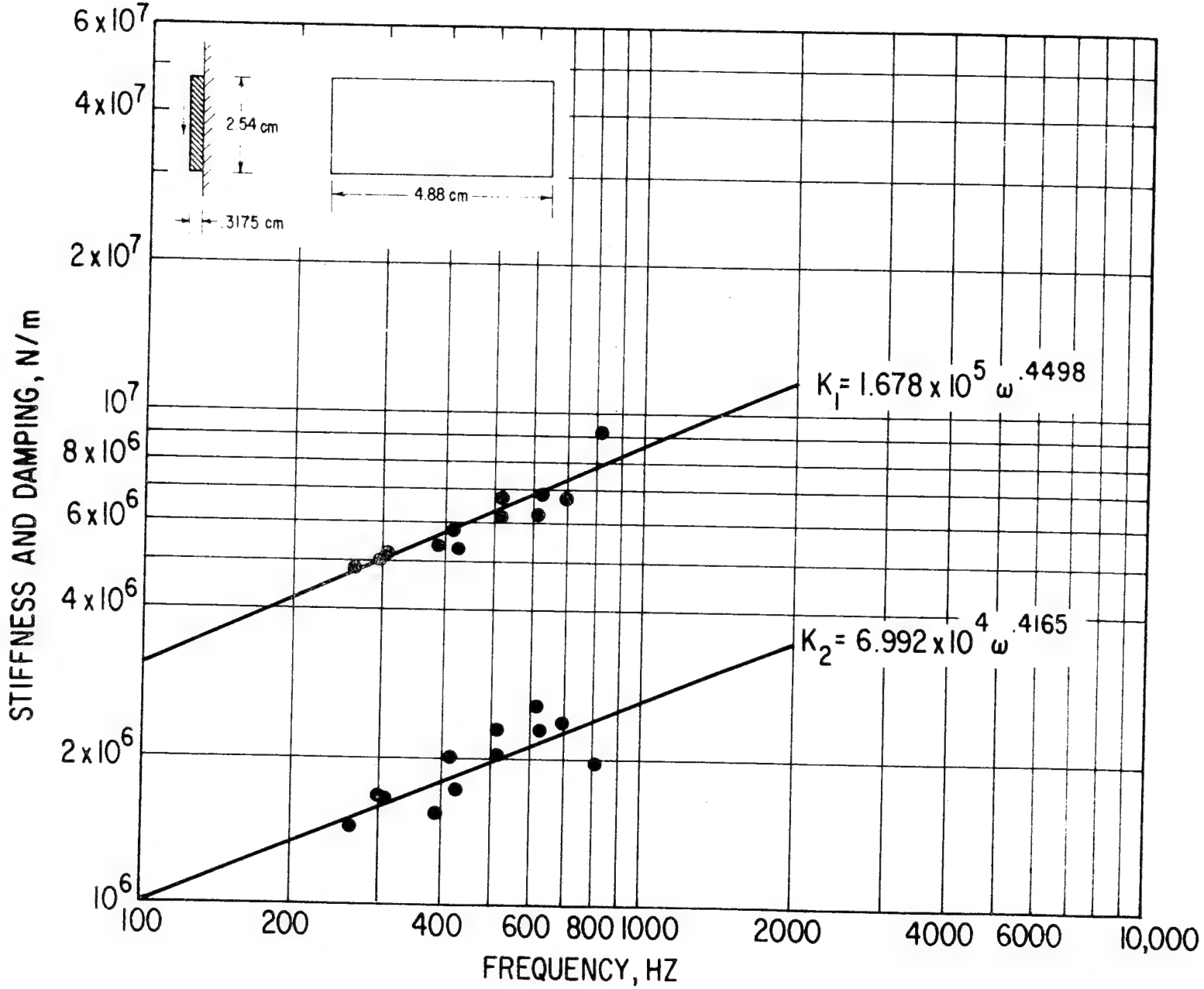

Fig. 81 Stiffness and Damping vs Frequency. Shear Specimens. Zero Preload, 32 C. Nominal Dissipation 4.40 watts/cm^3

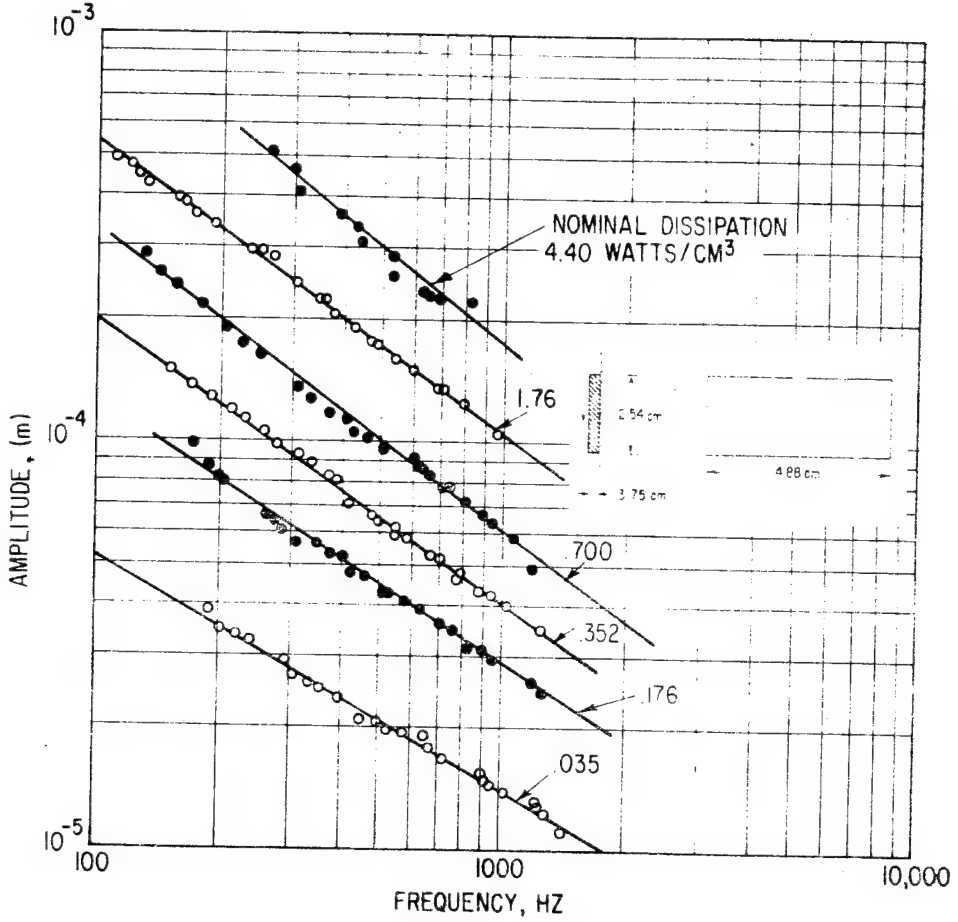

Fig. 82 Amplitude as a Function of Frequency. Shear Specimen. Zero Preload, 32 C

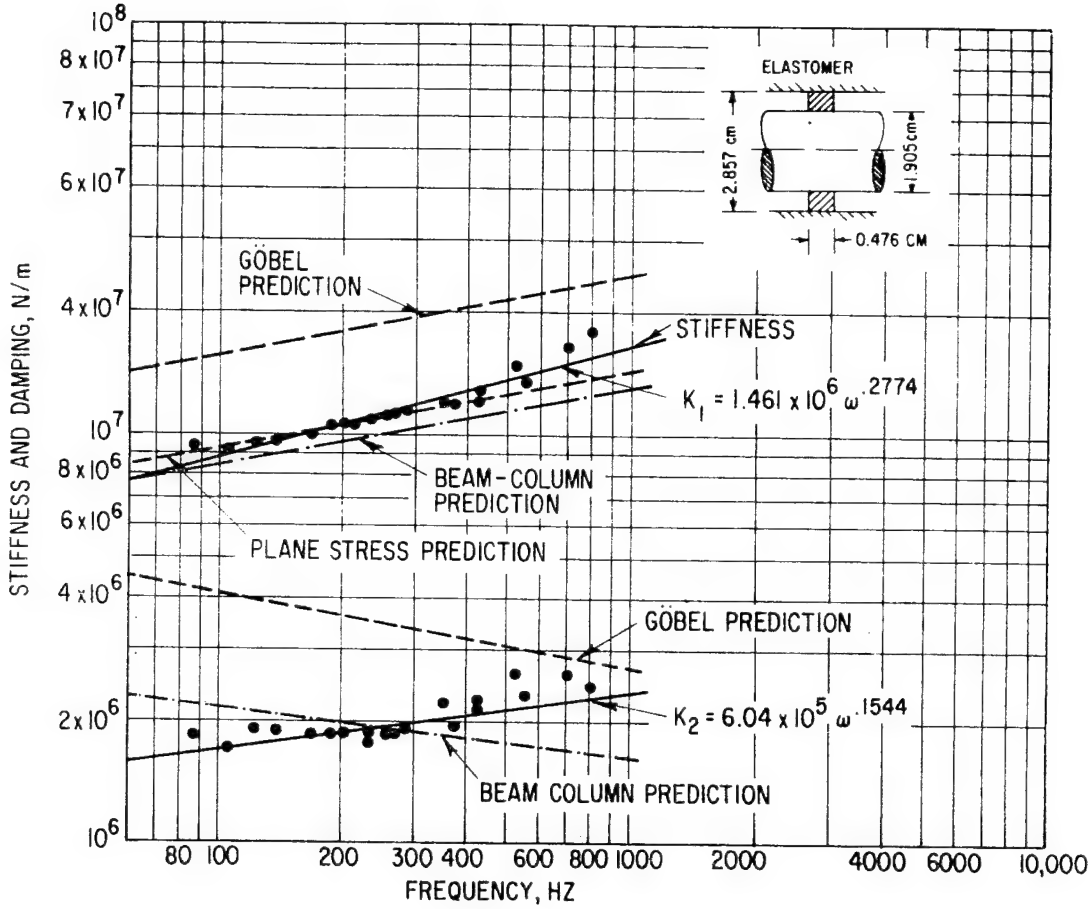

Fig. 83 Stiffness and Damping for Cartridge Specimen. 32 C. Nominal Dissipation 0.022 watts/cm^3

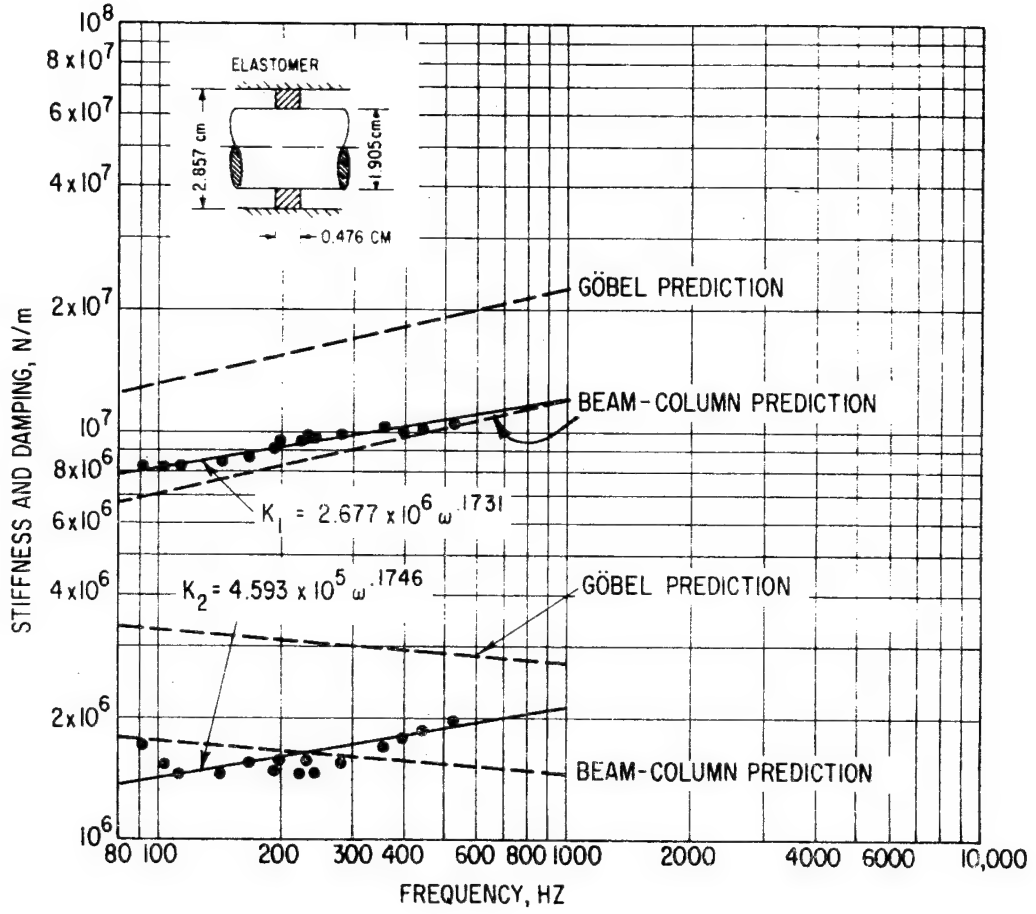

Fig. 84 Stiffness and Damping for Cartridge Specimen. 4° C. Nominal Dissipation 0.022 watts/cm^3

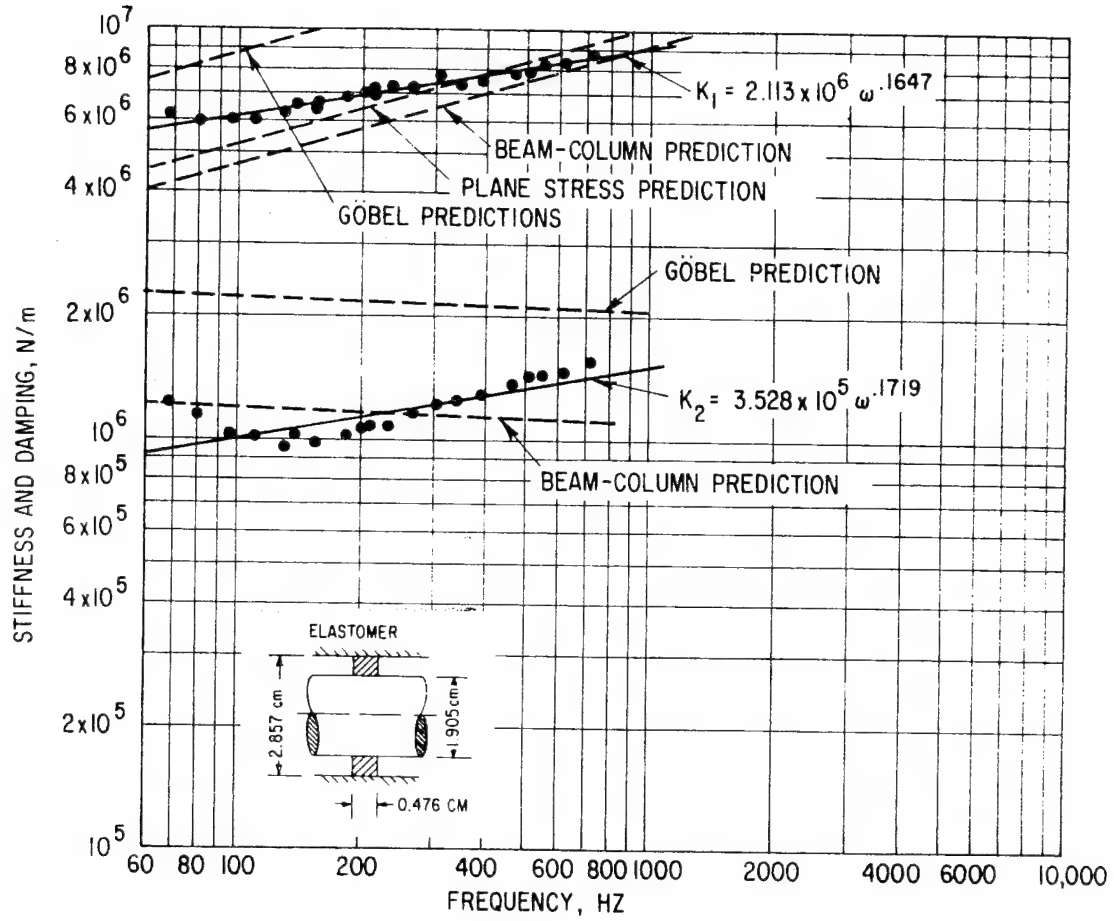

Fig. 85 Stiffness and Damping for Cartridge Specimen. 66 C. Nominal Dissipation 0.022 watts/cm^3

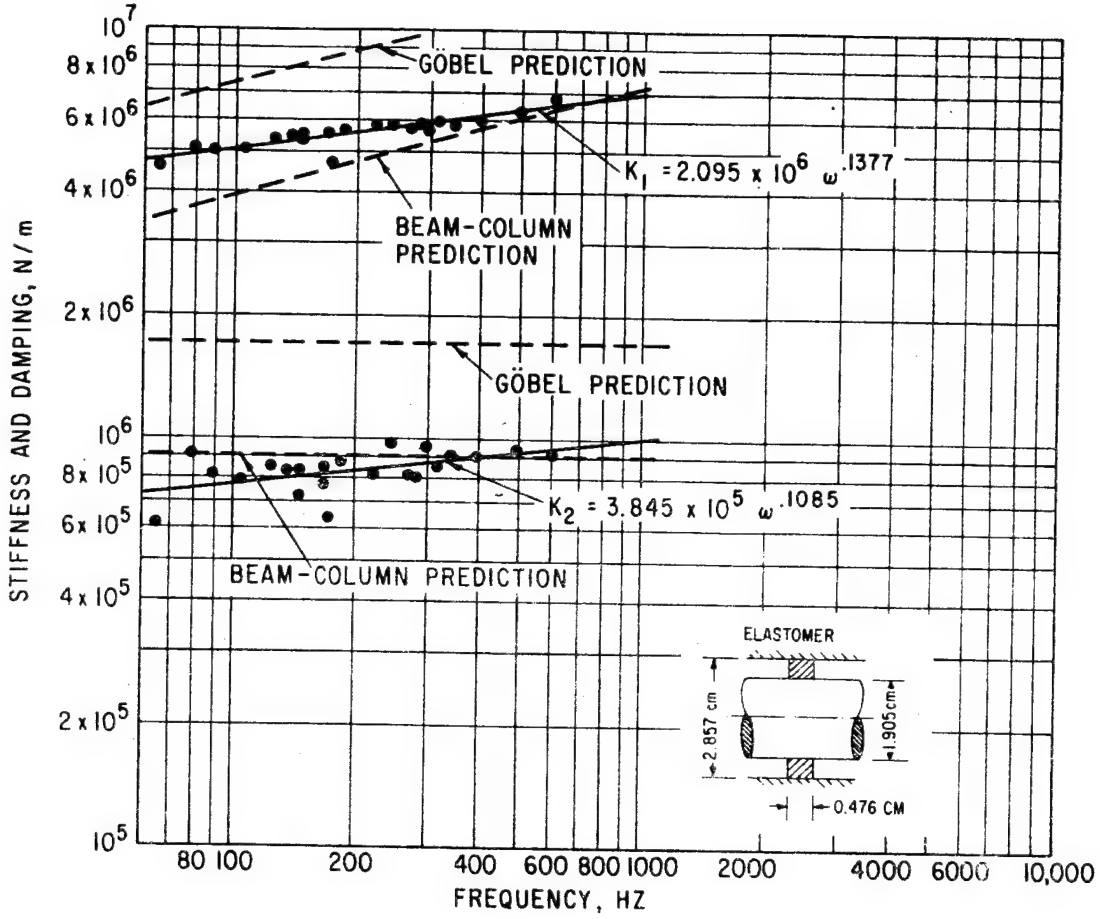

Fig. 86 Stiffness and Damping for Cartridge Specimen .0 C.
Nominal Dissipation 0.022 watts/cm^3

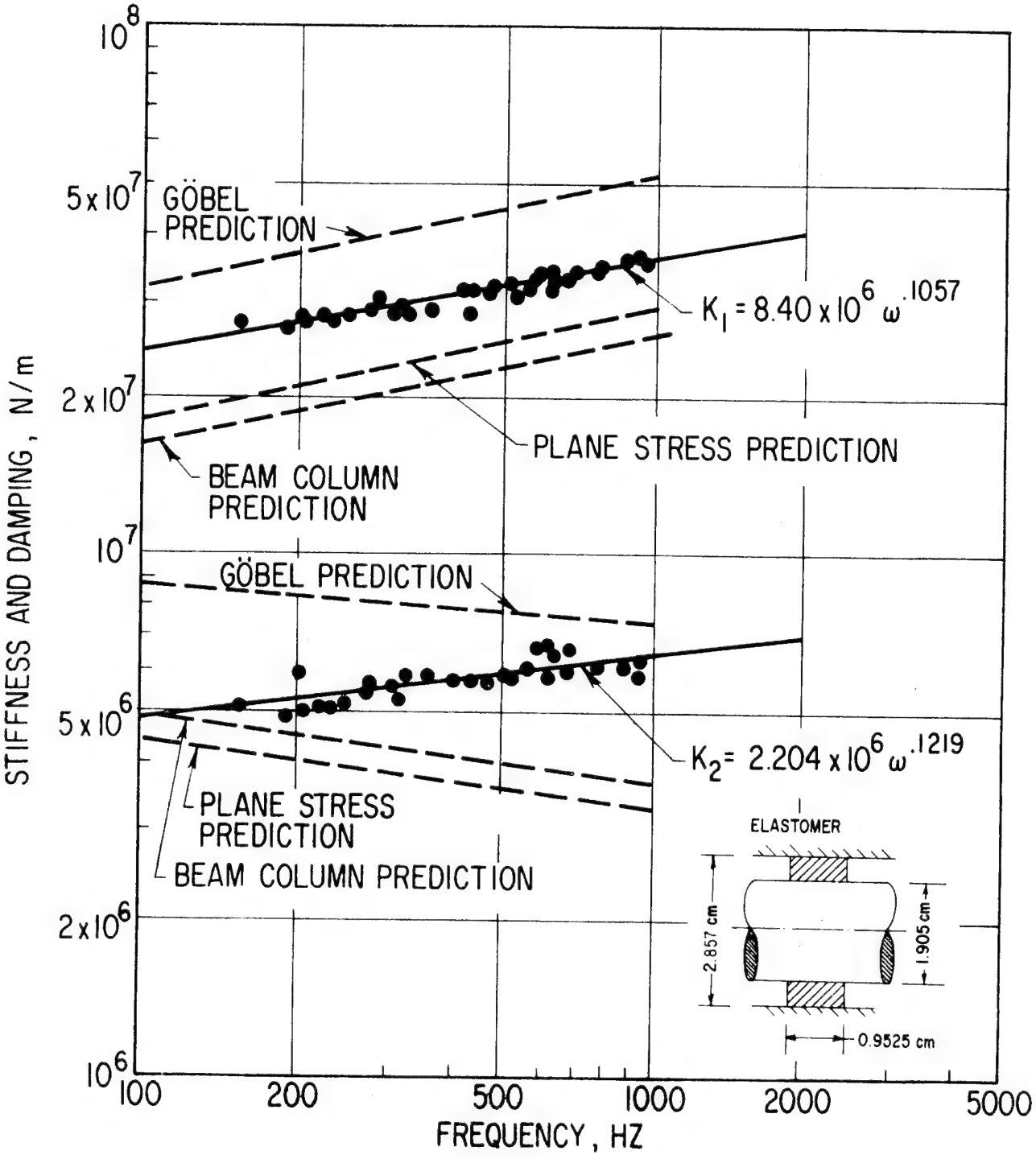

Fig. 87 Stiffness and Damping for Cartridge Specimen. 32 C. Nominal Dissipation 0.022 watts/cm^3

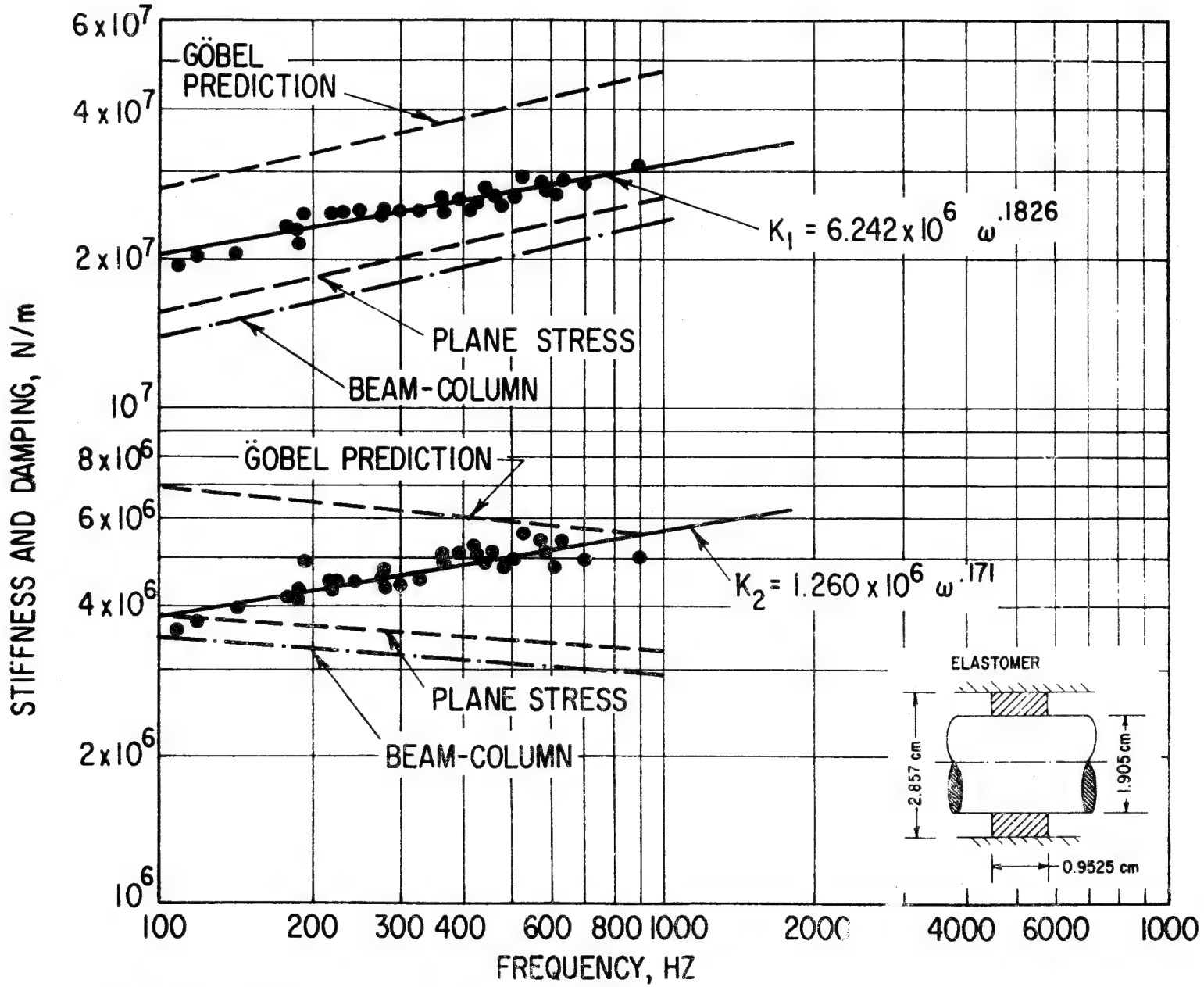

Fig. 88 Dynamic Stiffness and Damping for Cartridge Specimen. 44 C. Nominal Dissipation 0.022 watts/cm^3 (Four Elements as Shown) (Dimensions as Shown).

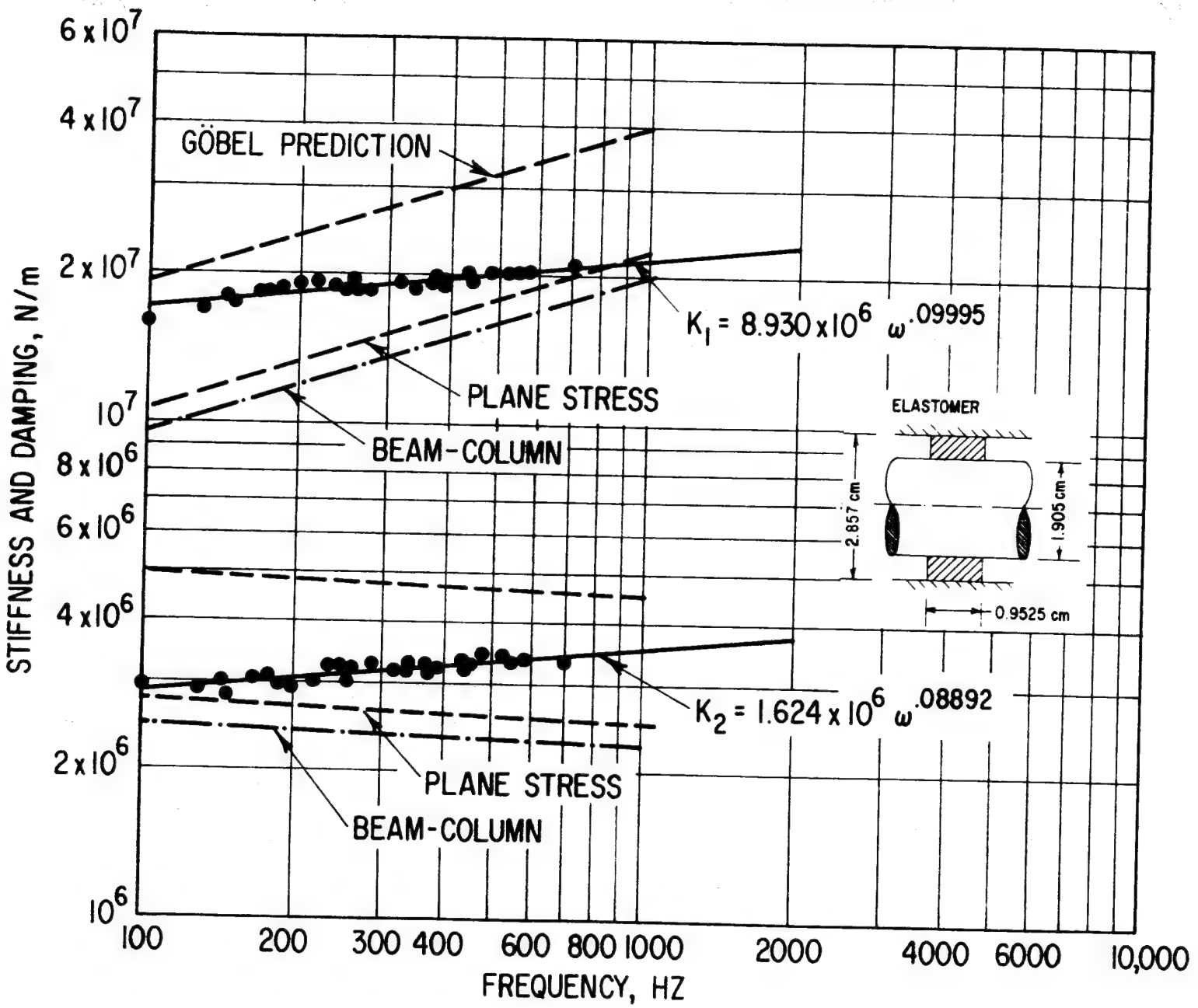

Fig. 89 Dynamic Stiffness and Damping for Cartridge Specimen. 64 C. Nominal Dissipation 0.022 watts/cm^3 (Four Elements as Shown)

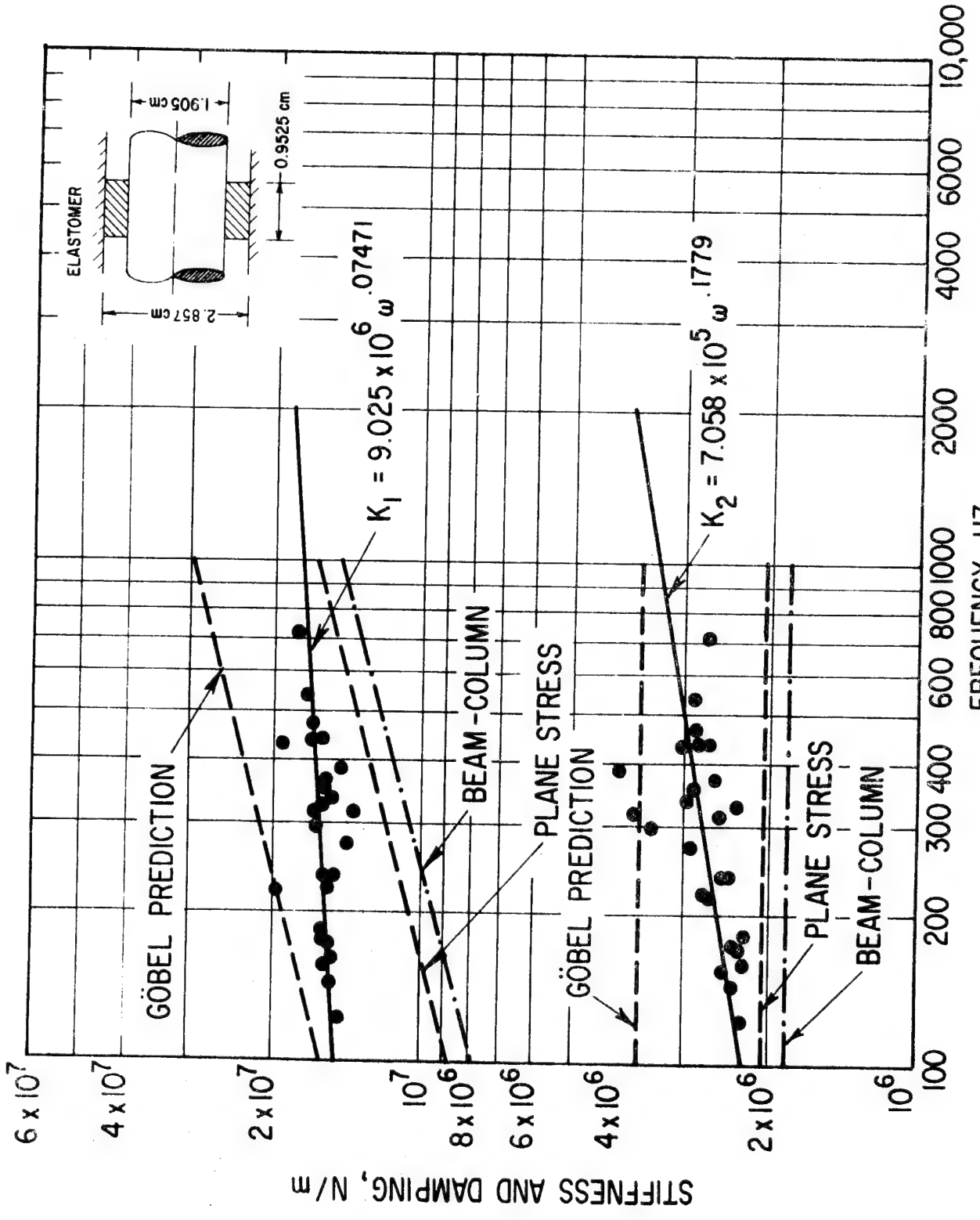

Fig. 90 Dynamic Stiffness and Damping for Cartridge Specimen. 80 C.
Nominal Dissipation 0.022 watts/cm^3 (Four Elements as Shown).

With some exceptions, for damping of the shorter specimen, the test data lies within the band defined by the highest and lowest prediction lines. The shorter specimen data generally approaches the Beam-Column predictions most closely, while the longer specimen data more generally lies midway between the Beam-Column and Gobel prediction lines.

The stiffness data shows a similar slope to the predictions, whereas the damping test data shows a different trend from the predictions. The material properties for the elastomers obtained from shear specimen tests indicate a slight decrease in loss modulus with frequency. Since the cartridge damping predictions are related to the loss modulus via a frequency independent geometry factor they also reflect this decrease with frequency. The cartridge test data, however, shows a consistent increase with frequency.

Cartridge Tests at Different Dissipation Levels

These tests are performed with the same two cartridge test specimens as for the tests at different temperatures. The temperature for these tests was 32 C. Data for the shorter specimen are presented in Figures 91 through 96 and for the larger specimen in Figures 97 through 101. In Figures 96 and 101, corresponding to each plot of stiffness and damping versus frequency, is a line showing amplitude as a function of frequency. With one exception, there is good distinction between the lines on Figures 96 and 101. However, in Figure 96, above 210 Hz, the points identified as 1.32 watts/cm^3 nominal dissipation lie very close to the line for 0.88 watts/cm^3. Apparently the required test conditions for 1.32 watts/cm^3 were not maintained above 210 Hz. Comparison of Figures 94 and 95 confirm that, below 210 Hz, there is significant difference in the stiffness and damping data, whereas, above 210 Hz, the two figures present very similar results. Figure 95 is intended, for completeness since, toghether with the data of Figure 96 it fully defines the test conditions for individual points.

The effects of dissipation level are, generally, to decrease both stiffness and damping although this trend is less pronounced at high frequency than at low frequency. In other words, the lines of stiffness and damping versus frequency becomes steeper at high dissipation levels.

Specimen Catalog

The power law curve fit coefficients for all the specimens whose stiffness and damping are plotted in Figures 57 through 101 are summarized as a function of temperature, dissipation and geometry in Tables XI, XII and XIII. These tables form the Specimen Catalog for shear, compression and cartridge geometries.

Transient Behavior

In high dissipation tests with the compression specimens, a level of dissipation was reached at which it was no longer possible to maintain a subresonant condition. When the input acceleration to the shake table

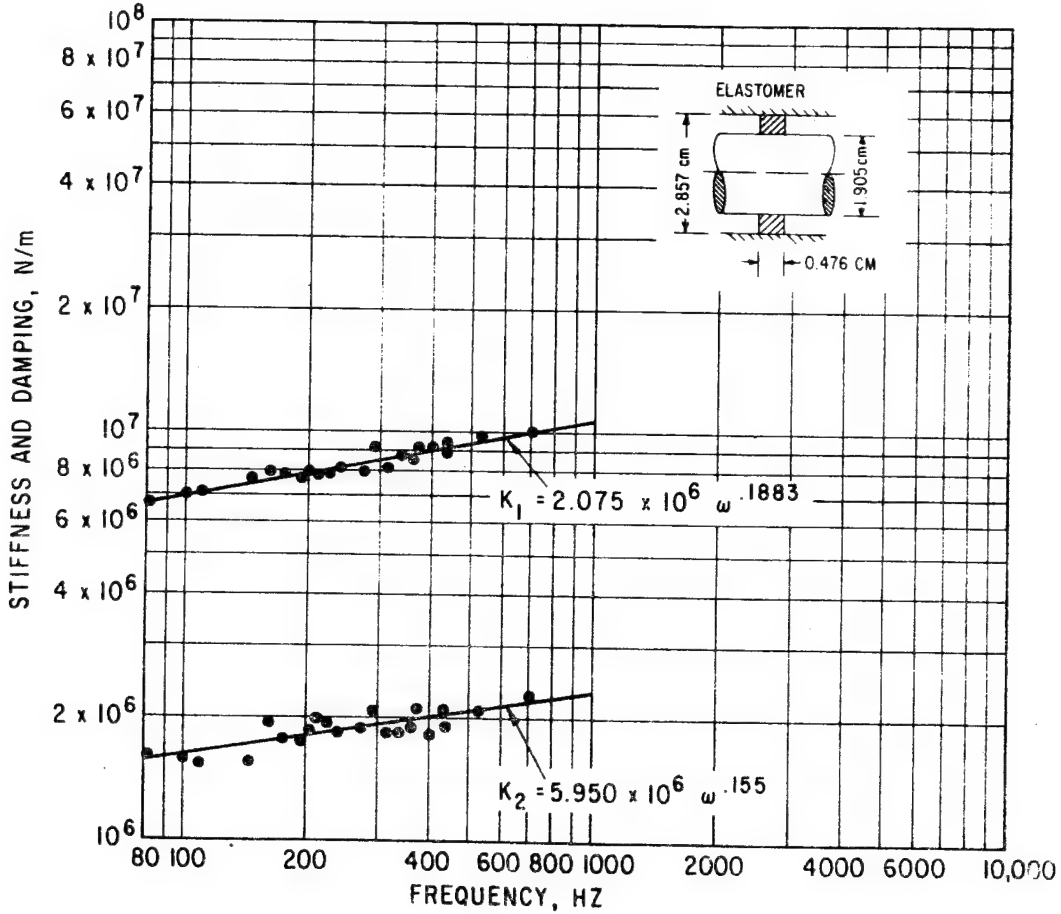

Fig. 91 Stiffness and Damping for Cartridge Specimen. 32 C. Nominal Dissipation 0.11 watts/cm^3

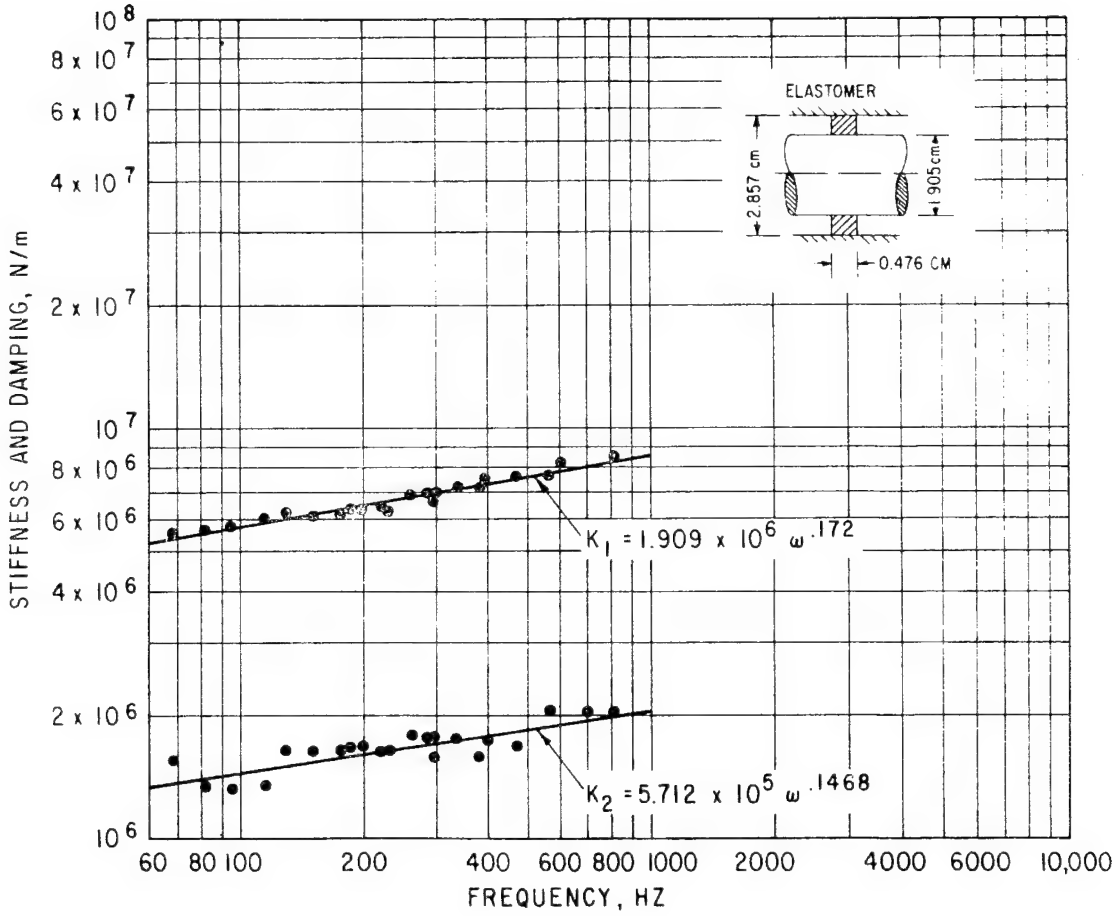

Fig. 92 Stiffness and Damping for Cartridge Specimen. 32 C. Nominal Dissipation 0.22 watts/cm^3.

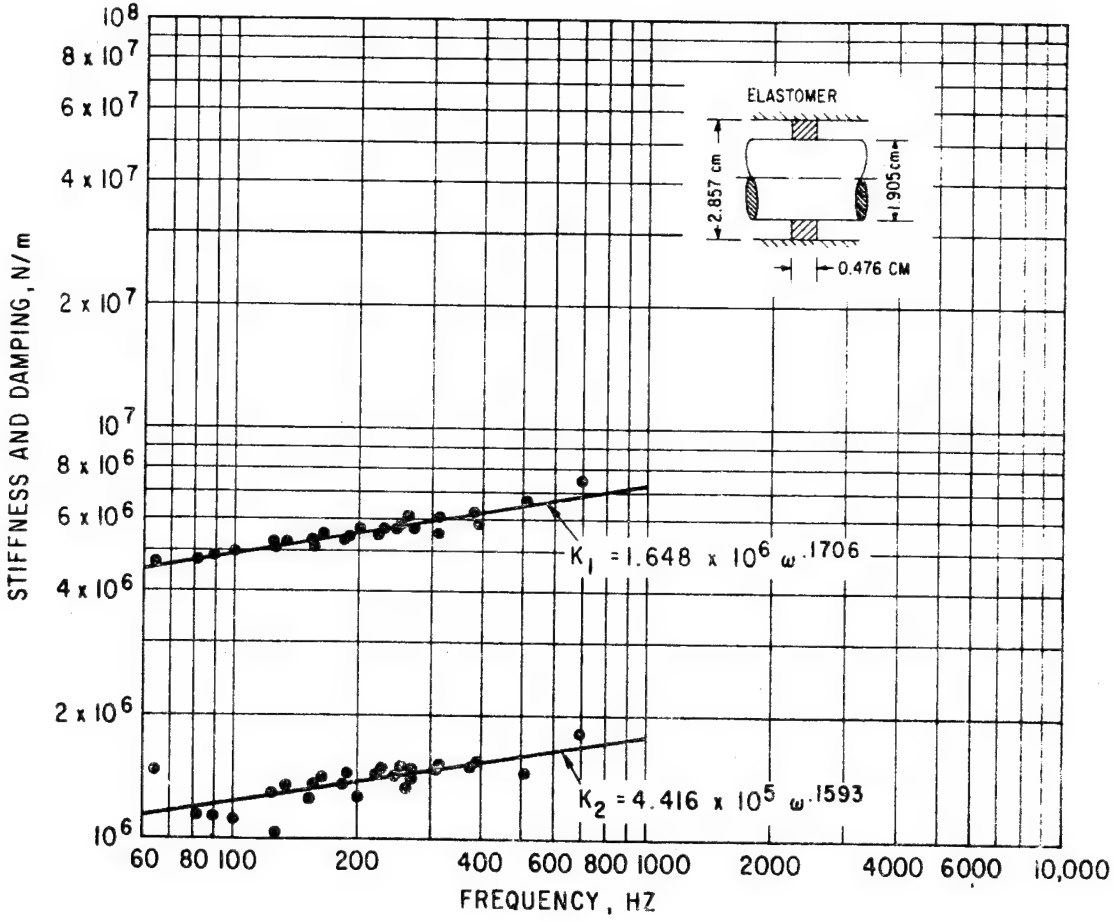

Fig. 93 Stiffness and Damping for Cartridge Specimen. 32 C. Nominal Dissipation 0.44 watts/cm^3

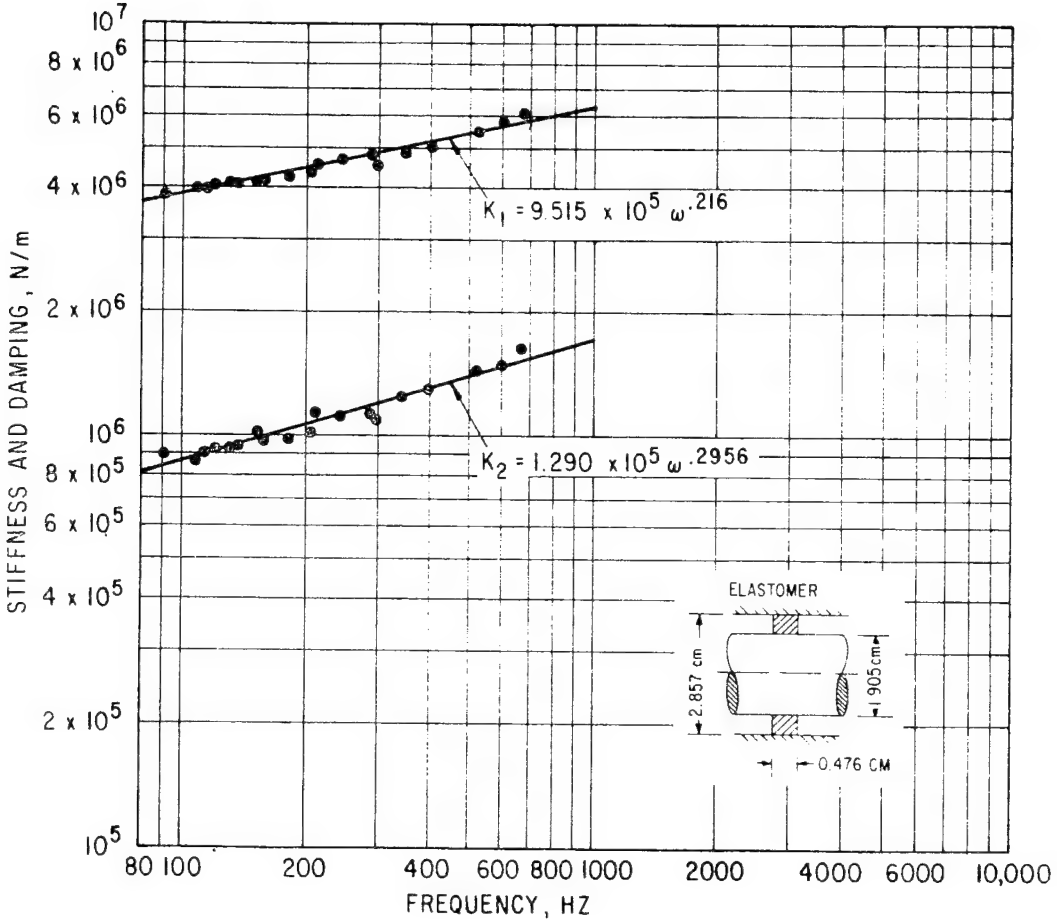

Fig. 94 Stiffness and Damping for Cartridge Specimen. 32 C. Nominal Dissipation 0.88 watts/cm^3

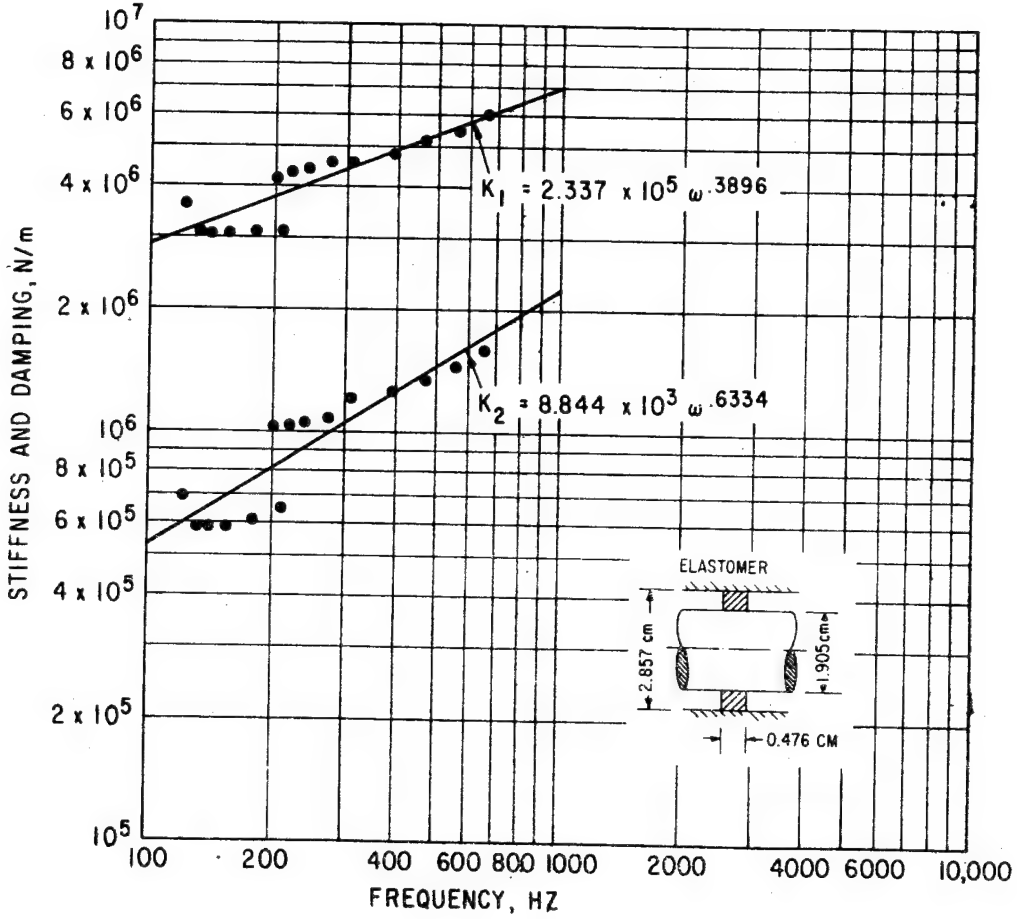

Fig. 95 Stiffness and Damping for Cartridge Specimen. 37 C. Nominal Dissipation 1.32 watts/cm^3

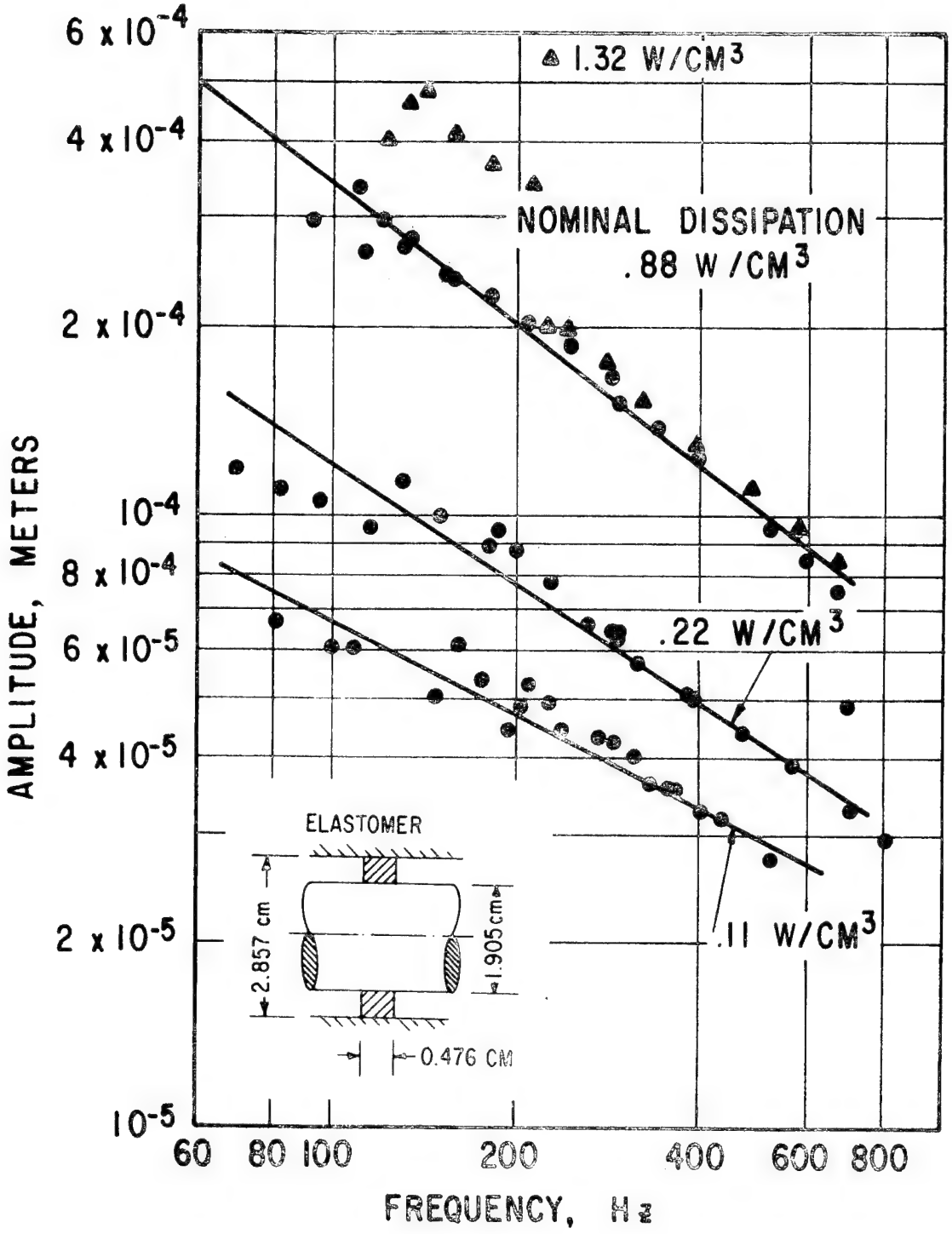

Fig. 96 Amplitude vs Frequency. Narrow Cartridge Specimen. High Dissipation Tests. 32 C (Four Elements with Detail as Shown)

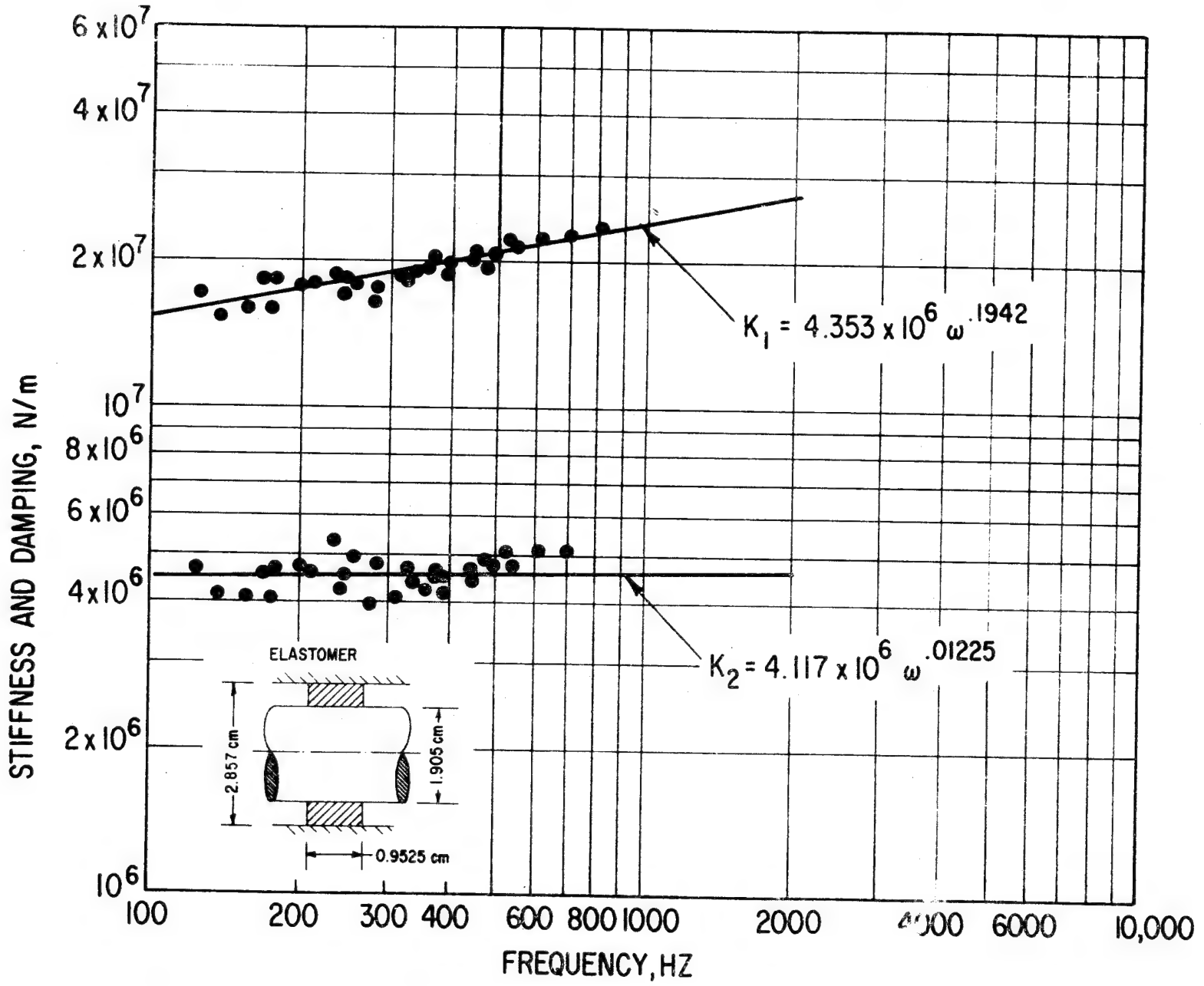

Fig. 97 Dynamic Stiffness and Damping for Cartridge Specimen. 32 C. Nominal Dissipation 0.16 watts/cm^3 (Four Elements as Shown)

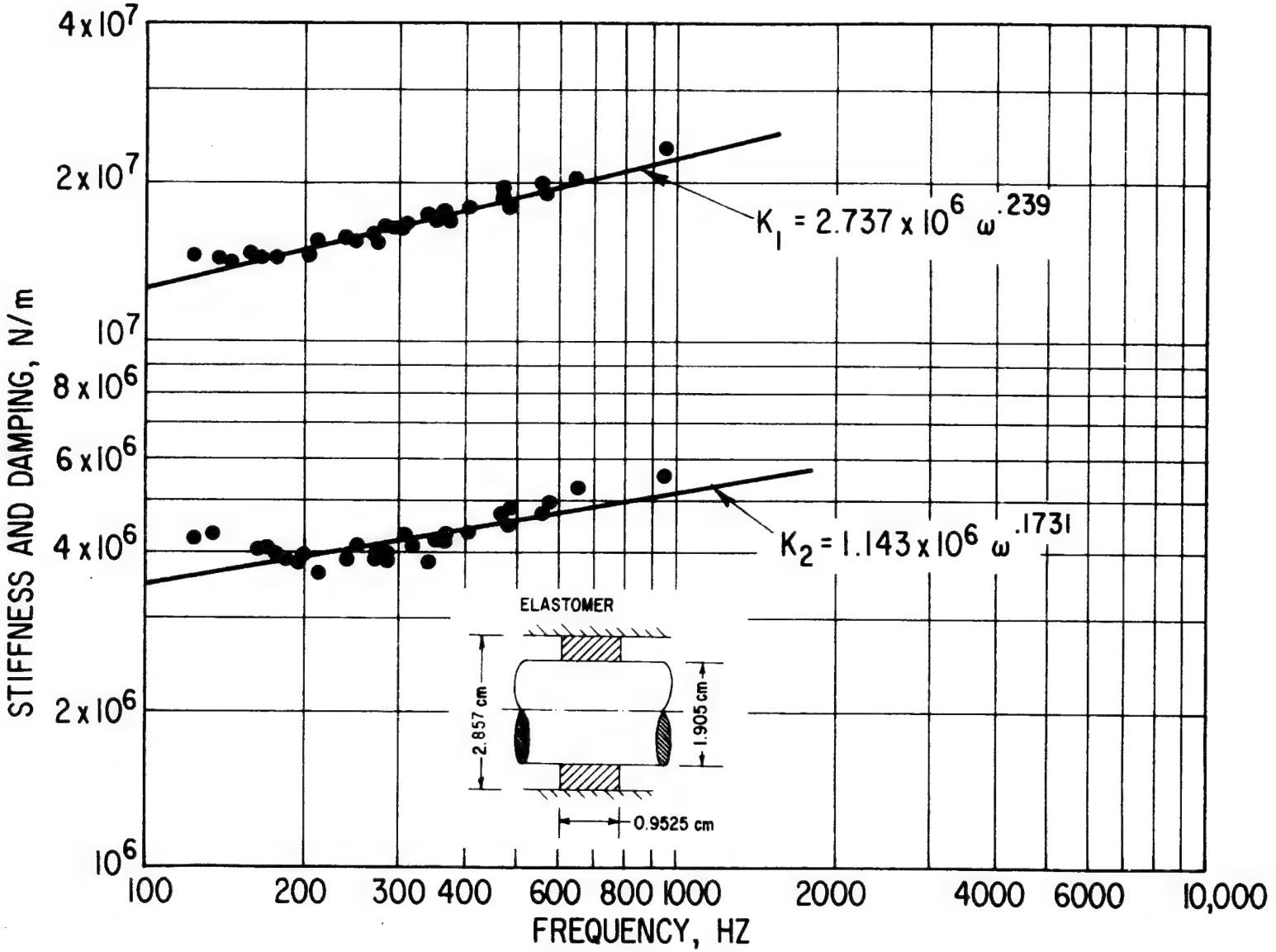

Fig. 98 Dynamic Stiffness and Damping for Cartridge Specimen. 32 C. Nominal Dissipation 0.50 watts/cm^3 (Four Elements as Shown)

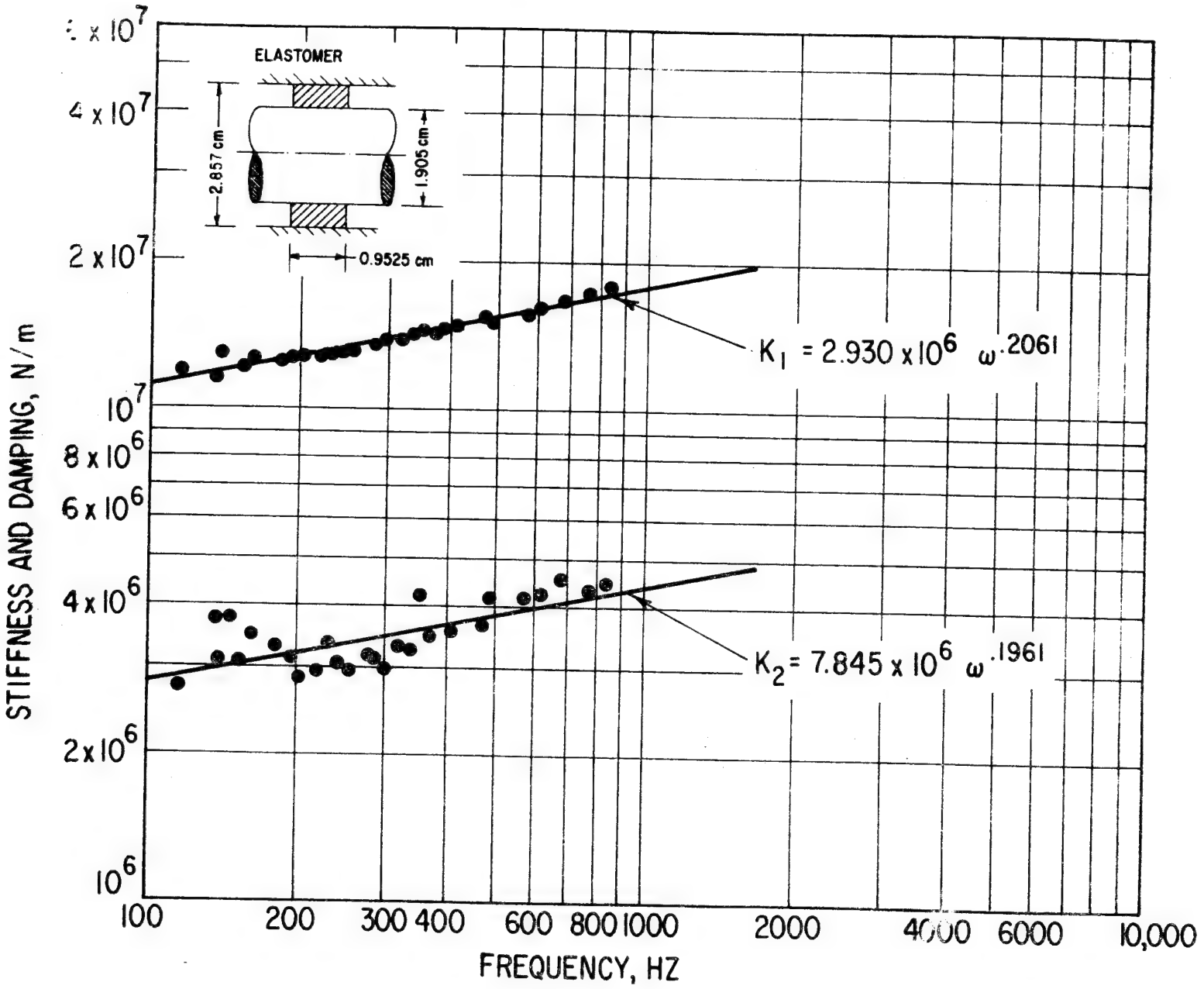

Fig. 99 Dynamic Stiffness and Damping for Cartridge Specimen. 32 C. Nominal Dissipation 1.00 watts/cm^3 (Four Elements as Shown).

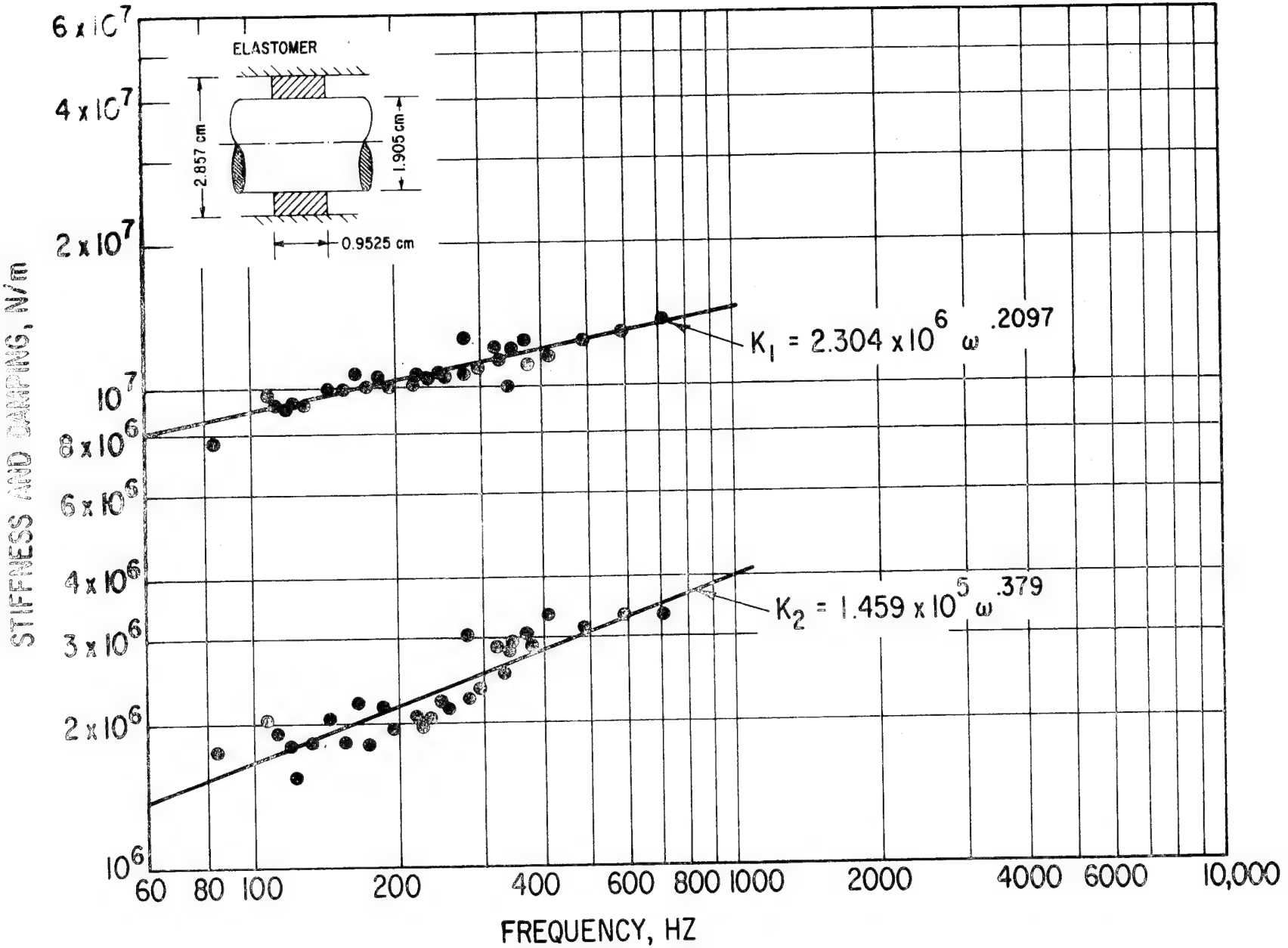

Fig. 100 Dynamic Stiffness and Damping for Cartridge Specimen. 32 C. Nominal Dissipation 1.8 watts/cm^3 (Four Elements as Shown)

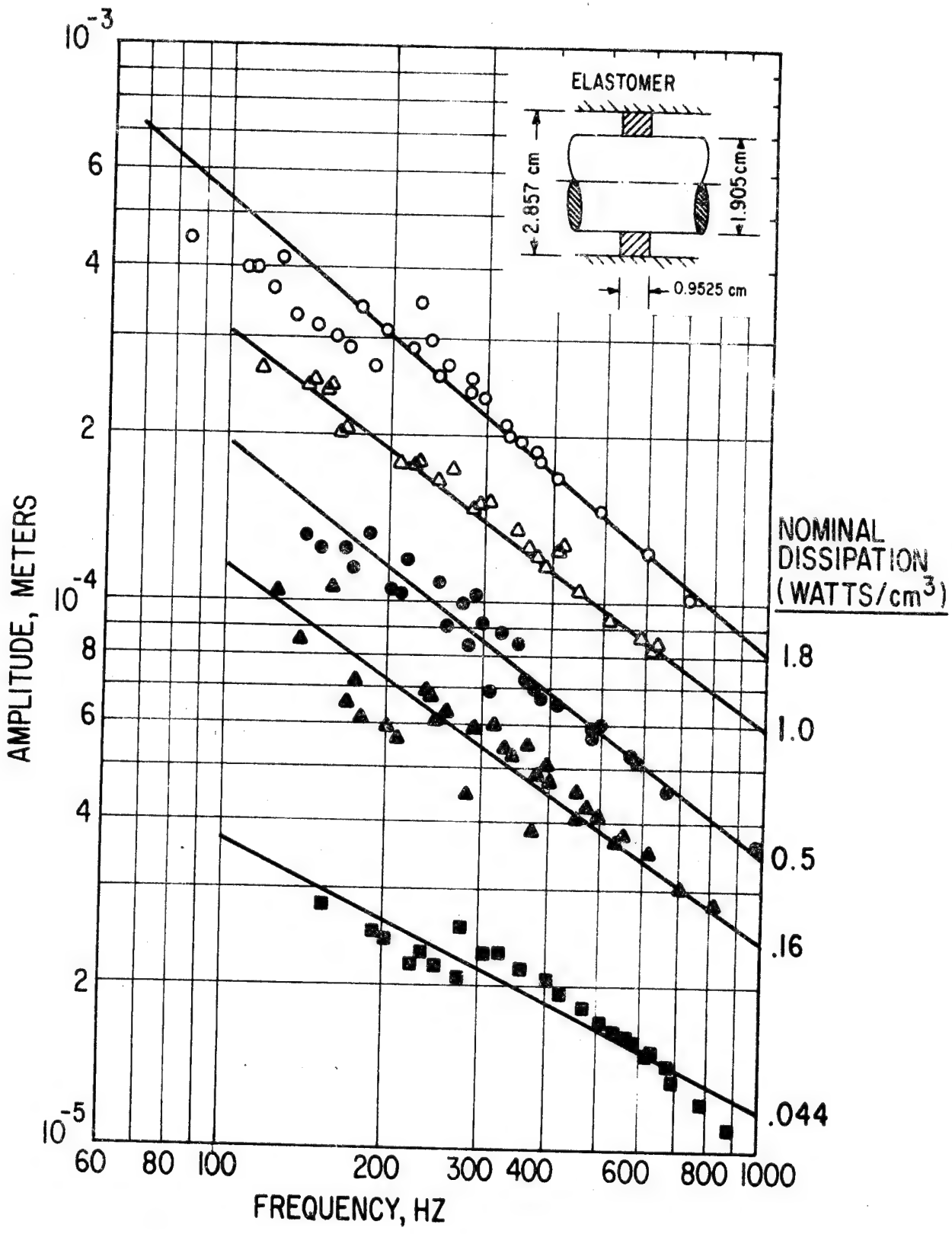

Fig. 101 Amplitude vs Frequency. Wide Cartridge Specimen. High Dissipation Tests. 32 C (Four Elements with Detail as Shown)

TABLE XI. SPECIMEN CATALOG
(SHEAR SPECIMEN)

$$\left[\text{Stiffness: } K_1 = A_1\,\omega^{B_1};\ \text{Damping: } K_2 = A_2\,\omega^{B_2}\right]$$

Temp (C)	Pre-load	Dissi-pation w/cm^3	Dimensions*			No.	Stiffness, N/m		Damping, N/m		Run No.	Fig. No.
			(h)	(b)	(x)		A_1	B_1	A_2	B_2		
32	--	0.062	0.3175	1.27	4.88	8	5.752×10^{6}	0.2037	1.30×10^{7}	-0.1277	8-01→06	57
50	--	0.062	0.3175	1.27	4.88	8	2.971×10^{6}	0.2677	6.197×10^{6}	-0.06372	8-07→11	58
66	--	0.062	0.3175	1.27	4.88	8	1.710×10^{6}	0.3037	3.782×10^{6}	0.03011	8-12→16	59
93	--	0.062	0.3175	1.27	4.88	8	1.868×10^{6}	0.245	1.06×10^{6}	0.0225	8-17→21	60
32	--	0.035	0.3175	2.54	4.88	4	5.088×10^{6}	0.1914	4.451×10^{6}	0.03608	4-62→67	76
32	--	0.176	0.3175	2.54	4.88	4	2.448×10^{6}	0.2509	1.999×10^{6}	0.07099	4-68→73	77
32	--	0.352	0.3175	2.54	4.88	4	1.355×10^{6}	0.3009	8.545×10^{5}	0.1729	4-74→79	78
32	--	0.704	0.3175	2.54	4.88	4	1.014×10^{6}	0.3066	2.767×10^{5}	0.2998	4-80→85	79
32	--	1.76	0.3175	2.54	4.88	4	7.086×10^{5}	0.304	6.916×10^{4}	0.436	4-86→91	80
32	--	4.40	0.3175	2.54	4.88	4	1.678×10^{5}	0.4498	6.992×10^{4}	0.4165	4-92→95	81

*Dimensions are for thickness (h), width (b), and length (x).

TABLE XII. SPECIMEN CATALOG
(COMPRESSION ELEMENTS)

[Stiffness: $K_1 = A_1 \omega^{B_1}$; Damping: $K_2 = A_2 \omega^{B_2}$]

Temp (C)	Pre-load	Dissi-pation w/cm^3	Dimensions* (d)	Dimensions* (h)	No.	Stiffness, N/m A_1	Stiffness, N/m B_1	Damping, N/m A_2	Damping, N/m B_2	Run No.	Fig. No.
66	2.5	0.062	1.27	0.635	10	1.921×10^6	0.2102	7.145×10^5	0.09152	10-01→05	63
66	5	0.062	1.27	0.635	10	2.525×10^6	0.1812	6.073×10^5	0.1101	10-06→09	64
93	2.5	0.062	1.27	0.635	10	2.042×10^6	0.1620	3.377×10^5	0.1444	10-10→13	65
93	5	0.062	1.27	0.635	10	3.084×10^6	0.1205	6.381×10^5	0.06282	10-14→17	66
32	2.5	0.44	1.27	0.635	10	1.853×10^6	0.2186	8.367×10^5	0.1154	10-18→21	69
32	2.5	1.1	1.27	0.635	10	7.561×10^5	0.3073	4.716×10^4	0.4613	10-25→28	70
32	2.5	2.2	1.27	0.635	10	1.198×10^6	0.2025	2.601×10^4	0.4839	10-37→39	71
32	5	0.55	1.27	0.635	10	1.270×10^6	0.2645	4.438×10^5	0.192	10-33→36	72
32	5	1.1	1.27	0.635	10	4.290×10^5	0.3896	3.425×10^4	0.505	10-29→32	73

*Dimensions are diameter (d), and height (h).

TABLE XIII. SPECIMEN CATALOG
(CARTRIDGE ELEMENTS)

$$\left[\text{Stiffness: } K_1 = A_1 \omega^{B_1};\quad \text{Damping: } K_2 = A_2 \omega^{B_2}\right]$$

Temp (C)	Pre-load	Dissi-pation w/cm^3	Dimensions*			No.	Stiffness, N/m		Damping, N/m		Run No.	Fig. No.
			D_i	D_o	ℓ		A_1	B_1	A_2	B_2		
32	--	0.022	1.905	2.858	0.476	4	1.461×10^6	0.2774	6.041×10^5	0.1544	4C2-01→04	83
43	--	0.022	1.905	2.858	0.476	4	2.677×10^6	0.1731	4.593×10^5	0.1746	4C2-05→08	84
66	--	0.022	1.905	2.858	0.476	4	2.113×10^6	0.1647	3.528×10^5	0.1719	4C2-09→12	85
80	--	0.022	1.905	2.858	0.476	4	2.095×10^6	0.1377	3.845×10^5	0.1085	4C2-13→16	86
32	--	0.044	1.905	2.858	0.953	4	8.400×10^6	0.1057	2.204×10^6	0.1219	4C-01→06	87
44	--	0.044	1.905	2.858	0.953	4	6.242×10^6	0.1826	1.260×10^6	0.171	4C-07→13	88
64	--	0.044	1.905	2.858	0.953	4	8.930×10^6	0.09995	1.624×10^6	0.08892	4C-14→20	89
80	--	0.044	1.905	2.858	0.953	4	9.025×10^6	0.07471	7.058×10^5	0.1779	4C-45→50	90
32	--	0.11	1.905	2.858	0.476	4	2.075×10^6	0.1883	5.950×10^6	0.155	4C2-17→20	91
32	--	0.22	1.905	2.858	0.476	4	1.909×10^6	0.172	5.712×10^5	0.1468	4C2-21→24	92
32	--	0.44	1.905	2.858	0.476	4	1.648×10^6	0.1706	4.416×10^5	0.1593	4C2-25→28	93
32	--	0.88	1.905	2.858	0.476	4	9.515×10^5	0.216	1.290×10^5	0.2956	4C2-29→32	94
32	--	1.32	1.905	2.858	0.476	4	2.337×10^5	0.3896	8.844×10^3	0.6334	4C2-33→36	95
32	--	0.16	1.905	2.858	0.953	4	4.353×10^6	0.1942	4.117×10^6	0.01225	4C-21→26	97
32	--	0.5	1.905	2.858	0.953	4	2.330×10^6	0.2597	7.924×10^5	0.2197	4C-27→32	98
32	--	1.0	1.905	2.858	0.953	4	4.445×10^6	0.154	1.455×10^5	0.1189	4C-33→38	99
32	--	1.8	1.905	2.858	0.953	4	2.304×10^6	0.2097	1.459×10^5	0.379	4C-39→44	100

*Dimensions are inner diameter (D_i), outer diameter (D_o), and width (ℓ).

reached a critical level, a slow but consistent change in system conditions would set in. With no further adjustments to frequency of input acceleration, the output acceleration would steadily increase with time, reach a peak, then reduce and settle at a steady value. During this change in acceleration the phase angle would increase from as low as 30° and stabilize at a value above 90°. This change in phase angle was a clear indication that the operating condition of the system had changed from subresonant to superresonant. This transient phenomenon was also accompanied by a significant increase by as much as 10 C in the temperature measured near the specimen.

With a higher input acceleration, the same phenonmenon would occur but its time scale would be reduced. When just above the critical acceleration level, the peak amplitude would occur after several minutes. However, levels of acceleration could be reached where the peak amplitude would occur within 15 seconds.

The phenomenon was not observed in the shear specimen tests or in the cartridge specimen tests.

Some typical traces of output acceleration as a function of time are shown in Figure 102. The frequency in all cases is 433 Hz and the supported mass is 0.908 kg. The lowest line on the figure illustrates the result of an input acceleration below the critical level at which the trnasient phenomenon sets in. In the center line on this figure the input acceleration is just above the critical level. Over several minutes the output acceleration increases at a slow steady rate and then increases sharply until a peak is reached, followed by a gradual drop to an asymptotic value slightly lower than the peak value. In the upper line of this figure, the rate of increase in output acceleration is high from outset. The peak is reached within 15 seconds but the gradual drop in amplitude to an aymptotic value still takes over a minute.

Phase angles at the beginning and end of each trace are shown as circled values. The increase in phase angle from below to above 90° for the two lines with a peak is apparent.

The fact that this is a transient phenomenon, the fact that a chnage in temperature is involved, and the fact that the time scale of the phenomenon is controlled by the input acceleration and hence by the dissipation rate, strongly suggests that the cuase is a time-varying change in the thermal state of the elastomer induced by internal heating.

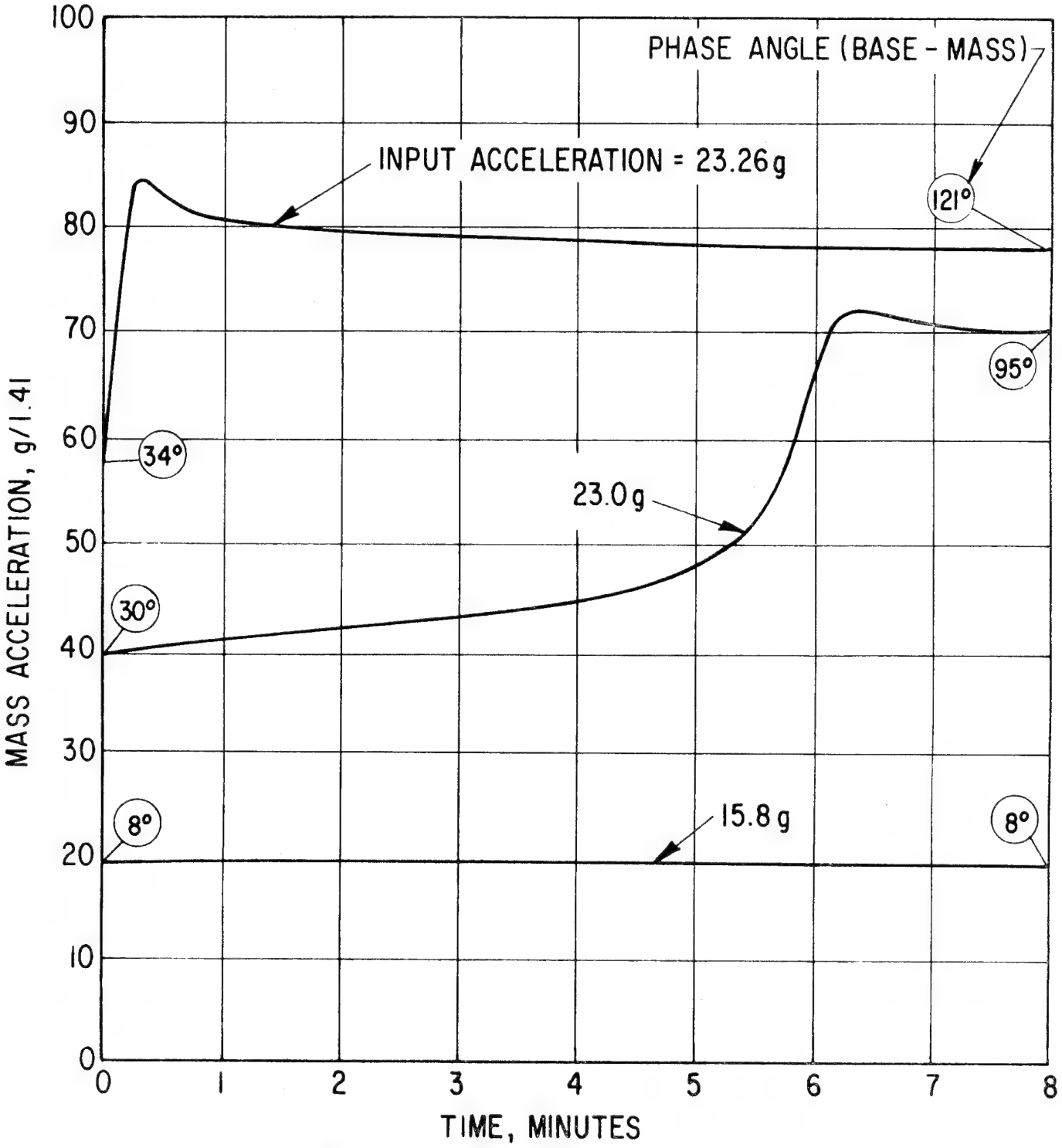

Fig. 102 Thermal Transient. Compression Specimen. Supported Mass, 0.908 Kg, Frequency 433 Hz

DISCUSSION

High Dissipation Results

As shown by the test data of the preceding section, the influence of a high dissipation rate is generally to reduce the effective stiffness and damping of an elastomer specimen. An obvious hypothesis is that internal heating reduces local material properties, and, on the basis of this hypothesis, the thermoviscoelastic model described earlier was developed. The hypothesis can now be tested by comparing the predictions of this model with the test data.

A parameter required by the model is thermal conductivity, and no value of conductivity is available for the material tested. However, since all other parameters of the model can be assigned values, once material properties and geometry factors are available, the approach taken has been to exercise the model for a range of reasonable values of conductivity, and to determine the value giving the best agreement. The initial object of this comparison is the compression test data. In Figures 103, 104 and 105 stiffness and damping are plotted against amplitude for frequencies of 175, 380 and 600 Hz. Superimposed on the compression specimen test data are predictions of the model for conductivity values of 20×10^{-4} and 6.7×10^{-4} watts/(cm C). It may be seen that the predictions for a conductivity of 6.7×10^{-4} match the test data with reasonable success, both in terms of trends and in absolute values of stiffness and damping.

The value of 6.7×10^{-4} for conductivity is not unreasonable (rubber conductivity is 1.49×10^{-3}) but there is no evidence, apart from the empirical comparison that this value is correct for polybutadiene nor, therefore, is this comparison absolute evidence of the validity of the model.

The observed transient change in amplitude and phase angle under certain high dissipation conditions, as presented in the Results Section, is qualitatively predictable by the one-dimensional thermoviscoelastic analysis described earlier. As an exercise for the model, an attempt was made to reproduce the conditions of Figure 102, and to predict comparable transient results. In addition to conductivity no value is available for specific heat for this material, although a density value was obtained from the manufacturer (0.043 lb/in.^{3}). The conductivity and specific heat values used were 6.7×10^{-4} watts/(cm C) and 0.0622 nm/kg C. The frequency was 433 Hz and the supported mass was 0.908 kg.

Figure 106 presents some of the results of this prediction for two levels of input acceleration (17.25 and 24 g), which are similar to those applied to produce the transient phenomenon in Fig. 102. A thermal transient phenomenon with a transition through resonance is predicted for both input accelerations, but the resonant peaks are much sharper than those found in a similar time scale in the corresponding test conditions shown in Figure 102. The predicted internal peak temperatures are surprisingly high, although no measurements of internal temperature are available for comparison.

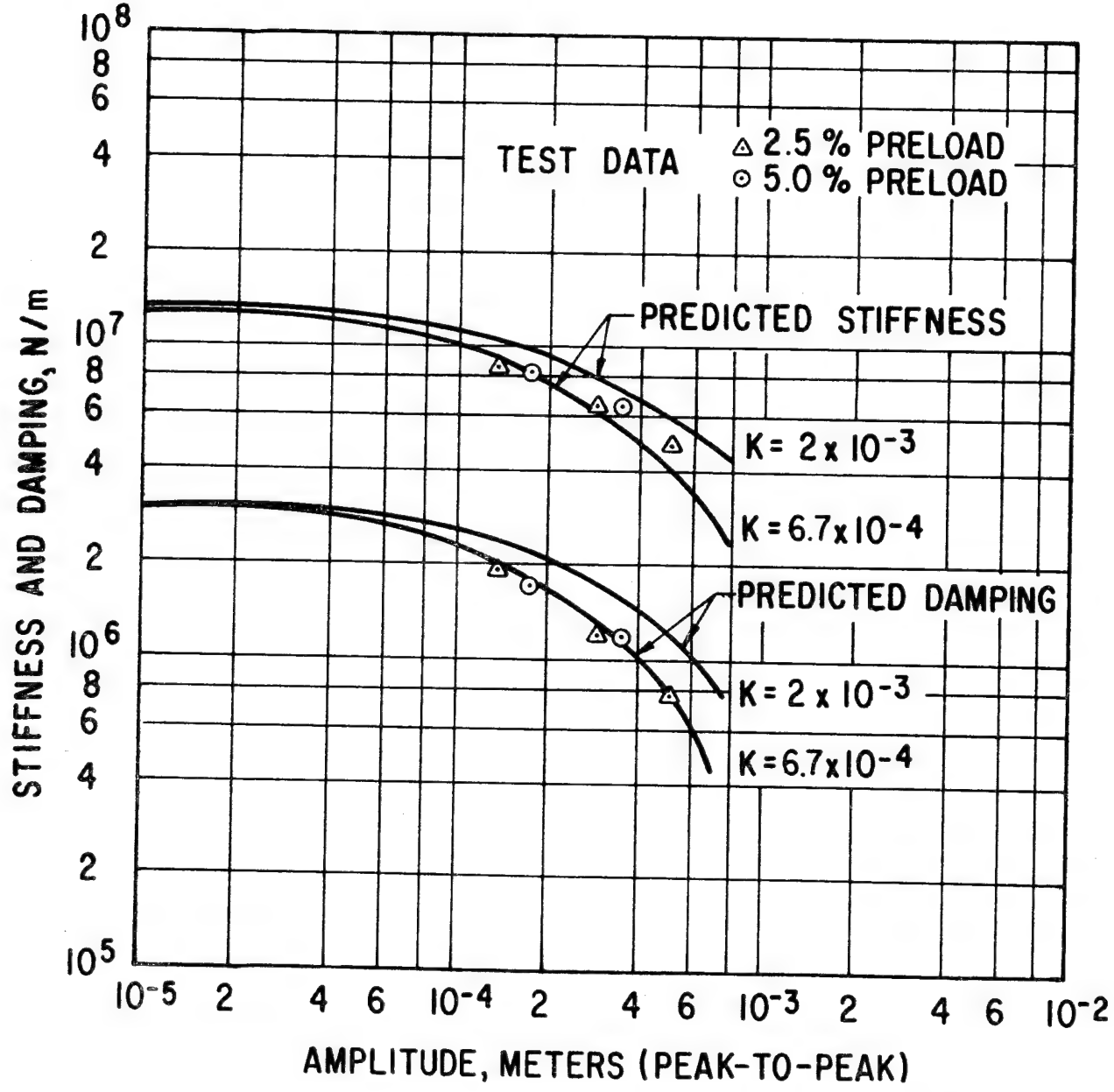

Fig. 103 Stiffness and Damping vs Amplitude for Compression Specimen, 175 Hz. Comparison of Prediction and Measurements for Two Different Values of Thermal Conductivity

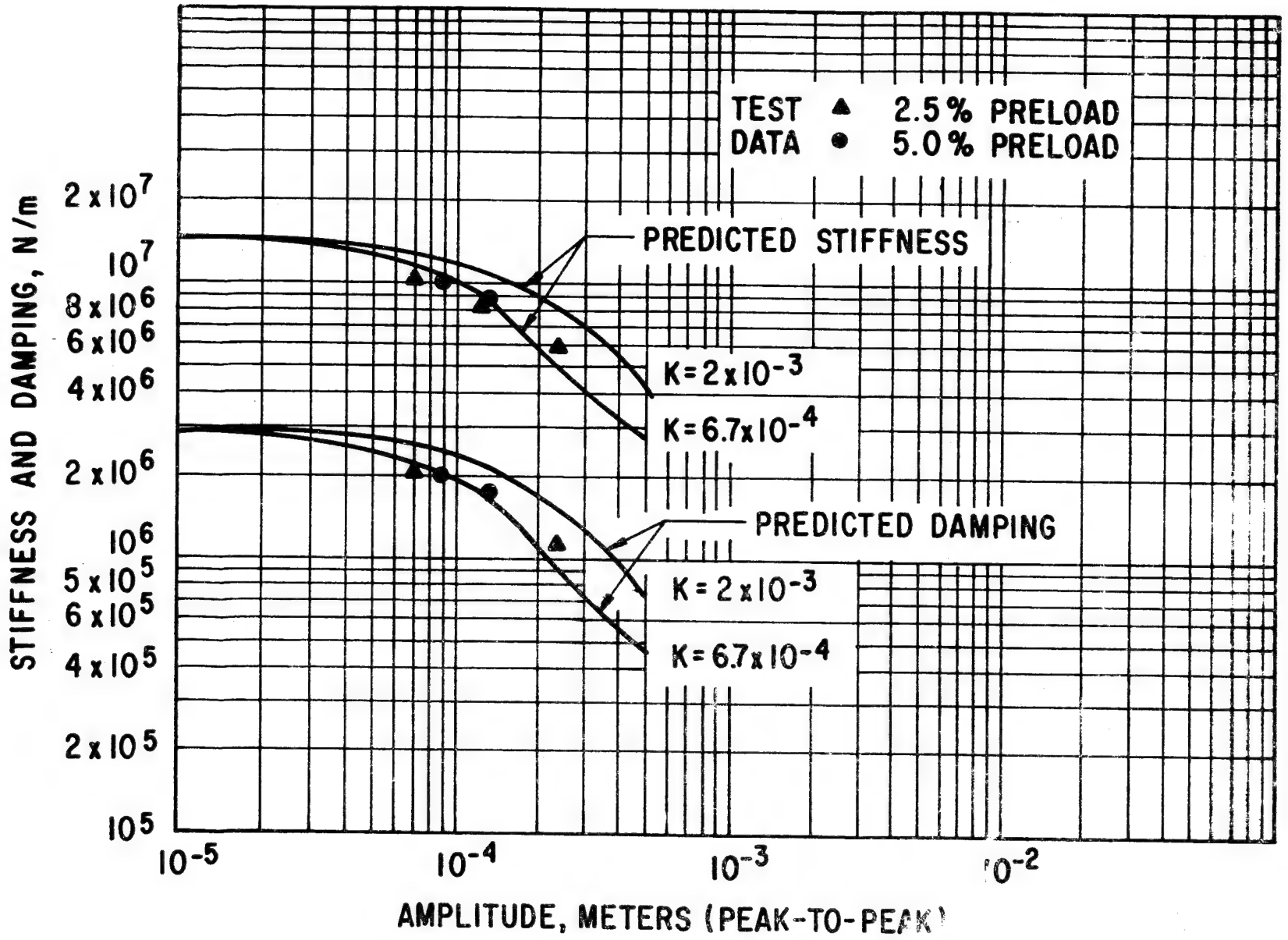

Fig. 104 Stiffness and Damping vs Amplitude for Compression Specimen, 380 Hz, 32 C. Comparison of Prediction and Measurement for Two Different Values of Thermal Conductivity

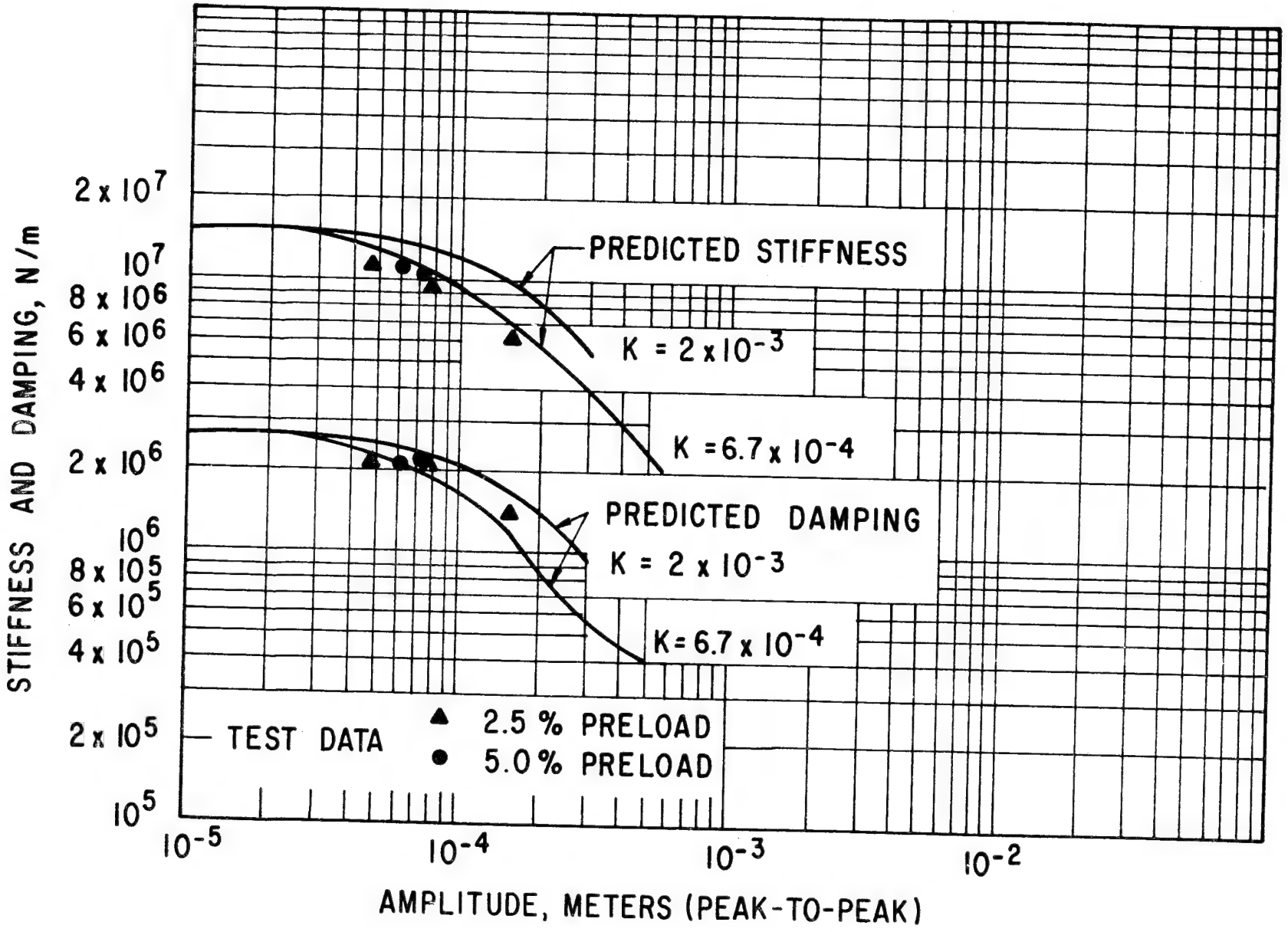

Fig. 105 Stiffness and Damping vs Amplitude for Compression Specimen, 600 Hz, 32 C. Comparison of Prediction and Measurement for Two Different Values of Thermal Conductivity.

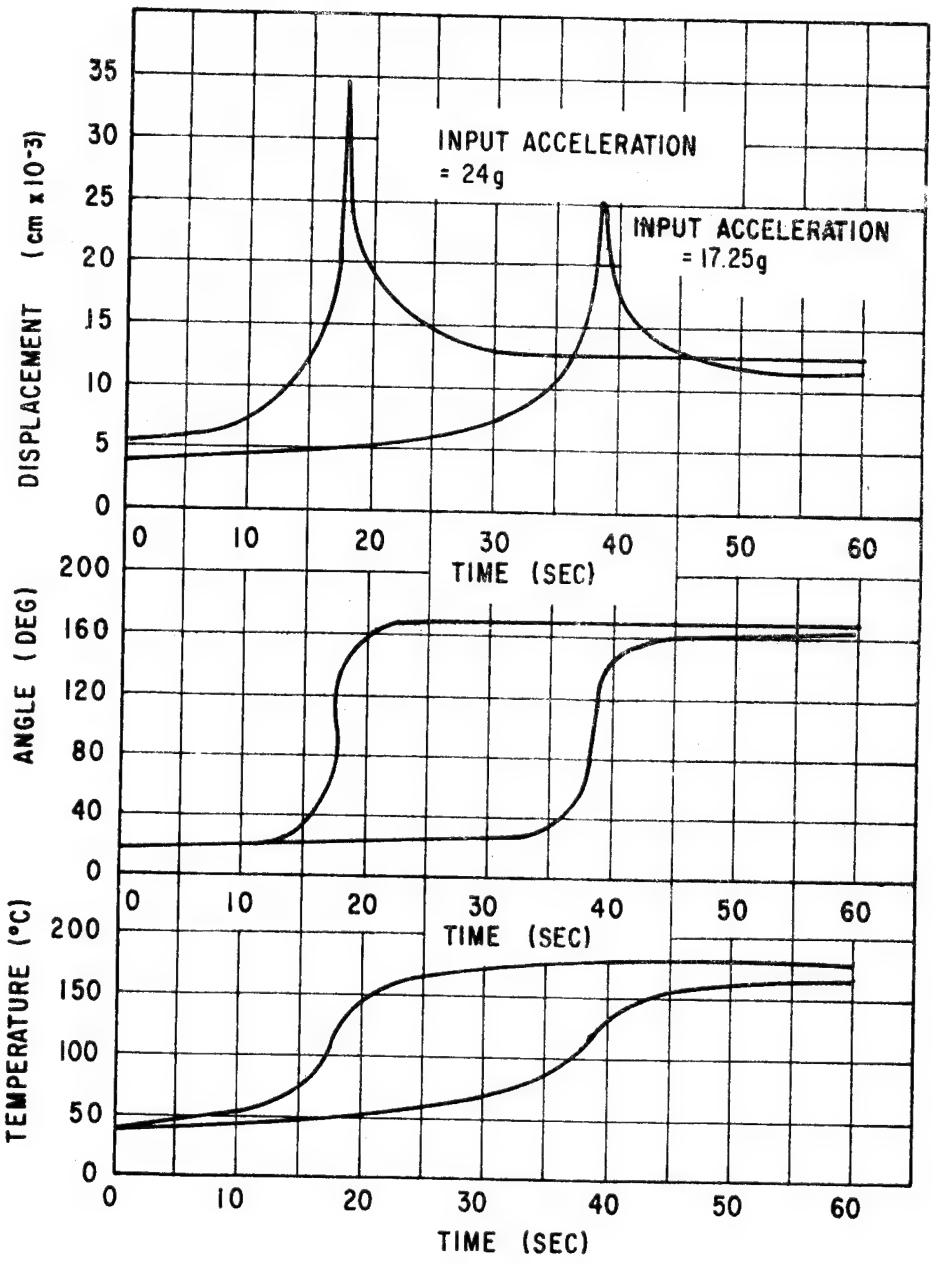

Fig. 106 Prediction of Thermal Transient for Comparison With Figure 102, 433 Hz, 0.908 Kg, Supported Mass. Compression Specimen. Conductivity 6.7 x 10^{-4} watts/cm C

The inability to completely recreate the transient conditions is not surprising, since very close simulation of the mechanical properties of the elastomer specimen and its dependence on temperature and dissipation would be required. However, the ability qualitatively to predict the phenomena on the basis of a thermoviscoelastic model with similar levels of input acceleration is evidence of the importance of thermal effects in determining the high dissipation behavior of the compression specimens.

A further check on the model was sought by comparison of its predictions with test data for the shear specimen. The same value of conductivity most successful for the compression specimens has been applied ($K = 6.7 \times 10^{-4}$ watts/cm C). Figures 107 through 110 show typical results which exhibit significant differences, both qualitative and quantitative,between tests and predictions. The predictions give much higher stiffness than the test data. It turns out that the area for heat flow is so large and the length of the heat flow path so small in the shear specimens, that temperature levels are much lower than in the compression specimens. Thus, the predictions based on internal heating and a corresponding reduction of material property values show only minor deviations from the isothermal values.

It becomes clear that some other mechanism is influential in reducing stiffness and damping of the shear specimens. Reference to available literature on the subject shows that another mechanism has, indeed, been recognized though not, as yet, analyzed or understood. This mechanism shows itself as a softening of shear elements at moderate to high strains. A transition region in amplitude has been identified as lying between strains of 0.001 and 0.005. Below this strain level the stiffness and damping are independent of strain. Above this level of strain a fall-off in stiffness occurs. It is reported by Warnaka (ref. 4) that consistent behavior is obtained for different materials.

This softening effect has not been previously reported at these frequencies for compression loading and there is apparently some difference in the behavior of compression and shear specimens with respect to high dissipation. Thermal effects clearly account for more of the stiffness degradation in compression elements than in shear elements.

In an attempt to clarify the relative importance of thermal effects and the 'strain softening' effect, stiffness and damping data for the compression and shear specimens has been plotted, separately, against strain and against dissipation rate, as independent variables. The results are shown in Figures 111 and 112 for shear, 113 and 114 for compression. The compression specimen plots include data from the Phase II series of tests. Some interesting observations may be made:

1. The shear specimen stiffness and damping data shows reasonably close correlation with strain.

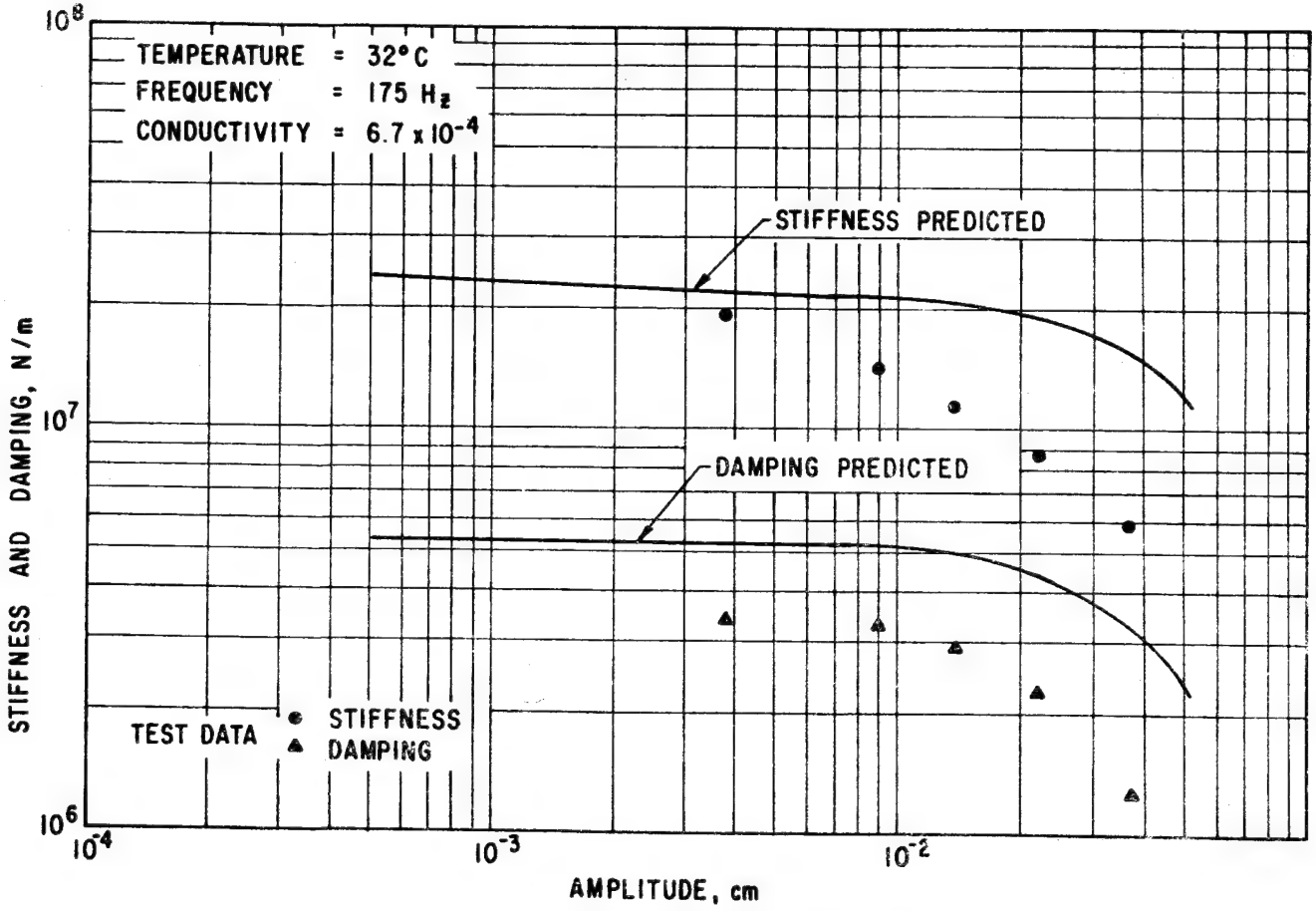

Fig. 107 Comparison of Predictions and Measurements of Stiffness and Damping Under High Dissipation Conditions. Shear Specimen. (Four Elements)

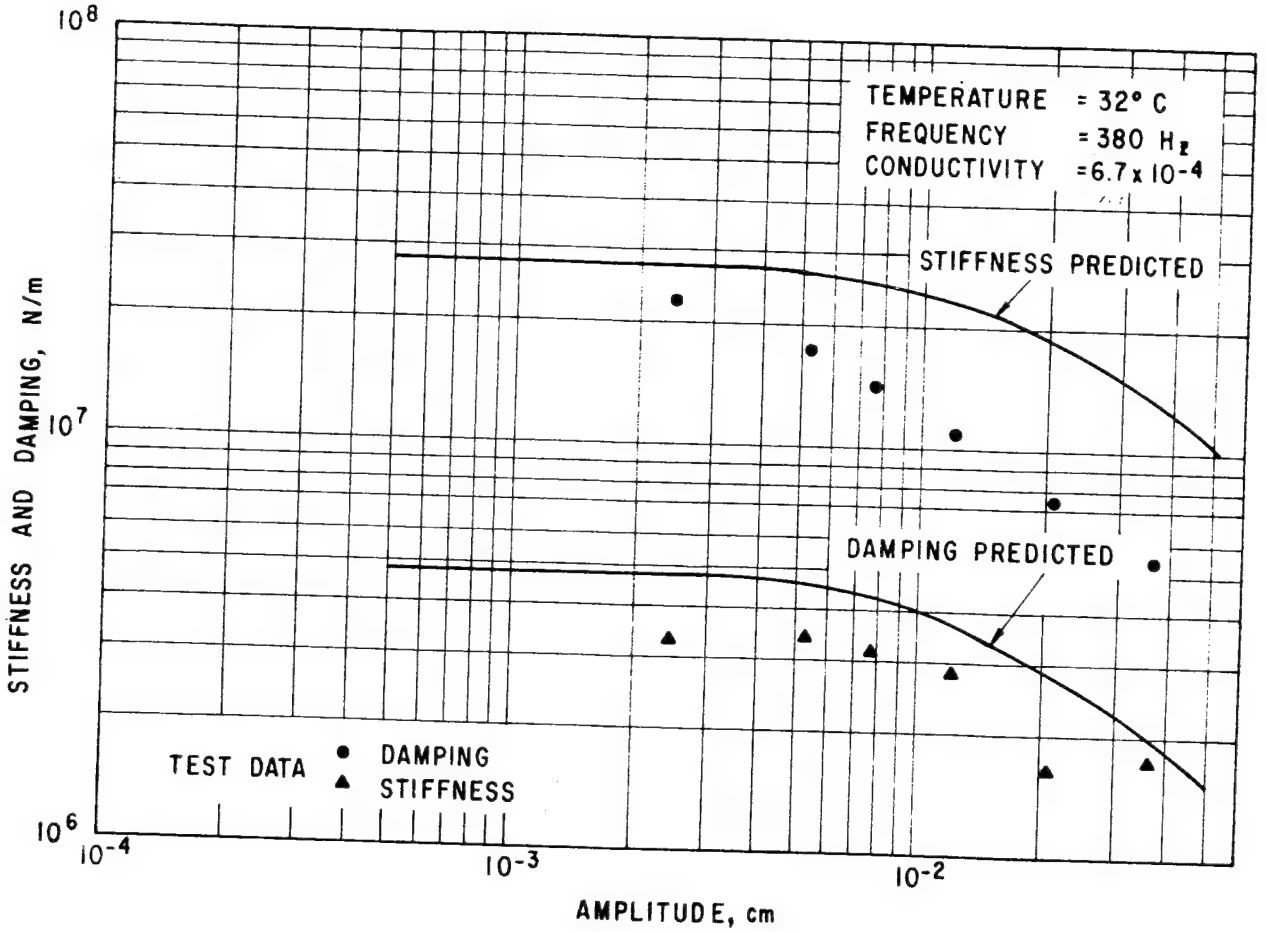

Fig. 108 Comparison of Predictions and Measurements of Stiffness and Damping Under High Dissipation Conditions. Shear Specimen. (Four Elements).

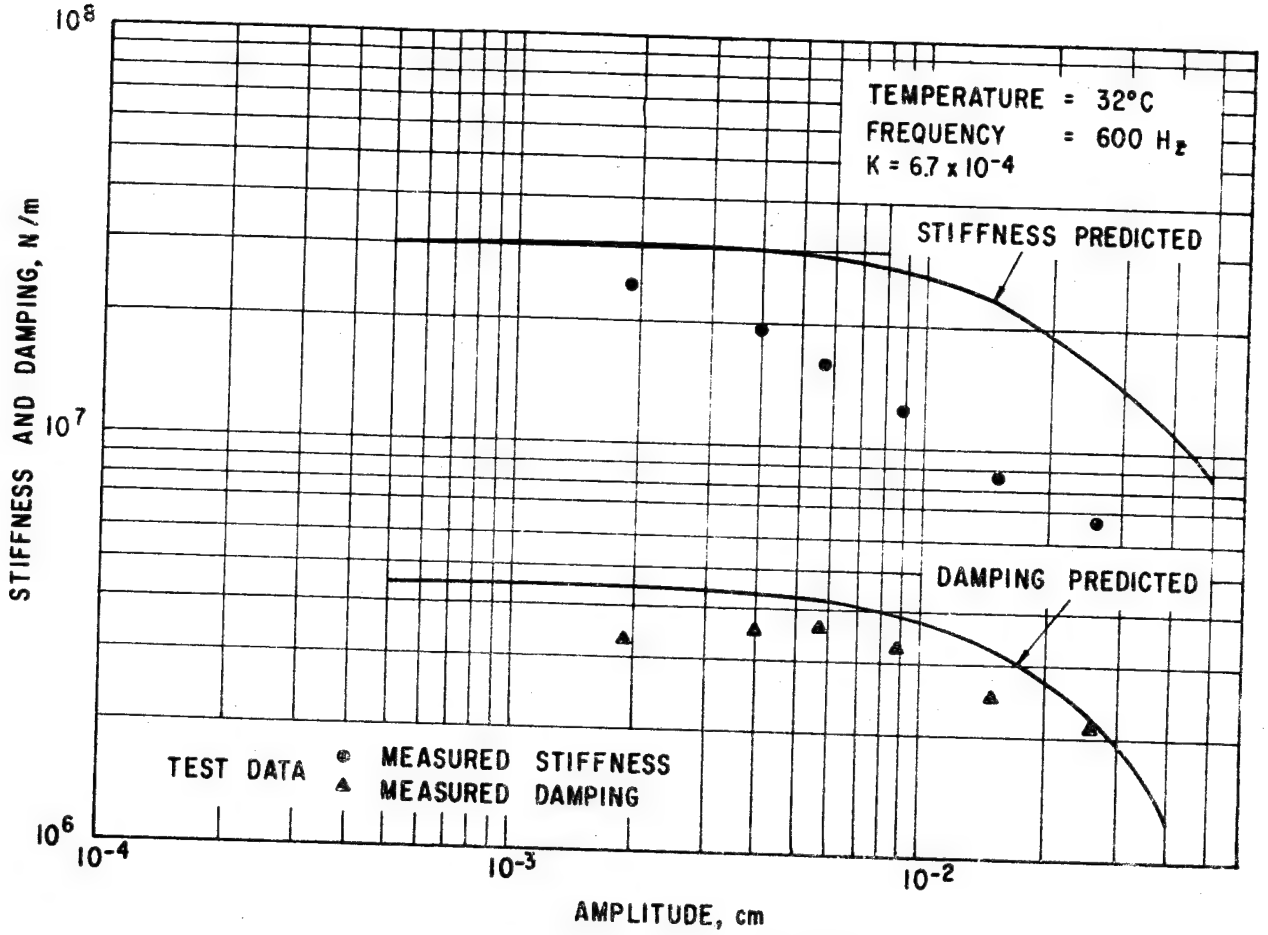

Fig. 109 Comparison of Predictions and Measurements of Stiffness and Damping Under High Dissipation Conditions. Shear Specimen. (Four Elements)

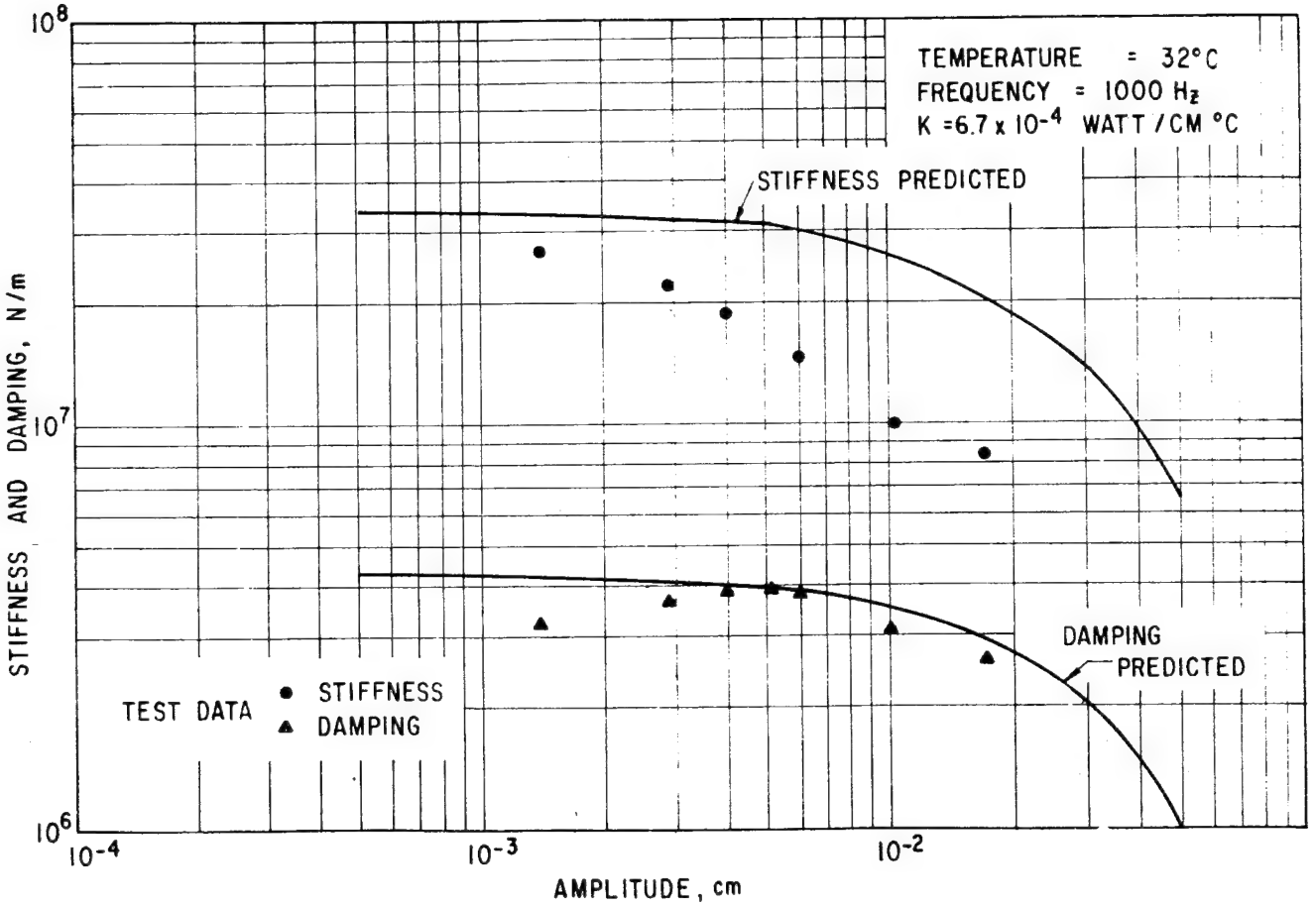

Fig. 110 Comparison of Predictions and Measurements of Stiffness and Damping Under High Dissipation Conditions. Shear Specimen. (Four Elements)

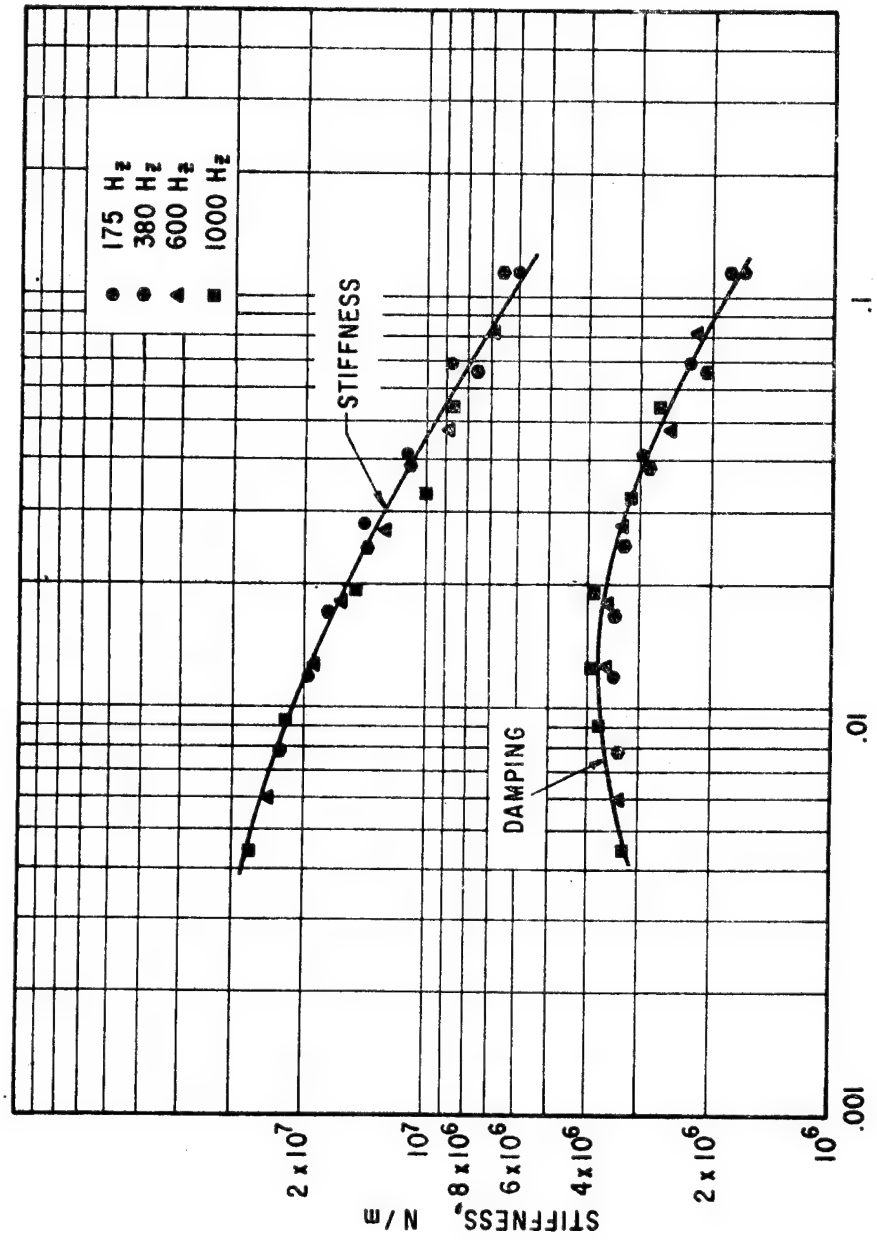

Fig. 111 Stiffness and Damping as a Function of Strain. Shear Specimen. 32 C (Four Elements)

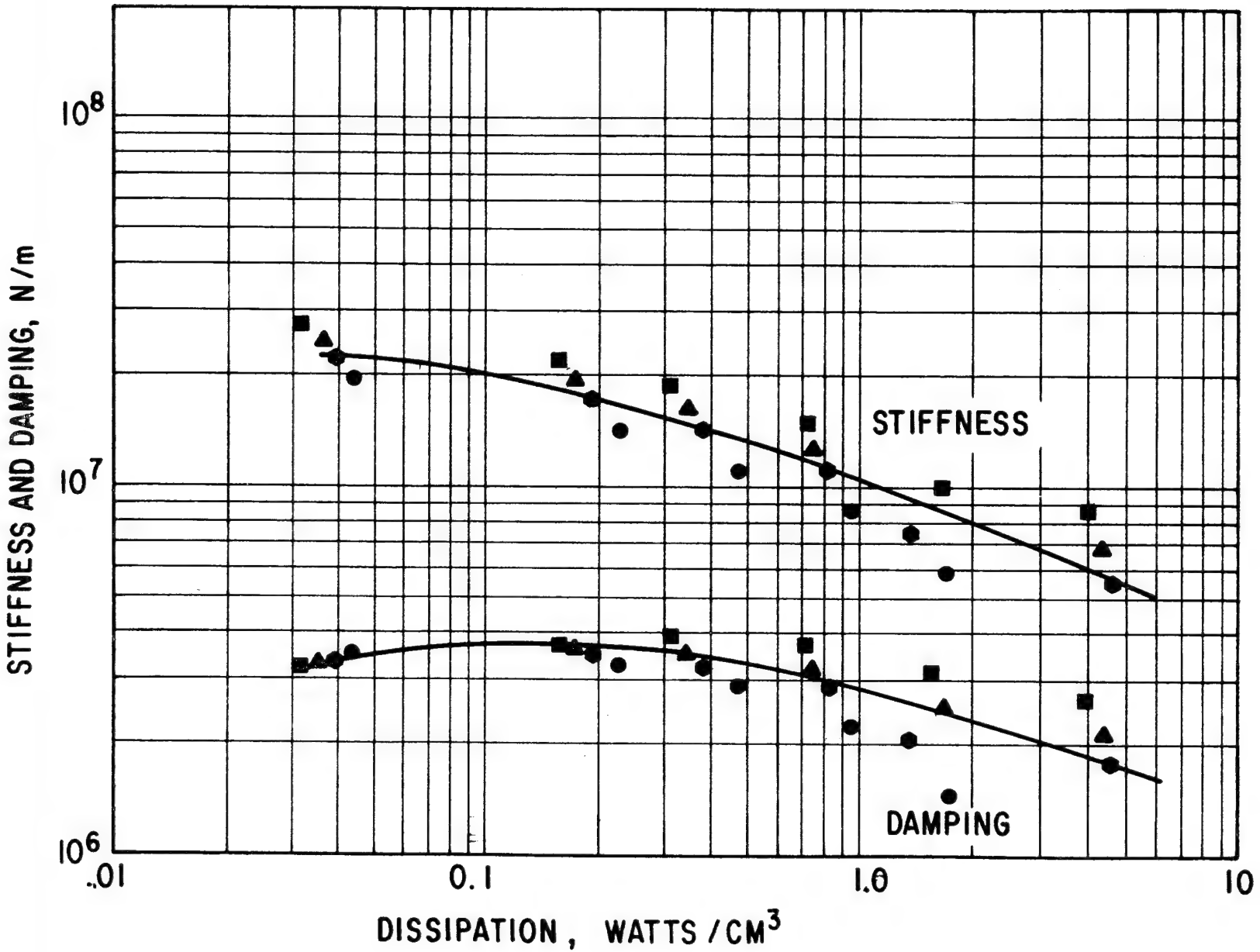

Fig. 112 Stiffness and Damping as a Function of Dissipation. Shear Specimen. 32 C (Four Elements)

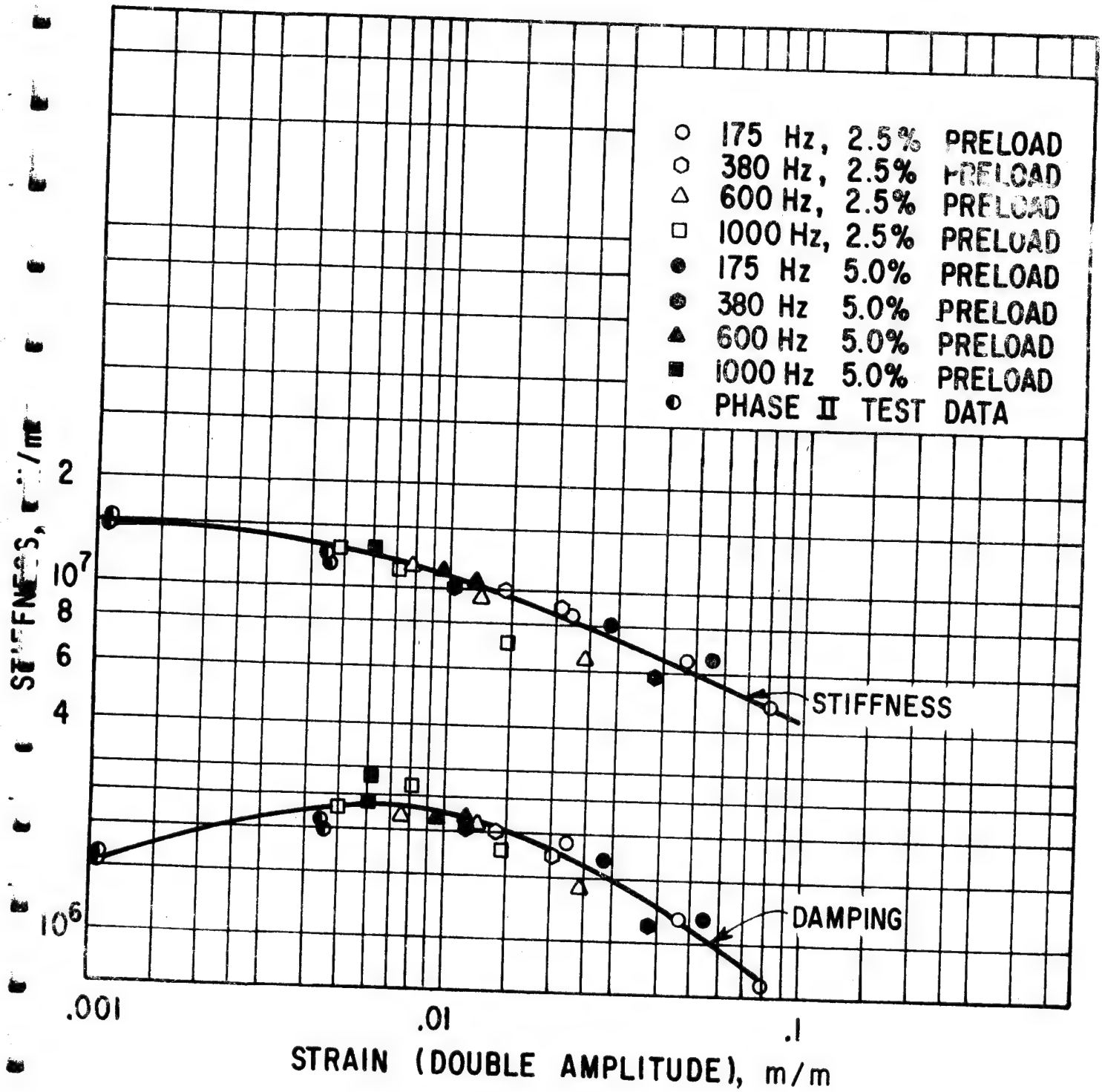

Fig. 113 Stiffness and Damping as a Function of Strain. Compression Specimen. 32 C. (Ten Elements)

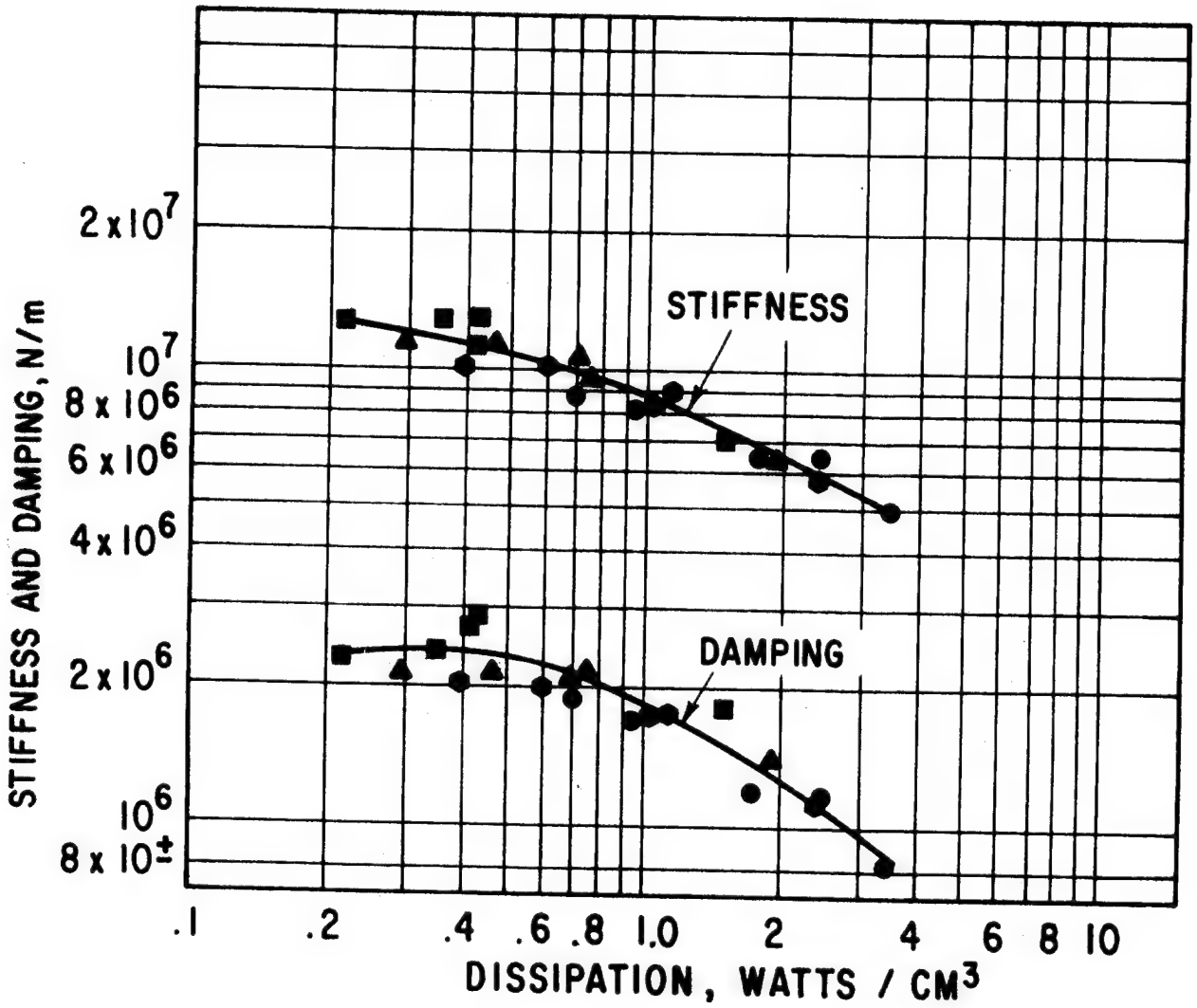

Fig. 11a Stiffness and Damping as a Function of Dissipation. Compression Specimen. 32 C (Ten Elements)

2. The shear specimen data shows poor correlation with dissipation rate.

3. The compression specimen data shows reasonably close correlation either with strain or with dissipation rates.

4. The data is generally at a high enough strain rate that strain independence is not apparent, (although more extensive data would be required, at low strains, to determine where strain independence does occur).

5. Damping values exhibit a peak, in the case of the shear and compression specimens, for strains in the region of one percent.

In summary, these results justify the following statements:

Stiffness and damping of elastomer elements in the frequency range 100 to 1000 Hz are influenced by two aspects of vibration amplitude: firstly strain, which has a 'softening effect' above a certain transition value; secondly, self-heating due to thermal dissipation, which causes reduction in values of local material properties. The relative importance of these two effects is governed by the geometry, type of loading, and, probably, by frequency and material. The strain softening effect appears to dominate for the shear specimens of polybutadiene.

Further information will be required before the relative contributions of thermal and strain softening can be established for the compression specimens. The conductivity must be separately determined before the one-dimensional thermoviscoelastic model can be tested further. The low strain region must be more extensively explored to verify the existence of a strain 'transition' region, to determine what conditions are required to establish strain independence, and to establish the influence of geometry on the strain dependence. Temperature measurements within the material under high strains would provide additional insight.

The present indications are that high amplitude stiffness and damping follow closely a unique relationship with strain. If this observation can be supported with further test data it offers an interesting and simple approach to accounting for high amplitude effects in design.

Damping Performance

The effect of strain on damping performance is further illustrated in Figure 115. Here the loss coefficient, η, has been plotted as a function of strain. The loss coefficient is a good measure of the elastomer's ability to damp vibrations of a mechanical system and,

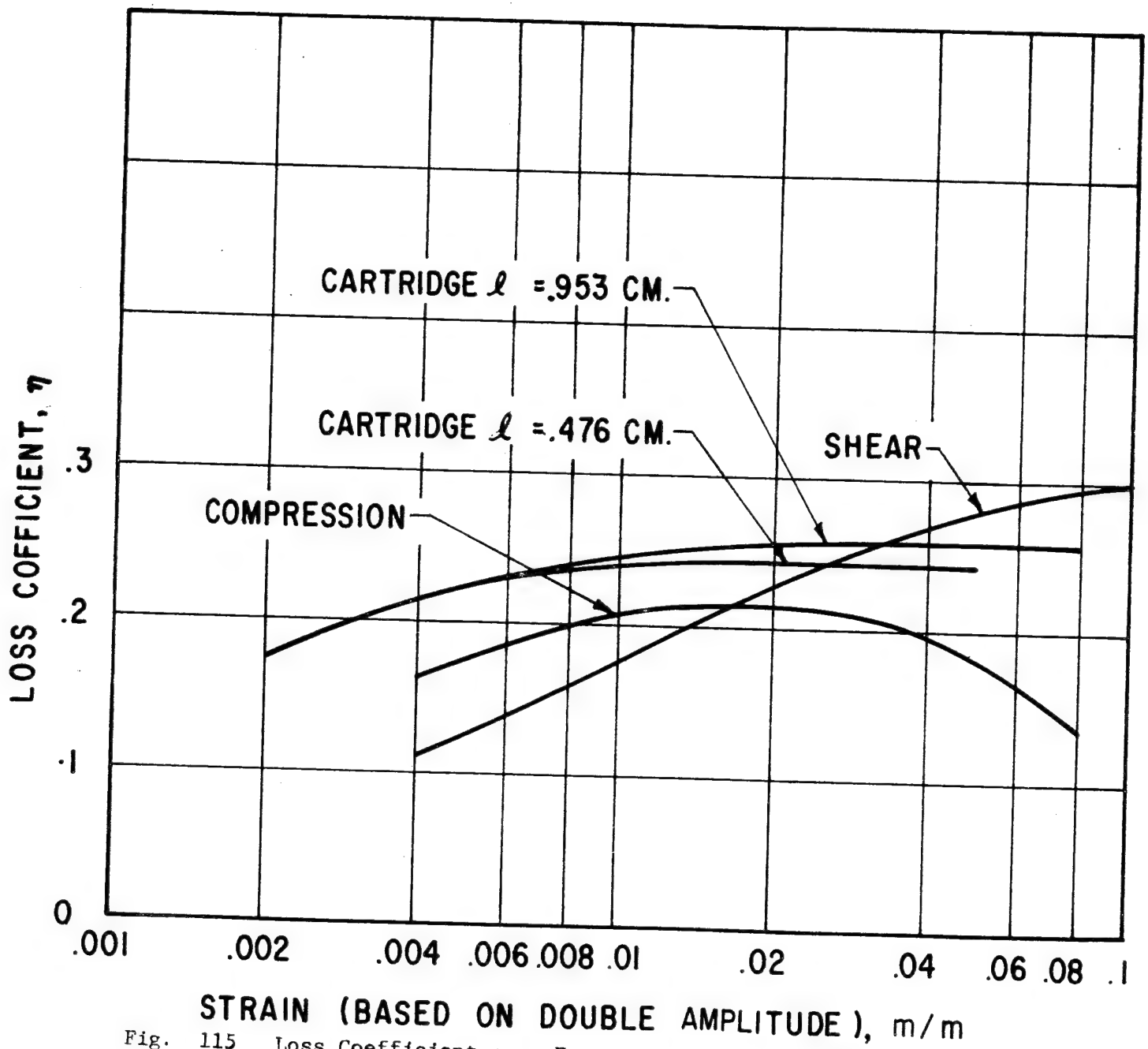

Fig. 115 Loss Coefficient as a Function of Strain. Elastomer Specimen

for a one-degree-of-freedom system such as is used for the Base Excitation Resonant Mass tests, the damping ratio ($\zeta = C/C_c$) is equal to one-half of the loss coefficient. Consider Figure 115: for strains below 0.02 there is a universal increase in loss coefficient for all specimens; at a strain of 0.02 all specimens show a loss coefficient in the range 0.21 to 0.26 (10.5 to 13 percent of critical damping). Above a strain of 0.02, however, there is some divergence in loss coefficient behavior between the different specimens. The shear specimen reveals a steady increase in loss coefficient to a value of 0.3 at a strain of 0.1. The cartridge specimen loss coefficient remains constant and the compression specimen loss coefficient falls above a strain value of 0.02

Based on these results, the generally best operating condition is with a double amplitude strain of 0.02. Of course, the question of survivability and life must be assessed further before any overall conclusion about operating conditions are drawn. For shear elements the temperature developed due to self-heating are unlikely to be a problem, but fatigue life for significant strain amplitude at frequencies in the range 100 to 1000 Hz must be determined to be acceptable. For compression elements and probably for cartridge elements, the temperatures developed are likely to be a problem in addition to fatigue life.

It is of particular interest that the two different cartridge geometries show such similarity of loss coefficient dependence on strain. It is also of importance to note that the cartridge geometry indicates the least overall sensitivity of loss coefficient to strain, and achieves a loss coefficient value of 0.2 or greater for all strains above 0.003.

High Temperature Results

As expected the test results show a significant influence of temperature on stiffness and damping and on the material properties inferred from the shear specimen results. The method of reduced variables (the WLF law) was discussed in a previous section of this report as a means of unifying the effects of temperature and frequency.

The availability of test results for material properties over a range of temperatures now allows the method of reduced variables to be tested for this material.

As identified the method of reduced variables requires knowledge of the characteristic temperature. No information is available as to the characteristic temperature or transition temperature for the material tested and it has been necessary to seek to infer the characteristic temperature from the test data. To do this the method has been applied for a range of characteristic temperatures. Reduced storage and loss moduli, referred to 32 C, have been calculated for each test data point

for each temperature tested. The result is a set of discrete, reduced storage and loss modulus values, covering a wide range of reduced frequency values (from 11 to 1600 Hz), referred to 32 C. Power law relationships between reduced moduli and reduced frequency have been fitted to the data and, as a measure of the consistency of the reduced data, the rms deviation between test data and the power law lines have been calculated. The characteristic temperature has then been sought as that value which minimizes the rms deviation.

In Figures 116 and 117 rms deviation, for reduced storage and loss moduli, respectively, are plotted against characteristic temperature. The deviation for storage modulus shows a minimum at a characteristic temperature of -50 C. The deviation for loss modulus however shows no sign of possessing a minimum. There is a continual decrease in deviation as the characteristic temperature is increased from -100 to +32 C.

Accepting the storage modulus minimum as indicating the transition temperature and the loss modulus data as anomalous, reduced moduli have been plotted against reduced frequency for a characteristic temperature of -50 C in Figures 118 and 119. These plots reflect the minimization results. The reduced storage modulus follows, with reasonable consistency a single straight line on a log-log plot; the reduced loss modulus data remains a series of individual curves corresponding to the four different temperatures tested.

What are the explanations? In summary, either polybutadiene does not fall into the category of materials satisfying the reduced variables law or some other parameter besides frequency and temperature is affecting the damping and loss modulus data. In the light of the preceding discussion of high dissipation results the possibility exists that the influence of strain softening is reflected even in the low (reference) dissipation results for the shear specimens.

Since increasing frequency at constant dissipation means a reduction in strain, the low dissipation test data for damping is likely to reflect the effects of strain if these are significant. If now we review the effects of strain on damping for shear specimens (Fig. 111), it is apparent that decreasing strain will also decrease damping. Thus, on the basis of strain effects alone, "low dissipation" damping would be expected to fall with increasing frequency. This anticipated trend is a plausible reason for the inconsistency of loss modulus data and the method of reduced variables.

Stiffness is seen to increase with decreasing strain and, therefore, with increasing frequency at constant dissipation. This is a trend which is consistent with the method of reduced variables, one of whose basic tenets is that an increase in frequency has an effect corresponding to a decrease in temperature.

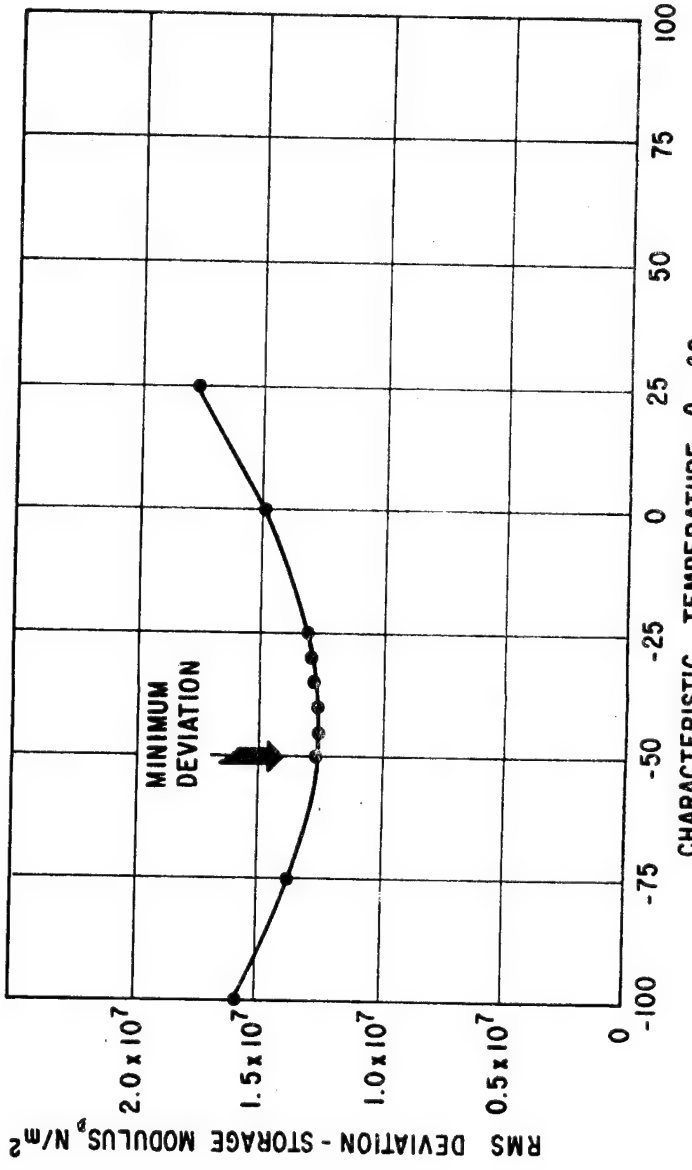

Fig. 116 RMS Deviation in Storage Modulus vs Characteristic Temperature. Shear Specimen (Eight Elements)

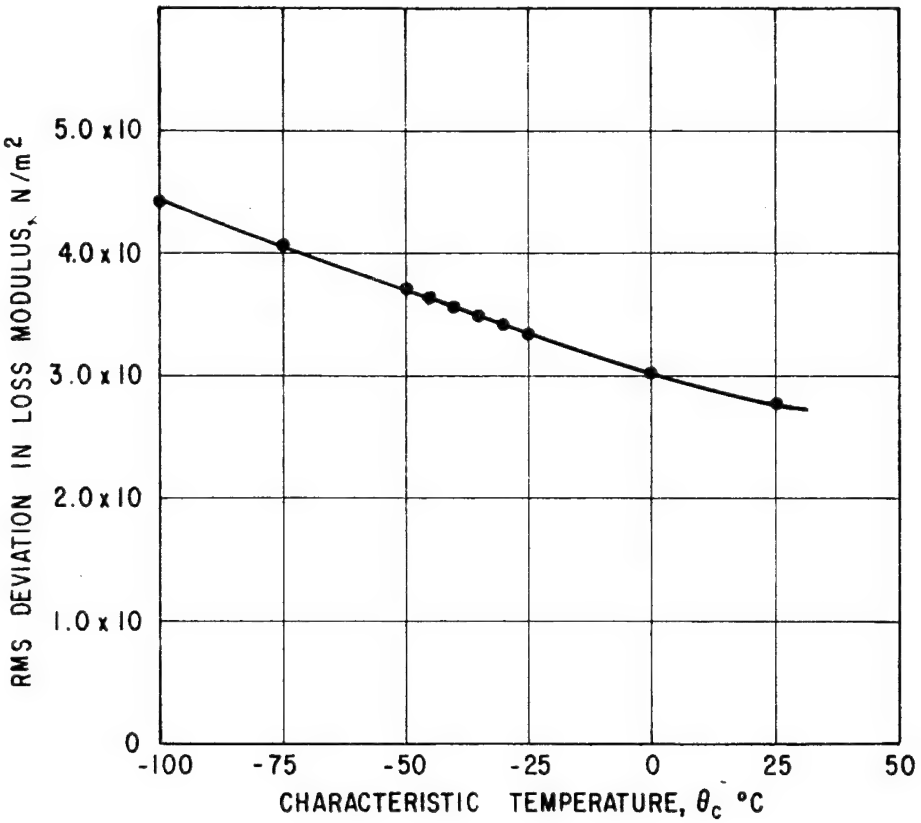

Fig. 117 RMS Deviation in Loss Modulus vs Characteristic Temperature. Shear Specimen (Eight Elements)

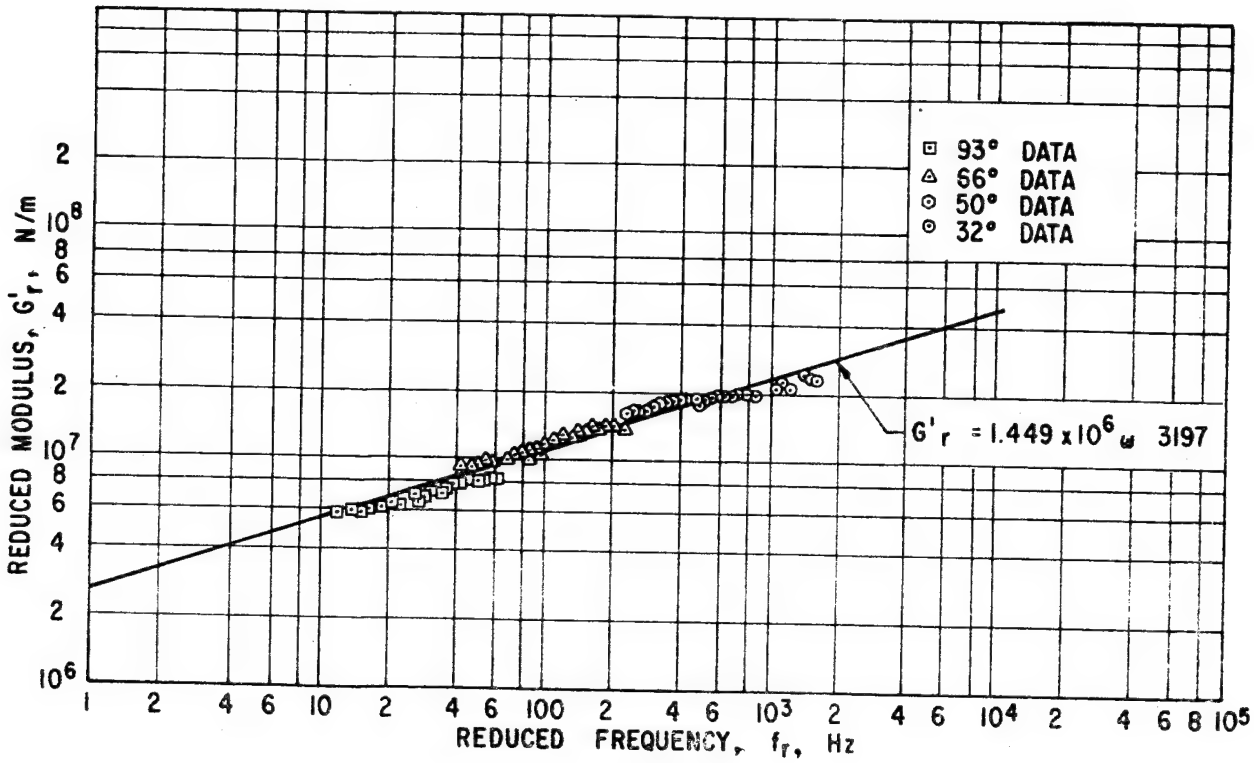

Fig. 118 Method of Reduced Variable. Reduced Storage Modulus vs Reduced Frequency. Reference Temperature, 32 C. Characteristic Temperature, -50 C

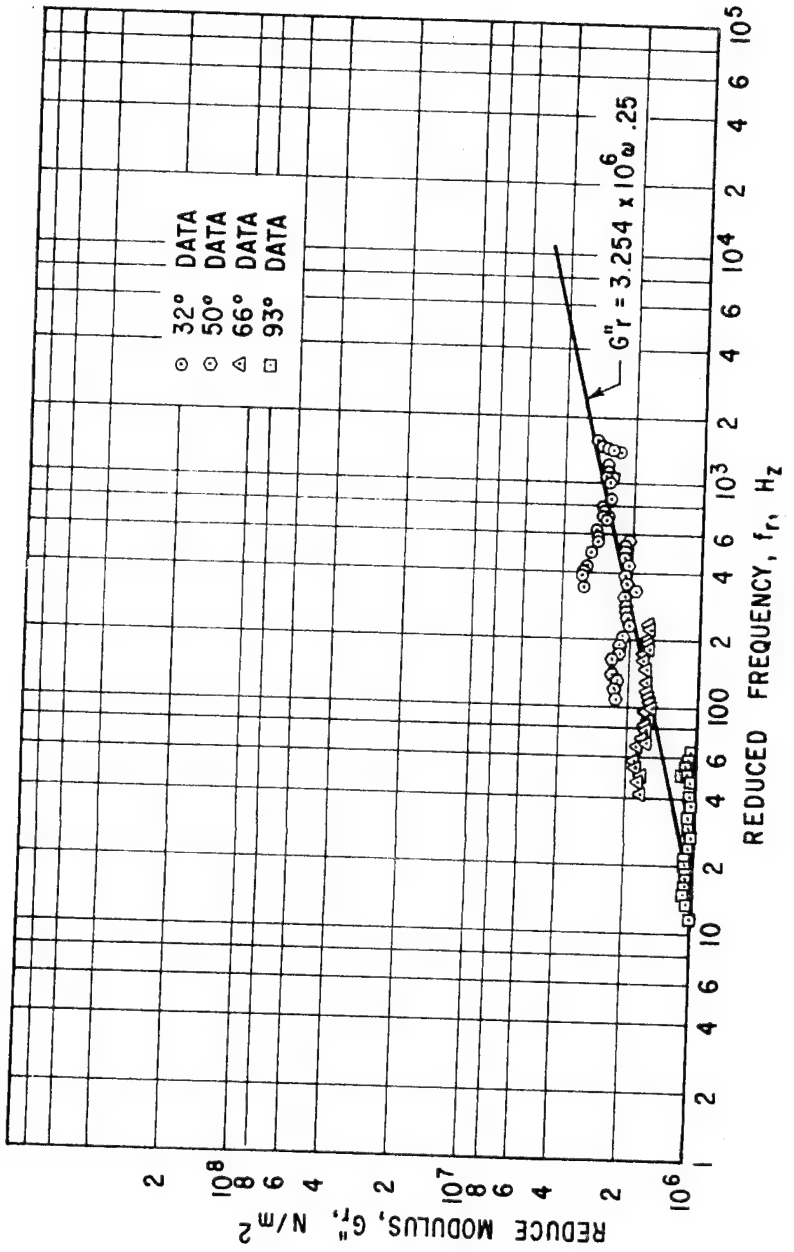

Fig. 119 Method of Reduced Variables. Reduced Loss Modulus vs Reduced Frequency. Reference Temperature, 32 C. Characteristic Temperature, -50 C

Before any conclusion can be drawn with respect to the validity of the reduced variables method for the particular material it is necessary to obtain further shear specimen values at amplitudes sufficiently low to exhibit strain independence of the material properties. In addition data at constant amplitude should be obtained to eliminate this influence of strain.

With the present material property data for polybutadiene there is limited benefit in applying the reduced variables method as a method of combining the effects of frequency and temperature. Since data is available at a range of temperature values of interest it has been summarized and stored directly in that form.

For application the curves of Figure 120 have proved most useful. In these curves storage and loss modulus at 100 and 1000 Hz are plotted against temperature. Values at these two frequencies may therefore be read for any temperature between 32 and 93 C. To calculate stiffness and damping at these two frequencies for a particular element the appropriate geometric relationships are applied, and plots of stiffness and damping against frequency are made which exhibit a straight line variation on log-log paper. This is how the predicted data for cartridge and cylindrical specimens presented in the preceding Section were generated.

Consistency of Phase II And Phase III Results

To provide a check on consistency, the material property data obtained from Phase II tests (as described earlier in this report) has been compared with the Phase III material property values of Table X for 32 C. The comparison, presented in Table XIV shows that there is good consistency between the two test series for storage modulus, but that the loss modulus values obtained from the most recent series of tests are substantially higher than the Phase II values.

TABLE XIV. COMPARISON OF PHASE II AND PHASE III VALUES FOR STORAGE AND LOSS MODULUS

Test Series	G' 100 Hz N/m^2	G' 1000 Hz N/m^2	G'' 100 Hz N/m^2	G'' 1000 Hz N/m^2
Phase II	1.353×10^7	2.067×10^7	2.021×10^6	1.684×10^6
Phase III	1.369×10^7	2.189×10^7	3.659×10^6	2.728×10^6

The reason for the discrepancy in loss modulus is the simplified, more accurate test method for material properties employed in the most recent series of tests. By eliminating the preload piston from the shear tests a source of error has been eliminated - an error which had been exaggerated (rather than reduced) by the "corrections" applied to account for it in

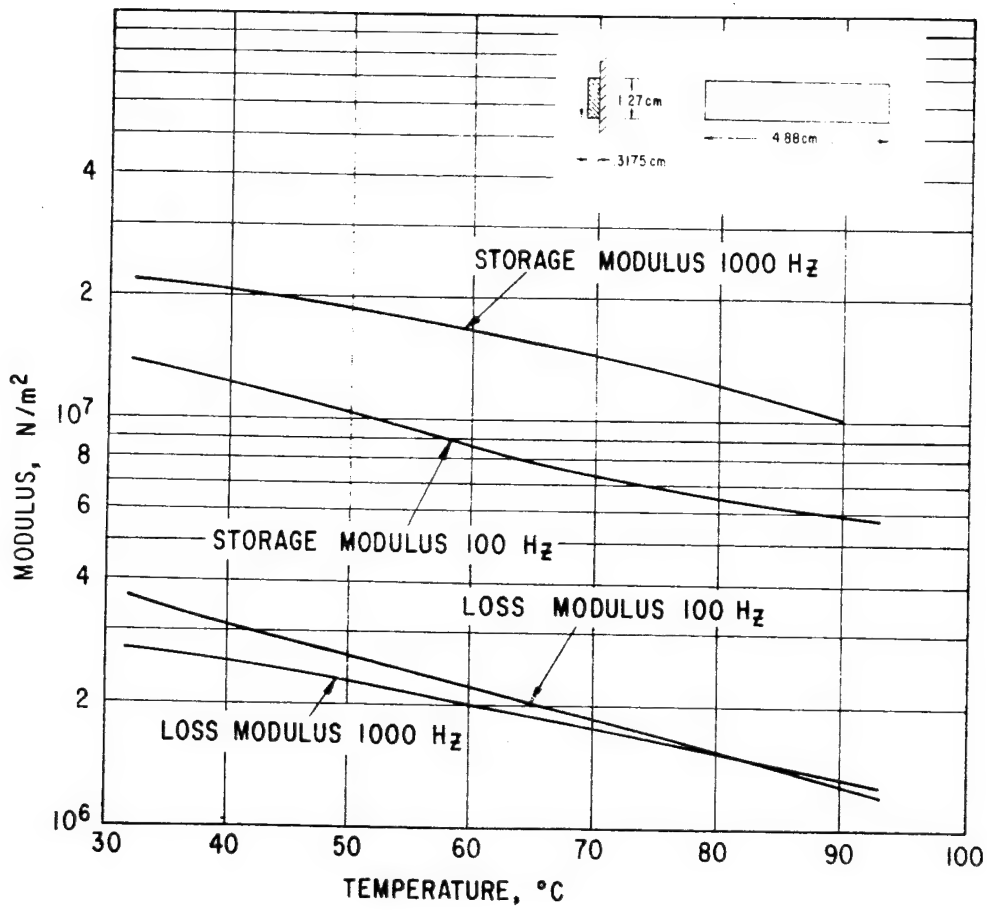

Fig. 120 Influence of Temperature on Dynamic Modulus at 100 Hz and 1000 Hz Based on Shear (Eight-Element Test Data)

reducing the Phase II data! Contrary to expectations based on an analysis of the mechanical system, assuming rigid system elements (ref. 2), the effect of the piston's presence is to reduce the apparent damping as described earlier in this report. Since the correction was based on the analysis of the mechanical system, the correction was applied with the wrong sign. The reasons for this anomalous effect of the piston are not clearly understood, but may well result from flexibility of such elements as the piston itself. The fact that the present test data for shear specimens is more reliable is not, however, in doubt.

Comparison of Prediction And Test Data

The test data for cartridge stiffness and damping and for compression element stiffness and damping at different temperatures and the comparison with prediction methods, has provided a basis for assessing the worth, in particular applications, of the prediction methods discussed earlier

For cartridge stiffness and damping predictions, the available methods are based on static stiffness analysis. Two simple methods, the Beam-Column analysis and the method of Göbel predict stiffness and damping which generally bracket the test data.

The difference in results of these two prediction methods is close to a factor of two. The limitation in state-of-the-art prediction for this geometry may, therefore, be summarized as follows:

Using static analysis-based predictions, dynamic performances of a ring cartridge may be predicted with a band of uncertainty which represents a factor of two in stiffness and damping; if this geometry is to be employed in a particular application, it should be ensured that satisfactory performance can be obtained for values of stiffness and damping which cover this band of uncertainty in cartridge predictability.

For cylindrical compression specimens there exists a static prediction method, employing a constant shape factor coefficient value (β) of two. Based upon this method, dynamic stiffness and damping may be predicted using the frequency dependent material properties of storage and loss modulus. Alternatively, using previously generated dynamic test data for cylindrical cartridge specimens with various d/h ratios, a function has been developed empirically which provides frequency dependent values for shape factor coefficient. These frequency dependent coefficients may again be used, in conjunction with the frequency dependent storage and loss module, to predict stiffness and damping.

For the Phase II test data, the static based method generates discrepancies of as much as 50 percent relative to the test data.

For the Phase III test data, at temperatures of 66 and 93 C, the two prediction methods produce discrepancies of similar magnitude. Figures 63 through 66 show the discrepancies graphically. The worst discrepancies between the prediction methods and test data points for all test condition of preload and temperature are summarized in Table XV. For stiffness the worst discripancies vary from 8 to 25 percent; for damping the discrepancies are in the range 20 to 30 percent, with measurements lower than predicted.

TABLE XV. CYLINDRICAL COMPRESSION SPECIMEN

[Maximum Discrepancies Between Measured And Predicted Stiffness And Damping Value]

Fig. No.	Temp. (C)	Pre-load (%)	Stiffness		Damping	
			Discrepancy	Percent*	Discrepancy	Percent
			$\beta' = 2$	$\beta' = f(\omega)$	$\beta'' = 2$	$\beta'' = f(\omega)$
63	66	2.5	-8.8**	+10.8	-23.7	-25.8
64	66	5	+12.1	+13.4	-28.6	-30.8
65	93	2.5	+13.0	+14.4	-20.7	-23.5
66	93	5	+22.9	+25.0	-21.8	-25.2

*Percentage referred to predicted value.

**Negative sign indicates measured data lower than predicted. Positive sign indicates measured data higher than predicted.

In terms of performance, there is nothing to choose between the two approaches for cylindrical compression elements. When either method is to be used in design of a system component, it is necessary to ensure that satisfactory system performance can be achieved allowing for uncertainties of the magnitude indicated in Table XV.

Test Method

The ability of the base excitation resonant mass method to provide stiffness and damping data for a variety of geometries and over a range of temperatures and dissipation levels has been convincingly demonstrated by the results presented in this report. It has been determined that the "cleanest" test condition occurs when the resonant mass is supported solely by the test specimen, without either of the lower or upper loading and unloading pistons. This simple test condition introduces no uncertainty with respect to tare stiffness and damping.

The simple test condition with no pistons can be achieved for the cartridge and shear specimens, without danger of putting the elastomer metal bond in tension. The compression specimen as presently designed requires the preloading effect of the piston to maintain the bond in compression. A modified design can be envisaged in which a self-preloading mechanism is employed.

Future Directions

The results presented in this report make clear the need for further work to improve fundamental understanding and applications capability.

The influence of strain amplitude as a parameter independent of thermal dissipation level must be further investigated as a function of geometry for polybutadiene and for different materials. The present results indicate that, over a significant range of strains, stiffness and damping are governed by strain rather than frequency. This must be further tested. In addition, the conditions of strain for which the stiffness and damping are independent of strain must be investigated, and related to geometry. It is anticipated that tests at very low amplitudes as well as high amplitudes will be required. The means to present the resultant information in a form suitable for use in design must also be developed. The information will be largely empirical, until the strain softening effect becomes better understood, and test methods must be evolved which can rapidly define the effect for different materials and geometries.

To improve understanding of the importance of thermal dissipation and its relationship to strain softening, thermal properties of conductivity and specific heat must be determined for the material being tested and included correctly in the thermoviscoelastic model. Direct measurements of temperature within the elastomer material, and comparison of these measurements with predictions will also provide improved understanding of thermal dissipation effects.

When strain softening is better understood, and stress independent results are available, the method of reduced variables as a means of conveniently presenting elastomer properties must be further evaluated.

As comparisons show, the uncertainty in prediction ability for a cartridge and of cylindrical compression elements when static geometry effects are applied, while significant, may be acceptable for some applications. The degree of predictive uncertainty should be investigated further for other materials. The need for, and potential benefits of, improved viscoelastic analysis methods must be identified and, if the need is shown to exist, appropriate methods of viscoelastic continuum analysis should be developed.

Tests over similar parameter ranges for geometries similar to those presently reported should be performed using other materials, including materials selected for known differences in hardness and loss coefficient. These tests will provide the basis for generalization of, or exception to, the results for polybutadiene.

In the case of a cartridge, the effect of a rotating load as opposed to a uniaxial load must be investigated. The anticipated application of the cartridge element is in rotating machinery where the load vector will be rotating. It is important to determine, under controlled conditions, whether there is a significant difference in the stiffness and damping under the action of rotating and uniaxial dynamic loads, and to establish the degree of uncertainty in prediction for a rotating load environment.

An important geometry to be tested is the O-ring. This is a compact, commercially-available, simple, elastomer element. O-rings are already in use as seals and flexible mounts in squeeze-film dampers where their stiffness properties in particular are important. Their use as flexible mounts independent of squeeze film dampers is anticipated, in which case their damping properties will also be important.

When testing O-rings, and other geometries, it is important to preserve the approach which has been inherent in the tests and analysis up to this point; that, for improved understanding, tests in shear, for general material properties, must be performed on the same material as is employed in the geometry of interest. In this way, meaningful predictive methods which relate stiffness and damping for storage and loss moduli can be evolved.

Analytical studies for representative machinery classes should be performed to establish the needs for damping elements and the ability and limitations of elastomers in filling these needs.

Application tests should be performed to demonstrate the vibration control capabilities of elastomer elements. Following successful application tests, the questions of life and survivability should be investigated.

APPENDIX A

THERMAL DISSIPATION IN AN ELASTOMER ELEMENT UNDER UNIAXIAL STRESS

As a result of imposed conditions an elastomer element, in the form of a right circular cylinder, is undergoing time varying changes in temperature, internal stress and displacement. The cylinder is as shown in Figure 121. It is assumed that stresses are uniaxial.

At any point

$$\sigma_z = \sigma(z,t)e^{i\omega t} \tag{72}$$

$$U_z = U(z,t)e^{i\omega t} \tag{73}$$

$$T_z = T_z(z,t) \tag{74}$$

where σ_z is the normal axial stress

U_z is the axial displacement; T_z is temperature;

and it is understood that only the real parts of expressions (72) and (73) apply.

σ and U are complex numbers containing both amplitude and phase information.

It is assumed that the amplitude functions σ,U are undergoing much slower changes with time than σ_z and U_z.

Axial equilibrium requires:

$$\frac{\partial}{\partial Z}(\sigma) = 0 \tag{75}$$

where Z is the axial coordinate and the inertia of the elastomer material is neglected.

The stress amplitude σ is evaluated as:

$$\sigma = 3G^*(Z,\omega)\frac{dU}{dZ} \tag{76}$$

where $G^* = G'(\omega,T) + i\,G''(\omega,T)$; T is the cycle average temperature; and G', G'' are the storage and loss moduli. T is a function of Z.

The instantaneous energy equation is:

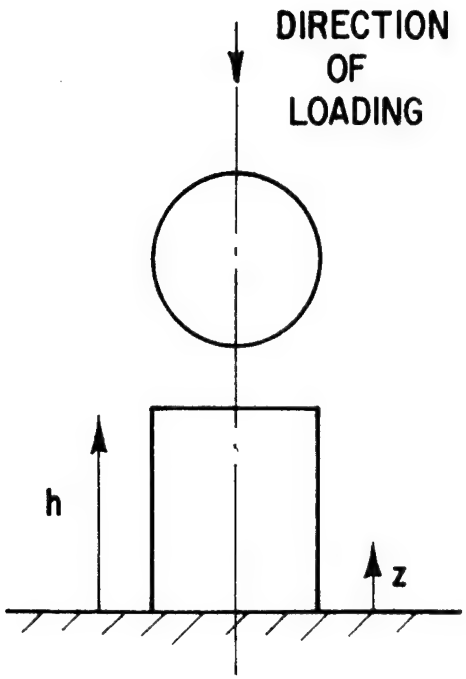

Fig. 121 Compression Loaded Cylinder

$$\rho C_p \frac{\partial T_z}{\partial t} = K \frac{d^2 T_z}{dZ^2} + S \qquad (77)$$

where $S = Re\ (\sigma_z)\ Re \frac{\partial}{\partial t}\left(\frac{dU_z}{dZ}\right)$

Now, assuming temperature to be changing slowly with time, we can take a cycle average as follows to get T:

$$T = \frac{\omega}{2\pi} \int_t^{t+2\pi/\omega} T_z(t')dt' \qquad (78)$$

thus the energy equation becomes:

$$\rho C_p \frac{\partial T}{\partial t} = K \frac{d^2 T}{dZ^2} + \frac{\omega}{2\pi} \int_t^{t+(2\pi/\omega)} S(t')dt' \qquad (79)$$

Now, if

$$I = \int_t^{t+(2\pi/\omega)} S(t')dt' \qquad (80)$$

then

$$I = \frac{1}{4} \int_o^{2\pi/\omega} \left(\sigma_z + \tilde{\sigma}_z\right) \frac{\partial}{\partial Z} \left(i\,\omega\, U_z - i\,\omega\, \tilde{U}_z\right)dt' \qquad (81)$$

where the superscript ~ implies the complex conjugate.

$$\therefore I = \frac{1}{4} \int_o^{2\pi/\omega} \left(\sigma\, e^{i\omega t} + \tilde{\sigma}\, e^{-i\omega t}\right) \frac{\partial}{\partial Z} \left(i\omega U\, e^{i\omega t} - i\omega \tilde{U}\, e^{-i\omega t}\right)dt'$$

$$= \frac{i\omega}{4} \int_o^{2\pi/\omega} \left[\sigma \frac{\partial U}{\partial Z} e^{2i\omega t} + \tilde{\sigma} \frac{\partial U}{\partial Z} - \sigma \frac{\partial \tilde{U}}{\partial Z} - \tilde{\sigma} \frac{\partial \tilde{U}}{\partial Z} e^{-2i\omega t}\right]dt'$$

$$= \frac{i\pi}{2} \left[\tilde{\sigma} \frac{\partial U}{\partial Z} - \sigma \frac{\partial \tilde{U}}{\partial Z}\right]$$

(continued on next page)

$$= \frac{i\pi}{2}\left[3\tilde{G}\ \frac{\partial\tilde{U}}{\partial Z}\frac{\partial U}{\partial Z} - 3G\ \frac{\partial U}{\partial Z}\frac{\partial\tilde{U}}{\partial Z}\right]$$

$$= \frac{3i\pi}{2}\left[\tilde{G} - G\right]\frac{\partial U}{\partial Z}\frac{\partial\tilde{U}}{\partial Z}$$

$$= 3\pi G''\left(\left|\frac{\partial U}{\partial Z}\right|\right)^2 \qquad (82)$$

Thus, the final form of the energy equation is:

$$\rho C_p \frac{\partial T}{\partial t} = K\frac{\partial^2 T}{\partial Z^2} + \frac{3\omega}{2} G''\left(\left|\frac{\partial U}{\partial Z}\right|\right)^2 \qquad (83)$$

and the equilibrium equation is:

$$\frac{\partial}{\partial Z}\left[3\ G^*\ (Z,\omega)\ \frac{\partial U}{\partial Z}\right] = 0 \qquad (84)$$

It is straightforward to perform a similar development for elements undergoing shear deformation (as shown in Fig. 122). In this case the energy equation is:

$$\rho C_p \frac{\partial T}{\partial t} = K\frac{\partial^2 T}{\partial Z^2} + \frac{\omega}{2} G''\left(\left|\frac{\partial U}{\partial Z}\right|\right)^2 \qquad (85)$$

where U is the amplitude of shear deformation (normal to Z) and the equilibrium equation is:

$$\frac{\partial}{\partial Z}\left[G^*\ (Z,\omega)\ \frac{\partial U}{\partial Z}\right] = 0 \qquad (86)$$

To further streamline Equation (83) through (86) to a single pair of equations, we can write (reorganizing slightly) for shear or compression elements:

Energy equation:

$$\frac{\partial}{\partial Z}\left[K\frac{\partial T}{\partial Z}\right] - \rho C_p \frac{\partial T}{\partial t} = -\gamma G''\left(\left|\frac{\partial U}{\partial Z}\right|\right)^2 \frac{\omega}{2} \qquad (87)$$

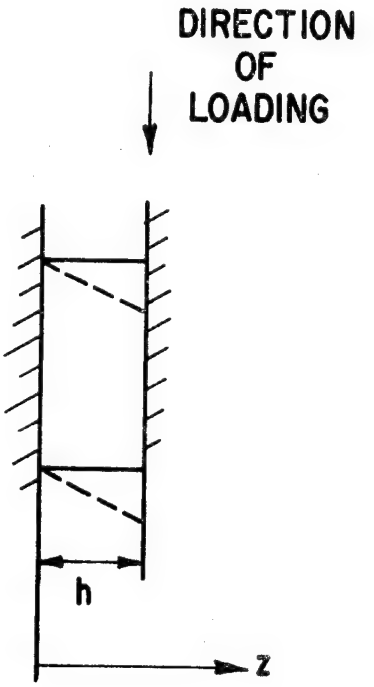

Fig. 122 Shear Element

Equilibrium equation:

$$\frac{\partial}{\partial Z}\left[G^* \frac{\partial U}{\partial Z}\right] \tag{88}$$

- where $\gamma = 1$ for a shear element, 3 for a compression element.

APPENDIX B

DATA REDUCTION ANALYSIS

For the Base Excitation Resonant Mass test method, test data consists of accelerometer and displacement sensor readings. The primary objective of data reduction is to interpret these signals in terms of stiffness and damping. The structure of this data and the method of reduction can best be defined in relation to a simple spring-mass-damper system subjected to base excitation, as shown in Figure 123.

The equation of motion for the mass is:

$$M\ddot{Y} + K_1(Y_m - Y_o) + C(\dot{Y}_m - \dot{Y}_o) = 0 \qquad (89)$$

where Y_m is displacement of mass
Y_o is displacement of base.

We will assume that the motions of base and mass are harmonic; so that:

$$Y_m = \text{Real}\left\{Y_m^* e^{i\omega t}\right\} \qquad (90)$$

$$Y_o = \text{Real}\left\{Y_o^* e^{i\omega t}\right\} \qquad (91)$$

and the equation of motion may be rewritten:

$$-\omega^2 M Y_m^* e^{i\omega t} + K_1(Y_m^* - Y_o^*)e^{i\omega t} + i\omega C(Y_m^* - Y_o^*)e^{i\omega t} = 0 \qquad (92)$$

Dividing through by $e^{i\omega t}$, we obtain

$$(K_1 + iK_2) = \frac{\omega^2 M Y_m^*}{Y_m^* - Y_o^*} \qquad (93)$$

where $K_2 = \omega C$

Now if φ is the phase angle between Y_o and Y_m we can write

$$Y_m^* = |Y_m^*|\cos\varphi - i\,|Y_m^*|\sin\varphi \qquad (94)$$

$$Y_o^* = |Y_o^*| \qquad (95)$$

and

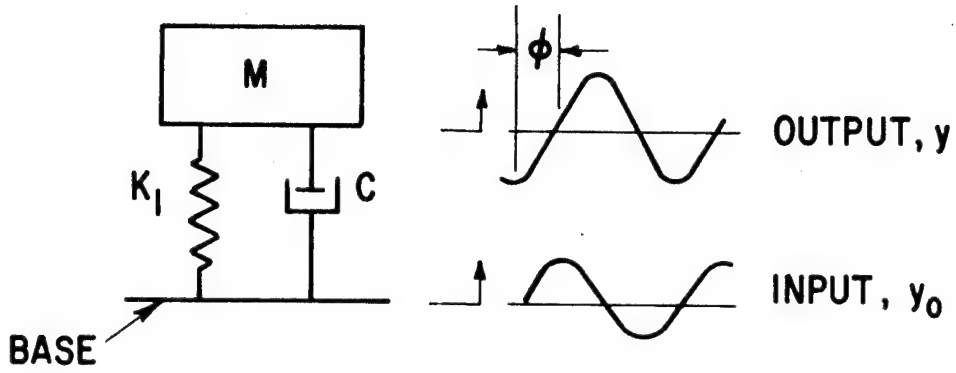

Fig. 123 Model of Base Excitation Resonant Mass System for Data Reduction Analysis

$$(K_1 + iK_2) = \frac{\omega^2 M(\alpha \cos \varphi - i \alpha \sin \varphi)}{\alpha \cos \varphi - i \alpha \sin \varphi - 1} \qquad (96)$$

where α is the transmissibility $\frac{|Y_m^*|}{|Y_o^*|}$. Thus,

$$K_1 + iK_2 = \frac{\omega^2 M (\alpha \cos \varphi - i \alpha \sin \varphi)(\alpha \cos \varphi - 1 + i \alpha \sin \varphi)}{(\alpha \cos \varphi - 1)^2 + \alpha^2 \sin^2 \varphi} \qquad (97)$$

or

$$K_1 = \frac{\omega^2 M [\alpha^2 - \alpha \cos \varphi]}{\alpha^2 - 2\alpha \cos \varphi + 1} \qquad (98)$$

and

$$K_2 = \frac{\omega^2 M \alpha \sin \varphi}{\alpha^2 - 2\alpha \cos \varphi + 1} \qquad (99)$$

Thus, if we determine α, the transmissibility, or ratio of output amplitude $|Y_m^*|$ to input amplitude $|Y_o^*|$, and φ the phase angle between input and output amplitudes, we can directly evaluate stiffness and damping (K_1 and K_2).

Note that these expressions are based on the simplest one-degree-of-freedom model with no correction for tare damping or stiffness. This is in contrast to the expressions used in Reference 2, which made corrections for effects of damping in preload and load support pistons. The simplicity of the present treatment results from the simplicity and accuracy of the test procedure performed for the majority of the tests, in which no external restraint of any kind was applied to the supporting mass. Only for the compression specimens was the preload piston employed. These expressions are, therefore, fully accurate for shear and cartridge specimens and subject to some uncertainty only in the case of the compression specimens.

NOMENCLATURE

A	stressed area, m^2
A_1, A_2	coefficients of power law relationship $K_1 = A_1\omega^{B_1}$; $K_2 = A_2\omega^{B_2}$, N/m^2
a_o, a_1, a_2, a_3	coefficients of force in generalized force-displacement relationship
a_θ	factor by which frequency is multiplied to get reduced frequency at temperature θ_c, corresponding to temperature θ
B	bulk modulus, N/m^2
b	width of shear element in direction perpendicular to direction of loading, m
B_1, B_2	exponents in power law relationship $K_1 = A_1\omega^{B_1}$, $K_2 = A_2\omega^{B_2}$
c_o, c_1, c_2, c_3	coefficients of displacement and its time derivative in generalized force-displacement relationship
C_p	specific heat, J/kg C
C_{T1}	damping coefficient of damping element in triparameter model, Ns/m
D	diameter of cylindrical compression element, m
da	elemental area, m^2
df_c, df_s	elemental forces in Beam-Column analysis, parallel and perpendicular to Beam-Column axis, respectively, N
D_i, D_o	inner and outer diameters of cartridge element, m
D_s	energy loss per cycle due to hysteresis, J
dt'	elemental time in cycle average integral
$d\theta$	elemental angle
E	Young's modulus, N/m^2
E_{eff}	effective Young's modulus for cartridge element, N/m^2

F	force exerted by elastomer, N
f	frequency, Hz
F_1	maximum force in hysteresis loop, N
f_1	factor used by Göbel to correct for shape effects in cartridge elements of finite length
f_r	reduced frequency, Hz
F^*	complex force amplitude, N
G	shear modulus, N/m^2
G^*	complex modulus $G' + iG''$, N/m^2
G', G''	storage, loss moduli in shear, N/m^2
G'_{eff}	effective storage modulus in shear, N/m^2
G''_{eff}	effective loss modulus in shear, N/m^2
G'_o	static shear modulus, N/m^2
G_r	reduced shear modulus, N/m^2
h	height of compression element; thickness of shear element (strained dimension for compression and shear elements)
I	$(2\pi/\omega)$ x cycle average of dissipation function, S, $J/m^3/cycle$
i	$\sqrt{-1}$
k	thermal conductivity, watts/cm C
K^*	complex stiffness, $K_1 + iK_2$, N/m
K_r	radial stiffness of cartridge, N/m
K_{T1}, K_{T2}	stiffness values in triparameter model, N/m
K_1	stiffness, N/m
K_2	damping, N/m
ℓ, L	length of cartridge element, m

M	supported mass, kg
n,N	number of elements in test specimen
$\bar{r}$	mean radius
R_t	right-hand side of energy equation in numerical solution at time, t, J/m^3S
r_1,r_2	inner and outer radius of cartridge, m
S	dissipation function, J/m^3S
s	shape factor - ratio of one loaded area to free area
T	temperature, C
t	time, s
t'	dummy time for cycle average integral, s
T_a	ambient temperature in metal to which elastomer is bonded, C
T_z	instantaneous temperature at axial coordinate Z, C
U	axial displacement, m
U_s	energy stored in element at maximum displacement, J
U_z	axial displacement (instantaneous), m
X	length of shear element in direction parallel to loading, m
Y	deflection of elastomer element, m
Y^*	complex amplitude of elastomer deflection, m
Y_m	absolute displacement of supported mass, m
Y_m^*	complex displacement amplitude of supported mass, m
Y_o	absolute displacement of base, m
Y_o^*	complex displacement amplitude of base, m
Y_1	maximum deflection of elastomer element, m
Z	axial coordinate, m

α	transmissibility, ratio of amplitude magnitudes: output acceleration to input acceleration
β	shape factor coefficient
β'	shape factor coefficient for use in calculating stiffness
β''	shape factor coefficient for use in calculating damping
γ	factor equal to 1 for shear elements, 3 for compression elements
Δt	time step in numerical solution of energy equation, s
η	loss coefficient, K_2/K_1
θ	angle in cartridge analysis
θ	absolute temperature in reduced variables analysis, K
θ_c	characteristic temperature for elastomer material, K
θ_T	transition temperature for elastomer
ρ	density of elastomer, kg/m^3
σ	complex stress amplitude, N/m^2
σ_z	normal axial stress (instantaneous), N/m^2
φ	phase angle between motions of base and supported mass
ω	frequency, rad/sec

REFERENCES

1. Chiang, T., Tessarzik, J.M., and Badgley, R.H., "Development of Procedures for Calculating Stiffness and Damping Properties of Elastomers in Engineering Applications. Part I: Verification of Basic Methods," NASA Contractor Report No. CR-120965, prepared by Mechanical Technology Incorporated for NASA-Lewis Research Center under Contract No. NAS3-15334, March 1972.

2. Gupta, P.K., Tessarzik, J.M., and Cziglenyi, L., "Development of Procedures for Calculating Stiffness and Damping Properties of Elastomers in Engineering Applications. Part II: Elastomer Characteristics at Constant Temperature," NASA Contractor Report No. CR-134704, prepared by Mechanical Technology Incorporated for NASA-Lewis Research Center under Contract No. NAS3-15334, April 1974.

3. Lazan, B.J., DAMPING OF MATERIALS AND MEMBERS IN STRUCTURAL MECHANICS, Pergamon Press, New York, 1968.

4. Warnaka, G.E., "Dynamic Strain Effects in Elastomers," Rubber Chem Technol, 1967, p. 407.

5. Holownia, B.P., "Effect of Carbon Black on Poisson's Ratio in Elastomers," Rubber Chem Technol, May-June 1975, pp 245-253.

6. Payne, A.R. and Scott, J.R., ENGINEERING DESIGN WITH RUBBER, Interscience Publications, New York, 1960.

7. Gent, A.N. and Lindley, P.B., "The Compression of Bonded Rubber Blocks," Proc Inst Mech Engrs, Vol. 173, No. 3, L59, pp 111-117.

8. Hattori, R. and Takei, K., J Soc Rubber Ind, Japan, Vol. 23, 1950, p. 194.

9. Payne, A.R., "Dynamic Properties of Vulcanized Rubbers: 5 - Shape Factors and Functions in Rubber Engineering," Research Report No. 84, Research Assoc of British Rubber Manufacturers, January 1975.

10. Maghe, S.R. and Neff, H.R., "Dependence of Compression Modulus on Poisson's Ratio," Rubber Chem Technol, 1973, p 207.

11. Cannon, C.M., Nashif, A.D., and Jones, D.I.G., "Damping Measurements on Soft Viscoelastic Materials Using a Tuned Damper Technique," Shock and Vibration Bulletin No. 38, Naval Research Laboratory, Washington, D.C., Part 3, November 1968, pp 151-163.

12. Snowden, J.C., VIBRATION AND SHOCK IN DAMPED MECHANICAL SYSTEMS, J. Wiley and Sons, Inc, New York, 1968.

13. Ferry, J.D., Fitzgerald, E.R., Grandiene, L.D., and Williams, M.L., "Temperature Dependence of Dynamic Properties of Elastomers: Relaxation Distributions," Ind Eng Chem, Vol. 44, No. 4, April 1952, pp 703-706.

14. Williams, M.L., Landel, R.F., and Ferry, J.D., "The Temperature Dependence of Relaxation Mechanisms in Amorphous Polymers and Other Glass-Forming Liquids," J Amer Chem Soc, 77, 370, 1955.

15. Sommer, J.G., and Meyer, D.A., "Factors Controlling the Dynamic Properties of Elastomeric Products," SAE Paper No. 720267, SAE/ ASTM Sym, Detroit, Michigan, January 1973.

16. Sircar, A.K., and Conrad, T.G., "Strain Dependent Dynamic Properties of Carbon Black Reinforced Vulcanizates: I - Individual Elastomers," Rubber Chem Technol, March-April 1975, p 71.

17. Carnahan, B., Luther, H.A., and Wilkes, J.O., APPLIED NUMERICAL METHODS, J. Wiley and Sons, Inc, New York, 1969.

18. Rightmire, G.K., "An Experimental Method for Determining Poisson's Ratio of Elastomers," J Lub Tech, July 1930, pp 281-388.

19. Göbel, E.F. Berechnung und Gestaltung von Gummifedern, Springer-Verlag, Berlin/Göttengen/Heidelberg, 1955.

NASA-Lewis Research Center
21000 Brookpark Rd.
Cleveland, OH 44135

Attention: Project Manager, MS 6-1
A. Ginsburg, MS 5-3
W. Loomis, MS 23-2
W. J. Anderson, MS 23-2
D. Drier, MS 21-4
L. W. Schopen, MS 500-206
N. Musial, MS 500-113
Report Control Office, MS 5-5
Library, MS 60-3
Reliability & Quality Assurance Office, MS 500-211
Technology Utilization Office, MS 3-19
Resources Management Office, MS 3-10

NASA Scientific and Technical Information Facility
Attn: Accessioning Department
P.O. Box 8757
Balt/Wash International Airport
Maryland 21240 (10 copies)

NASA Ames Research Center
Attn: Library
Moffett Field, CA 94035

NASA Flight Research Center
Attn: Library
P.O. Box 273
Edwards, CA 93523

NASA Goddard Space Flight Center
Attn: Library
Greenbelt, MD 20771

Jet Propulsion Laboratory
Attn: Library
4800 Oak Grove Drive
Pasadena, CA 91103

NASA Langley Research Center
Attn: Library
Langley Station
Hampton, VA 23365

NASA Manned Spacecraft Center
Attn: Library
Houston, TX 77058

NASA Marshall Space Flight Center
Attn: Library
Marshall Space Flight Center, AL 35812

NASA Headquarters
Attn: G. Deutsch (RW)
J. Maltz (RWM)
N. F. Rekos (RLC)
D. Miller (RLC) (1 copy ea.)
Washington, D.C. 20546

Aerojet-General Corporation
Attn: Library
1100 West Hollyvale
Azusa, CA 91702

Aerojet-General Corporation
Attn: Library
Aerojet Liquid Rocket Company
Sacramento, CA 98509

Aerospace Corporation
Attn: Library
P.O. Box 95085
Los Angeles, CA 91745

AiResearch Manufacturing Company
9851 Sepulveda Boulevard
Los Angeles, CA 90009

Air Force Aero Propulsion Laboratory
Attn: H. F. Jones
E. Lake (1 copy ea.)
SFL
Wright Patterson AFB, OH 45433

Batelle Memorial Institute
Attn: Library
C. M. Allen (1 copy ea.)
Columbus Laboratories
505 King Avenue
Columbus, OH 43201

Bendix Research Labs Division
Attn: Library
Detroit, MI 48232

Boeing Co.
Aerospace Division
Attn: Library
P.O. Box 3707
Seattle, WA 98124

Boeing Company
Vertol Division, Boeing Center
Attn: Library
P.O. Box 16858
Philadelphia, PA 19142

Continental Aviation and Engineering Corp.
Attn: Library
12700 Kercheval Avenue
Detroit, MI 48215

Curtiss-Wright Corporation
Wright Aero Division
Attn: Library
Main & Passaic Streets
Woodridge, NJ 07075

Fafnir Bearing Company
Attn: R. J. Matt
37 Booth Street
New Britain, CT 06050

Franklin Institute Research Labs
Attn: W. Shapiro
Benjamin Franklin Pkwy. at 20th St.
Philadelphia, PA 19103

General Electric Company
Aircraft Engine Technical Division
Bearings, Fuels and Lubricants
Attn: E. N. Bamberger

General Electric Company
Gas Turbine Division
Attn: C. C. Moore
Bldg. 53-330
Schenectady, NY 12345

General Electric Company
Mechanical Technology Laboratory
Attn: Library
R & D Center
Schenectady, NY 12301

General Motors Corporation
Allison Division
Attn: Library
Indianapolis, IN 46206

Hughes Aircraft Corporation
Attn: Library
Centinda & Teale Avenue
Culver City, CA 90230

Industrial Tectonics, Inc.
Attn: H. Hanau
18301 Santa Fe Avenue
Compton, CA 90024

Institute for Defense Analyses
Attn: Library
400 Army-Navy Drive
Arlington, VA 22202

Lockheed Missiles & Space Co.
Attn: Library
P.O. Box 504
Sunnyvale, CA 94088

Massachusetts Institute of Technology
Attn: Library
Cambridge, MA 02139

Mechanical Technology, Incorporated
Attn: Library
968 Albany-Shaker Rd.
Latham, NY 12110

National Science Foundation
Engineering Division
Attn: Library
1800 G Street, N.W.
Washington, D.C. 20540

Naval Air Systems Command
Attn: Library
Washington, D.C. 20360

Naval Ship Engineering Center
Attn: W. C. Lindstrom NSC 613D4B
Washington, D.C. 20360

Naval Ship Research & Development Center
Annapolis Division
Attn: Library
Annapolis, MD 21402

Naval Ship Systems Command
Attn: J. E. Dray SNHIP 6148
Washington, D.C. 20360

North American Rockwell Corporation
Space Division
Attn: Library
12214 Lakewood Blvd.
Downey, CA 90241

Office of Naval Research
Attn: S. W. Doroff ONR/438
Arlington, VA 22217

SKF Industries, Incorporated
Engineering & Research Center
Attn: T. Tallian
L. Sibley (1 copy ea.)
1100 First Avenue
King of Prussia, PA 19406

Sunstrand Denver
Attn: Library
2480 West 70 Avenue
Denver, CO 80221

TRW Accessories Division
Attn: Library
23555 Euclid Avenue
Cleveland, OH 44117

TRW Marlin Rockwell Division
Attn: A. S. Irwin
402 Chandler Street
Jamestown, NY 14701

U.S. Army Engineering R & D Labs
Gas Turbine Test Facility
Attn: W. Crim
Fort Belvoir, VA 22060

United Aircraft Corporation
Pratt & Whitney Aircraft Division
Attn: R. Shevchenko
P. Brown
Library (1 copy ea.)
400 Main Street
East Hartford, CT 06108

United Aircraft Corporation
Sikorsky Aircraft Division
Attn: Lester Burroughs
Stratford, CT 06497

U.S. Army Aviation Materials Labs
Attn: Library
Ft. Eustis, VA 23604

National Technical Information Service
Springfield, VA 22151 (20 copies)

Rensselaer Polytechnic Institute
Mechanics Division
Attn: F. F. Ling
Troy, NY 12181

Southwest Research Institute
Attn: Library
P.O. Drawer 28510
San Antonio, TX 78284

Pure Carbon Co.
MAIC Division
Attn: Library
441 Hall Avenue
St. Mary, PA 15847

Materials Science Corp.
Blue Bell Office Campus
Merion Tower Building
Blue Bell, PA 19422

Shaker Research Corp.
Attn: Dr. C. H. T. Pan
Northway 10 Executive Park
Ballston Lake, NY 12019

Marlin-Rockwell Co.
Division of TRW, Inc.
Attn: Anthony T. Galbato
402 Chandler St.
Jamestown, NY 14701

General Electric Co.
Attn: Dr. Alfred J. Martenson
P.O. Box 8, Malta Site
Schenectady, NY 12301

Northwestern University
Department of Mechanical Engineering
& Astronautical Science
Attn: Dr. R. Burton
Dr. H. S. Cheng (1 copy eal)
Evanston, IL 60201

Thiokol Corporation
Attn: Bliss Law, MS 308
P.O. Box 524
Brigham City, UT 84302

Teledyne CAE, Turbine Engines
Attn: R. Beck, Dept. Head
Materials Devel. & Man. Eng.
1330 Laskey Rd.
Toledo, OH 43697

Ingersoll-Rand Corp.
Attn: R. G. Kirk, Rotor Dynamics Div.
Phillipsburg, NJ 08865

United Technologies Corp.
Pratt & Whitney Aircraft Div.
Attn: Dr. F. C. Hsing
East Hartford, CT 06108

Deposits & Composites Inc.
Attn: R. E. Engdohl, President
318 Victory Dr.
Herndon Industrial Park
Herndon, VA 22070

Williams Research Corp.
Attn: George Rourk
2280 W. Maple Rd.
Walled Lake, MI 48088

University of Virginia
School of Engineering & Applied Science
Attn: Dr. Edgar J. Gunter
Dept. of Mechanical Engineering
Charlottesville, VA 22901